DRD No. SE-7
DRL No. 58

SILICON WEB PROCESS DEVELOPMENT

FINAL REPORT

C. S. Duncan, R. G. Seidensticker, J. P. McHugh,
M. E. Skutch, J. M. Driggers, and R. H. Hopkins

Contract No. 954654

DOE/JPL-954654-80/13
DIST. CATEGORY UC-63

October 1981

The JPL Low-Cost Silicon Solar Array Project is sponsored by the U. S. Department of Energy and forms part of the Solar Photovoltaic Conversion Program to initiate a major effort toward the development of low-cost solar arrays. This work was performed for the Jet Propulsion Laboratory, California Institute of Technology by agreement between NASA and DOE.

Westinghouse R&D Center
1310 Beulah Road
Pittsburgh, Pennsylvania 15235

DRD No. SE-7
DRL No. 58

SILICON WEB PROCESS DEVELOPMENT

FINAL REPORT

C. S. Duncan, R. G. Seidensticker, J. P. McHugh,
M. E. Skutch, J. M. Driggers, and R. H. Hopkins

Contract No. 954654

DOE/JPL-954654-80/13
DIST. CATEGORY UC-63

October 1981

The JPL Low-Cost Silicon Solar Array Project is sponsored by the U. S. Department of Energy and forms part of the Solar Photovoltaic Conversion Program to initiate a major effort toward the development of low-cost solar arrays. This work was performed for the Jet Propulsion Laboratory, California Institute of Technology by agreement between NASA and DOE.

Westinghouse R&D Center
1310 Beulah Road
Pittsburgh, Pennsylvania 15235

TABLE OF CONTENTS

TABLE OF CONTENTS (CONT.)

LIST OF ILLUSTRATIONS

LIST OF ILLUSTRATIONS (CONT.)

LIST OF TABLES

1. SUMMARY

Silicon dendritic web is a single crystal silicon ribbon material with unique advantages for the manufacture of low cost solar cells. Shaped by the interplay of natural crystallographic and surface tension forces, rather than by potentially contaminating dies, the web produces solar cells with excellent conversion efficiency. For example, the maximum demonstrated AM1 efficiency, 15.5%, is so far the highest value reported for a ribbon material. The web process also conserves expensive silicon: the ribbons are thin as grown, 100 to 200 μm, and the facet-smooth surfaces require no costly cutting or etching before cell fabrication. Because impurities are rejected from the ribbon during crystal growth, it is feasible to use cheaper, less pure "solar" grades of silicon as feedstock for the web process. Moreover, long flexible web strips facilitate automation of both crystal growth and the subsequent cell-manufacturing operations. Taken together, these characteristics have made the web process a leading candidate to achieve or better the 1986 Low Cost Solar Array (LSA) Project cost objectives of 70 cents per peak watt (1980 dollars) of photovoltaic output power.

During the past three and a half years of steady technical progress, the web process has evolved from one with all the potential advantages suggested above to a method very close to technology readiness for commercial development of low cost solar cells. Web output rates were raised more than ten fold to 27 cm^2/min, and cell efficiencies were increased to 15.5% from about 13%. Melt replenished growth, which was merely a concept in 1977, has now been demonstrated under operator control for a full one-day growth cycle and for periods of one eight-hour shift with complete closed-loop control. The melt level was maintained constant to $\pm$ 0.1mm, a degree of control better than the estimated requirements for automated continuous growth of web. The web produced

under continuous operation produced solar cells with excellent efficiency. Besides these systems-related developments, we have shown that silicon web can routinely be grown with thicknesses below 150 μm to conserve silicon, and that the resultant ribbons have dislocation densities less than 10^4 cm^{-2}. Silicon web has been grown from experimental "low-cost" silicon (Battelle), as well as from purposely contaminated feedstock, and yet has produced efficient solar cells. Hence, compatibility of the process with cheaper, less pure solar grade silicon seems likely.

Collectively these achievements imply that the web process has an excellent chance to better the DOE/JPL 1986 goal for sheet plus poly-silicon cost of 22.4 cents per peak watt (1980$). Our projected web cost is in fact 17.3¢ per peak watt assuming area throughput rates of 25 cm^2/min, 15% AM1 cell efficiency, a three-day melt replenished growth cycle, system automation, and silicon at $14 per kg. Aside from a three-day growth cycle and the silicon cost, these objectives individually have been met. The highlights of this work are the subject of this report. The next step is the design, assembly, and operation of a prototype automated web furnace to demonstrate the technology readiness of the process.

2. INTRODUCTION

This is the final report of a project to develop the silicon web process for low cost terrestrial solar cells. The work was carried out under JPL Contract 954654 as part of the Low Cost Solar Array Project.

The silicon web process takes advantage of natural crystallographic stabilizing forces to grow long, thin single crystal ribbons directly from liquid silicon. The ribbon, or web, is formed by the solidification of a liquid film supported by surface tension between two silicon filaments, called dendrites, which border the edges of the growing strip. The ribbon can be propagated indefinitely by replenishing the liquid silicon as it is transformed to crystal.

The dendritic web process has several advantages for achieving low cost, high efficiency solar cells.

- No dies or shapers are required; therefore, the silicon remains free from contamination.
- Since the faces of the web are natural crystal facets, the ribbon grows with mirror-smooth surfaces which are essentially ready for solar cell fabrication.
- Costly finishing steps of slicing, lapping, and polishing are not required to make cells; the result is a substantial savings in labor and equipment.
- Expensive silicon feedstock also is conserved by the web approach because the ribbons are thin - 5 to 6 mils - as grown, and because there is little subsequent cutting loss.
- Cell conversion efficiencies of > 15% (AM1) have been demonstrated.

The dendritic web process was recognized as a viable technique for the production of single crystal silicon ribbons in the early 1960's when it was used to provide material for solar cells in space applications, but it was the post-oil-embargo concern over fuel supplies which rekindled interest in the potential of the web technology to provide low cost photovoltaic power for terrestrial applications. At that time it was clearly recognized that improvements in output rate, higher solar cell efficiency, the introduction of melt replenishment and system automation for continuous growth, as well as a reduction in silicon price would all be required to reduce the price of solar panels. Thus, an important first step in this program—which began in April of 1977—was to identify the key technical developments required for web to achieve the national goal of $0.70 per peak watt of photovoltaic output power in 1986. Using experimental data, system modeling, and economic analysis, we found that the DOE/JPL 1986 wafer plus polycrystalline silicon cost goal of 22.4 cents per Wpk (1980 dollars) could be met or bettered for web as follows:

- Area throughput rate: $25 cm^2/min$ (> $18 cm^2/min$)
- Cell efficiency: 15% AM1
- Melt replenished growth: 3-day cycle (∿ 2 day cycle)
- Semi tomated growth

assuming:

- Polysilicon price: $14/kg in 1980 dollars (<$35/kg)
- Solar grade polysilicon is acceptable to the process.

Note that some tradeoffs exis among the requirements. Any one of the developments concerning throughput rate, melt-replenished growth, and polysilicon price may be relaxed as indicated in parentheses if all other requirements were met.

As Table 1 indicates, steady progress toward these objectives over the past three years has brought the web process close to technology readiness.

TABLE 1

SUMMARY OF ADVANCES IN PROCESS PARAMETERS

Process Parameter	April 1977	April 1978	April 1979	April 1980
Maximum Demonstrated Area Growth Rate (cm^2/min)	2.3	8	23	27
Maximum Demonstrated Width (cm)	2.4	3.5	4.0	4.7
Maximum Demonstrated Solar Cell Efficiency	∿13%	∿14%	∿15%	>15%

The current status of the silicon web process development is as follows:

- 27 square centimeters per minute growth demonstrated for short periods.
- One day manually controlled melt-replenished growth cycle demonstrated.
- Closed-loop melt level control ($\pm$ 0.1mm) of replenished growth for an 8-hour period.
- Functional semi-automated furnace design completed.
- Solar cell efficiency of 15.5% AM1 demonstrated. Average efficiency = 13.5% AM1.
- Efficient solar cells made on web grown from experimental "low cost" silicon.
- Thickness routinely 100-200 μm.
- Dislocation density routinely $<10^4/cm^2$.

Taken together, these achievements indicate that all key technical developments required for the web process to meet the 1986 cost goals have been individually met except for the three-day semi-automated growth cycle. (The development of $14/kg silicon is the subject of a separate JPL task; current results are promising.) Moreover, our studies indicate there are no inherent limitations to producing wider web at higher growth speeds. (See the analysis contained in reference 1, 1979-1980 Annual Report). For example, increasing the output rate to 35 cm^2/min, which we believe is a reasonable objective, would result in a 40% reduction in the projected price for web wafer plus polysilicon below the 17.3 cents per Wpk we now expect in 1986.

In the following sections of this report we have attempted to highlight the important developments of the past three and a half years. For details the reader is referred to past annual reports.[1-3]

3. WEB TECHNOLOGY DEVELOPMENT

3.1 Economic and Technical Requirements

Management and evaluation of silicon web growth process development requires a thorough understanding of the characteristic economic/technical relationship of the process. To obtain such understanding, an economic analysis was prepared, in accordance with the JPL SAMICS IPEG method, during Phase I of this program. At the time the economic analysis was prepared, a wealth of experimental experience with the process was available and provided sound technical judgements for incorporation into the economic analysis projection. The economic analysis has since become a key factor in the determination of technical goals and development tasks and in the evaluation of progress.

The initial economic analysis and its frequent updating served the dual purpose of predicting the 1986 costs and identifing the critical developments necessary to attain those predicted costs. The complete details of this analysis and its updating have been reported previously in annual and quarterly reports and are not repeated in this report. Instead, it is our intention to summarize the principal message of this analysis, the resulting development program undertaken, the progress and status of that program, and the remaining work to be done in order to satisfy the DOE/JPL 1986 goal.

3.1.1 Economic Analysis

The IPEG[4] analysis places annual expense into five categories in the following equation:

$$\text{ANNUAL EXPENSE} = C_1 \times \text{EQPT} + C_2 \times \text{SQFT} + C_3 \times \text{DLAB} + C_4 \times \text{MATS} + C_5 \times \text{UTIL}$$

where C for each category has been derived from the SAMICS model and EQPT = purchase cost of equipment to make QUAN per year, SQFT = floor space required by EQPT and its operator, DLAB = unburdened, unfringed cost of direct labor for QUAN, MATS = cost of direct materials and supplies (excluding polysilicon) to make QUAN, UTIL = cost of direct utilities to make QUAN, QUAN = amount of annual production in peak watts. The price is thus determined as

PRICE = ANNUAL EXPENSE/QUAN

The IPEG analysis, as previously reported[1,2,3,5] and updated, predicts that the silicon web process will reach or surpass the DOE/JPL 1986 goal. Table 2 shows the projected price of 17.3¢/Wpk as compared to the DOE/JPL 1986 goal of 22.4¢/Wpk (in terms of 1980 dollars) for the combined silicon and value-added wafer price. Note also, from the distribution of costs shown in Table 2, that no cost category is dominant. For example, the largest category, capital equipment (EQPT), constitutes just 26.7% of the total wafer price. Thus, if in actual production the capital cost were found to be double the projected cost, a very unlikely possibility, the total wafer price would be raised to just 21.9¢/Wpk which is still somewhat below the 22.4¢/Wpk 1986 goal. Other cost categories are smaller and consequently are proportionally less sensitive in terms of possible analysis adjustments.

3.1.2 Critical Developments

As is customary with economic projections, the silicon web economic analysis, from its inception, included assumptions of critical technical developments that were required in order to satisfy the DOE/JPL 1986 goal. In essence, these critical developments became the major technical objectives of this program. The following subsections, 3.1.2.1 through 3.1.2.6, review these developments, including their current status, and discuss what, if any, further work will be required. Completion of these developments will verify the conclusion of the economic analysis which predicts that the silicon web process can satisfy or even surpass the 1986 goal.

TABLE 2

Dwg. 7729A14

SUMMARY OF COSTS FOR SILICON WEB PROCESS
IPEG Projection for 1986
All Costs Shown in Terms of 1980 Dollars
Growth Parameters: Area Throughout Rate 25 cm^2/mm
Length of Growth Cycle 3 Days
Polysilicon Price $14/kg

Distribution of Costs, ¢/Wpk						Total Wafer Cost, ¢/Wpk
Polysilicon	EQPT	SQFT	DLAB	MATS	UTIL	
3.98	4.62	2.49	3.83	1.78	0.62	17.3

(DOE/JPL 1986 combined goal for silicon and wafers = 22.4¢/Wpk)

3.1.2.1 Area Rate of Growth

The cost sensitivity of the silicon web area rate of growth is shown in Figure 1. Using silicon priced at the DOE/JPL goal of \$14/kg, an area rate of growth of about 18 cm^2/min is required in order to satisfy the 1986 goal of 22.4¢/Wpk for the combined silicon and value-added wafer price. Note that the maximum demonstrated area rate of growth is 27 cm^2/min and that this rate corresponds to a projected cost of only 17.3¢/Wpk. Thus, the demonstrated rate is considerably better, by about 5¢/Wpk, than is required to satisfy the 1986 goal. Further refinement is required to assure that high-area growth rate will be routine. An extended analysis of the web process indicates that an area throughput of 35 cm^2/min is attainable and would bring the projected cost to 13.5¢ per peak watt.

3.1.2.2. Melt Replenishment

Melt replenishment is a mandatory requirement for satisfying the 1986 cost goal. The obvious contribution of melt replenishment is that of supplying silicon to the melt to sustain long (two to three day) periods of continuous growth. Another important but less obvious reason for melt replenishment is its relationship to web growth rate and quality. It has been proven experimentally that the speed of growth, the thermally generated stress and the width of growth are greatly affected by the silicon melt level. Thus, in a properly designed web growth system, these highly important parameters can be simultaneously optimized at only a single specific melt level, maintained by means of controlled melt replenishment.

The melt replenishment system developed for this program is working well and has been operated continuously with manual control during web growth for periods as great as seventeen hours. Seventeen hours is significant in that it corresponds to the actual growth hours in a one-day web growth cycle. Web grown during melt replenishment has demonstrated high quality, i.e., has cell efficiency equal to or better than web grown conventionally without melt replenishment.

Curve 713010-A

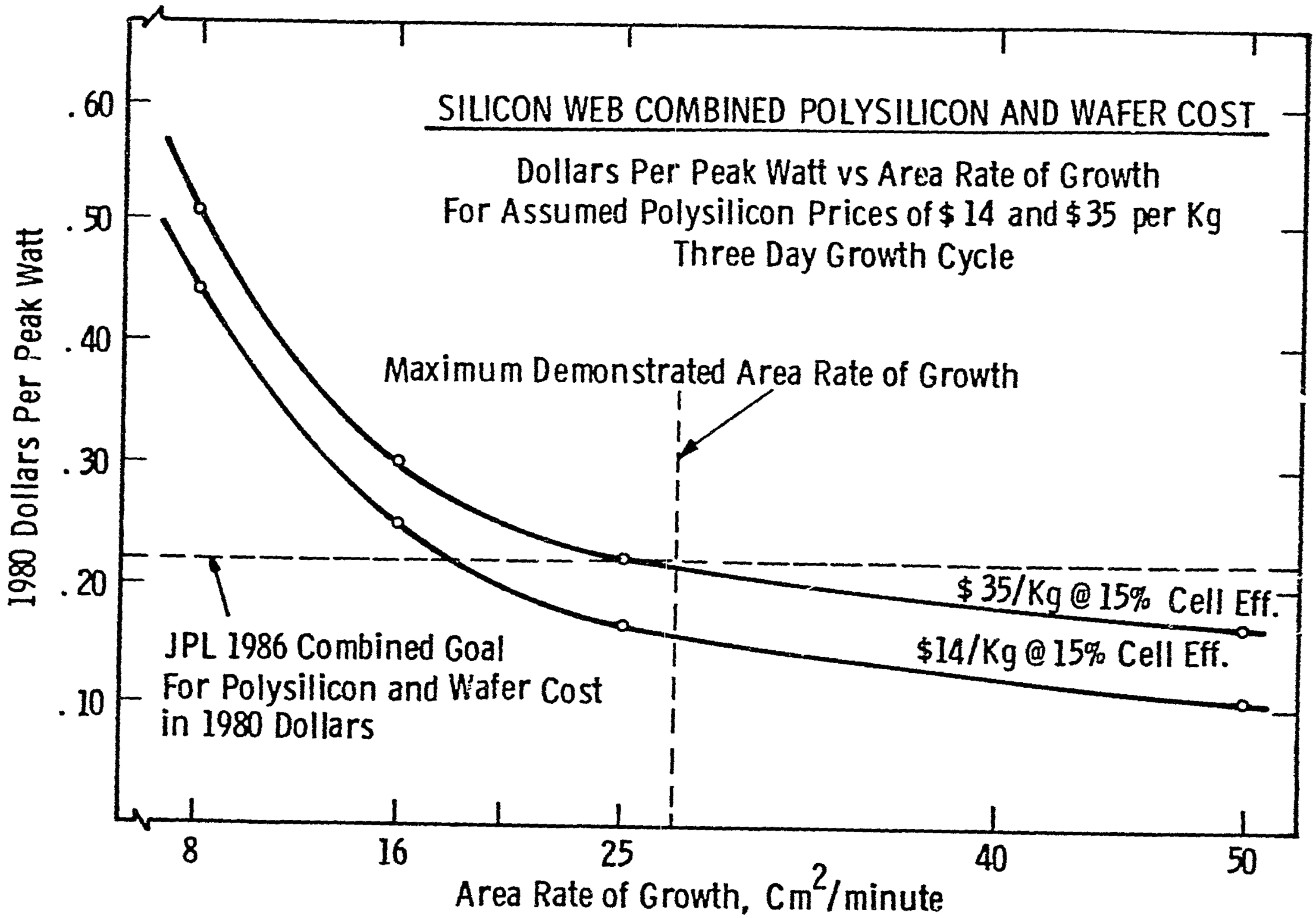

Figure 1 Silicon web combined polysilicon and wafer cost

ORIGINAL PAGE IS OF POOR QUALITY

The melt replenishment system is in an advanced state of development though minor redesign may be required to suit the size of solar grade polysilicon pellets, when available.

3.1.2.3 Automation

Automation of web growth is required in order to bring the direct labor cost to the level projected by economic analysis. The development of automated growth is being conducted in two successive steps, namely semi-automation followed by full automation. Demonstrated semi-automated growth, a goal of this program, has been achieved largely as a consequence of the development of closed-loop automated control of melt replenishment and melt level. The closed-loop system consists mainly of a motorized pellet feeder, a laser-based melt level sensor, and a control circuit which closes the loop with the pellet feeder and level sensor. This system provides semi-automatic control requiring very little operator input, and has been operated for periods up to eight hours. In this growth mode the constant-melt-level melt replenishment is fully automatic, while the operator must make only limited other adjustments. Figure 2 shows the cost sensitivity as it relates to the time length of automated melt-replenished growth necessary to satisfy the 1986 goal. Note that our goal of a three-day growth cycle results in a price of 17.3¢/Wpk as projected by the economic analysis, whereas a growth cycle of less than two days is required to satisfy the 1986 goal of 22.4¢/Wpk. The longest manually controlled melt replenished growth thus far demonstrated corresponds to a one-day growth cycle. The longest semi-automatic growth thus far demonstrated is eight hours, which equals the goal of this program.

In order to fully satisfy the economic analysis cost projection, a fully automatic three-day growth cycle is required. This will necessitate addition of a second closed loop for dimension control through fine adjustment of temperature, a function now performed through operator judgement.

Curve 719676-A

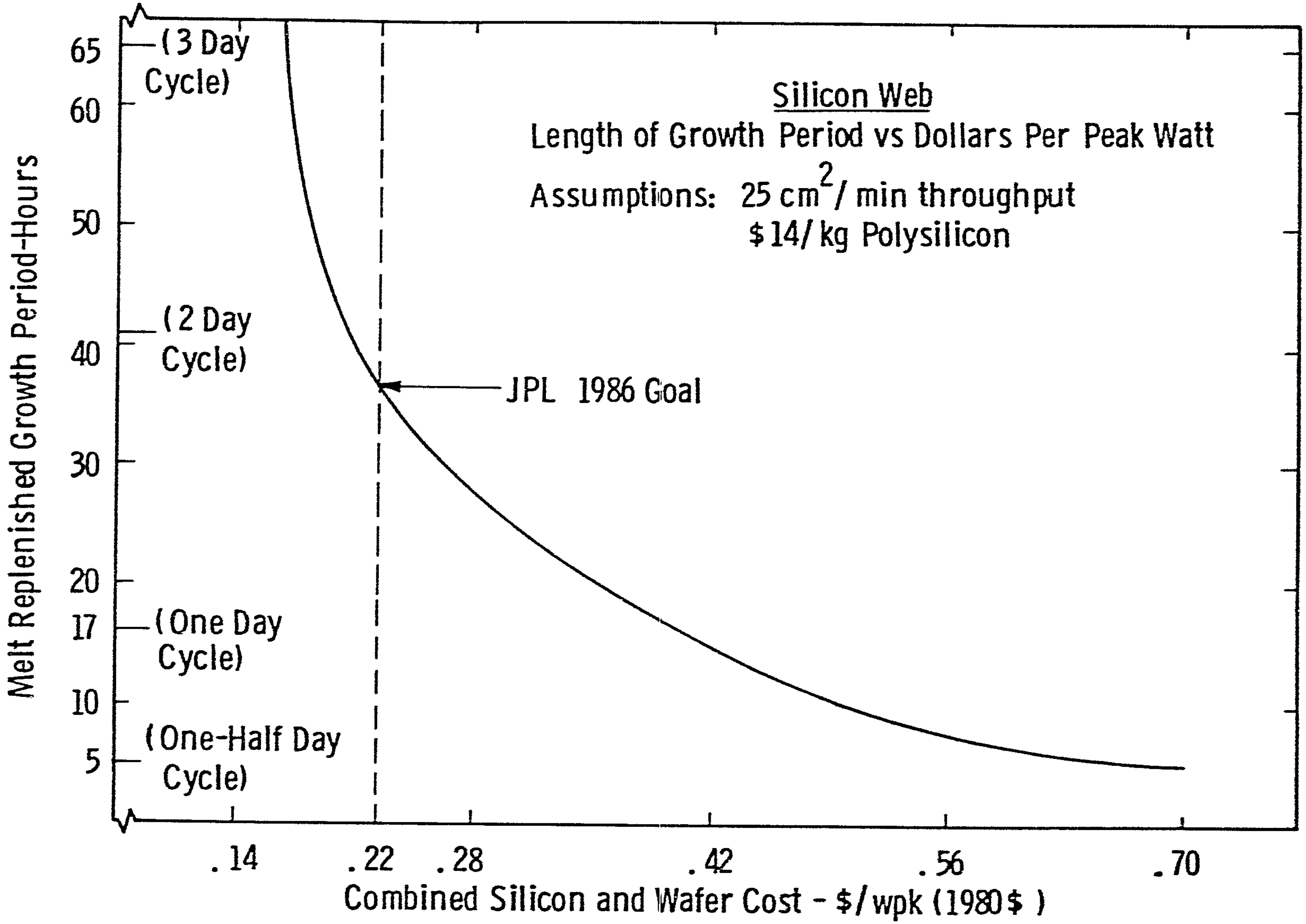

Figure 2 Effect of Replenishment Period on Web Wafer Cost

3.1.2.4 Silicon Economics

The silicon web process is inherently economical in its utilization of silicon for solar cells. Several properties of the process result in this economy, the most obvious being ribbon shape of growth. For this reason there is no loss due to slicing to wafer thickness as is required with Czochralski or other boule forms of growth. Also, as a result of the ribbon form of growth, rectangular-shaped solar cell wafers are achieved without material loss and provide the maximum packing factor in a solar panel. Cutting to wafer size is done by laser scribing and cleaving, again without loss of silicon. Finally, dendrites removed from solar cells can be returned to the melt without loss of silicon, other than that caused by clean-up etching before remelting. The wafer cost sensitivity related to salvaging dendrites is shown in Figure 3. We believe that the overall preference is for option three of Figure 3, despite the slightly higher wafer cost, because of the expected appreciably higher yield during cell fabrication if dendrites are removed after fabrication.

Another important silicon economy of the web process is its naturally thin growth, 150 microns (6 mils) being a typical, easily achieved growth thickness.

The polysilicon cost sensitivity for the web process is shown in Figure 4. Note that the process cost at six mils thickness is substantially below the DOE/JPL 1986 goal if it is assumed that the $14/kg polysilicon price goal is attained. Alternatively, the process shows considerable tolerance for higher priced silicon.

Another potential economy of the web process is its comparative tolerance of impurities in the silicon feedstock. Although no actual cost figures are available, a tolerance of impurities permits use of less pure and, presumably, less costly feedstock. Although solar grade polysilicon is not yet commercially available, good quality silicon web has been grown from experimental solar grade polysilicon prepared by Battelle under JPL contract #954339.

Dwg. 7729A63

ECONOMICS OF RECYCLING DENDRITES

Assuming the Key Developments Are Attained, Comparative Cost of the Three Dendrite Utilization Options Are:

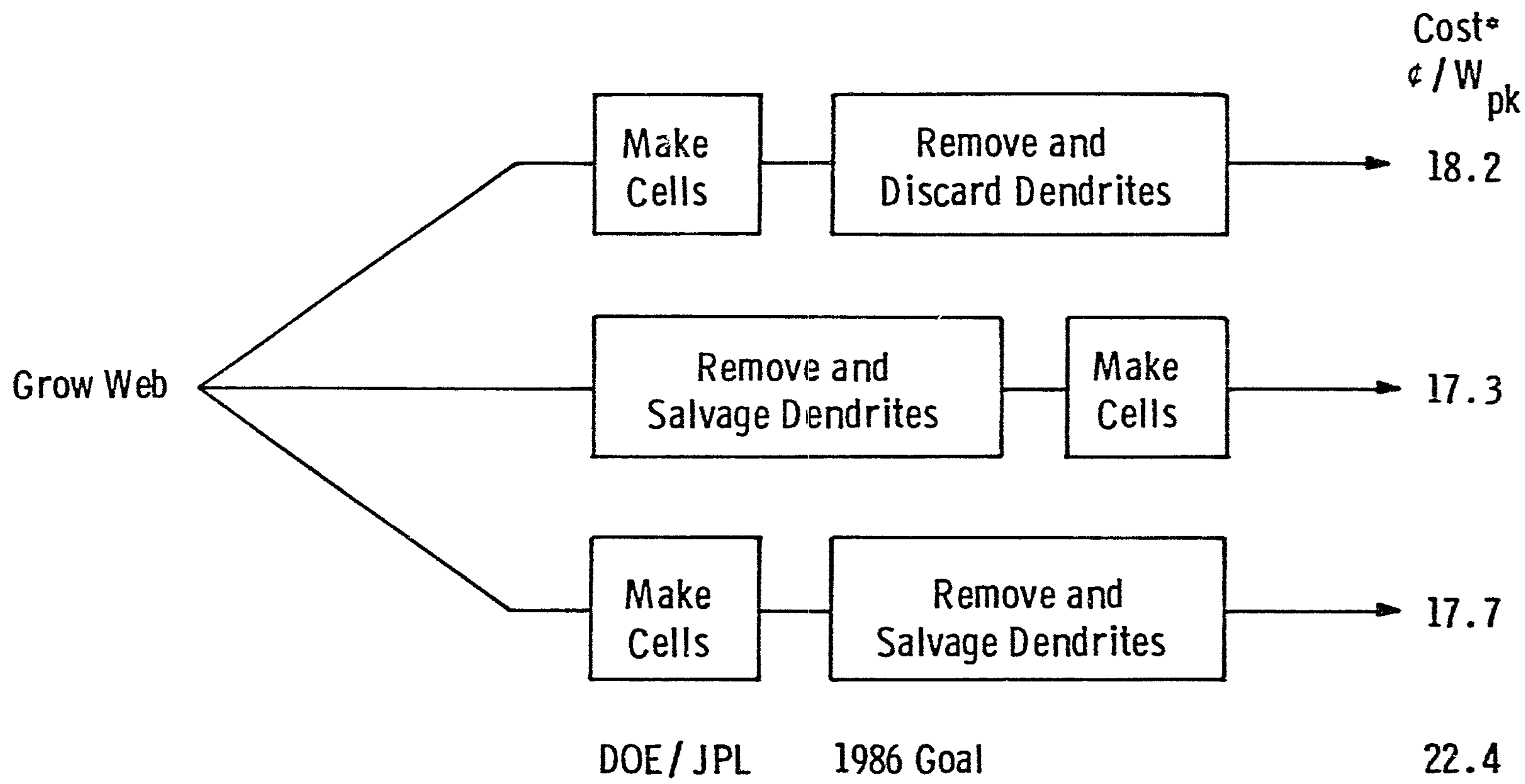

*Conbined polysilicon and value-added wafer cost in 1980 dollars

Figure 3 Economics of Recycling Dendrites

ORIGINAL PAGE IS OF POOR QUALITY

Curve 694242-A

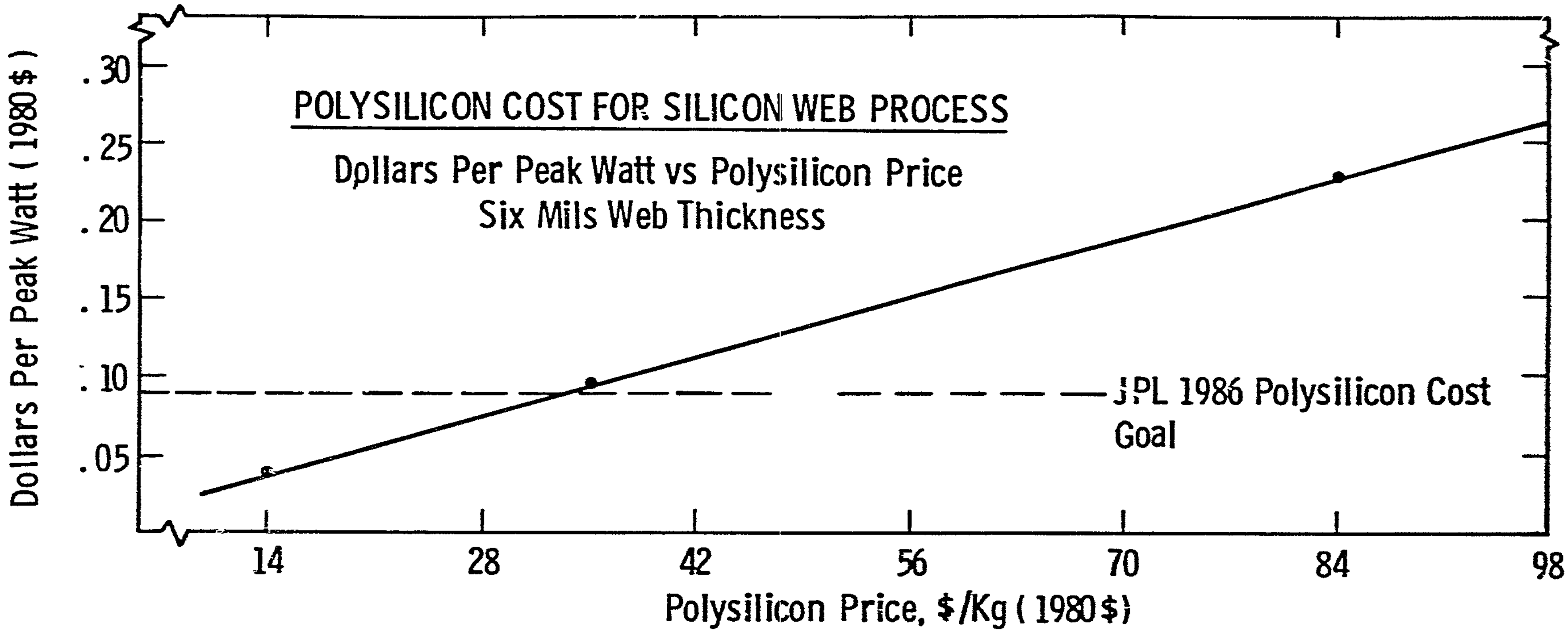

ORIGINAL PAGE IS
OF POOR QUALITY

Figure 4 Polysilicon Cost for Silicon Web Process

In summary, the silicon economy of the web process is primarily inherent, and our entire effort has been largely aimed at demonstrating this economy. No further development is needed.

3.1.2.5 Cell Efficiency

Cell efficiency is a very sensitive factor in determining the economics of a silicon sheet growth process. The SAMICS/IPEG analysis as prepared for the silicon web process includes efficiency insofar as only the wafer cost is concerned. Subsequent costs such as those related to cell fabrication, encapsulation, panel and support structure, etc. are also very sensitive to cell efficiency. For the economic analysis results shown earlier in Table 2, 15% cell efficiency was assumed.

Cell efficiency of 15% AM1 or higher has been demonstrated many times during this program. However, the yield of 15% cells is not high, and the best averages for batches of cells have tended to be nearer to 14%. Further process refinement of efficiency to produce an average efficiency of 15% or greater is recommended.

3.1.2.6 Equipment Design

The relationship of equipment cost to total wafer cost was shown earlier in Section 3.1.1 and Table 2. Ultimately, equipment design must satisfy two goals; namely, the functional features which are necessary to achieve the technical goals and the equipment (EQPT) cost as projected in the IPEG analysis. Although equipment design during this program has been concerned with the cost of the equipment, emphasis has heavily centered on functional features rather than the purchase cost of the equipment. Equipment costs projected in the economic analysis have been based on knowledge of the mechanical and electronic requirements of the equipment developed for the web process during this program. A complete, up-to-date detailed engineering design covering all developments of this program has been prepared and is appended to this report.

To satisfy the cost goal, additional design is needed in terms of functional performance and equipment cost. New functional design should include refinement of some existing design as well as a new dimension control loop (as discussed in Section 3.1.2.3). Some portions of the existing design should be redesigned for cost reduction but without any change in the functional specifications.

3.1.3 Summary

The economic analysis for silicon web was prepared early in this program and predicted that the process would equal or better the DOE/JPL 1986 price goal for wafers. The economic analysis also clearly identified the critical developments which were required in order to reach the 1986 goal. Tasks undertaken during the three now complete phases of this program were, in all instances, in close agreement with the long-term critical developments. The program tasks have been attained and all critical developments have been advanced to the status intended in this program.

To achieve full technology readiness for the 1986 goal, the critical developments must be taken to completion. The status of these developments are summarized briefly as follows:

- The area rate of growth goal has been demonstrated. Further refinement is needed in order that high throughput is attained routinely.
- Melt replenishment has been routinely demonstrated. This development is essentially complete.
- Closed loop control of the silicon melt level and semi-automatic web growth have been demonstrated. The achievement of fully automatic web growth requires the addition of a closed-loop control for web width.

- The projected silicon economics of the web process is in complete agreement with the inherent properties of the process. A commercially available supply of suitable pellet form solar guide polysilicon is needed in order to take full advantage of the process.

- Solar cell efficiency to as great as 15.5% AM1 has been demonstrated. Further development is needed so that an average cell efficiency of 15% or greater is attained.

- The functional features of web growth equipment design are nearly complete. The major exception is the need for an additional control loop as required for automatic control of width. The design also needs some simplification, without change of function, in order to minimize the cost to build.

Upon completion of the above critical developments, the process status will be that of full technology readiness for the 1986 goals.

3.2 Output Rate Technology

3.2.1 Introduction

The objective of the rate technology development has been to increase area throughput, i.e., area per unit time. The fundamental parameters that come into play are crystal width, growth velocity, stress levels and melt-level maintenance. Other concerns of interest are wider crystal starts and width control. Each of these parameters was addressed independently in the earlier developmental efforts and subsequently integrated into a functioning web growth system.

The general approach to the understanding and correlation of the various parameters involved in web growth has been a combination of thermal modeling and experimentation carried out in parallel, the results of each line of effort serving to supply information to the other. While the experimental effort has continued throughout the program, thermal modeling has been used as appropriate to guide the solution of specific throughput-related problems.

Section 3.2.3 presents a brief overview of the program as it developed; the sections which follow that will address the technical aspects of the experimental effort in terms of each parametric requirement in more detail.

3.2.2 Thermal Modeling

In order to provide a analytical tool for the design of dendritic web growth systems, several models were developed. The first of these models generated the temperature distribution in the susceptor, and the melt and was used for the design of slot shapes that would provide flat lateral temperature profiles in the growth region of the liquid.[3] Measurements of actual melt temperatures verified the analysis, and approximately flat melt profiles are presently routinely generated.

A second set of models generated the temperature distributions in the meniscus of a growing web and in the web itself. These models included the vertical aspects of the lid and shields as the variable parameters. Although the direct measurement of the temperatures in these regions is almost impossible to the accuracy required to verify the analysis, indirect evidence was obtained through the thickness velocity relationship of the growing ribbons. As is well known, the thickness of a ribbon crystal is related to its growth velocity by an inverse relationship such as $v = c + d/t^{1/2}$. Calculated values for the coefficients in such an equation agreed extremely well with the experimental data, giving at least indirect evidence for the validity of the analysis.[7]

The web temperature distribution models were further used to provide input data for calculation of the thermal stresses generated in the growing web. Again, while direct comparison of the calculations and experiment is difficult, the results of the stress models were consistent with the observed growth behavior.

Although these models provided valuable guidance in the design of real systems, they are of necessity only approximations of reality. Thus a comprehensive experimental effort was required to further develop the concepts and translate them into a functioning web growth system.

3.2.3 Overview of the Output Rate Technology Development Effort

At the start of this program in April 1977, the maximum demonstrated area growth rate was 2.3 cm^2/min and the maximum demonstrated width was 2.4cm. By the end of the program, these numbers had reached 27 cm^2/min and 4.7 cm respectively. In this section we will outline the steps taken to achieve these results in a loosely historical manner.

Although it was recognized at the start of the program that an elongated crucible and susceptor (as shown in Figure 5) would be the preferred configuration for the production of wide web crystals, a circular configuration was selected for the initial work on this program because of its simplicity and because it had in the past produced web on a regular basis, although not at widths consistent with the goals of this program. It was assumed that the knowledge and experience gained with this configuration would be applicable to an elongated configuration and this assumption was subsequently proved correct. When a second web growth facility, the J furnace, was constructed, it was equipped with an elongated susceptor that had a rectangular crucible configuration. This design incorporated those features which our experience with the circular geometry indicated were necessary for stable web growth and which modeling predicted would generate the desired thermal geometry for wide web growth. A substantial increment in web width to 3.5 cm was quickly achieved with the elongated geometry. Having established that this design functioned as expected, the round susceptor configuration in the first growth facility was replaced with an elongated susceptor of the same design, and this facility is now designated as the RE furnace. This configuration, including the lid and slot designs, had an experimentally verified design width capability, in terms of melt temperature profiles, in the range of 5 to 6 cm. However, as wider crystals were grown, the effects of thermal stress became evident as crystal deformation and degeneration of web quality at widths below that predicted on the basis of the melt profiles. This directed our attention to the temperature distribution in the web crystal just above the melt, i.e., the region of the lid and top shields.

ORIGINAL PAGE
BLACK AND WHITE PHOTOGRAPH

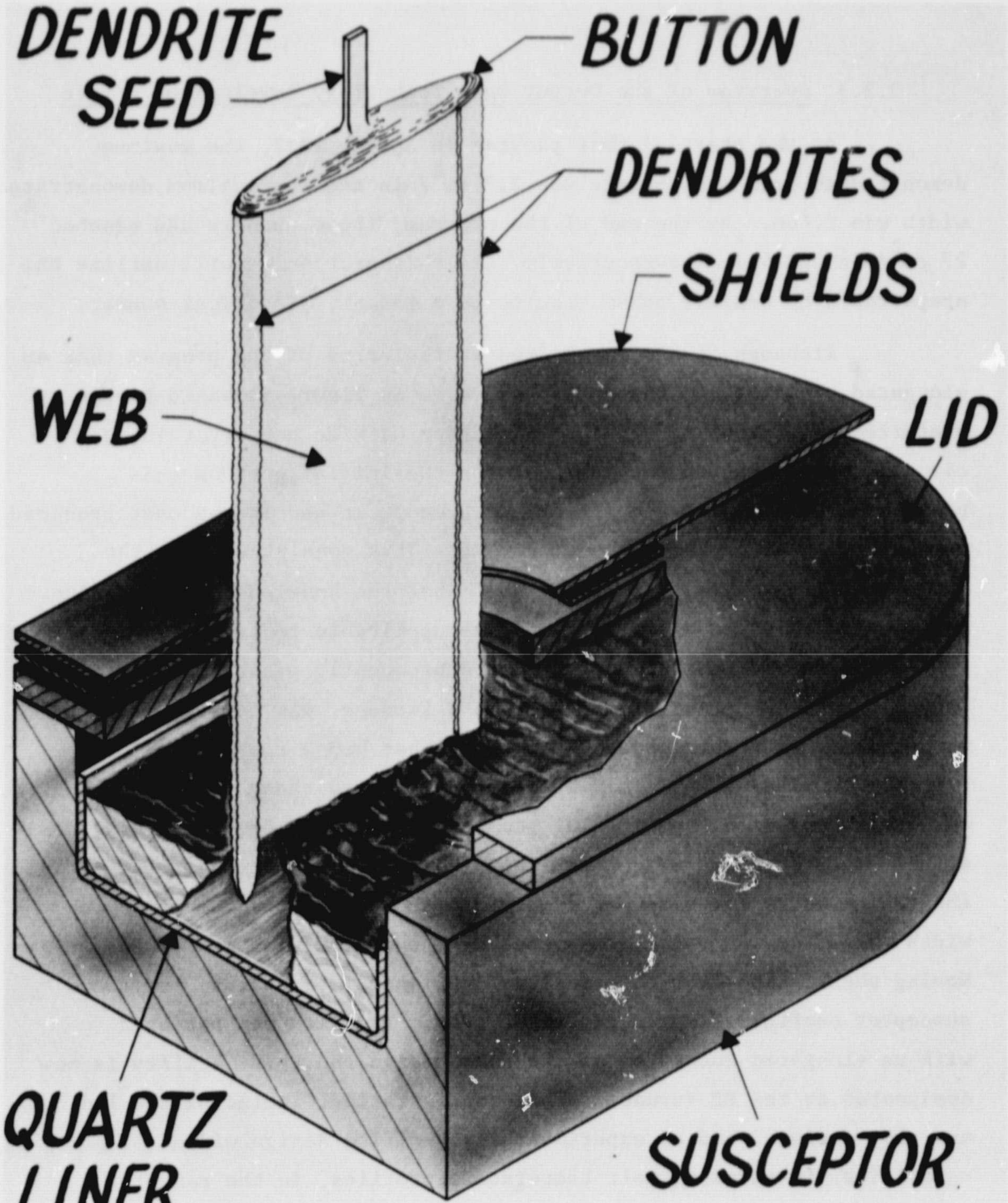

Figure 5   Web Growth Configuration with the Elongated Susceptor

Experimental results and thermal modeling were again combined to produce a lid and top shield configuration which substantially reduced stress levels in the web, leading to a further major increment in web width to 4.7 cm, with the crystal quality maintained to nearly the maximum width values. This progression in web width is illustrated in Figure 6.

Growth velocity is basically determined by the rate at which the heat of fusion can be dissipated from the growth front. For web growth, the two heat loss mechanisms are available: conduction into the supercooled melt and radiation from the web. The first is determined by the amount of melt undercooling and the second by the lid slot and top shield configuration as well as the melt level.[1-3] The configurations affecting radiative losses must also be compatible with minimizing stress in the web crystal so that designs aimed at improving one must be tested as to the effect on the other. Experiments aimed at increasing growth velocity were carried out in parallel with the experiments directed toward width enhancement.

In order to maintain an optimum melt level, one which maximizes web width and growth velocity while minimizing stress, melt replenishment is required. To this end, the RE facility has been largely dedicated, for more than a year, to developing and testing the various components and procedures necessary for melt replenishment, culminating in a functioning semi-automated web growth facility. This work is described in Section 3.3 and 3.4 in this report. During the later part of the program, the J-furnace was equipped with a manually controlled version of the replenishment system so that further work on output rate could be carried out under conditions compatible with melt replenishment.

For long-term automated web growth, it is desirable to grow web crystals at a controlled width. Thus, some recent work has been aimed at width control techniques. Although feasibility has been demonstrated, further work is needed in this area.

ORIGINAL PAGE
BLACK AND WHITE PHOTOGRAPH

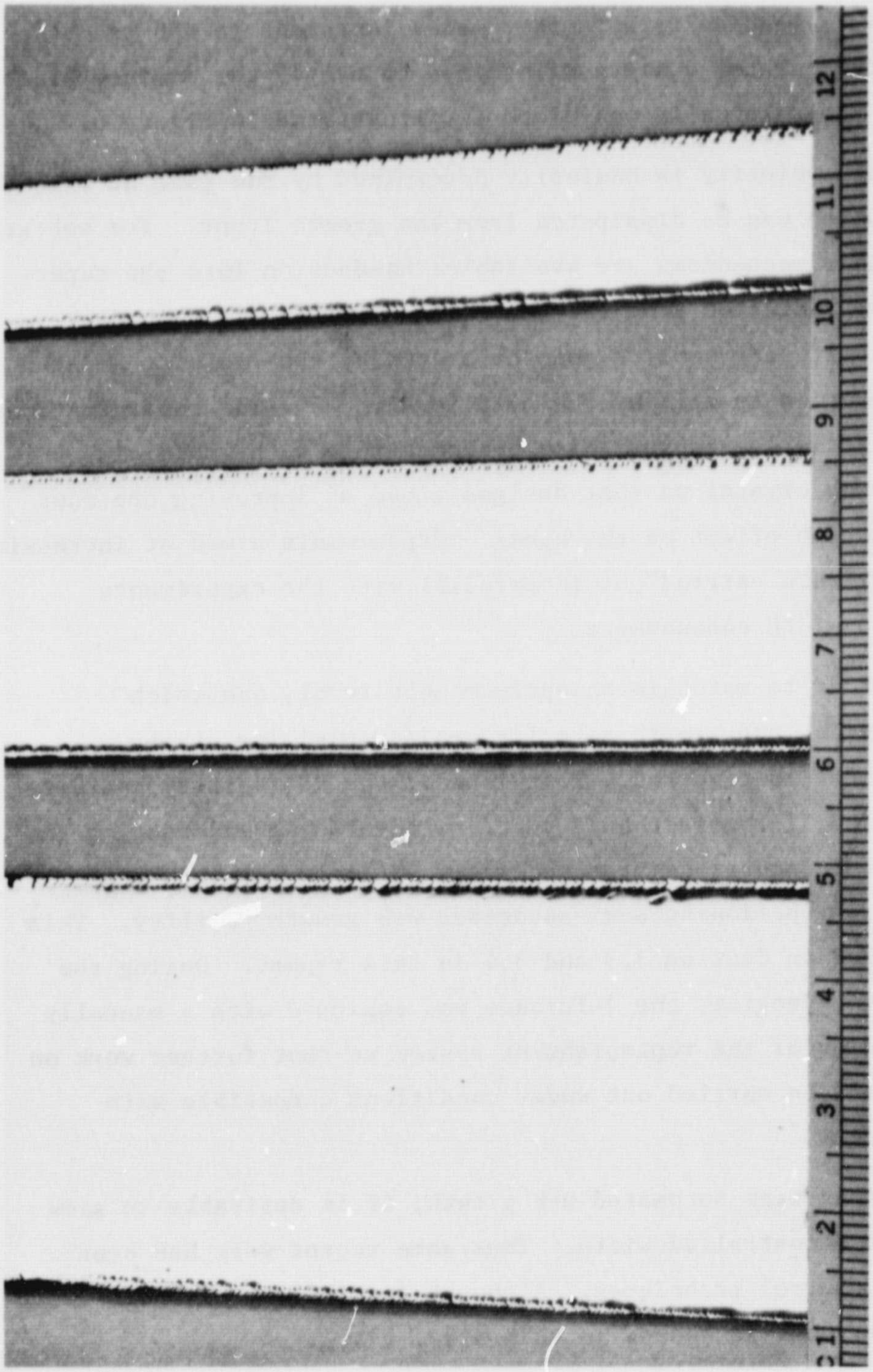

Figure 6 A Progression in Web Width with Advancing Growth Technology

In the following sections, the methods and experiments used to achieve the full order of magnitude increase in output rate will be discussed in more detail.

3.2.4 Web Width

Two thermal parameters affect the maximum width to which a high quality web crystal can be grown: the temperature profile in the melt and stress induced deformation. The former is determined by the susceptor configuration and the lid slot geometry, the latter by the temperature distribution in the web in the region above the growth interface.

The preferred melt surface temperature profile is essentially flat over a dimension comparable to the desired web width and rises toward the crucible walls, as shown schematically in Figure 7. Having fixed the susceptor configuration, the profile is determined by heat losses through the lid slot, which are, in turn, determined by the two-dimensional lid slot geometry. The desired profile can be obtained by enlarging the ends of a straight slot with "dogbone" holes (see Figure 8). If thermal stress was absent, such a design would easily produce crystals of about 6cm in width. However, the need to minimize thermal stress requires that the temperature distribution in the third or vertical dimension be controlled. This can be accomplished by the vertical geometry of the lid and top shields. Thermal modeling results indicate that the most important region in terms of thermal stress lies within about 2cm of the growth interface, which is consistent with the experimental results.

The thermal environment of a growing web crystal is shown schematically in Figure 9. Two overlapping critical regions for stress generation are shown: the plastic region and the elastic region. Stress generated in the plastic region causes lattice deformation and results in residual stress in the crystal.

ORIGINAL PAGE IS
OF POOR QUALITY

Dwg. 6438A24

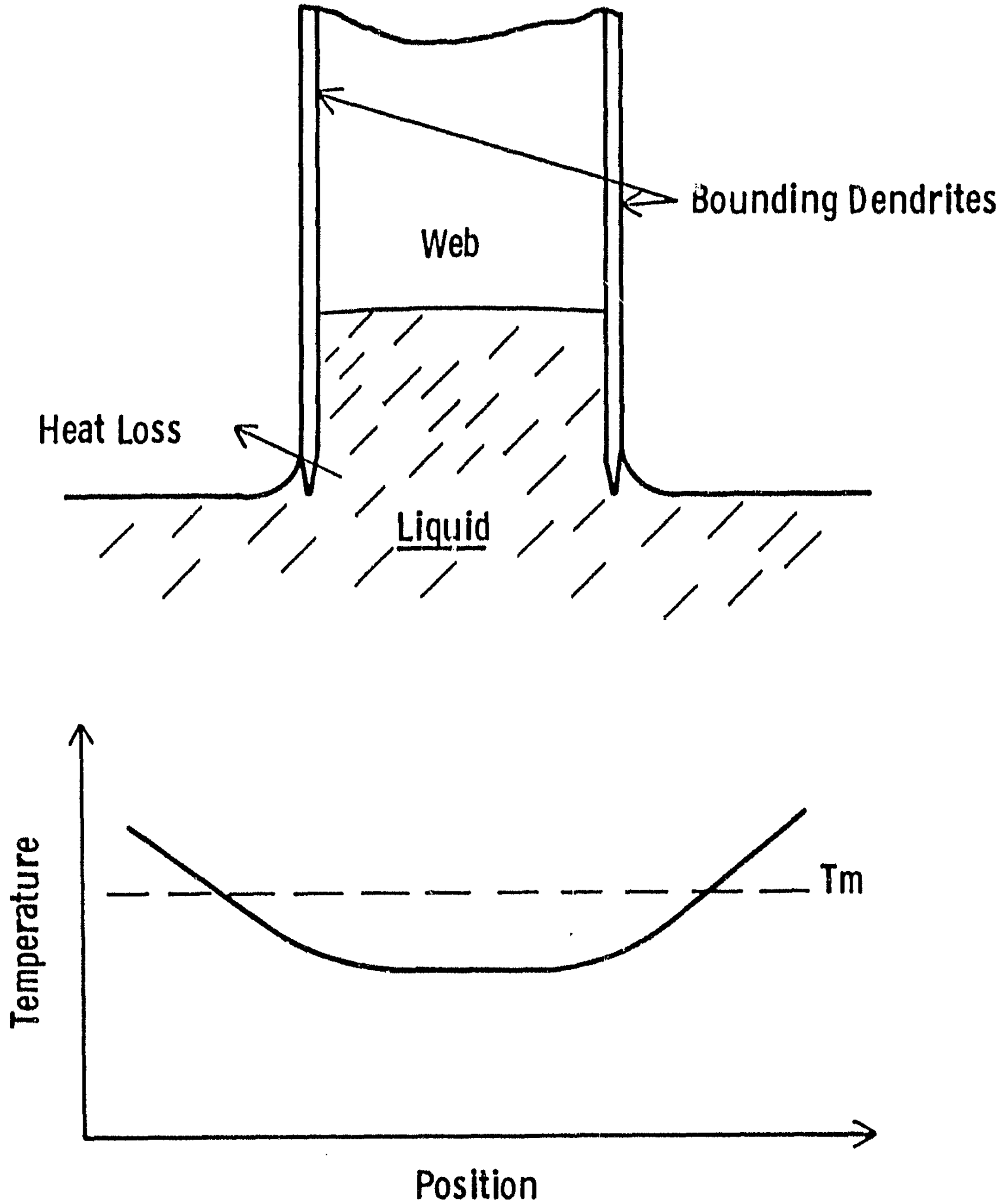

Figure 7 Schematic Illustration of a Growing Web Compared with Temperature Profile at Melt Surface.

Curve 714929-A

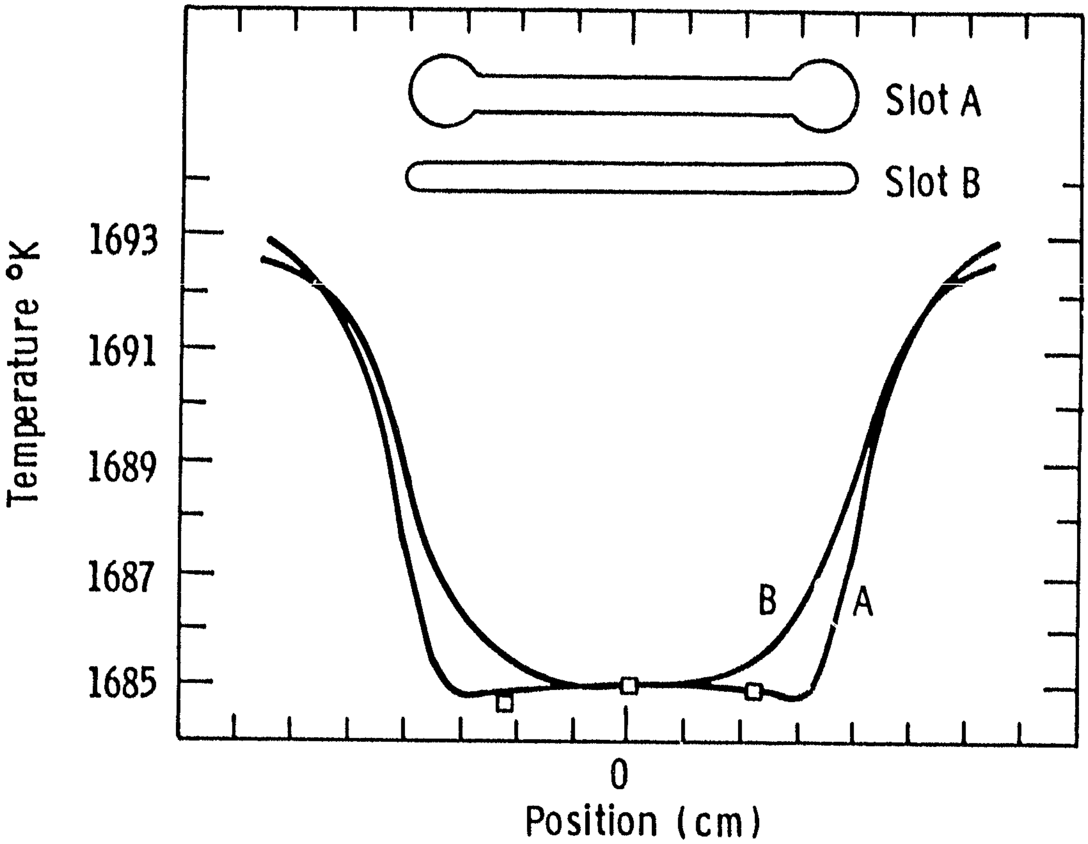

Figure 8 Lateral Melt Temperature Profiles Computed for a Long Slot Terminated by End Holes (A) and a Similar Straight Slot (B). Data Points were Determined from the Melting Temperature of a Fine Dendrite Seed.

ORIGINAL PAGE IS
OF POOR QUALITY

Dwg. 7701A17

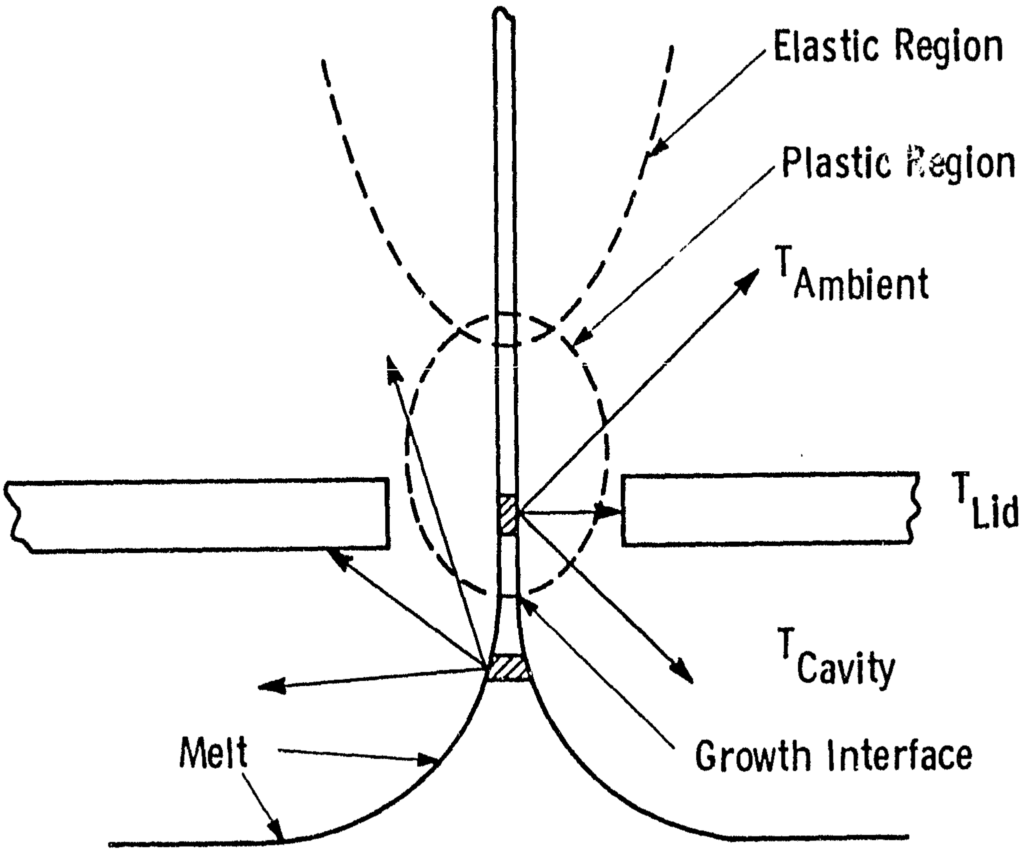

Figure 9 The Thermal Environment Around a Growing Web Crystal. Critical Regions for Stress Generation are Noted.

The magnitude of the residual stress can be quantitatively measured by splitting the crystal lengthwise, matching the halves at one end and measuring the gap between the halves as a function of distance along the length.[2] Stress generated in the plastic region can be minimized by proper design and control of the temperature distribution in the lid slot region and can be reduced to immeasurably low levels. Even without measurable residual stress, crystals can deform as a result of elastic buckling. The elastic bending causes the growth-stabilizing twin planes to outcrop at the web surface.[3] At this point the crystal quality rapidly degenerates. The temperature distribution in the elastic region is influenced not only by the lid slot, but by the number and configuration of the top shields.

It should be noted that the magnitude of the stress levels increases superlinearly with the width so that the tolerable stress level decreases as crystal width increases. For this reason, the reduction of stress has been a major effort during Phase III of this program. By means of the techniques described below, we have reduced web stress levels so that ribbons nearly 5cm wide can be grown.

Some examples of baseline lid and top shield configurations are shown in Figures 10 and 11. Figure 10 shows the RE-1 configuration which was developed for use in the early growth runs with the elongated susceptor. It proved to be a consistent producer of web crystals but maximum widths were limited by deformation to about 3.5cm. The J-181 design (Figure 11) was a considerable improvement in terms of web width and stress reduction, producing web crystals up to 4.7cm wide with slight modification in the top shield.

These two designs serve to illustrate a number of points relative to the importance of the temperature distribution in the region above the growth interface. The RE-1 configuration features a 6.3mm thick lid with a straight-sided slot. If the lid is made thicker, like the J-181 lid, and the slot is straight sided, the web is very highly stressed. However, beveling the slot in the thick lid reduces the

Dwg. 1703B17

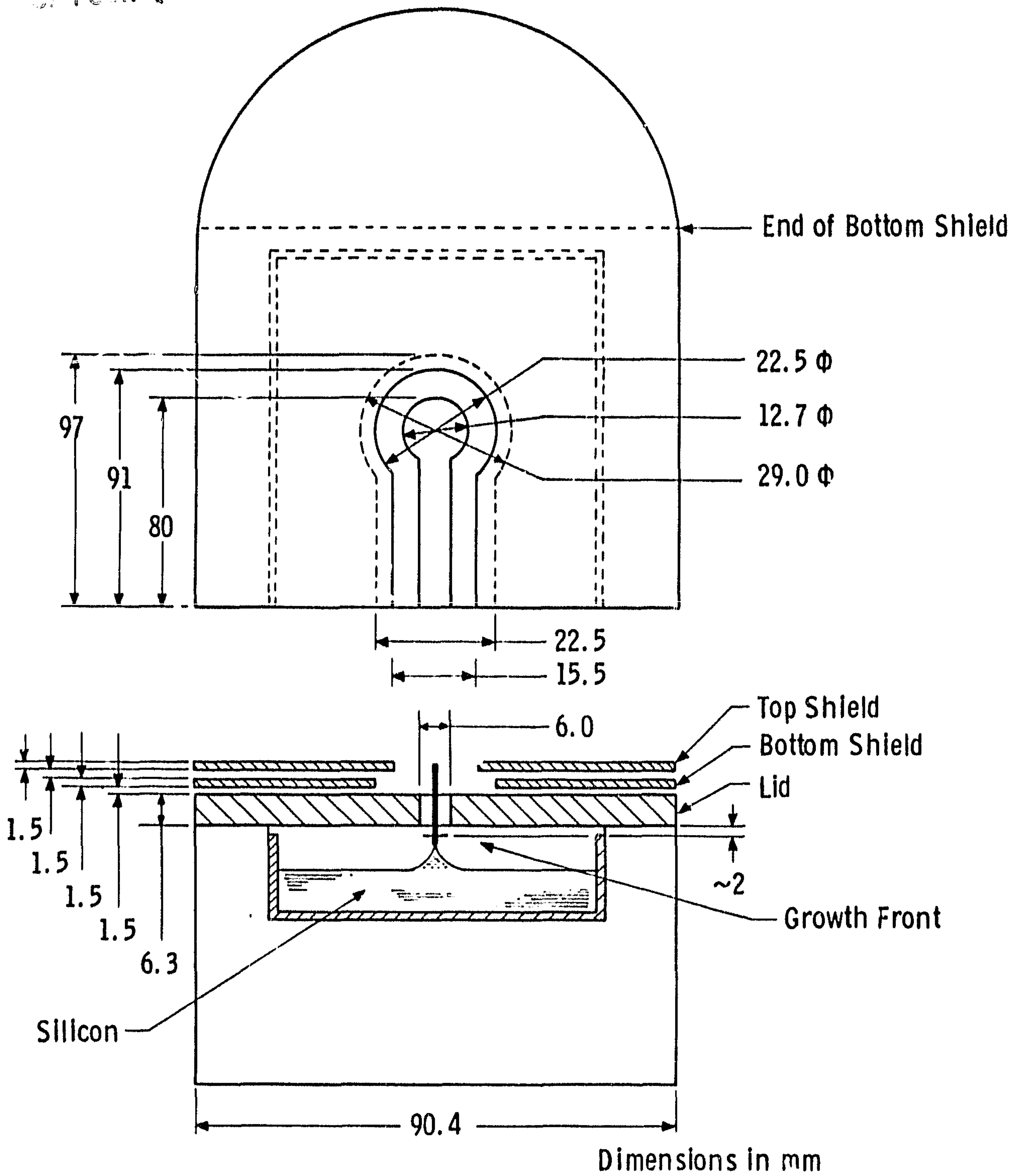

Figure 10 RE1 Growth Lid Configuration (schematic)

Dwg. 7702A61

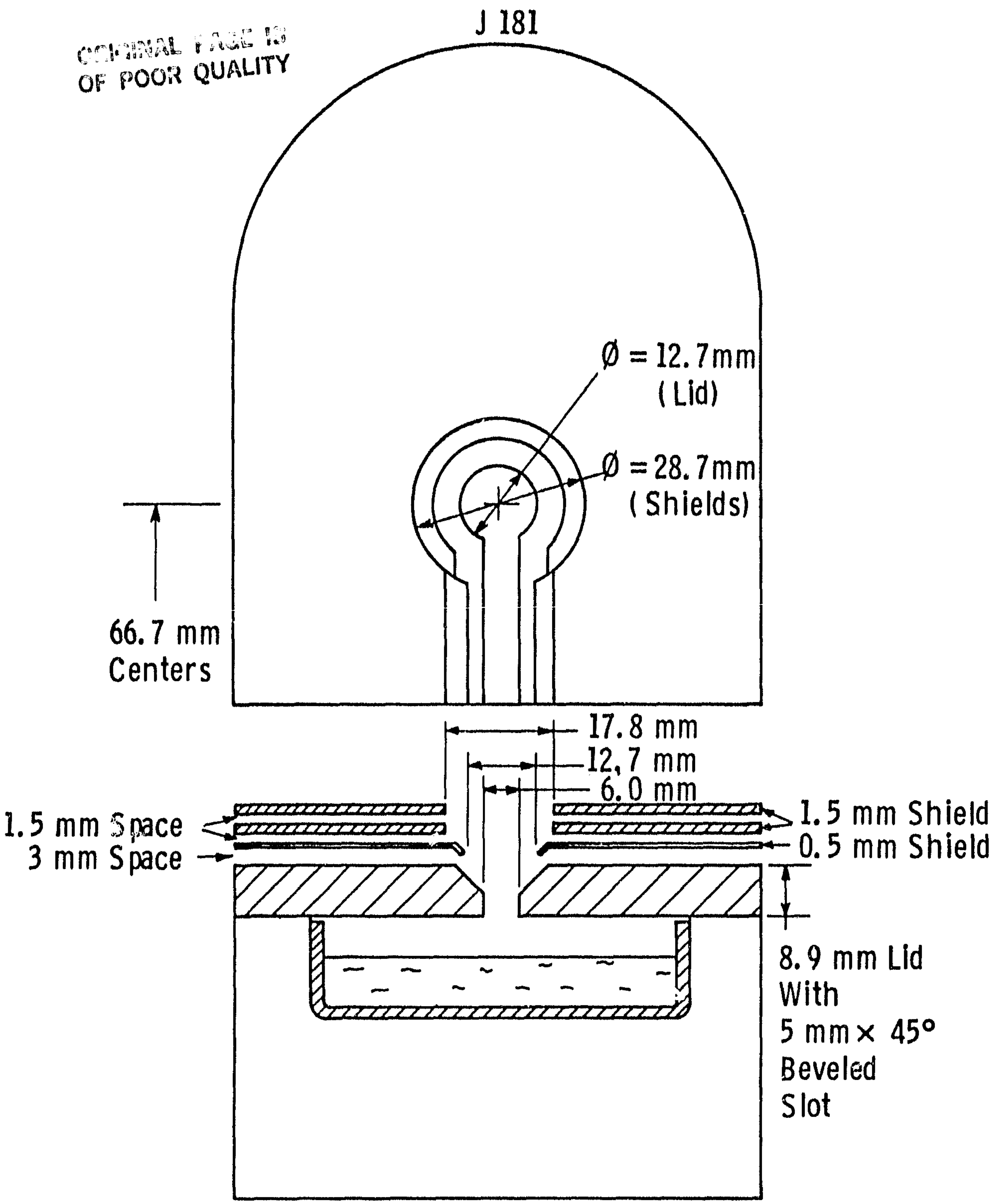

Figure 11 The J-181 Baseline Lid and Top Shield Configuration

elastic stress relative to that generated with the RE-1 lid. The thicker lid runs hotter in the slot region but with the bevel the thickness of the hot lid close to the web is less. The widest web crystals have been grown with an additional thin top shield added to the baseline J-181 configuration. Further improvements in the vertical temperature profile will lead to wider web crystals.

3.2.5 Growth Velocity

The growth velocity for a web crystal is determined by the rate at which the heat of fusion can be dissipated. In the web growth process, there are two mechanisms for heat loss: conduction through the meniscus to the supercooled melt and conduction and radiation from the web. It is in fact convenient to express the growth velocity in terms of two partial velocities, V_{melt} and V_{web}, where $V_{total} = V_m + V_w$. The melt component of the velocity is determined by the degree of melt undercooling and is thus limited by the amount of undercooling which can be used without adversely affecting crystal quality. As growth velocity increases, a higher proportion of the total velocity must come from the web component. This requires development of lid and shield configurations which allow more heat to be radiated from the web, especially near the growth interface.

Several design concepts for increasing radiative heat loss, suggested by the thermal modeling results, have been tested. Two configurations which significantly increase growth velocity are a thin lid and a widely beveled slot in a thick lid. Tests with a 3mm thick lid gave an increased growth velocity, but the lid tended to be too cold in the slot region. Rapid accumulation of oxide occurred in the slot. Growth could only be maintained for short periods of time. A thick lid runs hotter, inhibiting oxide deposition, and the radiative losses can be increased by increasing the amount of bevel along the slot. However, the effect is minimal unless the hot bevel is shielded from the web. This can be accomplished by bending a thin moly shield to match the slot bevel. Unfortunately, oxide tends to collect along the edge of the thin shield, limiting available growth time. Except for the oxide problem, both of these approaches show promise in terms of substantial increases in growth velocity.

Since growth velocity and web crystal thickness have an inverse relationship, velocity comparisons must be referenced to specific thicknesses. Thus velocity values have little meaning in isolation. For example, crystals have been grown at velocities up to 10 cm/min., but they were very thin (30-40 μm). Our objective is to develop configurations which permit high growth velocities with crystal thickness practical for solar cell fabrication. Configurations tested show great promise in satisfying this goal. Concepts have been devised to eliminate the problem of oxide deposition, and these will be tested during further development of higher throughput technology.

3.2.6 Area Throughput

While crystal width and high growth velocity have importance in and of themselves, the true objective of these efforts is to maximize the area throughput. Thus width and growth velocity are not isolated parameters in the sense that both must be enhanced in a single growth configuration in order to achieve higher area throughput rates. Thus for example, a higher growth velocity must be achieved without increasing stress to a level which impacts width. Maximizing throughput involves some degree of compromise in terms of growth configurations which produce maximum width or maximum growth velocity separately. The order of magnitude increase in area throughput to 27 cm^2/min achieved during the course of this program shows that this can be done.

3.3 Melt Replenishment

3.3.1 Concept

As was mentioned in Section 3.1 on the economic requirements of web development, it is necessary to have long (more than 1 day) crystal growth periods in order to meet the 1986 JPL cost objective for solar cells. As dendritic web development progressed, it became evident that the melt height relative to the lid has an indirect impact on material throughput. Since crystals become thinner at a given pull rate and stresses increase as the melt level decreases, maintaining a high melt level is necessary to keep web quality and throughput at the highest possible levels.

3.3.2 Development

In order to meet the goals of long growth runs and constant melt level, we chose to replenish the melt by adding silicon pellets as the web crystals are grown. This form was selected for the following advantages:

1) Pellets cause onlv slight temperature perturbations when fed into the melt.

2) Additional system power requirements are small.

3) Pellets are readily metered with simple, inexpensive equipment.

4) The approach lends itself to subsequent automation.

5) Polycrystalline silicon produced by the LSA Task 1 is very likely to be in pellet form.

Initial experiments used a manually actuated pellet feed system which can be seen in Figures 12 and 13. The functional parts of the feed system are a chamber which holds a supply of silicon pellets, a manipulator which allows the operator to drop pellets into the feed tube, and a feed tube. From the feed tube the pellets drop directly into the melt. The crucible was divided into two compartments, as seen in Figure 14, to prevent the solid pellet from migrating toward the growing crystal before it has completely melted. With this setup, several periods of simultaneous web growth and pellet feeding of up to an hour were achieved.

In the next phase of melt-replenishment development, the activity was transferred to the W furnace, which has a round susceptor. One of the reasons for this transfer was the greater sensitivity of the smaller system to thermal perturbations so that possible feed-related problems would be more readily apparent, and thus steps could be taken to solve the problems sooner. Another reason for the transfer was to permit the RE furnace to be used in throughput development. In these runs a mechanized feeder, as seen in Figure 15, replaced the manually operated feeder, making feed experiments much easier for the furnace operator.

ORIGINAL PAGE
BLACK AND WHITE PHOTOGRAPH

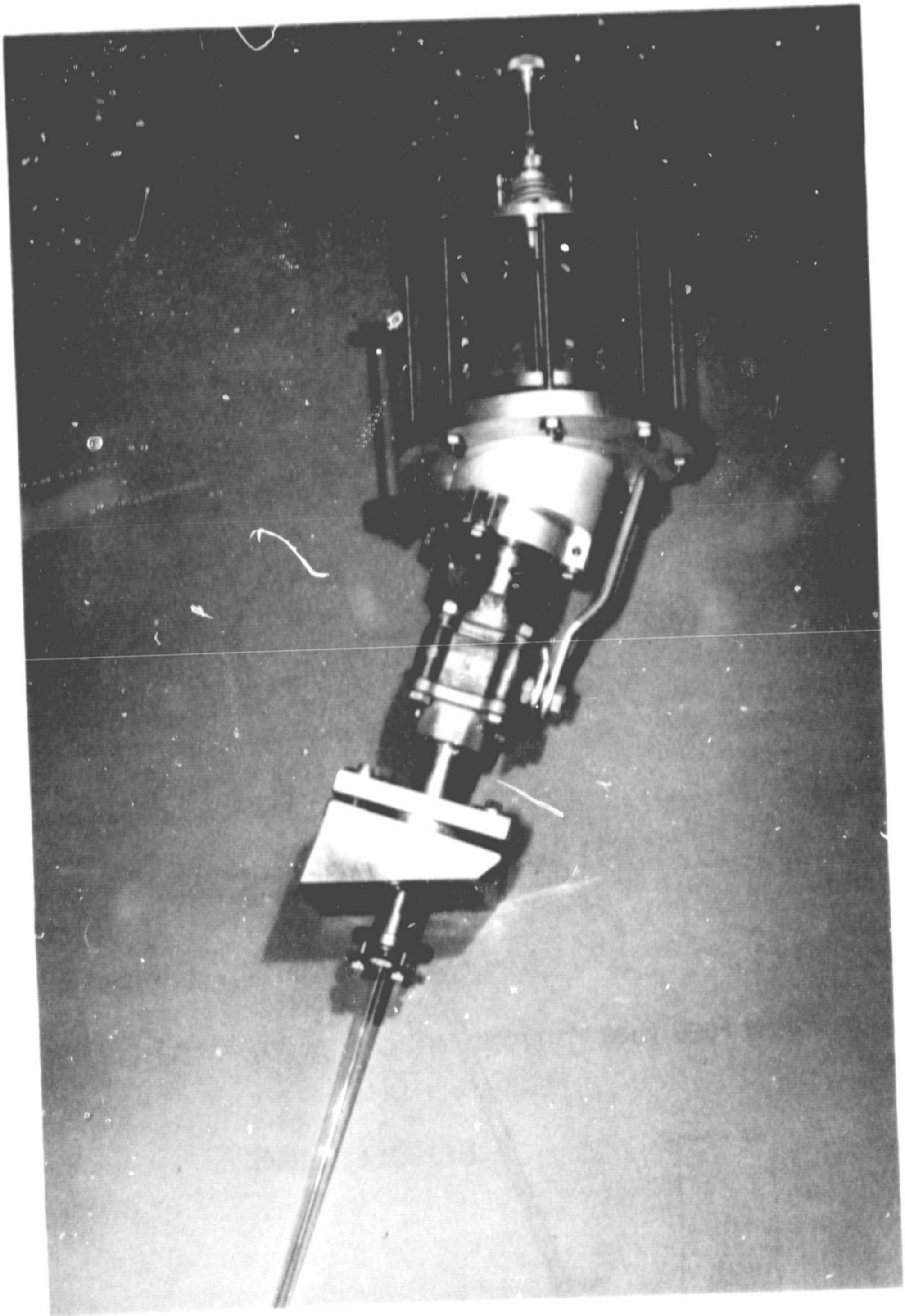

Figure 12 Photograph of manually actuated melt replenishment system.

Dwg.7684A15

Figure 13 Schematic of manually actuated melt-replenishment system

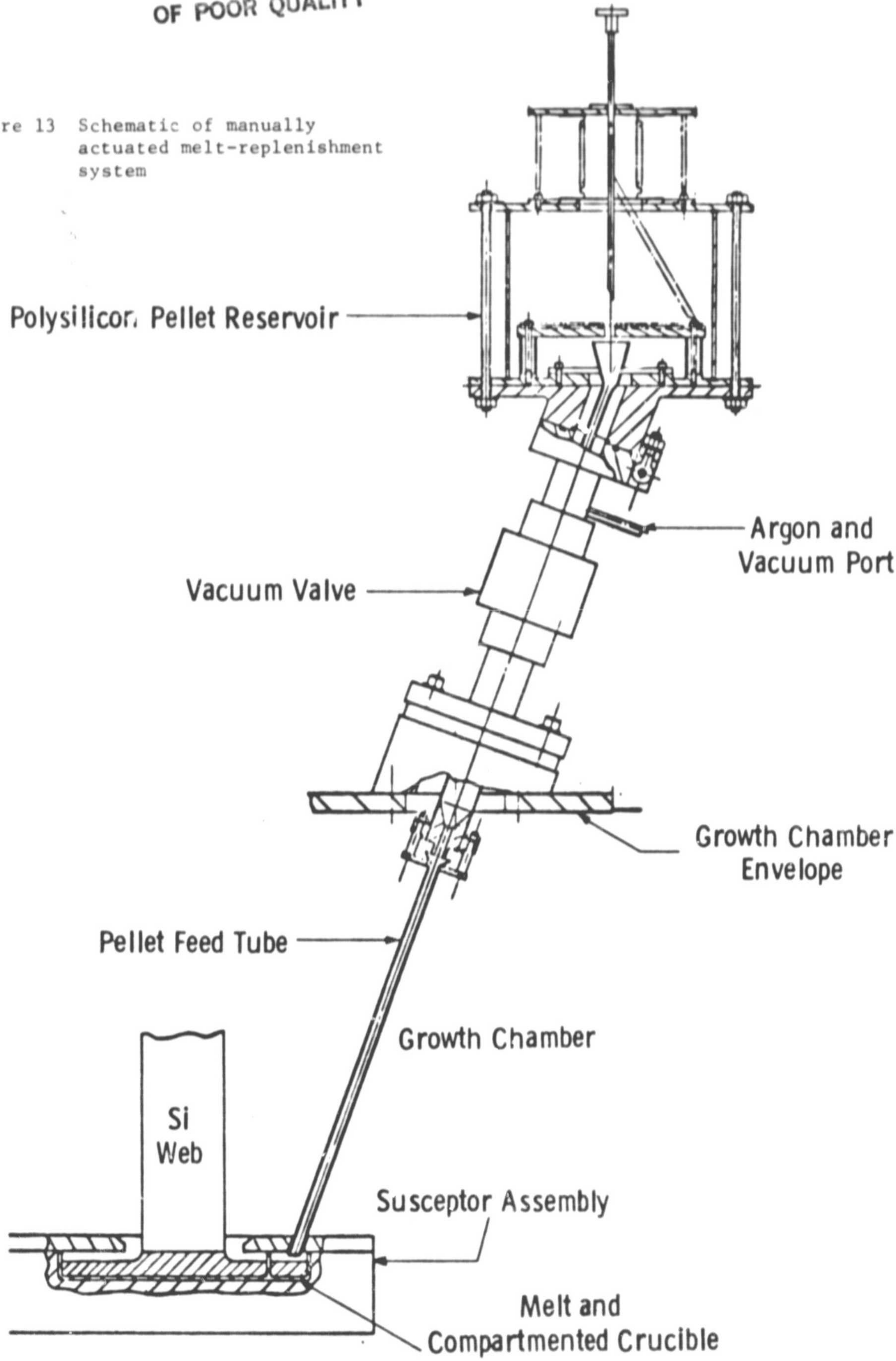

Dwg. 7695A07

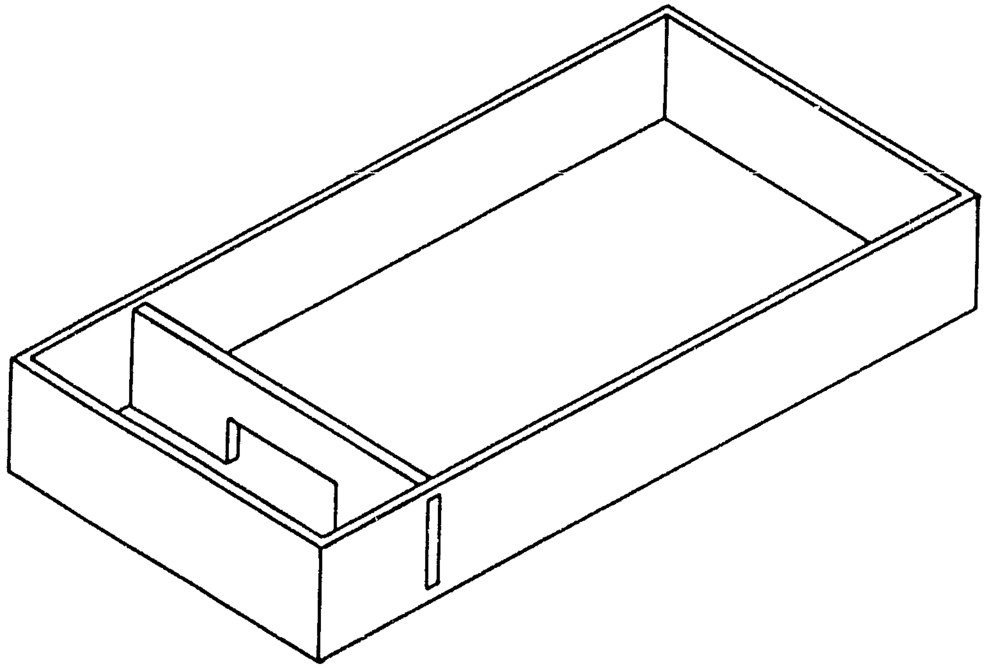

Figure 14 Compartmented crucible used in melt replenishment.

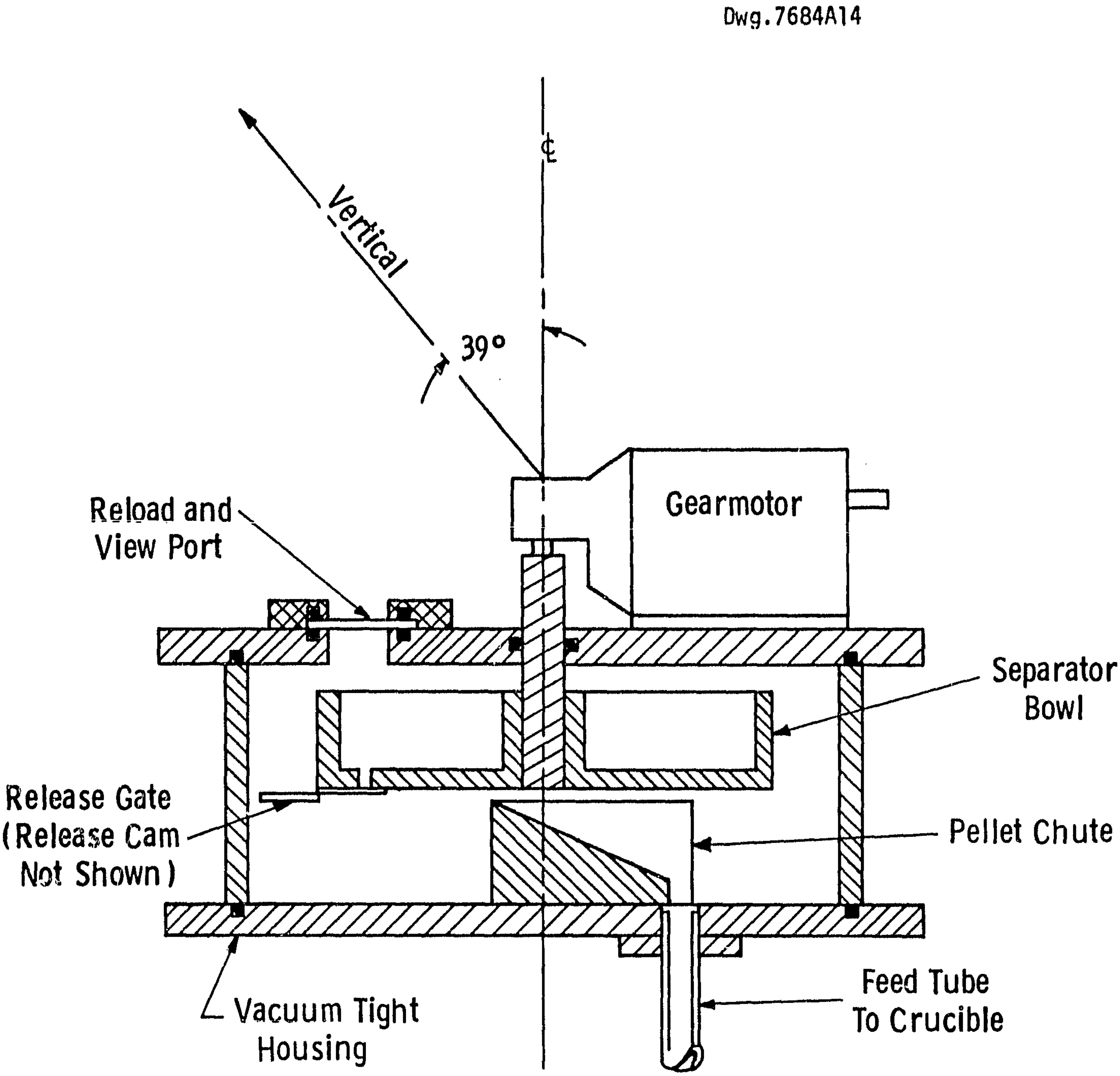

Figure 15 Mechanically actuated pellet reservoir and feed system.

The heart of the feed system is a rotating dish called a separator. The dish is inclined at a nominal 39° angle so that pellets would gravitate to the lower side. Holes in the bottom of the plate are just large enough to hold one pellet, and, as the dish turns, pellets drop into the holes and are separated from the mass of pellets in the dish. Spring-loaded gates which cover the bottom of the hole are actuated by a fixed cam, dropping the pellets through a funnel or chute into the feed tube.

In the development of melt replenishment in the W furnace, several problems were identified and solved. The first problem encountered was with feeding: even at low rates, ice fronts of solidifying silicon would occur due to the cooling effect of solid particles entering the melt near the supercooled web growth region. This problem was considerably lessened by the addition of shielding to the back of the crucible, where the pellets were being added. Feed periods of up to 35 minutes were then obtained. Longer runs were prevented by the occurrence of a second problem-that of floating ice.

The floating ice had two suspected sources, which are noted in Figure 16. The first, "oxide blow over," was caused by the pellets scraping oxide loose from the feed tube, the shields, or the lid, and gas flow under the lid carrying the loose particles over the barrier into the supercooled melt where they resulted in ice. Through the use of aspirators and changes in gas flow, this problem was alleviated and feed periods of up to an hour were achieved. The second cause, "dendrite nucleation," occurred when the barrier became cold enough to allow silicon to freeze along its edge. Thermal fluctuations from convection currents in the melt could cause the silicon dendrites to be melted free from the barrier and to be carried into the cooler area of the melt where they terminate crystal growth. This problem is due to proximity of the barrier to the growth region, and in the round susceptor little can be done to alleviate it. Because the feed chamber is farther from the colder growth region in the elongated susceptor, melting of pellets can be accomplished without adverse effect on web crystal growth. Thus "dendrite nucleation" would not be a problem in the other furnaces.

Dwg.7730A91

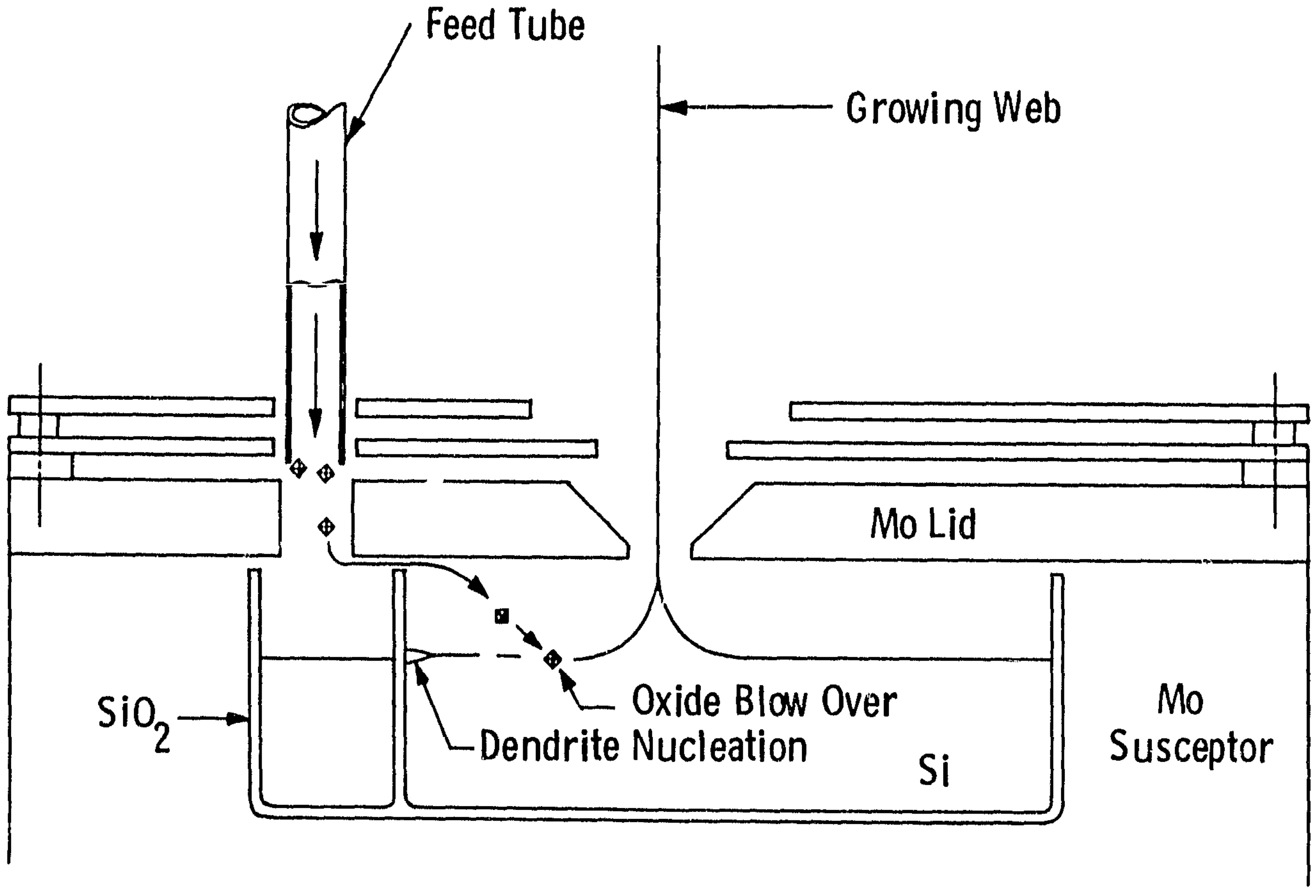

Figure 16 Mechanisms for the formation of free-floating silicon "ice" during melt replenishment.

At this point, development was returned to the elongated susceptor in the RE furnace. Based on experience gained from the W furnace, the mechanized feeder was moved to the longer susceptor, aspirators were added to the lid, and end shields were placed on the susceptor. As development continued, it was found that the aspirators were not necessary: by making a higher barrier which fit into a slot in the lid, oxide or particle blow over was prevented.

Through thermal probing and observations of crystal growth with various feed rates, it became clear that the thermal profile suitable for melting pellets at low feed rates would be inadequate for higher rates. To remove this problem moveable end shields[5] were made. By raising or lowering these shields the effect of a change in pellet feed rate can be largely balanced.

In order to use what had already been learned about melt replenishment in width development and to have additional facilities for further development of replenishment, a feeder was added to the J furnace. The design was similar to that on the RE furnace: changes were made on some seals and the pellet chute, and teflon replaced steel in the separator bowl to prevent the possibility of the silicon pellets chipping the steel and thus introducing impurities.

Both feeders have a limited pellet capacity and as the feed rates and run lengths increased, it became necessary to refill the feeders. To do this a batch feeder was constructed. A closeup view of the batch feeder installed on the J furnace is shown in Figure 17. As can be seen, the batch feeder is essentially a glass tube enclosing a plunger mechanism. Access to the batch feeder is through a port which permits additional pellets to be placed in the reservoir as required. This component can be isolated to prevent back diffusion of air while the reloading is taking place. For test purposes this isolation is accomplished with a simple mechanical clamp.

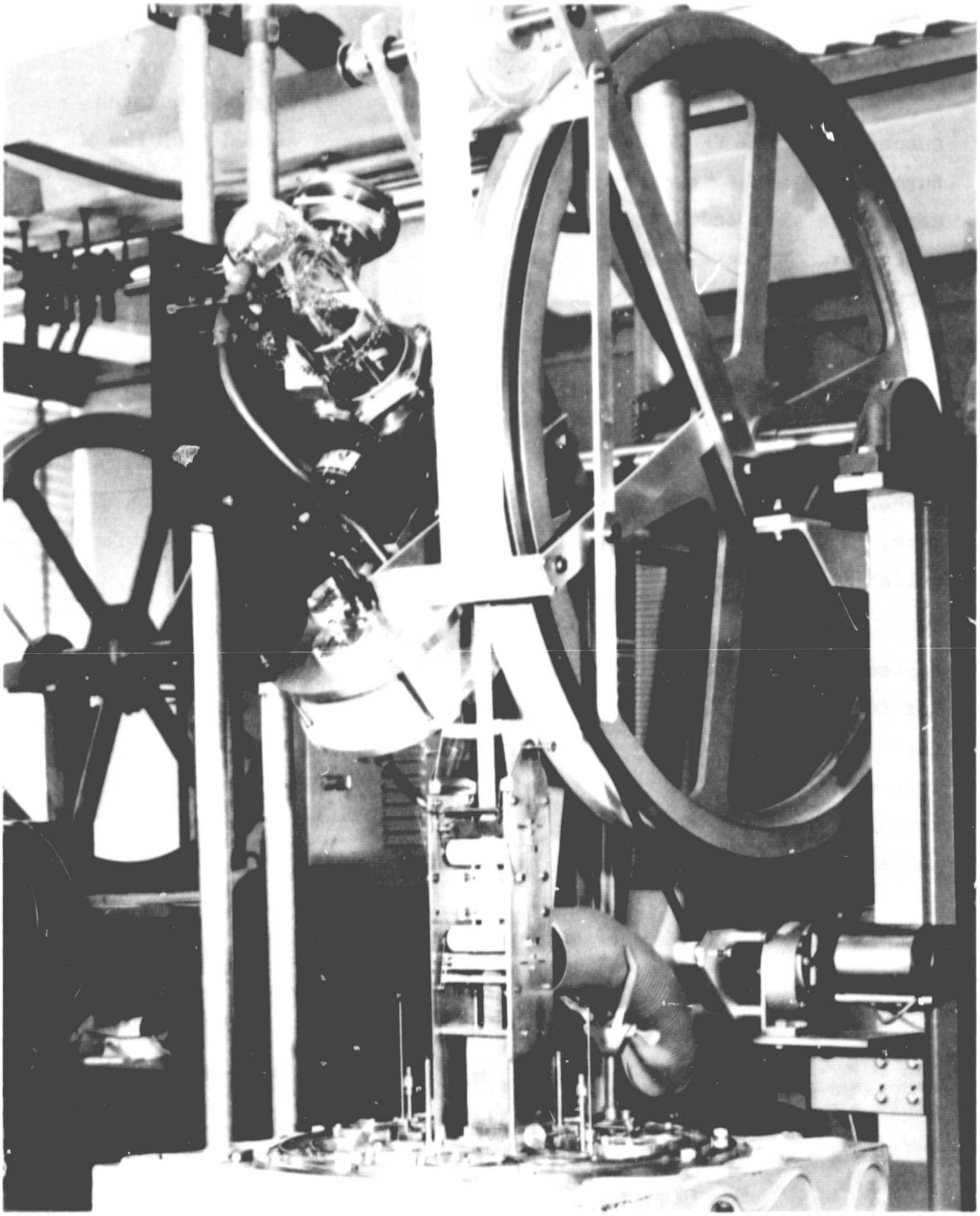

Figure 17 Batch Pellet Feeder Shown Installed on Web Growth Furnace.

As work progressed, the length of the melt-replenished (or "feed") runs increased. In the early runs about 2 hours was the longest feed period; this was increased to five hours of ice-free feeding on several occasions. Individual crystals were grown without problems for as long as 3 hours, 15 min with feeding. In order to determine whether there would be any special problems encountered in longer runs, two runs were made, one with 13 hours of feeding and one with 17 hours.

In the 13-hour run the lid and shield arrangement resulted in some ice from oxide which spalled from the shield edges. In the next run wider shield slots were used. This was insufficient to prevent some ice formation which prematurely ended some crystals grown in the 17-hour run. As a result, although the melt was fed continuously, crystal growth was not continuous. However, crystals were growing nearly 13 hours of the 17 hours of run time. An important observation was that solar cell performance was excellent for all material grown in the run.[1] Sample cells were made on six separate crystals. The results are listed below:

Crystal	Uncoated Efficiency (%)	AR-Coated Efficiency (%)
1	9.70	13.9
2	9.43	13.5
3	9.09	13.0
4	9.30	13.3
5	9.72	13.9
6	9.00	12.9

3.3.3 Summary

In the course of this contract melt replenishment has progressed from a concept to an experimentally proven procedure. Feed rates which correspond to the rates of crystal removal from the melt are presently standard, and feed runs of 13 and 17 hours in length have been made. Adding further encouragement, the solar cell efficiencies from crystals grown in the 17-hour feed run were excellent. No adverse effect from the replenishment was evident.

The next step in melt replenishment should be to increase the length of the runs from the present maximum of 17 hours to a length of 65 hours for a demonstration of technology readiness.

3.4 Semi-Automated Growth

3.4.1 System Concept

Semi-automated web growth is achieved by automatic control of the silicon melt level. Very little operator action is required since growth is essentially in steady state if melt level change is limited to a few tenths of a millimeter. In addition to the greatly reduced operator requirements, semi-automatic growth has the very important added advantage of maintaining optimum growth conditions.

The semi-automatic growth system[1] consists of three subsystems:

1) The melt replenishment system which includes a motor-driven pellet feeder, a pellet feed route for delivering pellets to the melt, and the susceptor, crucible, melt and thermal shield assembly as modified for melt replenishment. This system is shown schematically in Figure 18.

2) The melt level sensing system which includes a two-milliwatt helium-neon laser, a beam route through the growth chamber, a bandpass filter, a lens for focussing the beam as it is reflected from the melt, and a solid state position detector, Figure 19.

3) The circuit which closes the loop with the melt-replenishment system and the melt level sensing system. This circuit includes a sum and difference amplifier which accepts the solid state detector output, a sub-circuit which conditions the signal, a meter relay, and a sub-circuit to provide selectable two-speed control for the pellet feed motor.

Dwg. 7709A99

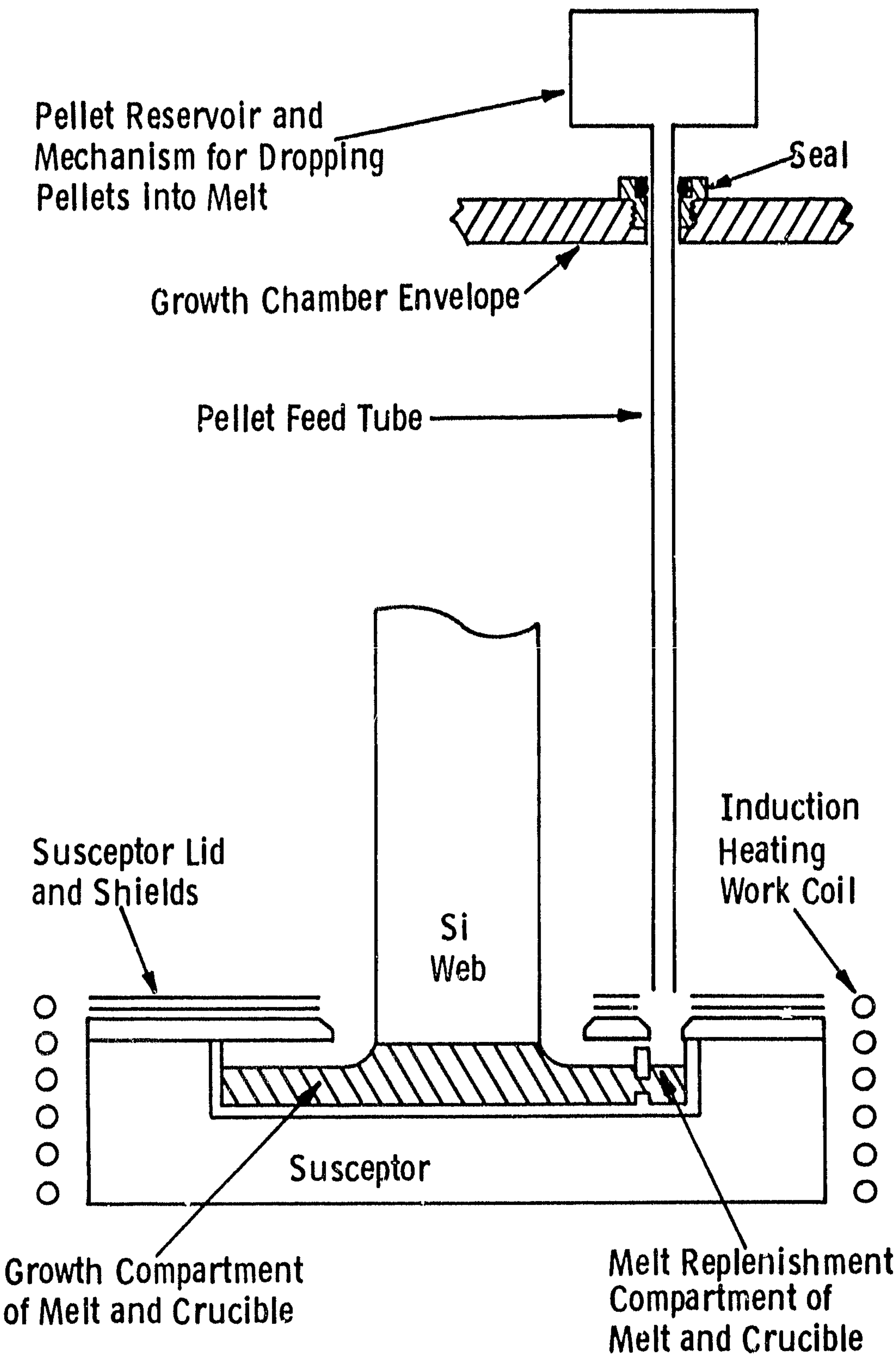

Figure 18 Simplified sketch of melt replenishment system

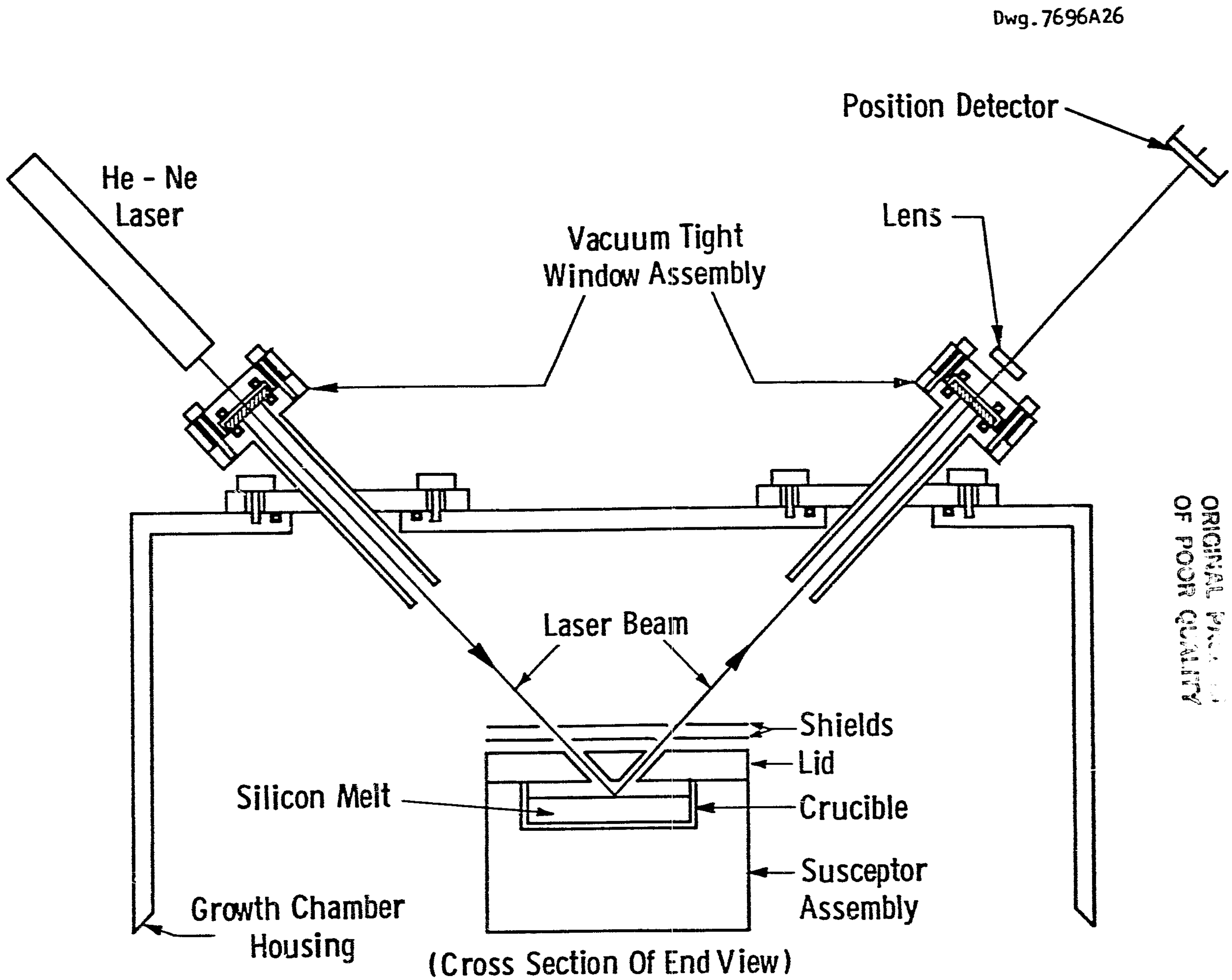

Figure 19 Schematic of melt-level sensor

The semi-automatic growth system utilizing the above subsystems, as shown schematically in Figure 20, has the capability of maintaining the silicon melt level to an accuracy of approximately 0.1 millimeter during web growth. By comparison, manual control of melt replenishment, which was used prior to the addition of the control loop, requires frequent operator adjustment in order to maintain an approximate melt level. The approximately constant melt level obtained manually will permit long periods of growth, but not at optimum conditions, and requires continual operator attention. With automatic control of the melt replenishment, the melt level can be maintained at an optimum growth level and little operator action is required after growth has been established. Subsequently, this semi-automatic mode of growth can be upgraded to fully automatic growth by addition of a web width-control loop as discussed in Section 3.1.

3.4.2 Closed-Loop Growth

In the development of a closed-loop melt-replenishment system, the first step was the evaluation of the sensitivity of the melt level sensing system. Figure 21 is a reproduction of the tracing on the strip chart recorder of the melt level sensor during web crystal growth. Prior to the start of crystal growth the trace is level, indicating no change in liquid level. After growth is initiated the trace is deflected, indicating a lowering of the melt level. In this example a total of 26 grams of silicon were removed by the crystal, making a 13 mV output change. A 1mm change in melt level corresponds to a change of 20 grams of silicon; this is equivalent to a 10 mV reading from the detector, a readily detectable change.

As the ability to replenish the melt at higher rates improved, the furnace operator was able to detect changes in the melt level from the detector output and to make feed rate changes to compensate. Frequently, the melt was controlled within 2mV or 0.2 mm with no great difficulty. However, one of the objectives of this program is to reduce the number of operator-dependent functions, and adding the chore of monitoring the melt level would be a step in the wrong direction.

Dwg. 7725A80

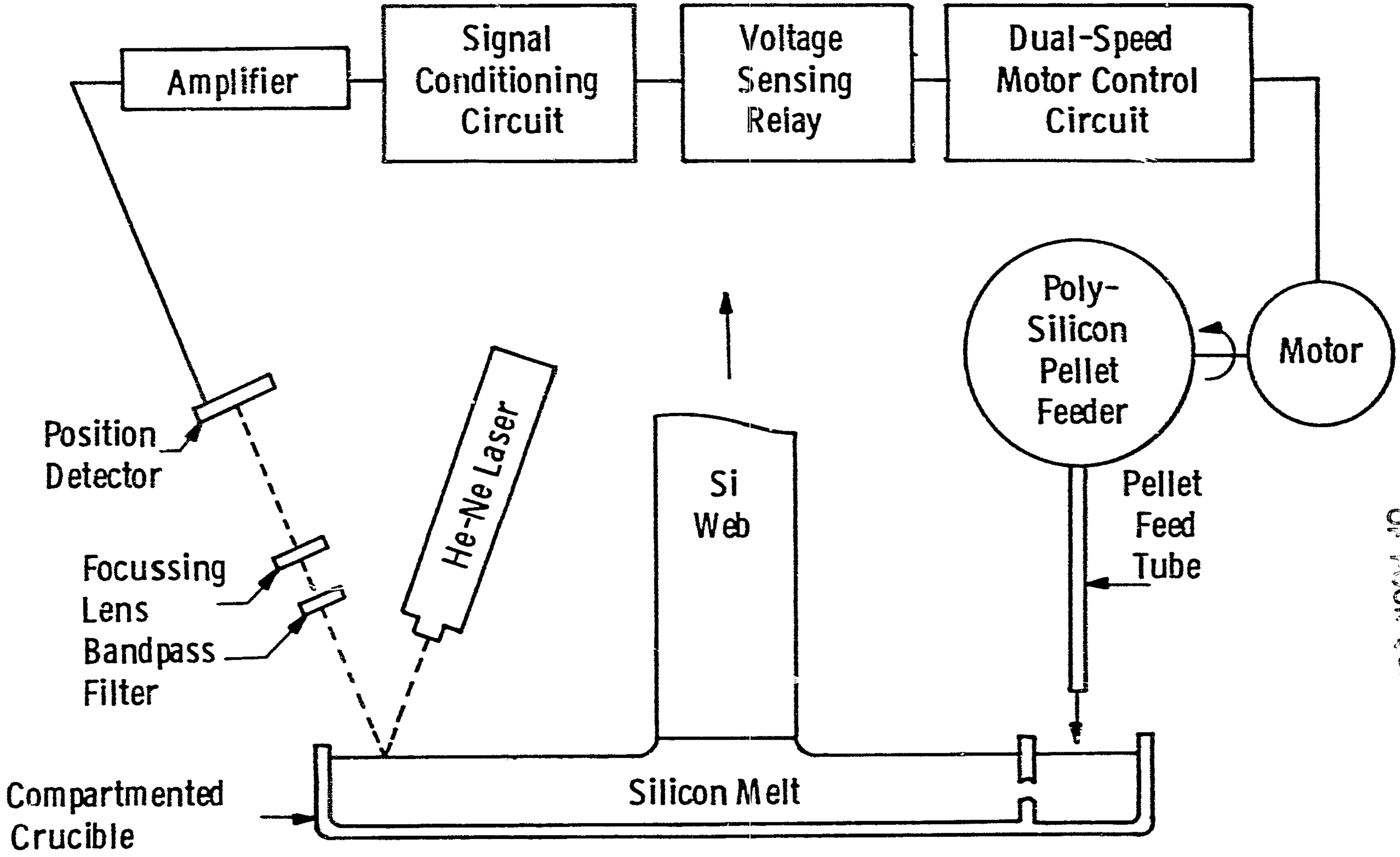

Figure 20 Block diagram of closed-loop circuit for control of melt level.

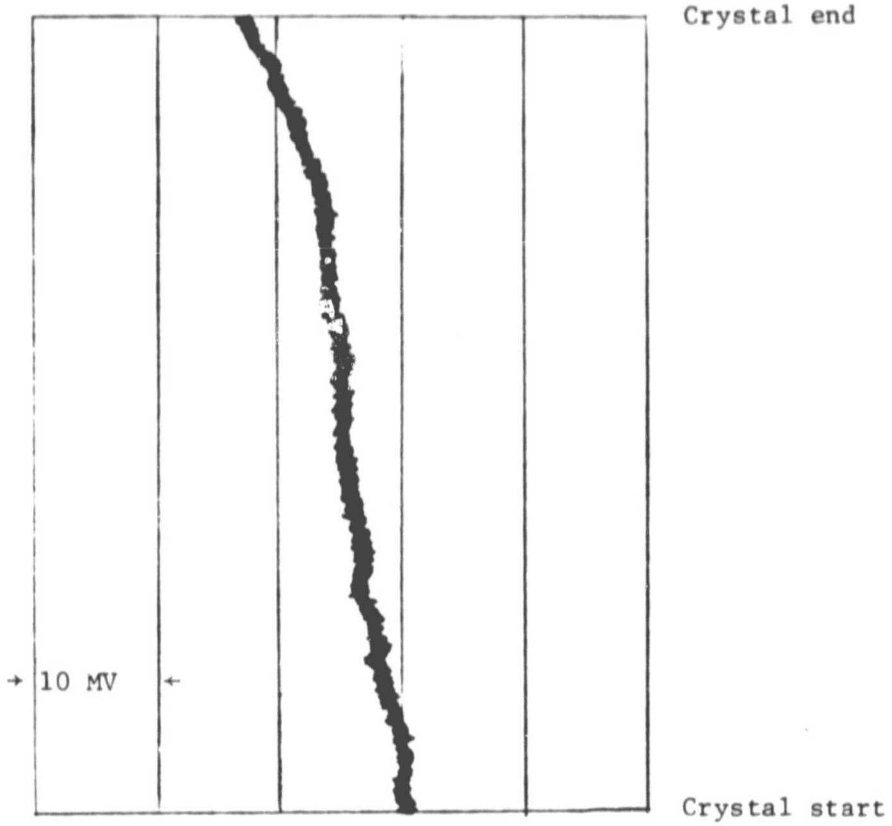

Figure 21 Example output of melt level position detector, taken without melt replenishment.

Since the melt level sensor worked well and had the desired sensitivity and since the feed rates were sufficient for the present rates of crystal growth, a controller was designed, constructed, and installed. The principle of operation is as follows: two independent feed rates are selected, one faster than the anticipated rate of silicon consumption by web growth and one slower. When the output signal of the melt level sensing system indicates that the level is above a predetermined set point, the controller switches to the slower feed rate. If the melt level falls during growth, the controller switches to the faster rate. The oscillation between the two feed rates maintains the melt at the desired level.

The results of the runs made with the closed-loop system have shown that the melt level is easily controlled within a few tenths of a millimeter, well within the range required for long-term stable web growth. The control system has been used in runs for up to eight hours. Figure 22 shows some of the level detector output from the eight-hour run.[7] (The largest perturbations of the melt level occur when growth is interrupted. The deflection, caused by a shock wave, has a negligible effect on the feed rate because it lasts for just 2 to 3 seconds.) During crystal growth the melt level remains quite stable and is easily controlled within a tenth of a millimeter.

These results demonstrate the successful operation of the closed-loop melt-replenishment system.

3.4.3 Summary

A system for semi-automatic growth of silicon web has been built and productively operated. The contract goal of an eight-hour semi-automated growth run has been demonstrated. The system meets all functional technical requirements as identified before start of design. However, some redesign is desirable for the purpose of reducing the cost of the system.

Successful operation of the semi-automatic growth system is essentially the prerequisite for fully automatic growth, which can be

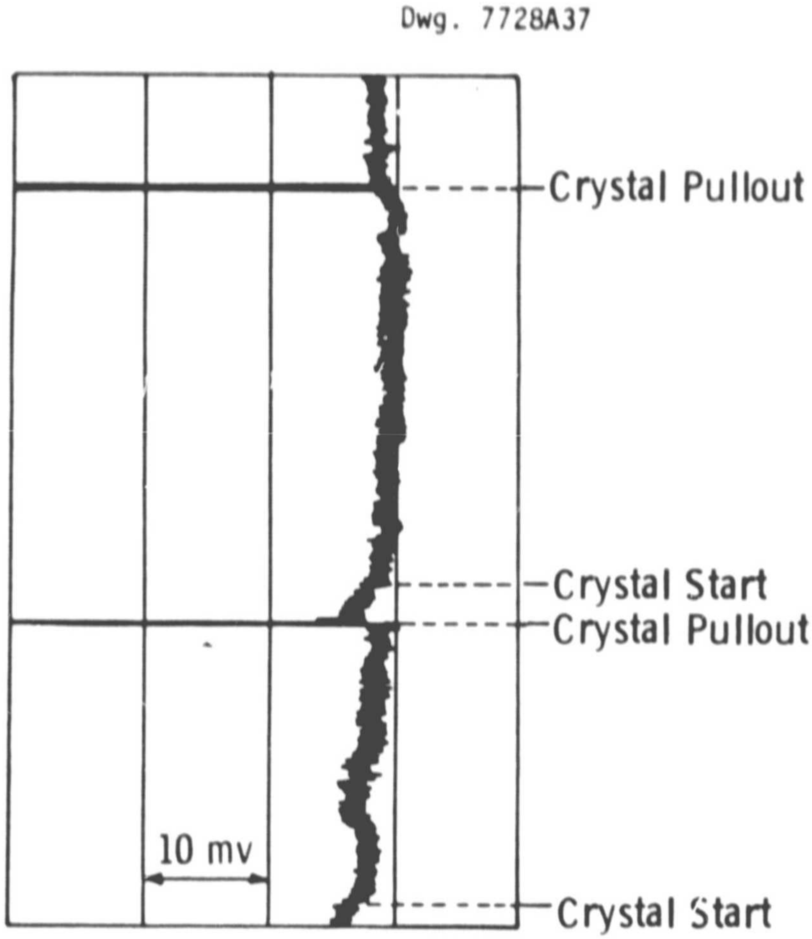

Figure 22 A portion of the melt level detector output from 8 hour semi-automatic web growth run.

obtained by addition of a closed loop for dimension control. This control loop, when used with a suitable thermal gradient within the susceptor system, will perform fine adjustments of the melt temperature to maintain constant web growth width. The effectiveness of this method has been demonstrated manually on numerous occasions and requires skilled operator attention. Application of a dimension control loop will eliminate all operator functions after growth is started and will provide fully automatic growth.

3.5 Feedstock Considerations for Dendritic Web Growth

At the present time, all silicon crystal growth processes utilize high purity "semiconductor grade" starting material, and cost reduction for this feedstock is an important consideration in meeting the future wafer cost goals. Although no specifications have yet evolved for such low cost material, there is the implicit expectation that low cost feedstock will have significantly greater impurity content than presently utilized material. At the inception of the Low Cost Solar Array program, there was relatively little knowledge of the effect of impurities on the performance of solar cells, and an investigation of the topic was undertaken as one aspect of Task I of the LSA program.[8]

Although a study of impurities in dendritic web was not a major thrust of the Task I program, analysis of several web crystals intentionally doped with nickel and with molybdenum suggested that these impurities were more strongly rejected than had been expected for such "high speed" growth. Subsequently, a small program was undertaken on Westinghouse funds to clarify the solute partitioning behavior of dendritic web. In that study, it was found that dendritic web rejected impurities with almost the same efficiency as in Czochralski growth, and a theoretical model which explained the mechanisms was devised.[9]

In the balance of this section, the results of these other studies will be summarized, and some more recent experience with non-standard feed stock will be presented. Specifically, dendritic web has been grown successfully from laboratory samples of a potentially low cost silicon from the Battelle Laboratories, and some experiments were done using dendrites reclaimed from solar cell-processing activities. In all cases not only was crystal growth accomplished without problem, but also the resulting diagnostic solar cells had very satisfactory performance.

3.5.1 Theory of Segregation in Dendritic Web Growth

The effectiveness of solute segregation in dendritic web growth is due in large part to the fact that solute rejected by the growing interface can diffuse laterally as well as normal to the growth front. In Czochralski growth, solute diffusion is effectively normal to the growth front except at the periphery of the crystal. In other ribbon growth techniques such as RTR and EFG, the rejected solute is effectively confined to a small molten zone near the interface. In web growth, however, the rejected solute can diffuse sidewise as well as ahead of the interface.

The geometry for the theoretical treatment of segregation in web growth is shown in Figure 23; the curved surface of the liquid meniscus is modeled as a wedge with included angle 2θ. Fluid flow in the system is determined by the growth rate of the crystal, and the diffusion equation must be solved in the appropriate moving reference frame.[9] The solution to the problem can be simplified under certain conditions; for example, if the equilibrium segregation coefficient k_o is small ($k_o \leq .001$), then the effective segregation coefficient k_{eff} is given by

$$k_{eff} = k_o(1 + vt/2D\sin\theta)$$

where v is the crystal growth velocity, t is the crystal thickness, D is the solute diffusivity in the melt and 2θ is the included angle of the wedge. Since the true meniscus spreads more rapidly than a wedge, the effective half angle is somewhat larger than the actual contact angle for silicon which is about 11°; 20° would probably be a reasonable value. Depending on the particular parameters for the solute and the growth conditions, k_{eff}/k_o should have a value somewhat between 1 and 10; most of the data available to date shows that it is more nearly unity than ten.

Dwg. 6407A45

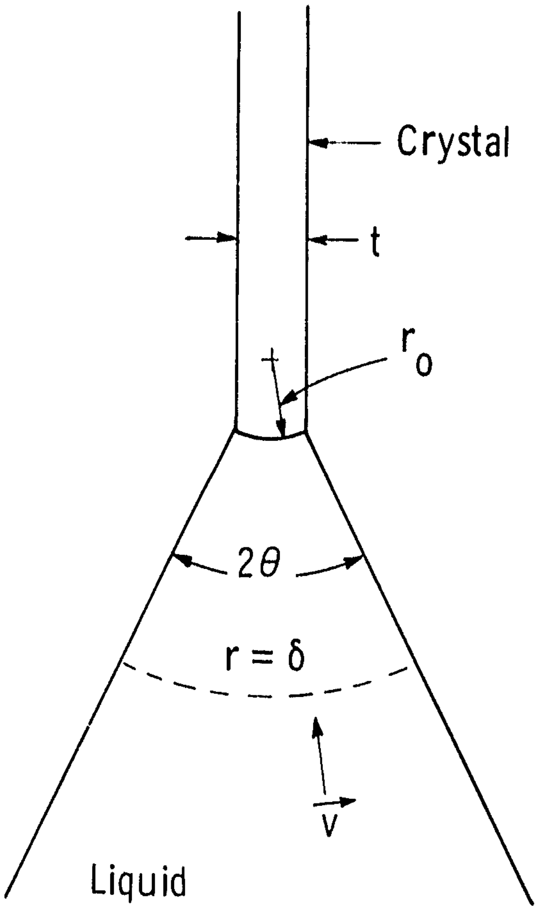

Figure 23 Geometry for calculating segregation in dendritic web.

3.5.2 Measured Segregation Coefficients

Measurement Techniques. Only electrically active impurities have been studied with regard to segregation behavior in dendritic web growth, and the impurity concentrations in the crystals have been determined electrically. Concentrations of those impurities which are carrier donors or acceptors were evaluated from electrical resistivity measurements using the four-probe technique.[5,6,7] For those impurities which act principally as minority carrier recombination centers, the concentrations were determined from DLTS (Deep Level Transient Spectroscopy) measurements; the work on these impurities was done primarily on the LSA Task 1 program on impurity effects in silicon solar cells.[10]

A detailed description of the DLTS for evaluating the concentration of impurities which affect carrier recombination is rather too complex to describe here. Basically, it uses the transient capacity of a junction to measure the emptying (or filling) of trapping centers. A thorough discussion of the theory and application of the technique is given in Reference 11.

Boron. In earlier reports on this project,[2,3] we discussed some preliminary data for the segregation coefficient of boron in dendritic web. The preliminary measurements seemed to indicate that $k_{eff} = 0.59$, which was significantly different from the commonly accepted value of $k_o = 0.80$. During the past year, additional data has been generated which has changed our measured value of k_{eff} to 0.7 but which still supports the observation that k_{eff} in dendritic web growth is less than k_o for boron, as determined from Czochralski crystal growth experiments.

The present value changed not only because of improved measurement techniques, but also because a much larger data base was accumulated. As usual, DopeSil* pellets were used to add specified amounts of boron to the silicon melt. The doping pellets were obtained from a number of different lots and presumably there could be lot-to-lot

*Trademark of Hemlock Semiconductor Co. (Dow Corning) variation within a given lot. The averaged segregation coefficients arranged by pellet lot number are given in Table 3. The data would seem to indicate that the lot-to-lot variation is insignificant compared with the pellet-to-pellet variation. Further, the final value of $k_{eff} = 0.70$ while closer to $k_o = 0.8$ is still an appreciable deviation.

Aluminum, Gallium and Indium. These three acceptor impurities were the first solutes for which segregation coefficients were measured in dendritic web. They were chosen because not only were the atoms electrically active, but also the equilibrium segregation coefficients were small compared to unity. The details of the measurements and analyses are given in Reference 6; the numerical results are presented in Table 4.

Phosphorus. Although most of the web crystals which have been grown were doped with boron, four crystals were grown using phosphorus doping (also in the form of DopeSil pellets). The resistivity of the webs ranged from 3 to 30 ohm-cm. For these crystals the segregation coefficient was found to be $k_{eff}(P) = 0.36 \pm .02$, which can be compared with the commonly accepted value of $k_o = 0.35$. Thus the effective p segregation coefficient in web is very nearly the same as the equilibrium value.

Transition Metals: Ti, V, Mn. Evaluation of the segregation coefficients of some transition group metals was done primarily on the LSA Task I impurity program and is included here for completeness.[8] Dendritic web crystals were grown from melts doped respectively with 1.77×10^{18} cm^{-3} Ti, 1.5×10^{18} cm^{-3} V and 2.0×10^{18} Mn. Additionally, boron was added to the melt to give about 8 ohm-cm material so that diagnostic solar cells could be fabricated. Impurity concentrations in the web crystals were determined from both the solar cell performance and from DLTS measurements. Since both techniques evaluate only the electrically active impurity concentrations, the total concentrations were determined using the ratios $C_{elect.}/C_{total}$ from work on Czochralski crystals.

TABLE 3

MEASURED BORON SEGREGATION COEFFICIENTS FOR SILICON WEB GROWTH

Dopant Lot Number	Nominal Boron Content	Number of Samples	Resistivity Range	Effective Segregation Coefficient
WPD-006	2×10^{17}	15	6.5-10.3	$.72 \pm .09$
WPD-007	3×10^{17}	12	1.7-4.6	$.67 \pm .07$
WPD-023	2×10^{17}	7	6.5-9.5	$.69 \pm .12$
WPD-026	2×10^{17}	21	5.9-10.5	$.72 \pm .14$
"Master Dope"		2	4.3-4.4	$.68 \pm .01$
		Grand Average		$.70 \pm .03$

TABLE 4

SEGREGATION COEFFICIENT DATA FOR Al, Ga, AND In IN WEB

Solute	Number of Crystals	Number of Samples	Initial Solute Concentration (atom fraction)	k_{eff}/k_o	k_o (Ref.12)
Aluminum	3	6	2.47×10^{-5}	1.47 ± 0.64	0.0028
Gallium	4	7	9.06×10^{-6}	0.97 ± 0.45	0.008
Indium	3	9	2.47×10^{-6}	0.93 ± 0.16	0.0004

Reasonably good results were obtained from the titanium- and vanadium-doped crystals, however no DLTS data were obtained from the manganese-doped crystal and only the solar cell data could be used to estimate the concentration. The final results can be summarized as follows:

Titanium: $k(web) = 4x10^{-6}$ ($= 2k(cz)$)

Vanadium: $k(web) = 1.7x10^{-5}$ ($=4.2k(cz)$)

Manganese: $k(web) = 3.4x10^{-5}$ ($= 2.5k(cz)$)

These values are in good agreement with the model of Section 3.5.1 and suggest that the dendritic web process is compatible with the use of solar grade silicon which might well contain transition group metallic impurities.

3.5.3 Web Growth from Non-Semiconductor Grade Silicon

Although segregation coefficient measurements indicated that the dendritic web process should be able to use starting material other than semiconductor grade silicon, direct evidence was needed. Accordingly, two types of feed stock were evaluated: 1) a potentially low cost silicon produced by the Battelle Laboratories, and 2) recycled dendrites which were removed from web crystals both before and after they had been processed into solar cells. The economic implications of both these materials are significant. In the first case, a possible low cost starting material was directly evaluated for dendritic web growth, and in the second case the material utilization efficiency of the process was evaluated.

Battelle Silicon. The material used in this growth experiment was an early laboratory sample produced by the Battelle Memorial Institute under an LSA Task I contract. The sample which we evaluated was supplied to us by JPL through Dr. R. Kachare. The fine granular character of the material made it of particular interest since it would be quite suitable for melt replenishment applications as well as being of potentially low cost.

The Battelle process utilizes the reduction of silicon tetrachloride by zinc in a fluidized bed and as a result the material as received had a high concentration of zinc. Before utilizing the sample for web growth, it was heated at about 1200°C in argon for 6 hours to remove entrapped zinc; this was the only pretreatment. There was no difficulty with web growth from the melt, and samples of the crystals were fabricated into solar cells. (Crystals W180-1, -2, and -3). Boron doping was also added to the melt to give material with a target resistivity of 12 ohm-cm based on the use of semiconductor grade silicon.

The resulting web crystals had a resistivity of 0.25 ohm-cm, indicating that some p-type impurity (possibly zinc) was present. Nevertheless, the resulting solar cells, fabricated from crystals W180-1 and W180-3, had efficiencies of 8.9% and 9.0%, respectively, <u>without AR coating</u> (estimated to be 12.6% and 12.8%, had AR coatings been applied). In summary, even this preliminary sample of a possible low cost silicon could be easily fabricated into reasonably good solar cell material by the dendritic web process.

<u>Recycled Dendrites</u>. One factor which limits total silicon utilization for the web process is the dendrites, which remain attached to the ribbon during solar cell processing. These dendrites serve to greatly strengthen the thin ribbons and permit relatively easy handling of the material, but unquestionably reduce the silicon "yield" of the growth process. This yield could be increased if these dendrites could be recycled and several experimental runs were made to demonstrate the feasibility of the approach.

In the first experiment, dendrites were removed from unprocessed web and used to make up 10% by weight of the growth charge. The dendrites were first given a light cleaning etch and were added to the usual semiconductor grade silicon to make up a total charge of 185 gm. Crystals grown in this run, J226, were processed into solar cells which showed an <u>uncoated</u> AM1 efficiency of 9.8%. The resistivity of the material was 5.7 ohm-cm as expected from the boron dope added to the melt.

In the second experiment, dendrites were obtained from the cell fabrication facility. These dendrites had coatings of aluminum and copper from the metallization steps as well as diffused layers of aluminum- and phosphorus-doped silicon from the junction formation processes. The cleaning was therefore a little more extensive. The scrap dendrites were first cleaned with hot HNO_3 to remove the AR coating and copper metallization and then with NaOH to remove the aluminum back metallization. Finally, 3:1 $HF:HNO_3$ was used to remove the diffused surface layers of phosphorus and aluminum. Again, 18 gm of reprocessed dendrites was added to semiconductor grade silicon to make a standard 185 gm melt. Samples from crystal J269-1 from the run were processed into solar cells which had an average uncoated efficiency of 8.5%.

All of the results on recycling dendrites indicate the feasibility of the concept; the desirability depends on a detailed cost analysis of the overall process.

3.5.4 Ancillary Considerations in the Use of Solar Grade Silicon

In the discussion of the preceeding sections, the solute segregation effects and the growth experience indicate that dendritic web growth can accommodate silicon feedstock less pure than semiconductor grade. There are a number of impurity-related effects which must be considered for all crystal growth techniques including the dendritic web process. If some sort of melt-replenishment technique is used, then impurities in the feed stock will accumulate in the melt and ultimately the impurity content of the growing crystal will increase over the content of the crystal in the early stages of growth. This is one of the phenomena considered in the impurity study[8] and the results have been published in the open literature.[13]

Briefly, the study showed that the buildup of impurity was dependent on whether the melt was replenished continuously or whether it was replenished periodically, e.g., between the growth of multiple crystals from the same melt. It was shown that the continuous replenishment scheme, such as would be used for the dendritic web process, results in a much slower buildup than the periodic replenishment procedure. For impurities with very small segregation coefficients, the solute concentration in the liquid at any given time, C_L, is related to the initial concentration, C_o, by the relation

$$C_L/C_o = 1 + M_C/M_o$$

where M_C is the total weight of crystal that has been grown and M_o is the weight of the melt. Thus if 3.8 Kg of web (e.g., 5cm wide x 150 μm thick x 200 m long) is grown from a continuously replenished 200 gm melt, then the solute concentration in the melt will increase 20 times.

What limiting concentration of impurity can be accommodated depends on the answer to two questions: what electrical effect will impurity have and what crystal growth effect will occur? Again, the impurity study program has addressed itself to the electrical effects of various solutes, and some of the results of these studies are summarized in Figure 24.[14] The figure shows the relative performance of solar cells having various concentrations of impurities in the base crystal. Since these impurities are generally strongly rejected to the melt, the limiting concentration in the melt is usually many orders of magnitude larger than for the crystal. A fuller discussion of this topic is beyond the preview of the present report.

The crystal growth aspect of the limiting concentration is related to the stability of the growth front in the presence of a large solute concentration. A treatment by the usual approach of interface stability or constitutional supercooling analysis is rather difficult since no adequate theory of constitutionally generated instability for web growth presently exists. An estimate of limiting solute concentration can be found from experimental work on the growth of web from melts doped with Mo, Cr, etc. In those experiments, it was found that growth was difficult and interface breakdown occurred when the solute content reached about 20 ppma, give or take a factor of 1.5.[15] Considering the segregation coefficients of most deleterious impurities, this concentration is below the value where serious cell degregation would occur.

Curve 696864-B

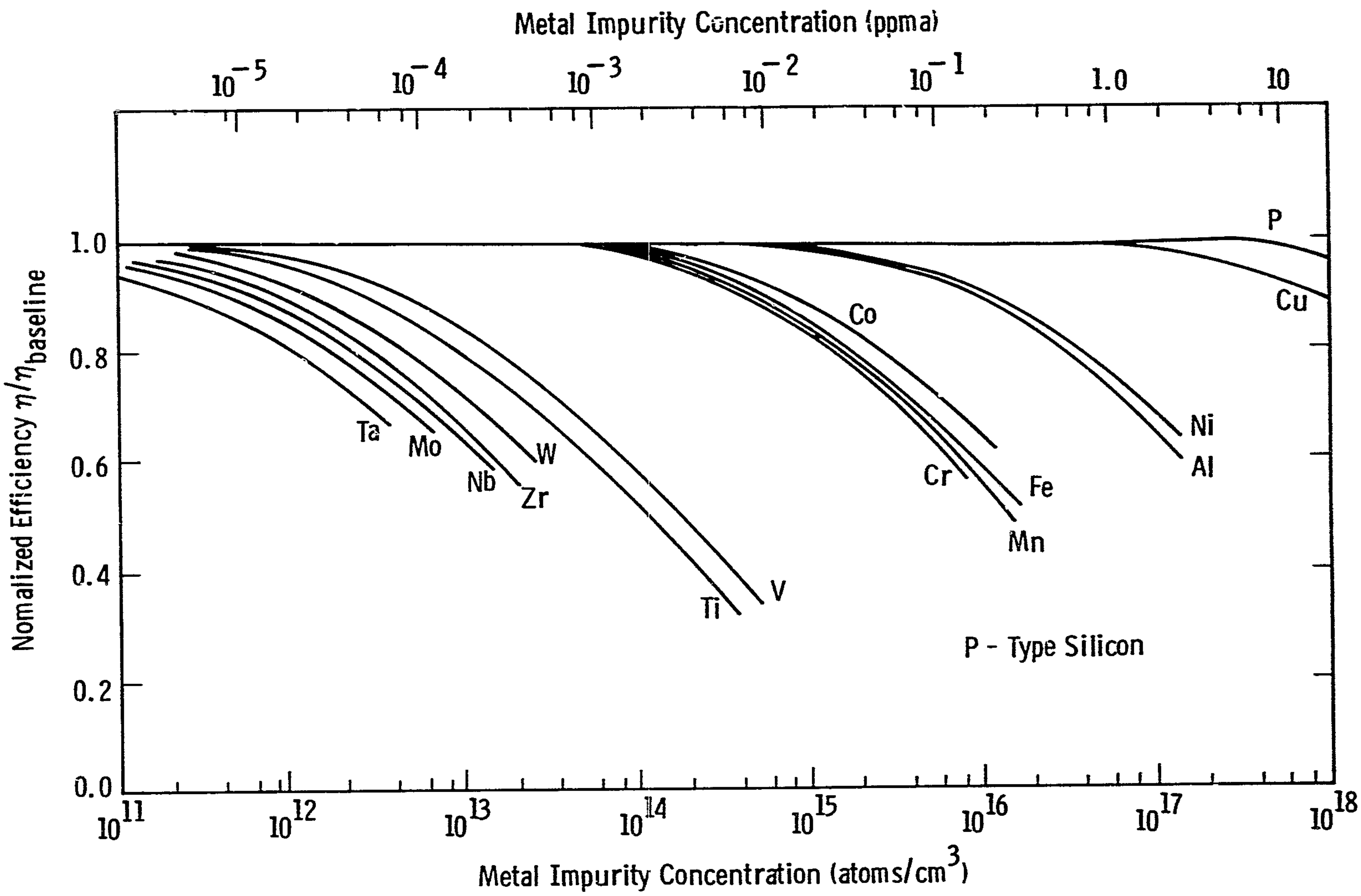

ORIGINAL PAGE IS
OF POOR QUALITY

Figure 24 Curves for the normalized solar cell efficiency as a function of metal impurity content for devices made on 4 ohm-cm, p-type silicon.

From these considerations of the effect of impurities on both the solar cells and on the growth process, it would appear that dendritic web crystals could be grown from silicon feedstock having a total impurity content of about 1 ppma (based on the equation given earlier). At least some material (the Battelle silicon) meets these requirements.

3.6 Dendritic Web Solar Cells

The attainable efficiency of a silicon solar cell depends on both the material properties of the wafer and the cell processing protocol. These two factors are not totally independent in that the cell design must complement the material; for example, thin wafers such as dendritic web require some sort of back-surface field device to prevent excessive loss of minority carriers at the back contact. Nevertheless, there are some general requirements that can be placed on the starting wafers if high quality solar cells are to be fabricated. First, the material should be of the proper conductivity type and resistivity to complement the cell design. Dendritic web silicon has been grown to specified resistivities from .01 to 20 ohm-cm. Second, the material should be of the proper size for the cell design. Dendritic web silicon has the inherent rectangular shape required for efficient packing of individual solar cells into a module or array; further, the thickness of the material is readily controlled by the pull speed. Third, the material should contain minimal chemical and physical imperfections which will lower the lifetime of minority carriers in the base region of the cell. Dendritic web silicon rejects impurities with almost the theoretical efficiency (see Section 3.5.2). Additionally, the web crystals can be grown with very low dislocation density. Further, the "imperfection" represented by the central twin planes in the web have no measureable effect on the carrier lifetime.[16] Finally, for both convenience and economics, the material should require a minimum of processing prior to device fabrication. Dendritic web emerges from the melt with a surface of high perfection requiring only minimal cleaning prior to the junction formation process.

Solar cell fabrication studies under the present program were limited to 10x10 mm diagnostic solar cells which · ·e used to evaluate web quality. Other programs, sponsored both by ··· as part of the LSA Program and by Westinghouse internal programs, investigated larger cells and cell modules. The present section will discuss both sizes of cells to present a more complete picture of the performance of dendritic web material.

3.6.1 Diagnostic Solar Cells

In the present program, solar cell fabrication and testing were used mainly as a tool to assess the quality of the web crystals. Instead of fabricating cells of a "commercial" size, the decision was made to use the 10x10 mm cell design developed for material evaluation in the LSA Task I impurity study program.[8]

The general design of the diagnostic cell is shown in Figure 25, which details the pattern used for the Czochralski or float zone wafers in the impurity study. For the present study, only the central 10x10 mm pattern was used for the web studies; the other devices, which have other diagnostic purposes, were eliminated. In practice, 25-mm long samples were cleaved from the web crystals and two cell patterns were fabricated on each blank; two or more blanks were cut from each crystal so that at least four cells were fabricated from a given crystal.

The cell-processing sequence generated an n^+pp^+ junction sequence so that the resulting cells included a back surface field to compensate for the thin web material. Generally, the cells were processed with the dendrites attached to the web samples for support during the processing steps; the active cell area was then defined by a mesa etch. A typical process run sheet defining the various process steps is shown as Figure 26. It should be noted that there is no antireflectance coating (AR) step in the processing sequence. It was felt that every process step adds the possibility of adding an artifact to the cell performance and therefore, since material evaluation was the goal of the operation, more reproducible results would be obtained without AR coating.

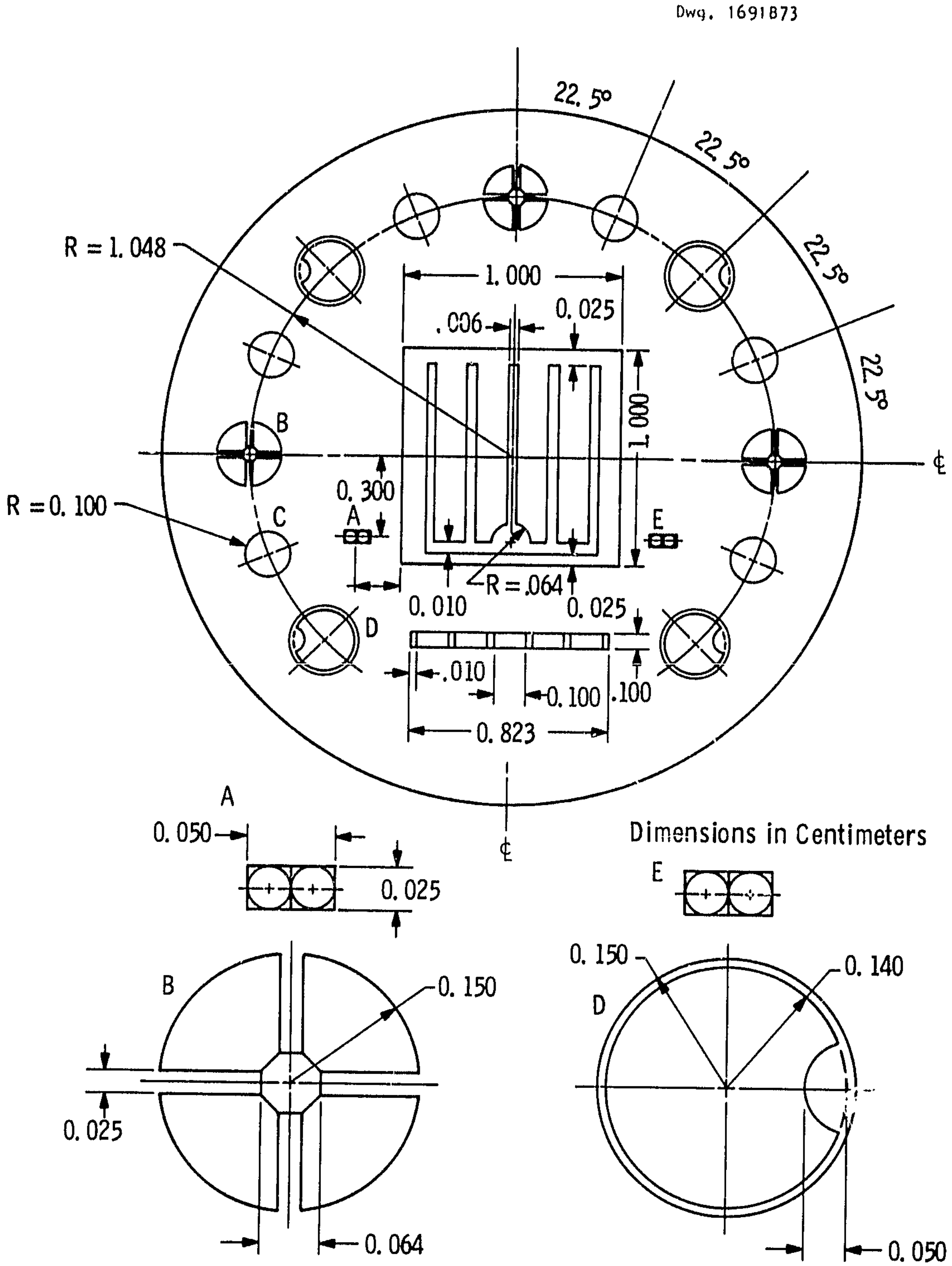

Figure 25 Diagnostic solar cell pattern design.

Start Date Material: Quantity: Engr.	PROCESSING LOG	Run or Sample Web Qual - Array Process

Date Tech.	Process	Special Instructions, Measurements, etc.
	IDENTI-FICATION (1)	Scribe serial numbers on either side of web near one end to identify P+ side of structure
	CLEAN (2)	Remove oxide coating by swabbing with cotton soaked with HF, rinse in D.I. H_2O; 4 min. H_2SO_4 - 160°C
		HF:H_2O (1 to 10 ratio) dip 15 sec. H_2O - NH_4, H_2O_2 - HCl
	SILOX (3)	Side not numbered 420°C; 5000Å TK: Speed = 100
	CLEAN (4)	HF:H_2O (1 to 10 ratio) dip 15 sec. H_2O - NH_4, H_2O_2 - HCl
	BORON DIFF. (5)	Boron Deposition, BBr_3 @ 960°C 2-20-2 min. Numbered side up. Very slow pull (5 min/2 inches)
	REMOVE OXIDE (6)	3:1 (H_2O:HF) until all oxide is removed R_s = ______ Ω/□ (Target value = 60 Ω/□)
	SILOX (7)	Numbered side 420°C; 5000Å TK; Speed = 100
	CLEAN (8)	HF:H_2O (1 to 10 Ratio) dip 5 sec. H_2O_2 - NH_4, H_2O_2 - HCl
	$POCl_3$ DIFFUSION (9)	Diffusion Temp. 850°C Time 35 min. source temp. = 0° Flow Rates 200 cc/min - N_2 Source; 1560 cc/min - N_2 Carrier 62.5 cc/min O_2 (Slow cool by pulling 3 in/5 min)
	REMOVE OXIDE (10)	Strip deposition oxide 3:1 (H_2O:HF) Measure, R_s = ______ Ω/ (Target value = 60 Ω/)
	PHOTO RESIST (11)	Apply photo resist by Photo resist AZJ (spin speed 4000 RPM). Bake at 90°C 15 min.
	MASK (12)	Expose as many cells as possible/piece 1 cm x 1 cm
	METAL FRONT (13)	Top side not numbered Ti Å Pd Å Ag A
	METAL BACK (14)	Ti 1500Å Pd 500Å Ag 20 KÅ
	REJECT METAL (15)	Reject excess material and PR coat by gentle agitation in acetone
	AG PLATE (16)	Apply 4 microns AG by electro plating process
	PHOTO-RESIST (17)	Mask #2 (Mesa) Waycoat SC, 7000 rpm, h - 4.0 μm (AP-100 before Waycoat SC) Exposure time = 15 sec (I_o = 0.6 μa). Apiezon wax back side
	ETCH SILICON (18)	44 cc HF + 26 cc HNO_3 + 29 cc Acetic 5°C, Etch time = 5-10 sec Etch silicon between 5 to 8 μm deep, Talystep ______ μm.
	TEST (19)	Return to Engr.

Rev. #3 - EJS

Figure 26 Processing sequence for fabricating diagnostic solar cells.

Other experiments indicated that the AR efficiency could be found by multiiplying the uncoated efficiency by the factor 1.43.

Testing of the cells was done using a tungsten-halogen lamp to simulate an AM1 spectrum. The lamp intensity was adjusted to give 91.60 mW/cm^2 as measured by a calibrated standard solar cell. Open-circuit voltage, short-circuit current, and four additional current-voltage points were measured on each cell and this data used to determine the parameters Log I_o, R, and N in the equation

$$I = I_{sc} + I_o \; [1 - \exp(V+IR)/V_{th}]$$

where I and V are the terminal voltage and current and $V_{th} = kT/q$. The maximum power point and hence efficiency and fill factor are determined from the above relation. Additionally, the open-circuit decay lifetime is measured separately and included in the cell analysis printout, a sample of which is given as Table 5. In order to be used for material analysis, the cell data for the various web samples is analysed to give the averages and standard deviations of I_{sc}, V_{oc}, FF, Eff, (no AR) and the OCD lifetime. A sample printout of these average values is given as Table 6.

Finally, the averages according to crystals (without the SD's) are tabulated in a computer data base as well as in earlier reports.[1-3]

A general summary of the results of the diagnostic cell data is given in Figure 27, which shows a histogram of cell efficiency distribution. In this figure, the raw data for the uncoated cells has been converted to the anticipated efficiency with an AR coating. It can be seen that the average cell efficiency is about 13% with some of the cells over 15%.

3.6.2 Larger Solar Cells

In addition to the diagnostic solar cells discussed in the preceeding subsection, a number of 16x40 mm solar cells were fabricated as deliverable items under the contract. All of the crystals used to fabricate these larger cells had been previously characterized with diagnostic cells, and it is of some interest to compare the two devices.

TABLE 5 Example of cell data

00603WQ WQ60
QUAL1 6 /24/80 AM1: P0=91.60MW/CM^2 NO AR COATING

ID	ISC	VOC	IP	LOG(IO)	N	R	FF	EFF	OCD	PCDA	PCDB
3R*	22.10	.553	19.92	-6.353	1.97	-.82	.735	9.50	.00	.00	.00
R11	19.90	.537	18.42	-8.157	1.39	-.15	.769	8.69	.91	.00	.00
R12	19.90	.537	18.25	-7.383	1.58	-.53	.759	8.58	.91	.00	.00
R21	20.20	.539	18.57	-7.550	1.54	-.48	.763	8.78	1.04	.00	.00
R22	19.80	.539	18.00	-6.801	1.77	-.84	.749	8.45	.91	.00	.00
R31	20.20	.543	18.52	-7.296	1.62	-.69	.761	8.83	1.30	.00	.00
R32	20.30	.544	18.77	-7.972	1.45	-.38	.772	9.01	1.56	.00	.00
R41	20.00	.539	18.39	-7.507	1.55	-.60	.765	8.72	1.30	.00	.00
R42	20.10	.538	18.38	-7.126	1.66	-.79	.759	8.68	1.17	.00	.00
R51	21.40	.529	19.68	-7.768	1.45	.09	.751	8.99	3.90	.00	.00
R52	21.30	.525	18.94	-5.719	2.17	-1.38	.723	8.56	3.12	.00	.00
R61	21.40	.523	19.46	-6.915	1.67	-.40	.742	8.79	3.64	.00	.00
R62	21.30	.524	19.28	-6.600	1.78	-.66	.739	8.72	3.38	.00	.00
R71	22.40	.549	20.60	-7.955	1.45	.53	.742	9.65	9.80	.00	.00
R72	22.30	.558	20.61	-8.318	1.40	.47	.753	9.91	11.70	.00	.00
R81	22.20	.540	20.54	-8.480	1.32	.63	.750	9.51	7.80	.00	.00
R82	22.10	.539	20.42	-8.441	1.33	.74	.746	9.39	3.38	.00	.00
R91	20.90	.535	18.83	-6.261	1.95	-1.18	.741	8.76	1.56	.00	.00
R92	20.80	.533	19.02	-7.136	1.63	-.61	.755	8.86	2.34	.00	.00
R101	21.50	.547	19.85	-7.962	1.45	-.12	.764	9.50	4.16	.00	.00
R102	21.40	.544	19.66	-7.531	1.55	-.35	.759	9.35	3.64	.00	.00
R111	22.00	.544	19.97	-6.827	1.76	-.38	.739	9.35	5.50	.00	.00
R112	21.90	.541	20.20	-7.853	1.46	-.19	.764	9.57	5.20	.00	.00
R121	21.90	.548	20.09	-7.435	1.58	-.29	.755	9.58	7.54	.00	.00
R122	21.60	.546	19.82	-7.474	1.57	-.26	.755	9.42	6.50	.00	.00
R131	22.30	.539	20.58	-8.020	1.41	.13	.757	9.63	8.06	.00	.00
R132	22.00	.544	20.43	-8.653	1.30	.35	.764	9.67	11.05	.00	.00
R141	22.20	.537	20.50	-8.176	1.38	.32	.754	9.51	8.45	.00	.00
R142	21.70	.534	19.46	-6.241	1.95	-.55	.722	8.84	7.02	.00	.00
R151.*	20.30	.517	17.33	-4.390	3.20	-3.74	.696	7.73	1.95	.00	.00
R161	21.70	.541	19.92	-7.678	1.50	.18	.746	9.27	5.90	.00	.00
R162	21.70	.544	19.99	-7.956	1.44	.22	.752	9.39	5.90	.00	.00
R171	20.20	.533	18.38	-6.917	1.70	-.59	.746	8.50	1.69	.00	.00
R172	20.10	.530	18.19	-6.563	1.82	-.87	.742	8.36	1.56	.00	.00
R181	20.30	.533	18.40	-6.737	1.77	-.53	.738	8.45	1.69	.00	.00
R182	19.90	.530	17.92	-6.335	1.91	-.99	.736	8.21	1.17	.00	.00
R191	21.20	.549	19.56	-7.869	1.48	-.22	.764	9.41	3.12	.00	.00
R192	21.00	.549	19.28	-7.440	1.59	-.49	.761	9.28	3.00	.00	.00
R201	21.20	.540	19.34	-7.069	1.67	-.45	.748	9.06	1.95	.00	.00
R202	21.00	.548	19.22	-7.312	1.62	-.33	.752	9.15	2.60	.00	.00
R211	20.50	.538	18.42	-6.153	2.01	-1.20	.736	8.58	1.43	.00	.00
R212	20.20	.532	18.33	-6.659	1.79	-.92	.747	8.49	1.04	.00	.00
R221	20.30	.537	18.59	-7.319	1.59	-.47	.756	8.71	1.43	.00	.00
R222	20.30	.537	18.62	-7.434	1.56	-.40	.757	8.73	1.69	.00	.00
R231	19.80	.524	17.72	-5.985	2.04	-1.40	.733	8.04	1.04	.00	.00
R232	19.60	.527	17.43	-5.640	2.24	-2.00	.732	7.99	.91	.00	.00
R241	19.50	.531	17.47	-6.095	2.02	-1.16	.729	7.99	1.04	.00	.00
R242	19.60	.530	17.62	-6.205	1.97	-1.24	.737	8.10	.91	.00	.00

TABLE 6

EXAMPLE OF PRINTOUT OF CRYSTAL AVERAGES (WQ60)

CRYSTAL NUMBER	WEB QUAL	THK (MICRONS)	RHO (OHM-CM)	ISC(MA) AVG	ISC(MA) STDV	VOC(VOLT) AVG	VOC(VOLT) STDV	FILL FACTOR AVG	FILL FACTOR STDV	EFFICIENCY AVG	EFFICIENCY STDV	OCD(MICRO-S) AVG	OCD(MICRO-S) STDV
AA0011-4.1	WQ60	151	15.33	21.35	.06	.525	.003	.739	.012	8.76	.18	3.5	.3
AA0011-5.2	WQ60	167	16.29	22.25	.13	.546	.009	.748	.005	9.61	.22	8.2	3.6
J163-1.4	WQ60	204	5.51	21.45	.07	.545	.002	.762	.004	9.42	.11	3.9	.4
J165-1.3	WQ60	285	6.86	21.85	.17	.545	.003	.753	.010	9.48	.11	6.2	1.1
J187-3STD	WQ60	202	2.9	20.05	.18	.539	.003	.762	.007	8.72	.17	1.1	.2
J241-1.2	WQ60	318	7.23	22.05	.26	.538	.004	.749	.019	9.41	.39	8.6	1.7
J294-1.1	WQ60	215	8.03	21.70	.00	.542	.002	.749	.004	9.33	.08	5.9	.0
J297-2.3	WQ60	200	3.8	20.12	.17	.531	.002	.740	.004	8.38	.13	1.5	.2
J297-4.2	WQ60	168	4.15	21.10	.12	.546	.004	.756	.007	9.22	.15	2.7	.5
J299-4.2	WQ60	168	3.59	20.32	.13	.536	.003	.749	.010	8.63	.11	1.4	.3
RE286-2.4	WQ60	210	3.49	20.20	.24	.532	.012	.748	.007	8.51	.36	1.3	.5
W211-1.2	WQ60	170	3.20	21.40	.00	.562	.001	.782	.000	9.94	.02	4.6	.3
W213-1.3	WQ60	130	3.15	21.10	.14	.544	.017	.699	.064	8.50	.98	2.1	1.6
W214-1.1	WQ60	175	3.26	21.70	.35	.544	.013	.746	.004	9.31	.35	3.4	1.2
W214-2.3	WQ60	112	3.16	.00	.00	.000	.000	.000	.000	.00	.00	.0	.0
WA30-1.3	WQ60	190	7.89	20.00	.16	.515	.001	.735	.003	8.01	.04	1.4	.2
WA87-1.2	WQ60	222	3.76	20.42	.13	.541	.003	.760	.003	8.88	.04	2.0	.4
WB54-1.2	WQ60	195	17.55	21.30	.00	.519	.000	.513	.000	6.00	.00	3.9	.0

ORIGINAL PAGE IS
OF POOR QUALITY

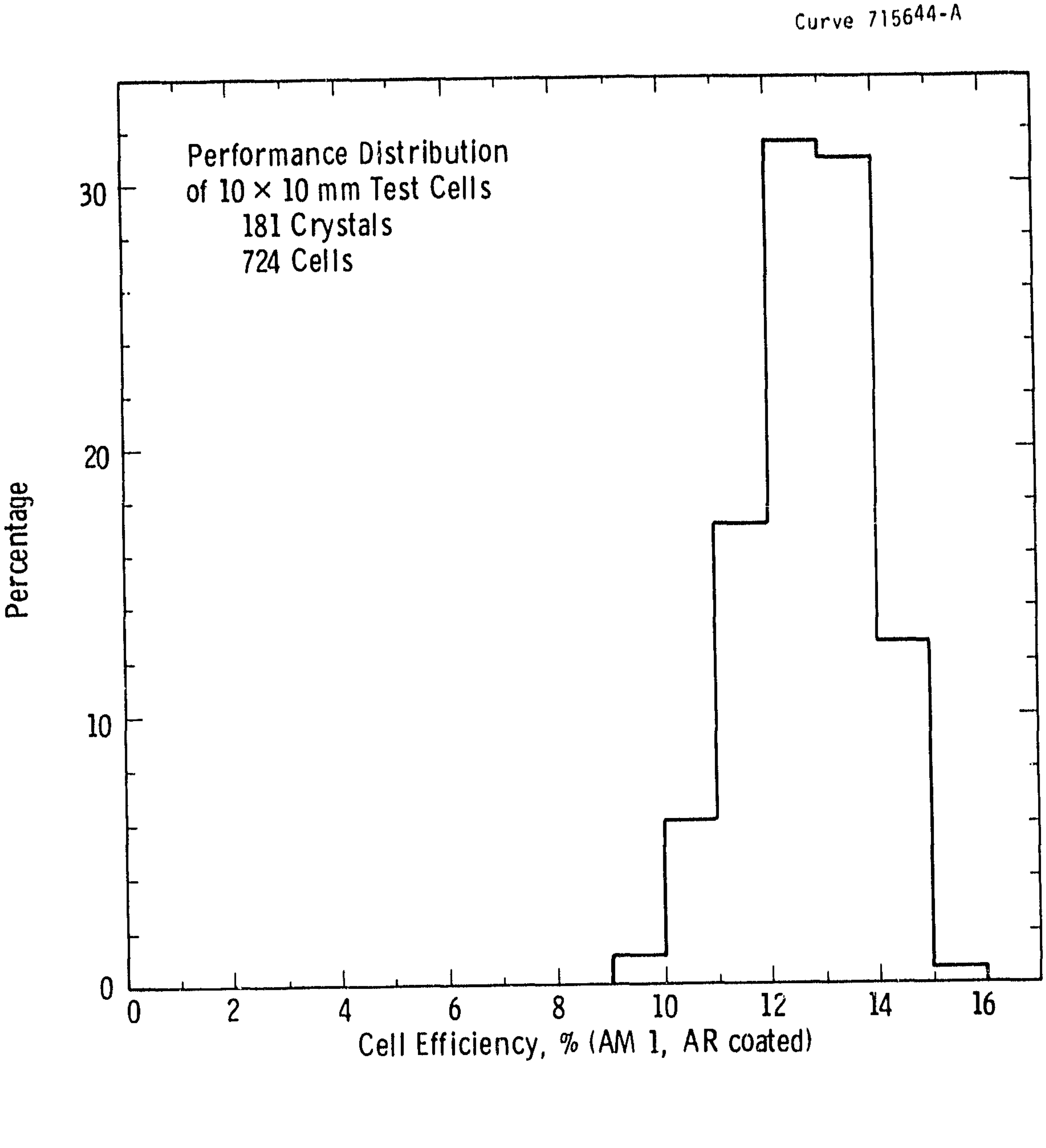

Figure 27 Distribution of diagnostic solar cell efficiencies.

Figure 28 shows the comparison, by crystal, for the efficiencies of the two types of cells; the data for the 16x40 mm cells are measured values for AR-coated devices, while the values for the 10x10 mm cells are calculated from the uncoated cells using the factor 1.43. The straight line in the figure is the 1:1 relationship, not a line fitted to the data. Generally, the two types of devices would seem to correlate quite well although the scatter indicates that there is some variation in either the processing or material. If one takes the data averages, $\eta_{AR} = 13.65 \pm .79\%$ for the larger cells and $\eta_{AR} = 13.04 \pm .64$ for the smaller cells, there is even some indication that the larger cells have greater efficiencies than expected from the diagnostic cell data, a result which might be related to a slightly more efficient grid pattern and larger area to periphery ratio.

In general, one may conclude that the 10x10 mm diagnostic cells are valid predictors of the performance of larger devices. Further, the factor 1.43 seems to be a reasonable value to ascribe to the ratio of AR-coated efficiencies to uncoated efficiency.

3.6.3 Solar Cell Modules using Dendritic Web Cells

Recently, four photovoltaic cell assemblies or modules were constructed using dendritic web solar cells. Although this work was performed under the Automated Assembly Task of the LSA Program, the results will be summarized here as an example of the application of dendritic web to a "practical" device. The details of the module program are given in Ref. 16.

Each of the modules was constructed from 72 series-connected cells, each 16x70 mm; the final module geometry was 284x294 mm (30x30 cm). A completed module with some individual cells, together with some processed and unprocessed web, is shown in Figure 29. The cell design used in the modules differed from the diagnostic and the 16x40 mm cell in several ways. Probably the most significant was the use of an aluminum alloy rather than a diffused boron p^+ layer for the BSF. Additionally, the antireflection coating was applied by a dipping technique done prior to the generation of the contact pattern with a photoresist process.

Curve 718929-A

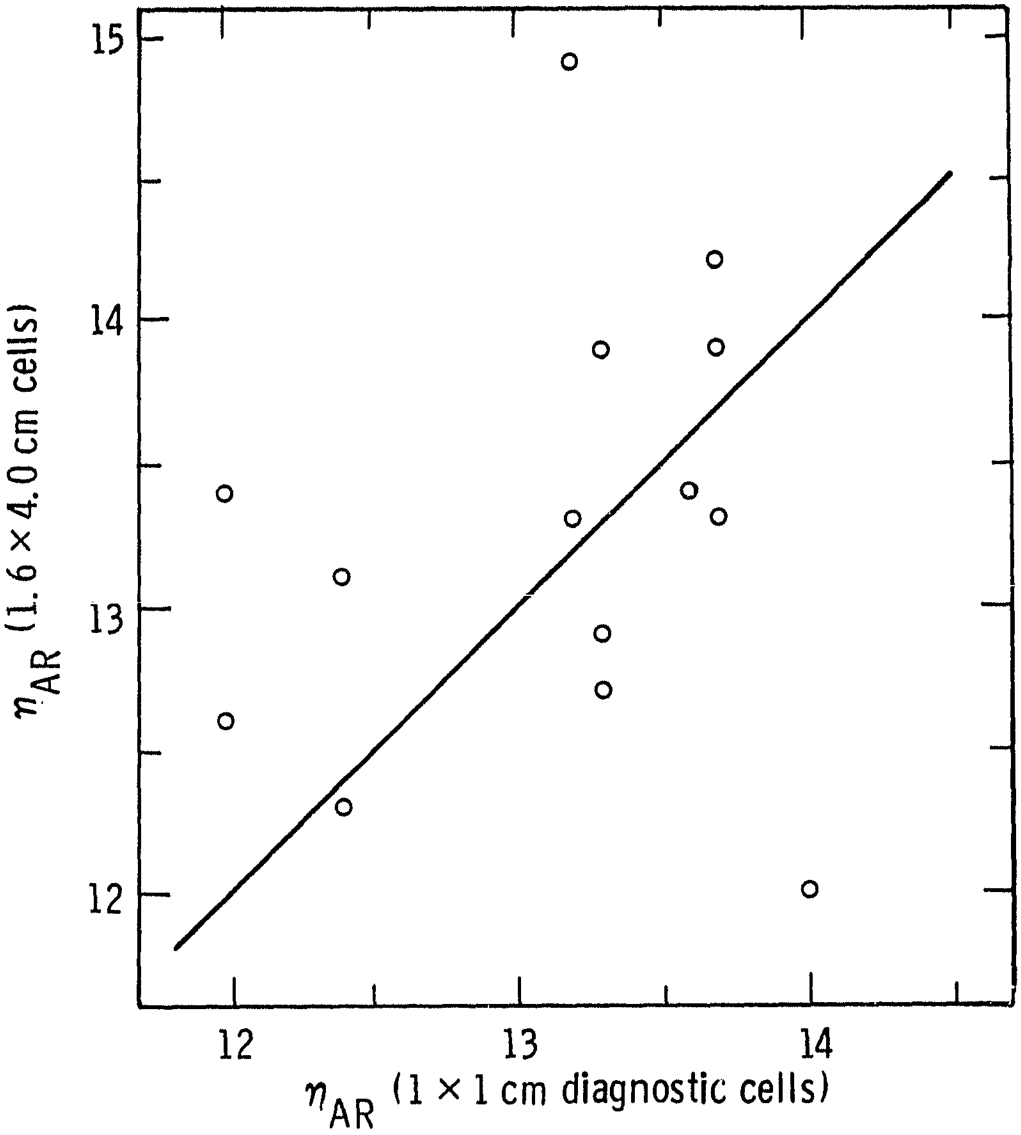

Figure 28 Comparison of cell efficiency for 16x40 mm and 10x10 mm solar cells made on the same web crystals.

ORIGINAL PAGE
BLACK AND WHITE PHOTOGRAPH

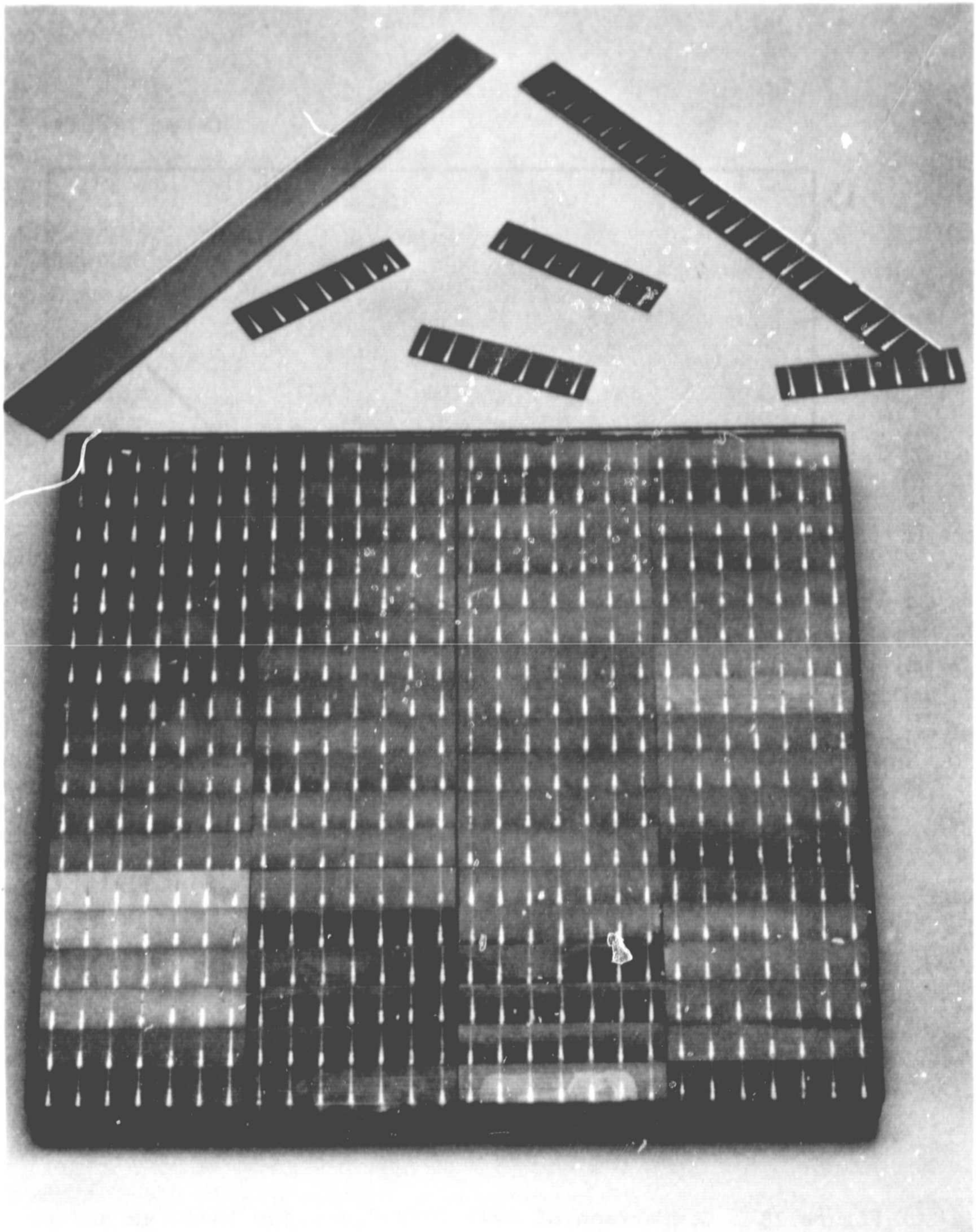

Figure 29 One foot square solar cell module constructed from 72 1.6x7 cm web solar cells connected in series. Also illustrated are web starting material and individual cells.

The general parameters of the cells used in the module were commensurate with the properties of the 10x10 mm and 16x40 mm cells. The distribution of efficiencies for the individual cells is shown as a histogram in Figure 30. The average efficiency of the cells shown in the figure is about 12%, which is slightly lower than the data obtained for the cells in Figure 27; this would indicate that some fine tuning of the processing may still be required.

The performance of the assembled modules was in very good agreement with the cell performance: 10.44, 11.24, 10.93 and 11.01% as measured at the NASA Lewis Research Center. The excellent packing factor of the rectangular cells thus gives an average module efficiency of 10.91% or 91% of the average cell efficiency. Dendritic web solar cells are capable of being used in a satisfactory power-generating module.

3.7 Equipment Design

All of the web growth developments of this program have been incorporated in a fully detailed engineering design. The furnaces shown in Figure 31 are similar in appearance to the new design. Unlike the furnaces shown in the photograph, however, the new design includes critical developments such as melt level sensing, continuous melt replenishment and melt level control. The fully detailed drawings of this design are given in the appendix and are identified as Design Specification D903190.

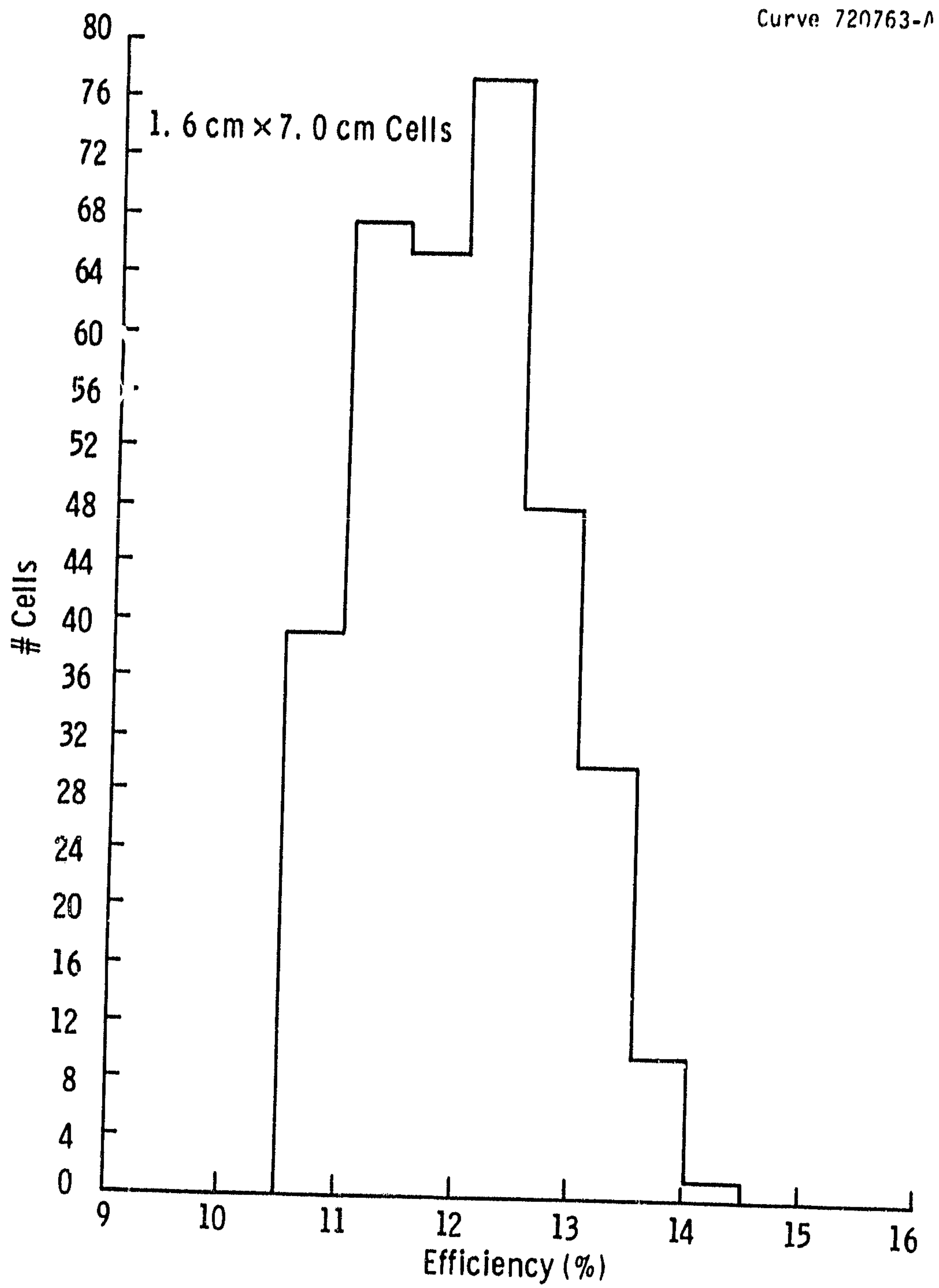

Figure 30 Efficiency distribution of cells used in demonstration modules.

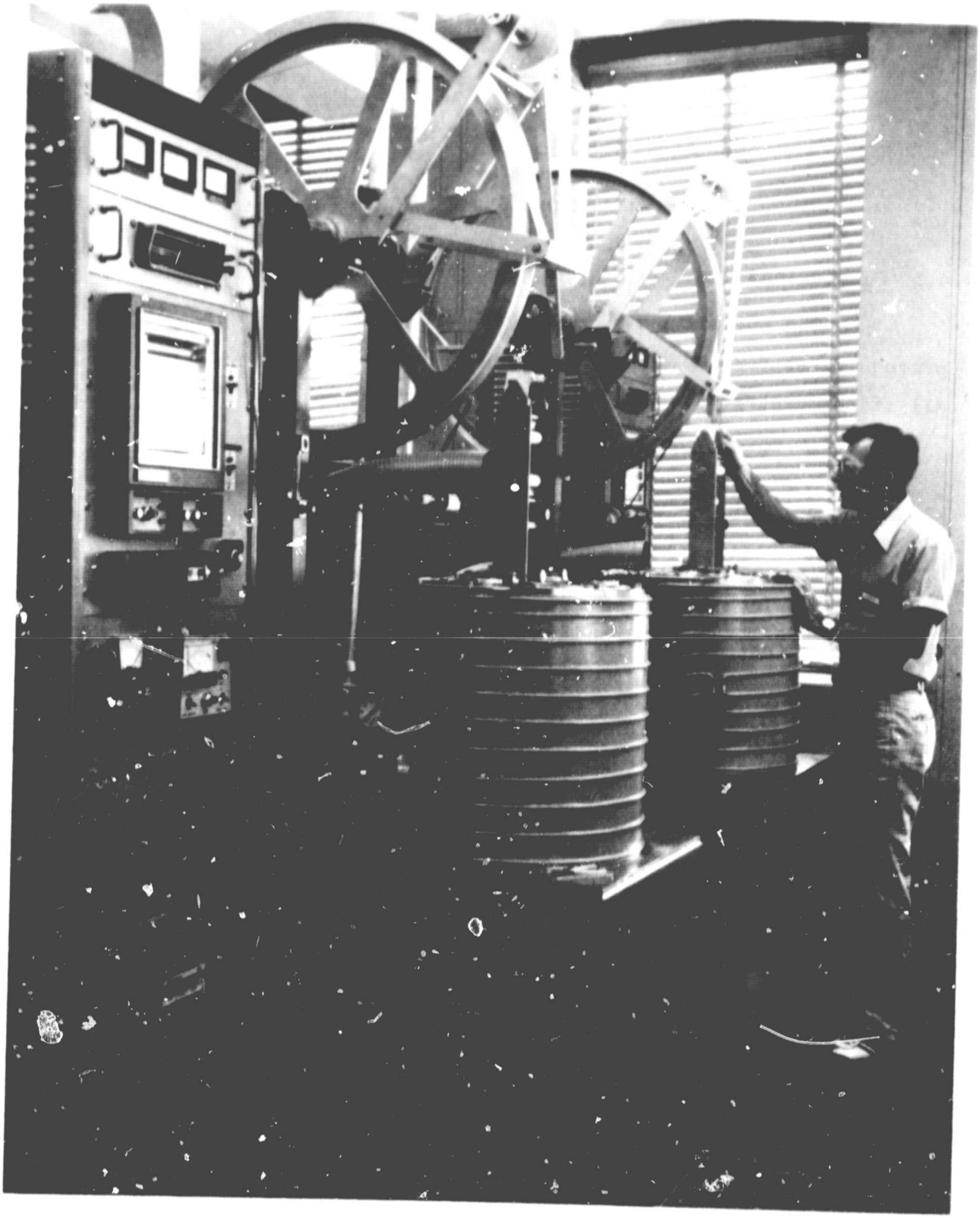

Figure 31 Second generation silicon web furnaces.

4. CONCLUSIONS AND RECOMMENDATIONS

4.1 Conclusions

The overall purpose of this program was to demonstrate the prerequisites for the technology readiness of the silicon web process. All of the contract goals have been met, the principal goals being:

- Web growth area throughput rate of 25 cm^2/min.
- Long-term continuous melt replenishment.
- Semi-automatic growth.
- Cell efficiency $\geq$ 15% AM1.

4.2 Recommendations

As a consequence of all prerequisites for technology readiness having been achieved, the prime recommendation is to proceed with a program to demonstrate technology readiness. The principal effort of such a program should be to design, build and operate an automated web growth apparatus to demonstrate performance sufficient to meet or exceed the DOE/JPL 1986 goal. The design portion of the recommended effort should be based upon, and be a continuation of, the design prepared under this contract.

5. NEW TECHNOLOGY

New technology items developed during this program are:

1) Thermal design for an elongated susceptor, crucible, melt and shield system for growth of wide web crystals.
2) New apparatus having greater capacity for web growth than with prior technology.
3) Method for continuous melt replenishment during web growth.
4) Method for melt level sensing.
5) Method for controlling temperature gradients in the susceptor, crucible and melt during dendritic web growth.
6) Barrier for use in melt replenishment for silicon web growth.

6. REFERENCES

1. C. S. Duncan, et al., Silicon Web Process Development, Annual Report, DOE/JPL 954654-80/11, April (1980).

2. C. S. Duncan, et al., Silicon Web Process Development, Annual Report DOE/JPL 954654-79/2, April (1979).

3. C. S. Duncan, et al., Silicon Web Process Development, Annual Report, DOE/JPL 954654-78/2, April (1978).

4. R. W. Aster and R. G. Chamberlain, Interim Price Estimation Guidelines: A Precursor and an Adjunct to SAMICS III, JPL 5101-33, Sept. 10, 1977.

5. C. S. Duncan, et al., Silicon Web Process Development Quarterly Report, DOE/JPL 965654-80/10 December (1979).

6. C. S. Duncan, et al. Silicon Web Process Development, Quarterly Report, DOE/JPL 954654-80/13, August (1980).

7. C. S. Duncan, et al., Silicon Web Process Development, Quarterly Report DOE/JPL-954654-80/12 June (1980).

8. A good review of the LSA Task I impurity study is given in R. H. Hopkins et al., "Effects of Impurities and Processing on Silicon Solar Cells, Phase III Summary and Seventeenth Quarterly Report, Vol. 1: Characterization Methods for Impurities in Silicon and Impurity Effects Data Base; Vol.2: Analysis of Impurity Behavior." DOE/JPL-954331-80/9.

9. R. G. Seidensticker, R. H. Hopkins and A. M. Stewart, "Solute Partioning during Silicon Dendritic Web Growth," J. Crystal Growth 46, 51 (1979).

10. See Ref. 8, V2, p. 131.

11. See Ref. 8, V1, p. 17.

REFERENCES (CONT'D)

12. H. Kodera, "Diffusion Coefficients of Impurities in Silicon Melt," Japan. J. Appl. Phys. 2, p. 212 (1963).

13. R. H. Hopkins et al., "Crystal Growth Considerations in the Use of 'Solar Grade' Silicon," J. Crystal Growth 42, 493 (1977).

14. See Ref. 5, V2, 42.

15. C. S. Duncan, et al., "Development of Processes for the Production of Low Cost Silicon Dendritic Web for Solar Cells," Conference Record, 14th IEEE Photovoltaic Specialists Conference, IEEE, New York, 25 (1980).

16. R. G. Seidensticker, L. Scudder and H. W. Brandhorst, Jr., "Dendritic Web: A Viable Material for Silicon Solar Cells," Conference Record, 11th IEEE Photovoltaic Specialists Conference, p. 299. IEEE, New York (1975).

17. R. B. Campbell et al., Final Report for Contract 954873 DOE/JPL 945873-80.

7. ACKNOWLEDGEMENTS

We would like to thank P. A. Piotrowski, H. C. Foust, L. G. Stampahar, E. P. A. Metz, W. B. Stickel, J. M. Polito, A. M. Stewart, J. P. Fello, and C. H. Lynn for their contributions to the web growth studies and P. Rai-Choudhury, R. B. Campbell, E. J. Seman, J. B. McNally, W. Cifone, D. N. Schmidt, and H. F. Abt for the processing and testing of the web solar cells. The report typescript was prepared by D. Todd and edited by G. Law, and we gratefully acknowledge their important contribution to this effort.

8. APPENDIX

Silicon Web Furnace Design Specification D903190.

ORIGINAL PAGE IS
OF POOR QUALITY

ROUTING					
FIREPROOF VAULT					

DRAWING LIST

INDEX	LINE	TITLE OF DRAWING	DRAWING NO.	MULTIPLIER	ITEMS OR STYLE NO.	CHECKED	DATE CHECKED
	1	GEN ASSY	1290J44				
	2	GEN ASSY	1290J45				
	3						
	4						
	5	FRAME ASSY	639F605				
	6	FURNACE WELDMT.	639F606				
	7	TOP COVER PLATE ASSY	639F607				
	8	TOP COVER PLATE DET.	639F608				
	9	BOT HEAT SHIELD COIL LIFT DETAILS	639F609				
	10	PELLET FEEDER ASSY	639F611				
	11						
	12						
	13	WEB GUIDE DETAILS	8536D11				
	14	HEAT SHIELD & OVAL SUSCEPTOR HEAT SHIELD	8536D12				
	15	LASER VEE BLOCK & GUIDE DETAILS	8536D13				
	16	BELLOWS DET. & WINDOW DET.	8536D14				
	17	XYZ POST WELDM'T & WEB GUIDE DET.	8536D15				
	18	LASER HOLDER ASSY	8536D16				
	19	LENS & DETECTOR ASSY	8536D17				
	20	CURVED HT. SHIELD ASSY	8536D18				
	21	PORTHOLE FLANG ASSY	8536D19				
	22	PORTHOLE FLG, & WINDOW DET.	8536D20				
	23	LASER HOLDER WELD'MT	8536D21				
	24	LENS & DETECTOR FASTENER DET.	8536D22				
	25	LENS & DETECTOR WELD'MT	8536D23				
	26	CURVED HT. SHIELD DET.	8536D24				
	27	BASE PLATE DET.	8536D25				
	28	BOT COVER PLATE DET.	8536D26				
	29	DETALS BOT. COVER PLATE	8536D27				

STOCK ORDER (1ST S.O. ON WHICH INF. HAS BEEN SENT TO SHOP) | LIST FINISH DATA. IN SPECIFYING THIS D NO. ON A STOCK ORDER THE ENGINEER MUST GIVE: —

NAME OF APPARATUS SILICON WEB FURNACE

ENGR. S. DUNCAN

CHECKED BY AND DATE TPG 10-29-80

DESIGN SPEC. D 903190

SUB. LETTER	SUB. LETTER	SUB. LETTER	SUB. LETTER	SUB. LETTER
SUB. LETTER	SUB. LETTER	SUB-LETTER	SUB. LETTER	SUB. LETTER

WESTINGHOUSE FORM 6541 J

PAGE 1 OF 3

ORIGINAL PAGE IS OF POOR QUALITY

ROUTING						
FIRE PROOF VAULT						

DRAWING LIST

INDEX	LINE	TITLE OF DRAWING	DRAWING NO.	MULTI-PLIER	ITEMS OR STYLE NO.	CHECKED	DATE CHECKED
	1	XYZ SUPPORT WELD'MT	8536D28				
	2	SENSOR SUB ASSY	8536D29				
	3	WEB WITHDRAWAL DUCT DET.	8536D30				
	4	RIBBON GUIDE ROLL DET.	8536D31				
	5	DET. SENSOR & PULLEY	8536D32				
	6	TOP ROLLER SYSTEM DET	8536D33				
	7	COIL DETS. OVAL SUSCEPTOR	8536D34				
	8	TAPE REEL DETAILS	8536D35				
	9	POST & BASE PL. DET.	8536D36				
	10	REWIND BRACKET LIFTER, SHOLDER SCR. DET.	8536D37				
	11	POST HSG. & DUCT GUIDE ASSY	8536D38				
	12	DUCT DETAILS	8536D39				
	13	RF & VAC. ADAPTER DET.	8536D40				
	14	DRIVE MOTOR DETAILS	8536D41				
	15	TAPE REEL DETAILS	8536D42				
	16						
	17	OVAL SUSCEPTOR DETAILS	8536D44				
	18	OVAL SHIELD & SUPPORT PLATE DET.	8536D45				
	19	OVAL WORK COIL ASSY	8536D46				
	20	LID HOLDING FIXTURE	8536D47				
	21	R.F. FITTING DET. (BRASS)	8536D48				
	22	CAPACITOR COVER ASSY	8536D49				
	23	OVAL SUSCEPTOR LID & SHIELD DET.	8536D50				
	24	(PELLET) TOP COVER PL. MTR. SPACER DET.	8536D84				
	25	BOTTOM COVER PLATE DET. (PELLET FEEDER)	8536D85				
	26	PELLET FEEDER DET	8536D86				
	27	PELLET DROPPER DETS.	8536D87				
	28	PELLET FEEDER BRKT. ASSY	8536D88				
	29	PELLET DROPPER DETS.	8536D89				

STOCK ORDER (1ST S.O. ON WHICH INF. HAS BEEN SENT TO SHOP) | IDENTIFYING DATA: IN SPECIFYING THIS D NO. ON A STOCK ORDER THE ENGINEER MUST GIVE: —

NAME OF APPARATUS SILICON WEB FURNACE

ENGR. S. DUNCAN

CHECKED BY AND DATE TPG 10-29-80

DESIGN SPEC. D 903190

WESTINGHOUSE FORM 6541 J

PAGE 2 OF 3

SUB. LETTER	SUB. LETTER	SUB. LETTER	SUB. LETTER	SUB. LETTER
SUB. LETTER	SUB. LETTER	SUB- LETTER	SUB. LETTER	SUB. LETTER

ORIGINAL PAGE IS
OF POOR QUALITY

ROUTING					
FIREPROOF VAULT					

DRAWING LIST

INDEX	LINE	TITLE OF DRAWING	DRAWING NO.	MULTI-PLIER	ITEMS OR STYLE NO.	CHECKED	DATE CHECKED
	1						
	2						
	3						
	4						
	5						
	6	FINGER GUIDE & ADJ. SCR ASSY	5592C28				
	7	STORAGE REEL WELD'MT	5592C29				
	8	STORAG REEL SHAFT DET.	5592C30				
	9	OVAL WORK COIL DET.	5592C31				
	10	ARGON DISTRIBUTION MANIFOLD ASSY	5592C32				
	11	TAPE REEL BRACKET	5592C33				
	12	SIDE HEAT SHIELDS (OVAL)	5592C34				
	13	CAPACITOR, CONNECTING STRAP DET	5592C35				
	14	PROBE HOLES ROUND & OVAL SUSCEPTOR	5592C36				
	15	GUIDE DET. PELLET FDR.	5592C52				
	16	HOUSING DET. PELLET FDR.	5592C57				
	17						
	18						
	19	OVAL CRUCIBLE DET.	1691B62				
	20	OVAL CRUCIBLE ASSY.	1711B33				
	21	DOOR SUB ASSY PELLET FEEDER	1713B80				
	22						
	23						
	24						
	25	PELLET DROPPER	7727A96				
	26						
	27						
	28						
	29						

STOCK ORDER (1ST S.O. ON WHICH INF. HAS BEEN SENT TO SHOP) | IDENTIFYING DATA: IN SPECIFYING THIS D NO. ON A STOCK ORDER THE ENGINEER MUST GIVE: —

NAME OF APPARATUS SILICON WEB FURNACE

ENGR. S. DUNCAN

CHECKED BY AND DATE TPG 10-29-80

DESIGN SPEC. D 903190

SUB. LETTER	SUB. LETTER	SUB. LETTER	SUB. LETTER	SUB. LETTER

WESTINGHOUSE FORM 6541 J

PAGE 3 OF 3

SUB. LETTER	SUB. LETTER	SUB- LETTER	SUB. LETTER	SUB. LETTER

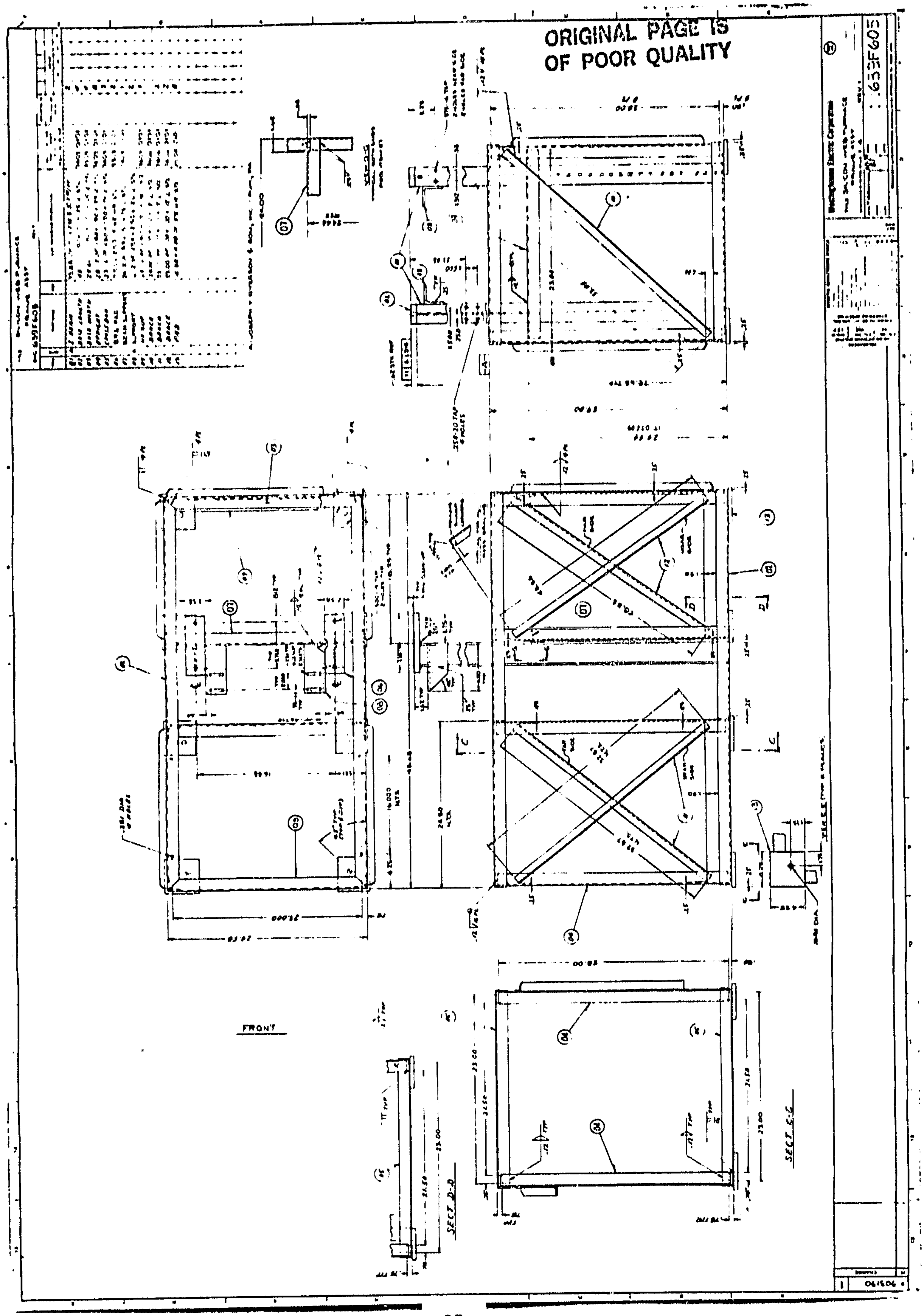
FRONT
SECT C-C
SECT D-D
Westinghouse Electric Corporation
633F605

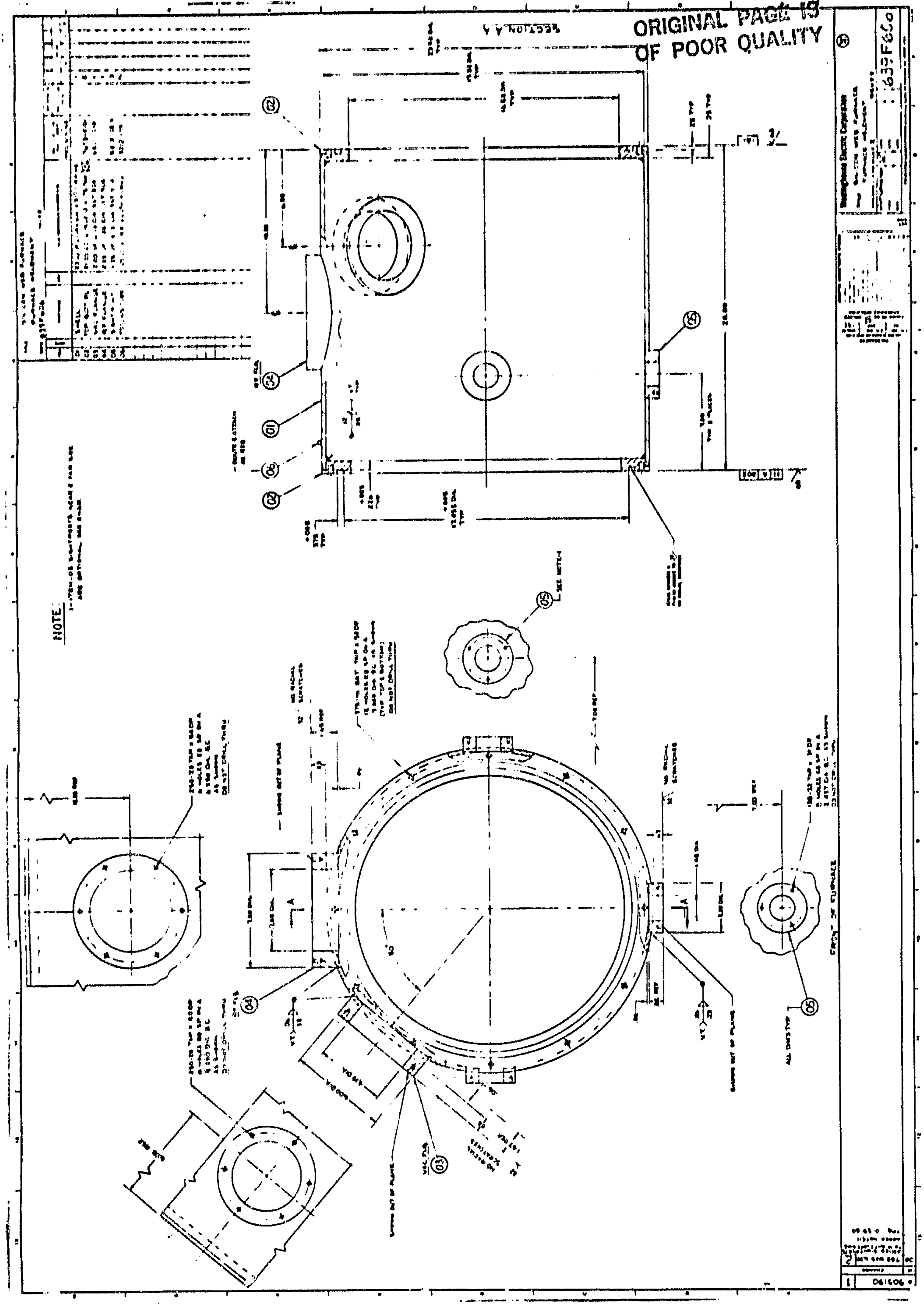

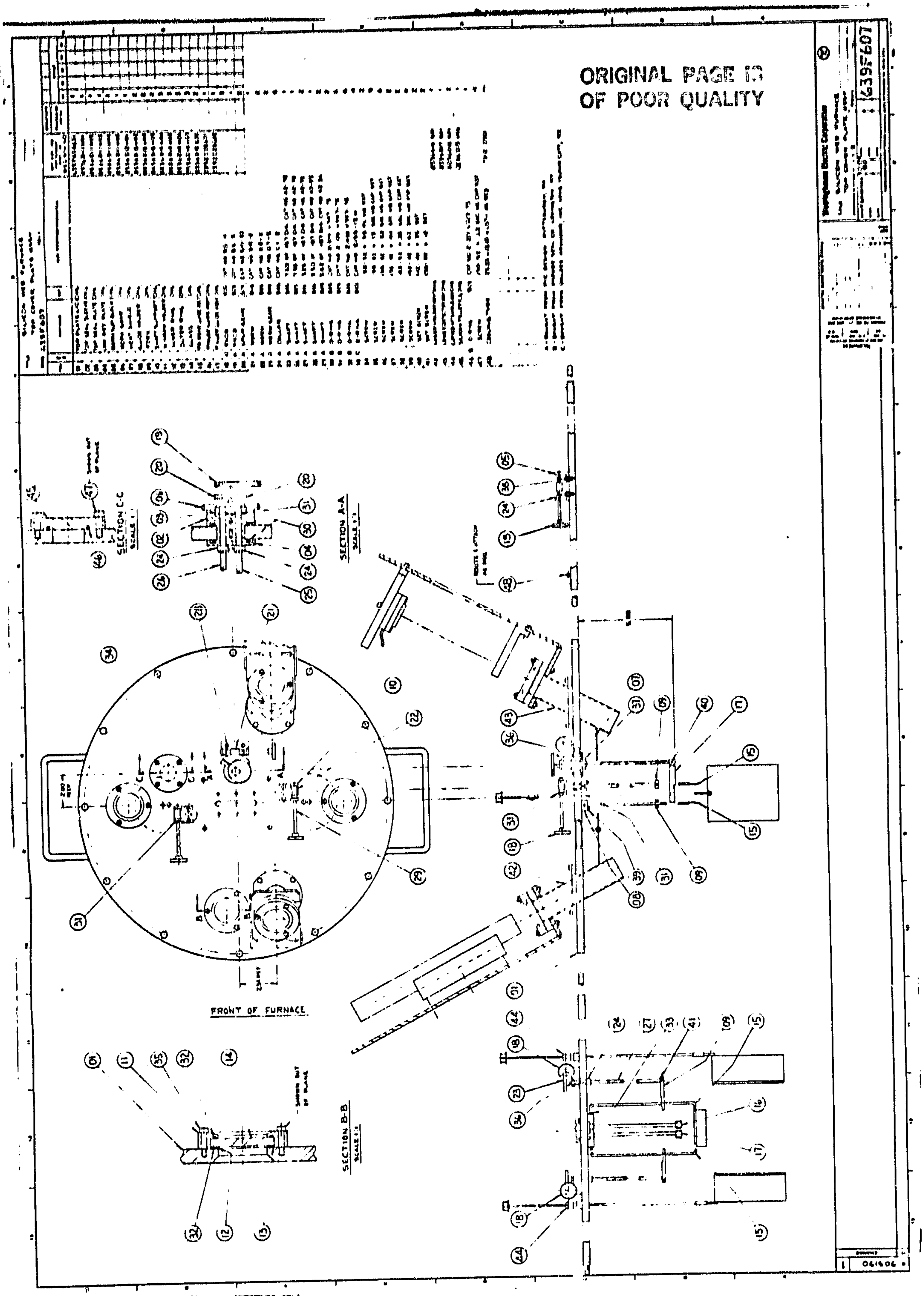
SECTION A-A
SECTION B-B
SECTION C-C
FRONT OF FURNACE
639F607

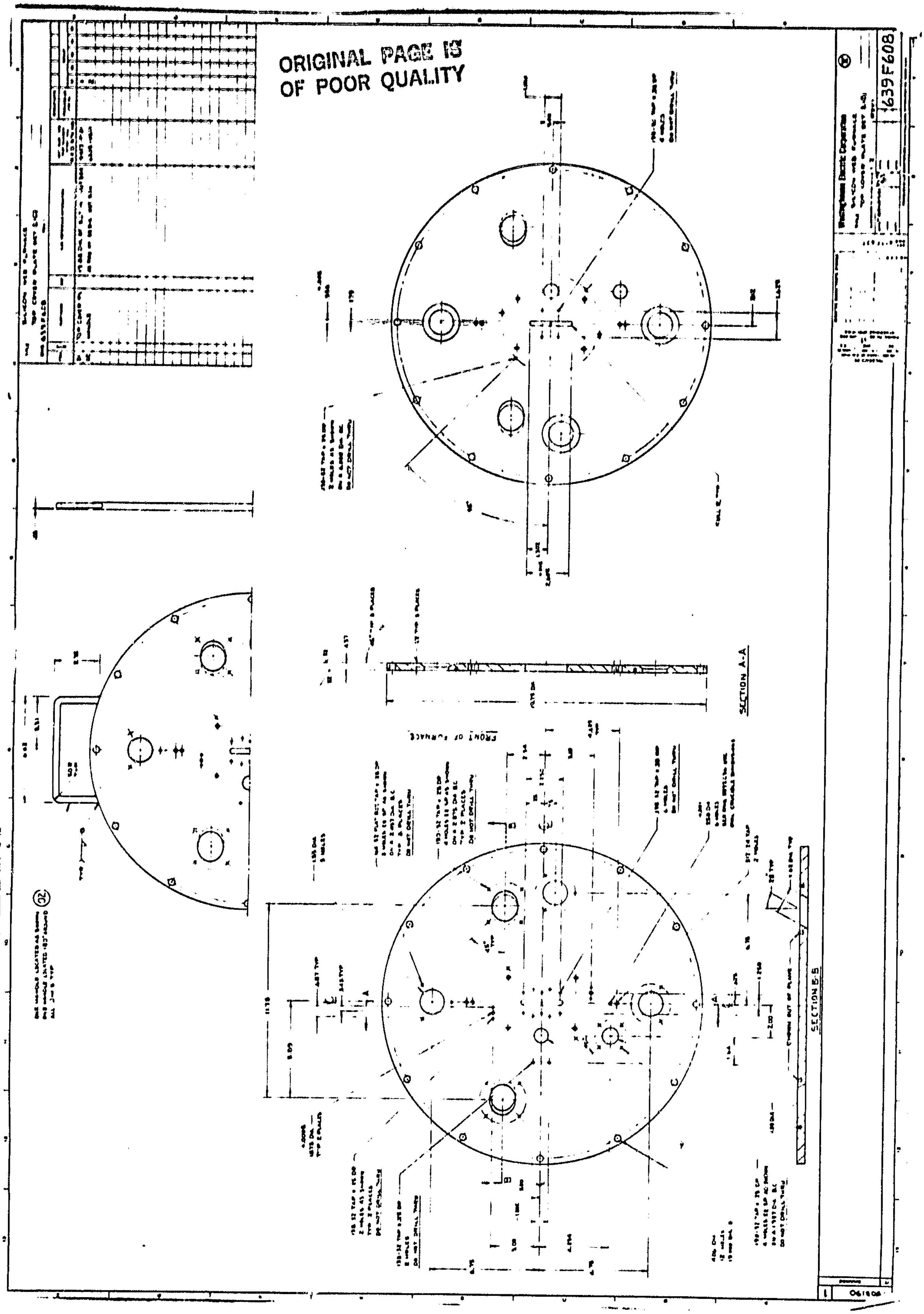
639F608
SECTION A-A
SECTION B-B
FRONT OF FURNACE

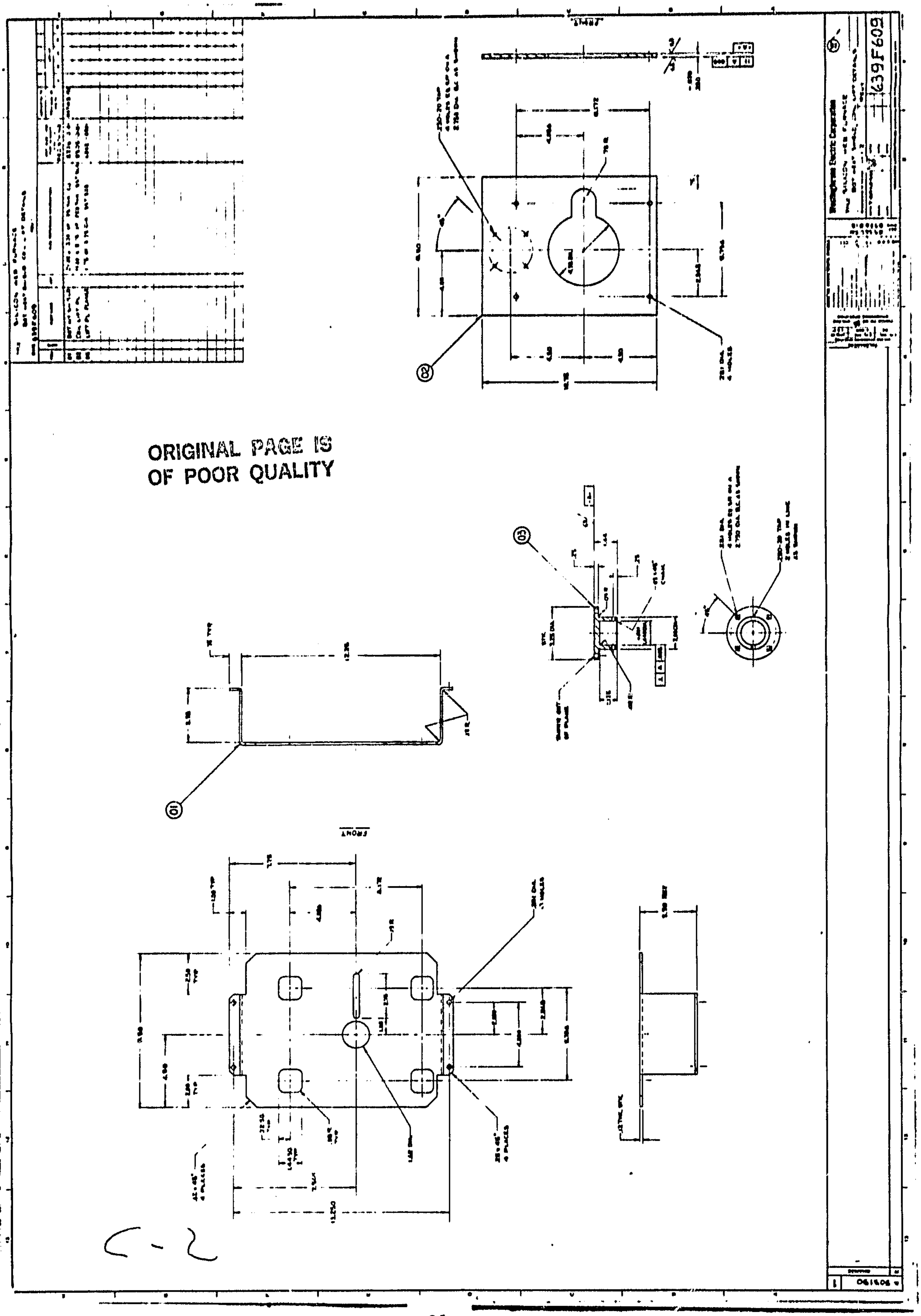

ORIGINAL PAGE IS
OF POOR QUALITY

C-2

ORIGINAL PAGE IS
OF POOR QUALITY

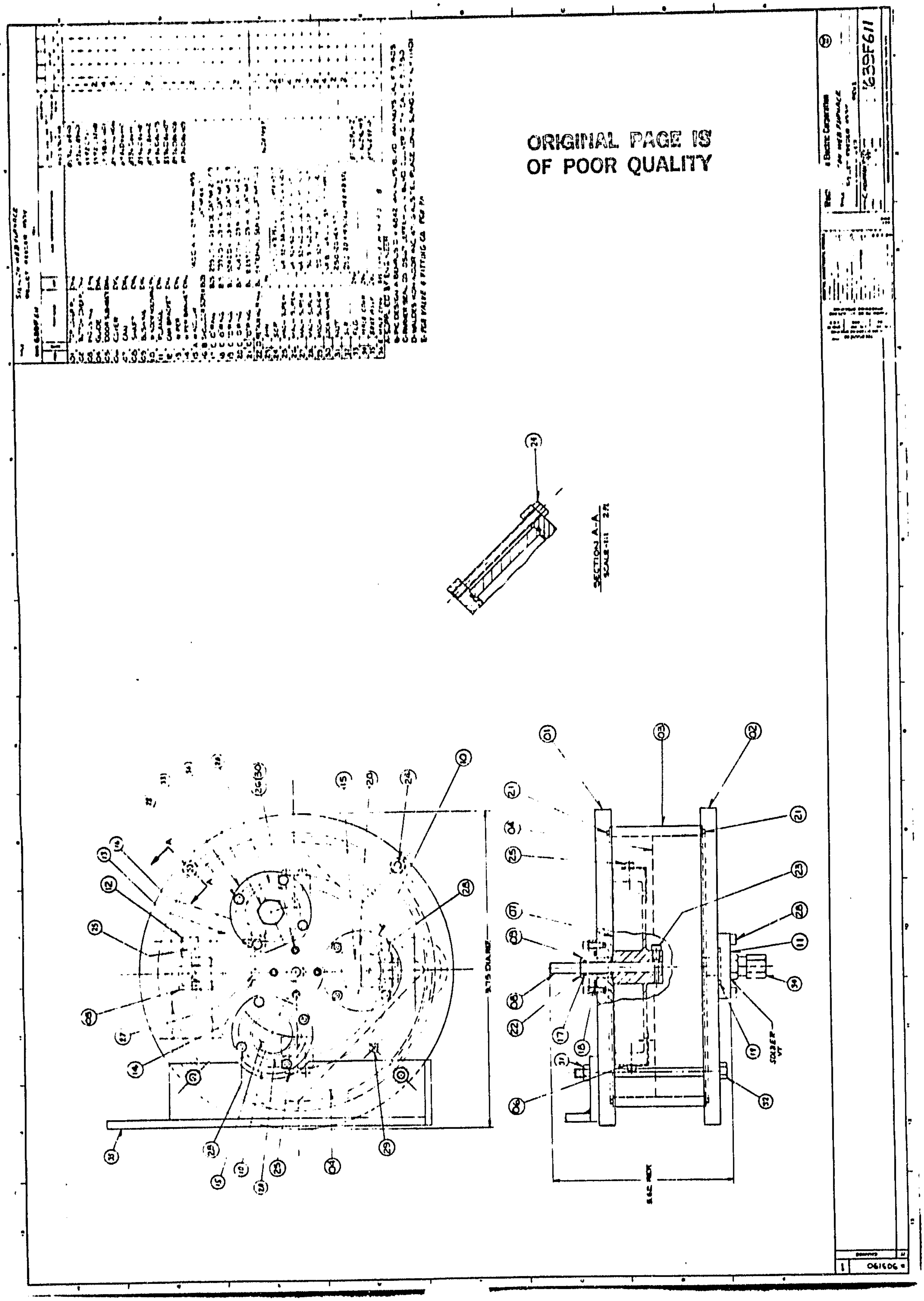

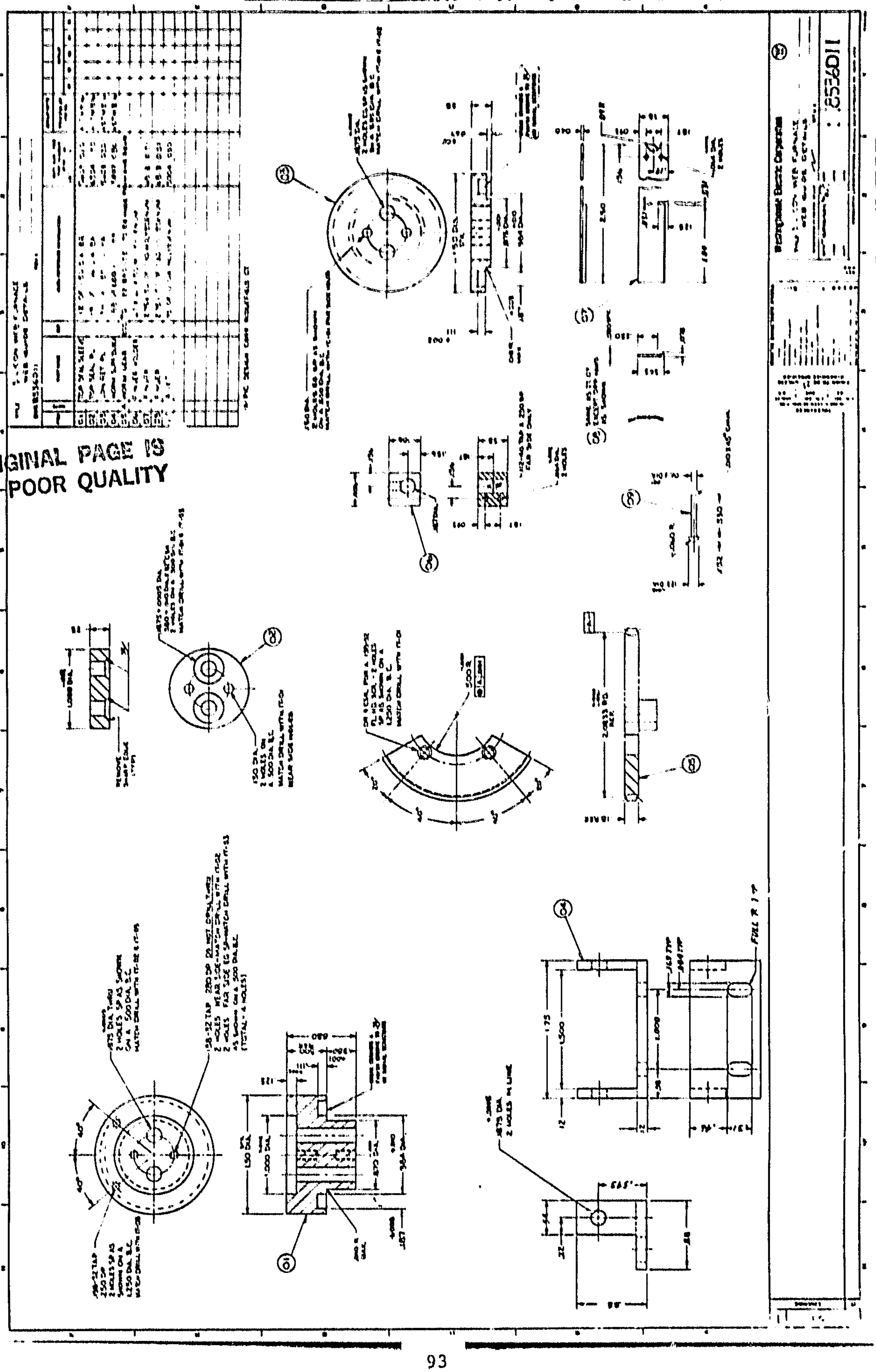

ORIGINAL PAGE IS
OF POOR QUALITY

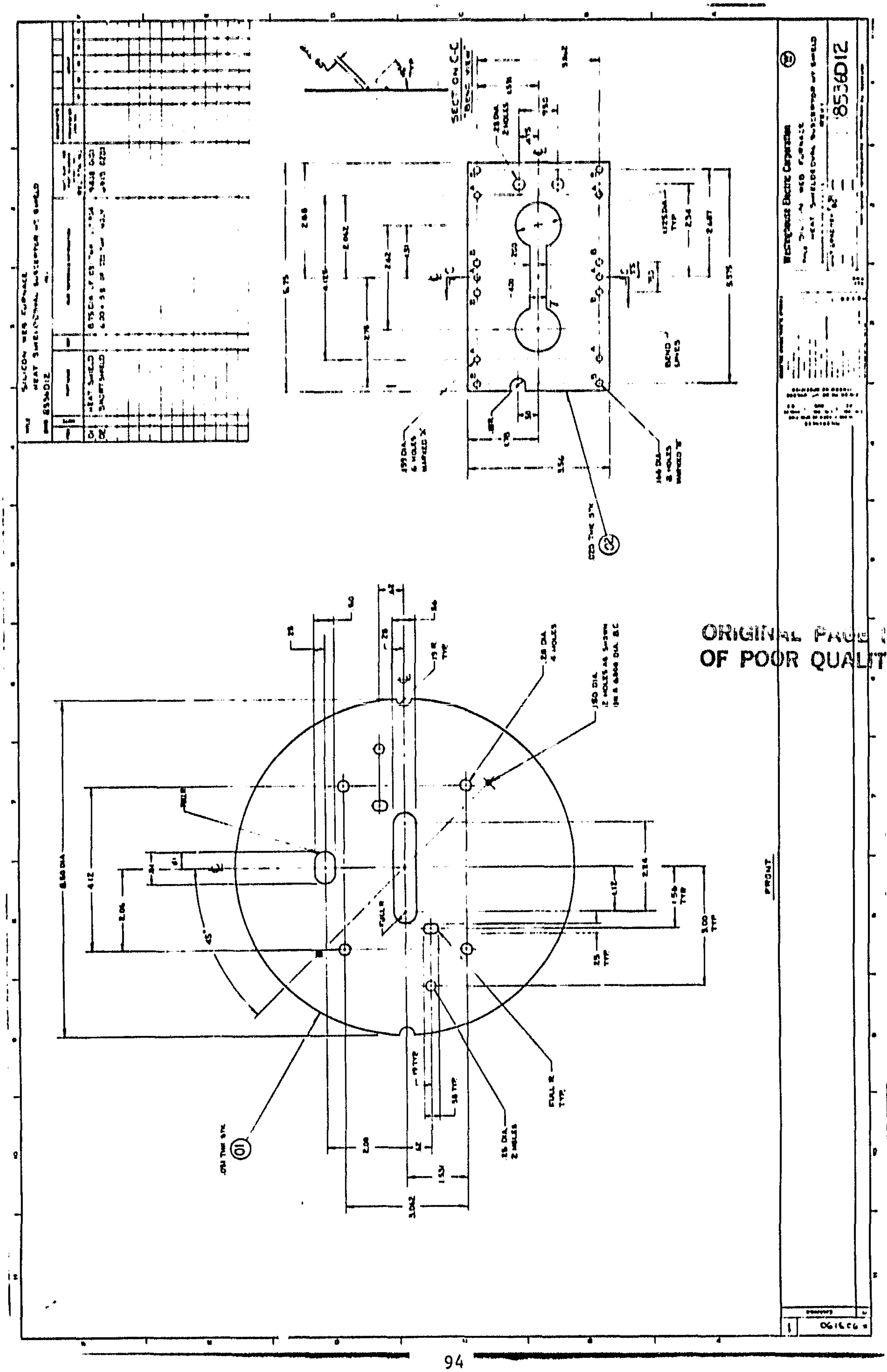

ORIGINAL PAGE IS
OF POOR QUALITY

ORIGINAL PAGE IS
OF POOR QUALITY

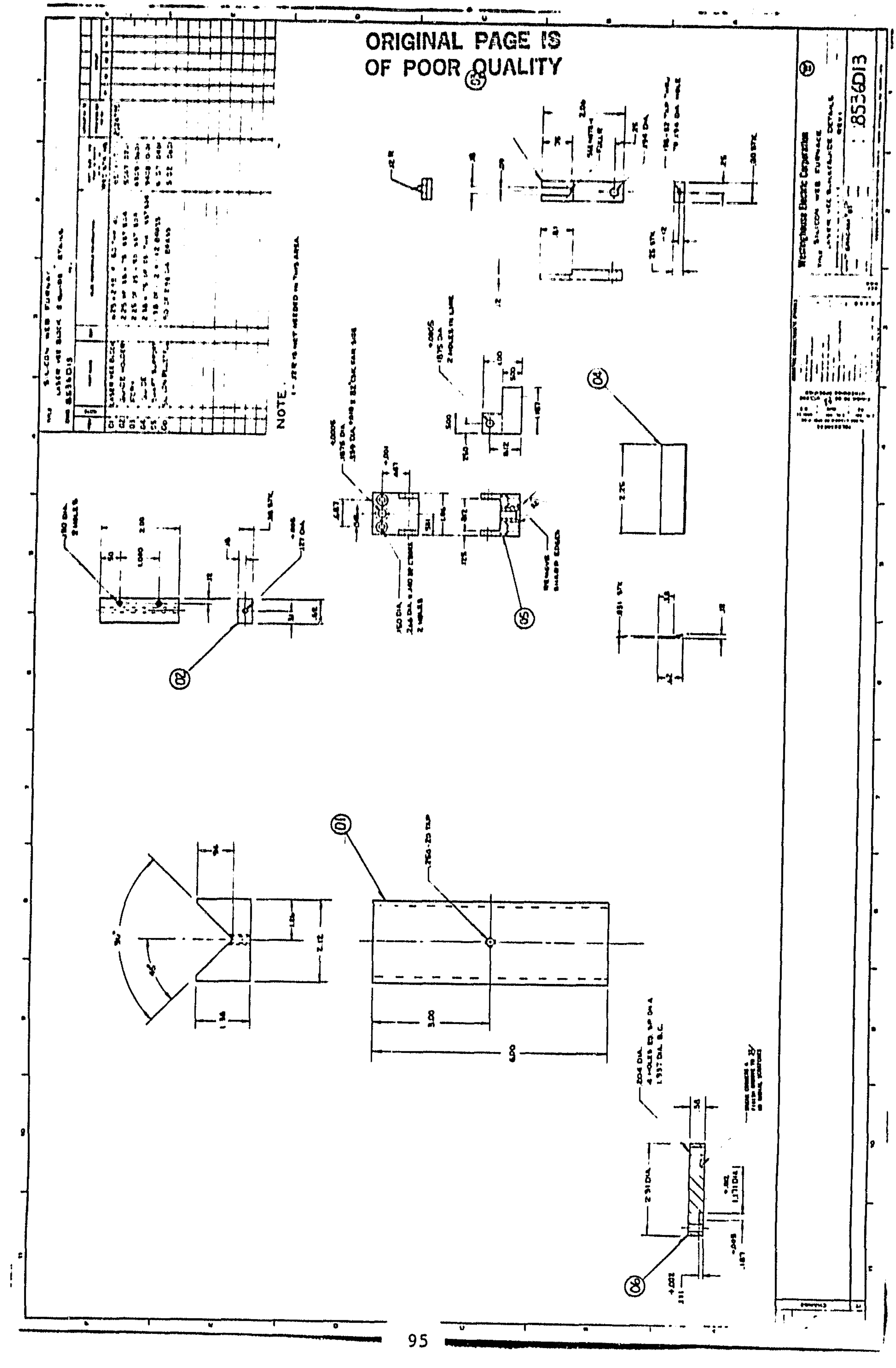

ORIGINAL PAGE IS
OF POOR QUALITY

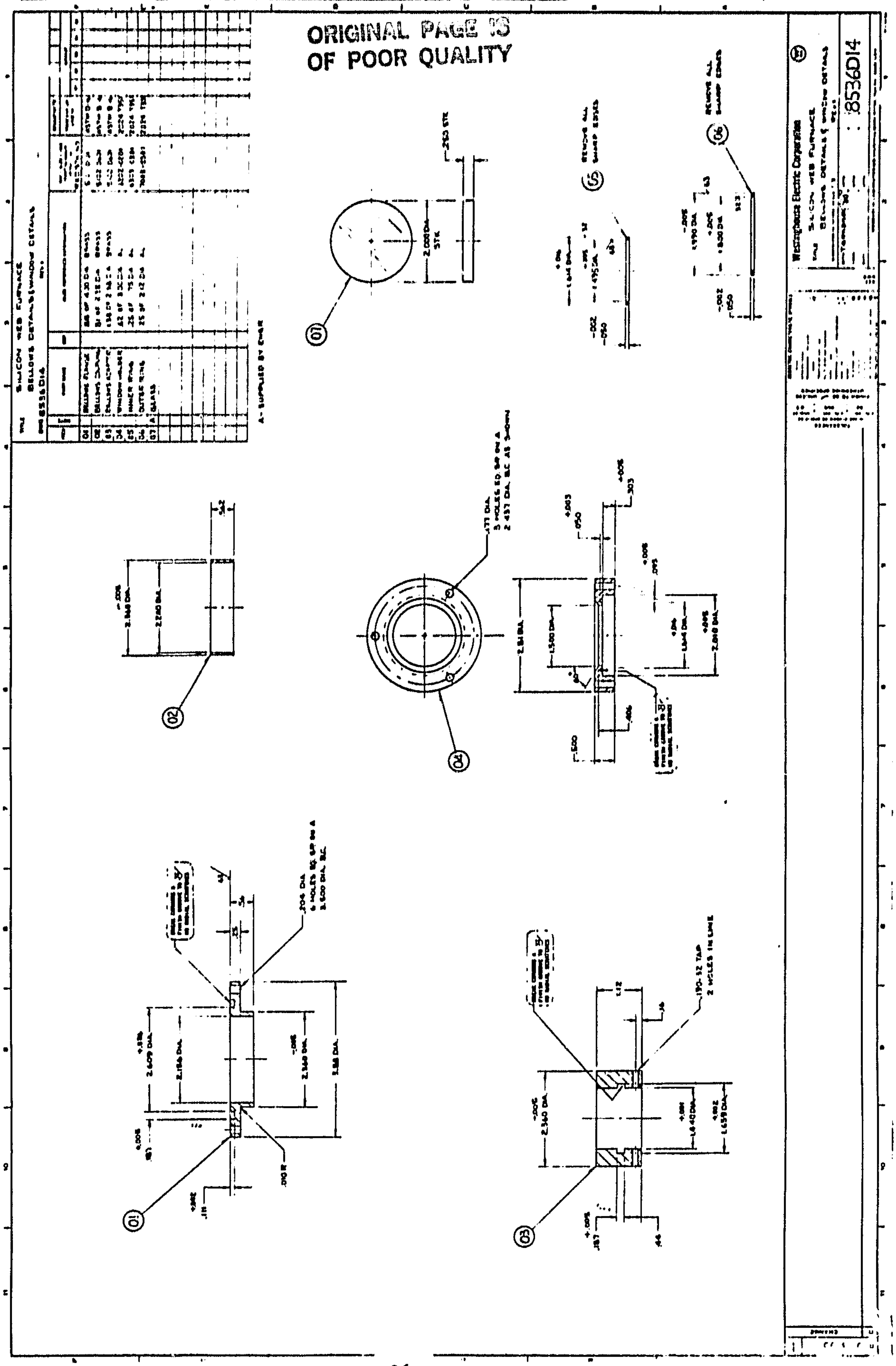

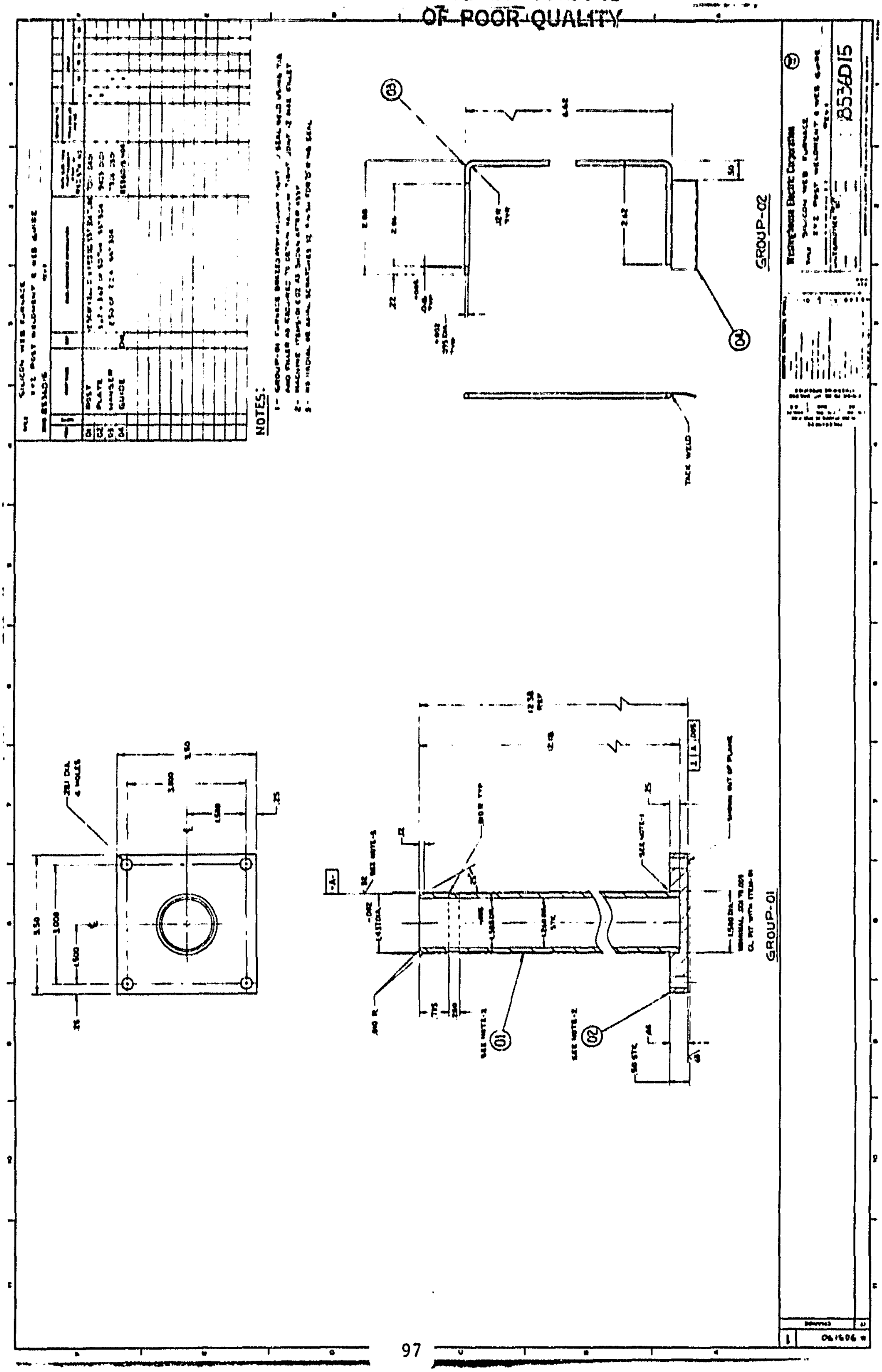
NOTES:
GROUP-01
GROUP-02
TACK WELD
8536D15

Item	Code	Part name		Description	Drawing no.		Group 01				
01		LASER PORT FLA.	DWG		8536D[illegible]		1				
02		LASER HOLDER	DWG		8536D22-[illegible]		1				
03		LASER HOLDER BLOCK	DWG		8536C[illegible]		1				
04		WINDOW HOLDER	DWG		8536D2[illegible]		1				
05		GLASS	DWG		8536D[illegible]		1				
06		O-RING		CAT NO 2-033 V747 75			2				
07		O-RING		CAT NO 2-223 V747 75			1				
08		SPRING					1				
09		SCREW		.250-20 x .50 SOC HD CAP			1				
10		SCREW		.250-20 x .75 SOC HD CAP			4				
11		SCREW		.190-32 x .50 SOC HD CAP			4				
12		ALL THREAD		.190-32 x .75	[illegible]		3				
13		HEX NUT		.190-32			6				
14	A	LASER		SEE NOTE-1			1				

A- CW RADIATION INC. 101 ZETA DRIVE, PGH., PA. 15238

NOTE:

1- MODEL LSP-2 2 W RANDOMLY POLARIZED REMOTE HEAD LASER SYSTEM WITH CONCENTRIC AND PARALLEL TUBE ALIGNMENT

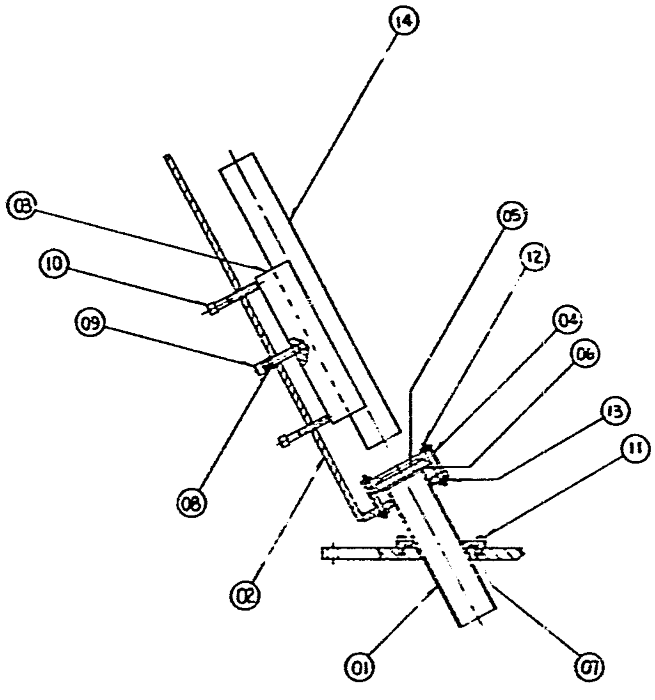

GROUP-01

ORIGINAL PAGE IS OF POOR QUALITY

Westinghouse Electric Corporation

SILICON WEB FURNACE LASER HOLDER ASSY

8536D16

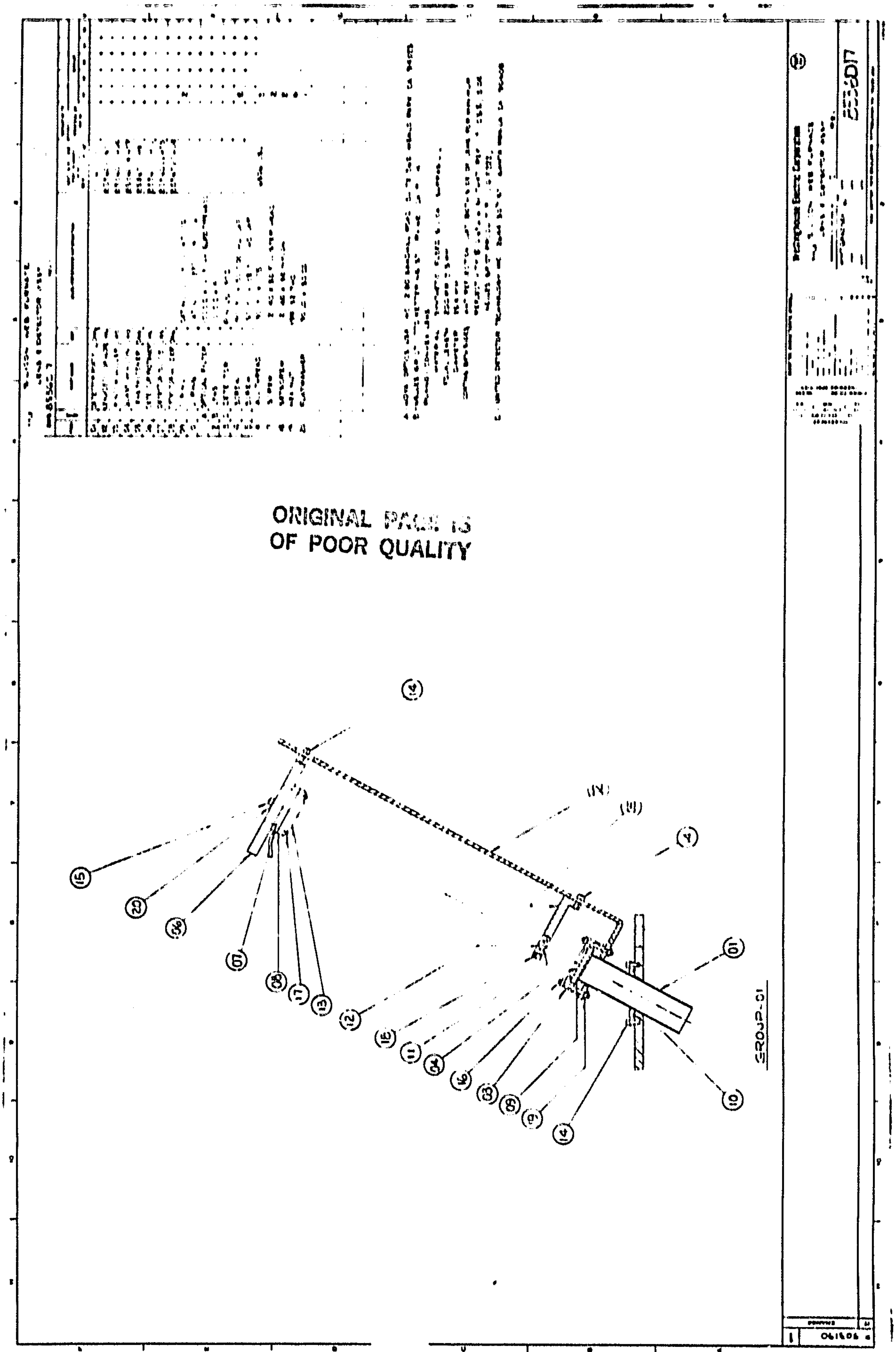
GROUP-01

TITLE	SILICON WEB FURNACE					
	CURVED HEAT SHIELD ASSY					
DWG	8536D18					

Item		Name		Description	Part No.	Qty
01		SHIELD			8536D24H01	1
02		SHIELD RIB			8536D24H02	1
03		POST			8536D24H03	1
04		COUPLING			8536D24H04	1
05		CONTROL ROD			8536D24H05	1
06		O-SEAL CONNECTOR			8536D24H06	1
07		NUT			8536D24H07	1
08		SCREW		[illegible] FILLISTER HD SST		4
09	A	O-RING		CAT NO 2 [illegible]		3
10		KNOB			[illegible]	1

A - PARKER SEAL CO., LEXINGTON, KY

NOTE:

1- REMOVE FRONT AND BACK FERRULE. PLACE O-RINGS (ITEM-09) ON CONTROL ROD (ITEM-05). TIGHTEN NUT (ITEM-07).

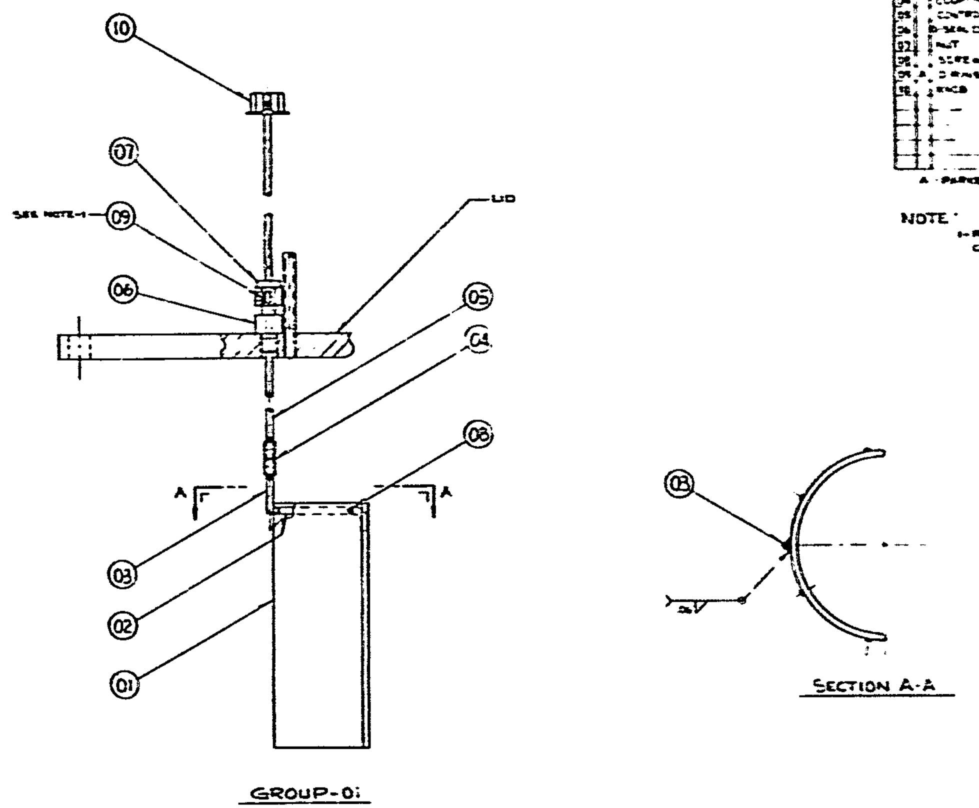

Westinghouse Electric Corporation

TITLE SILICON WEB FURNACE CURVED HEAT SHIELD ASSY

8536D18

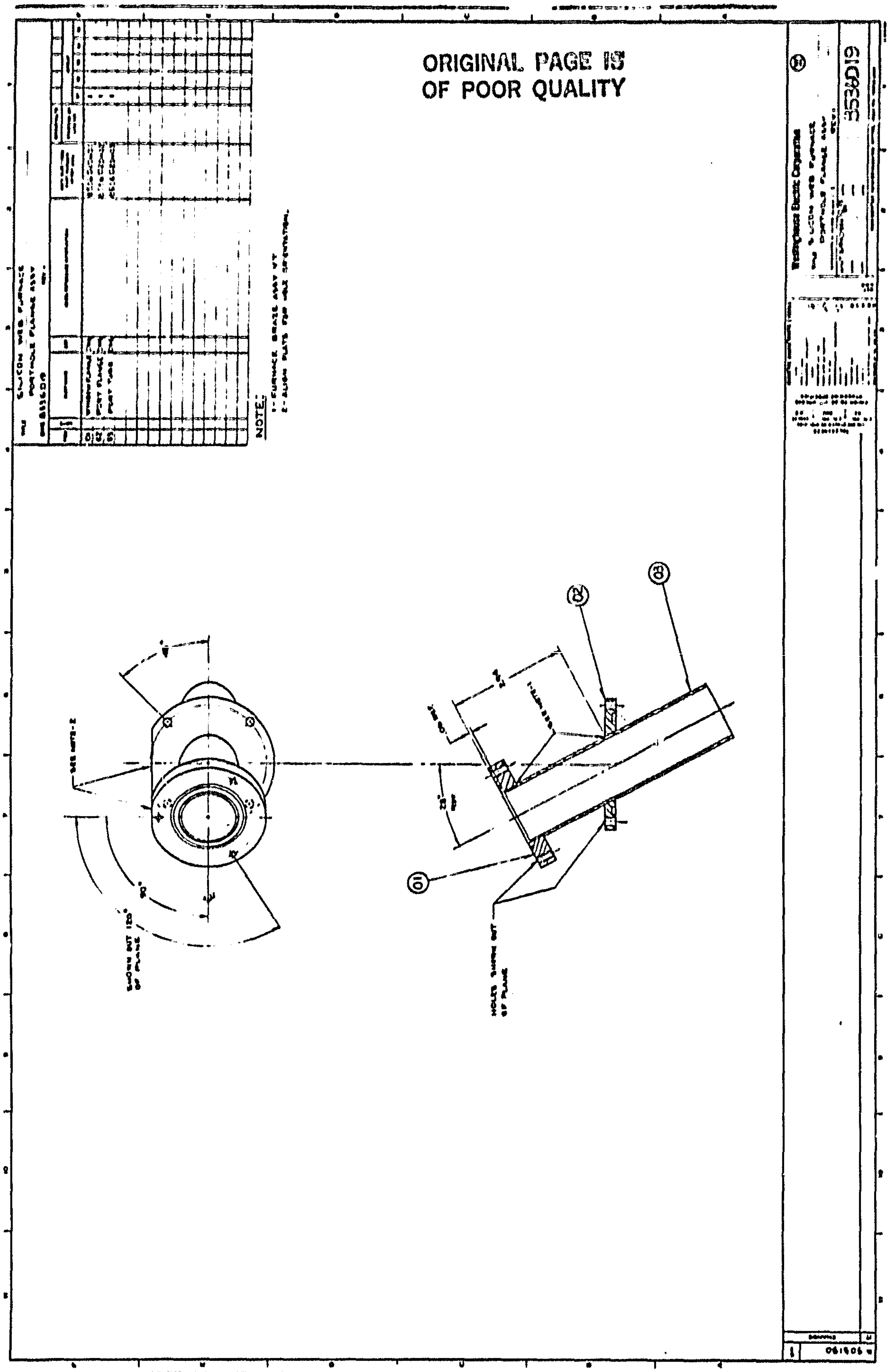
NOTE:
353D19

ORIGINAL PAGE IS
OF POOR QUALITY

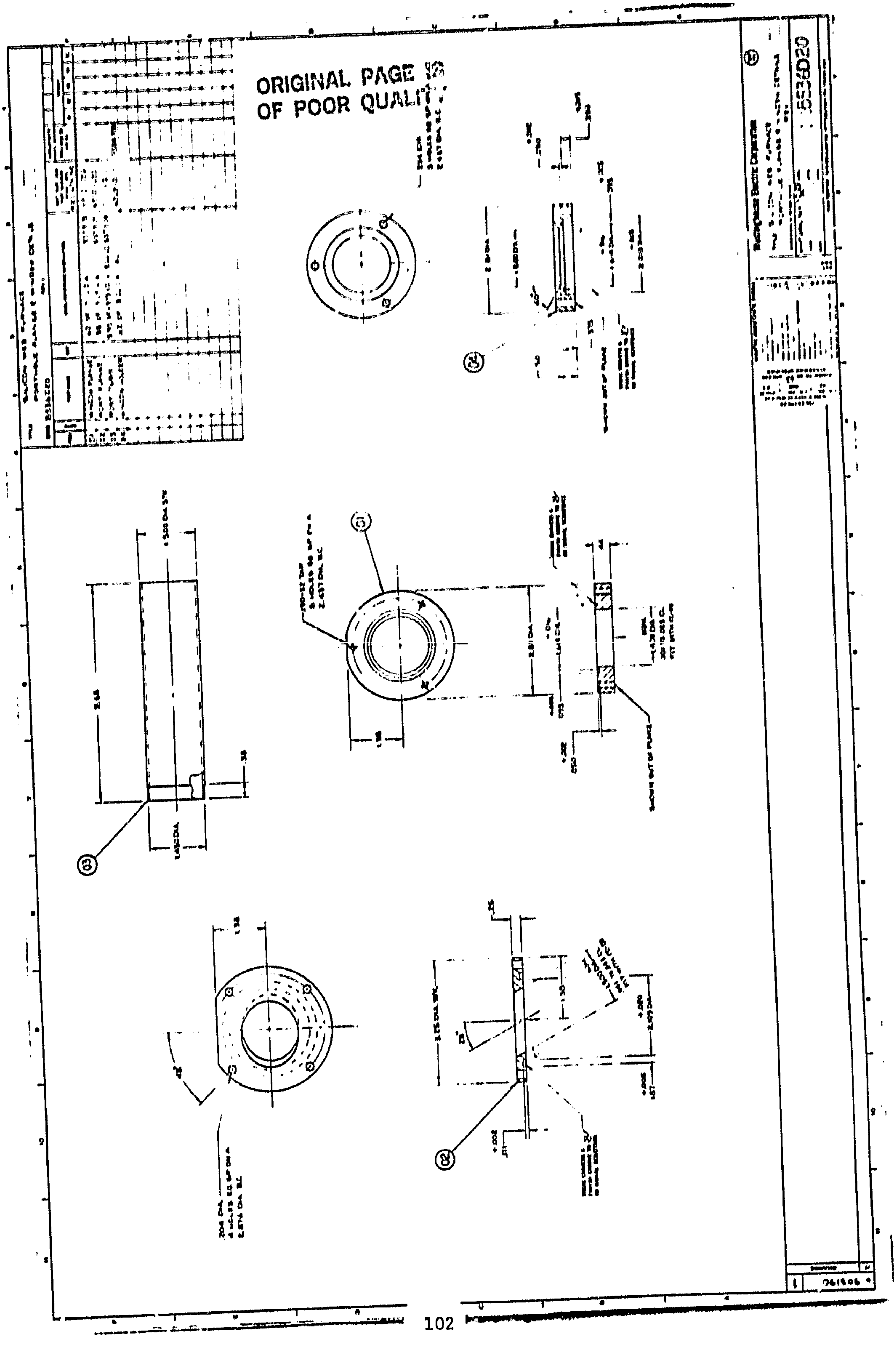

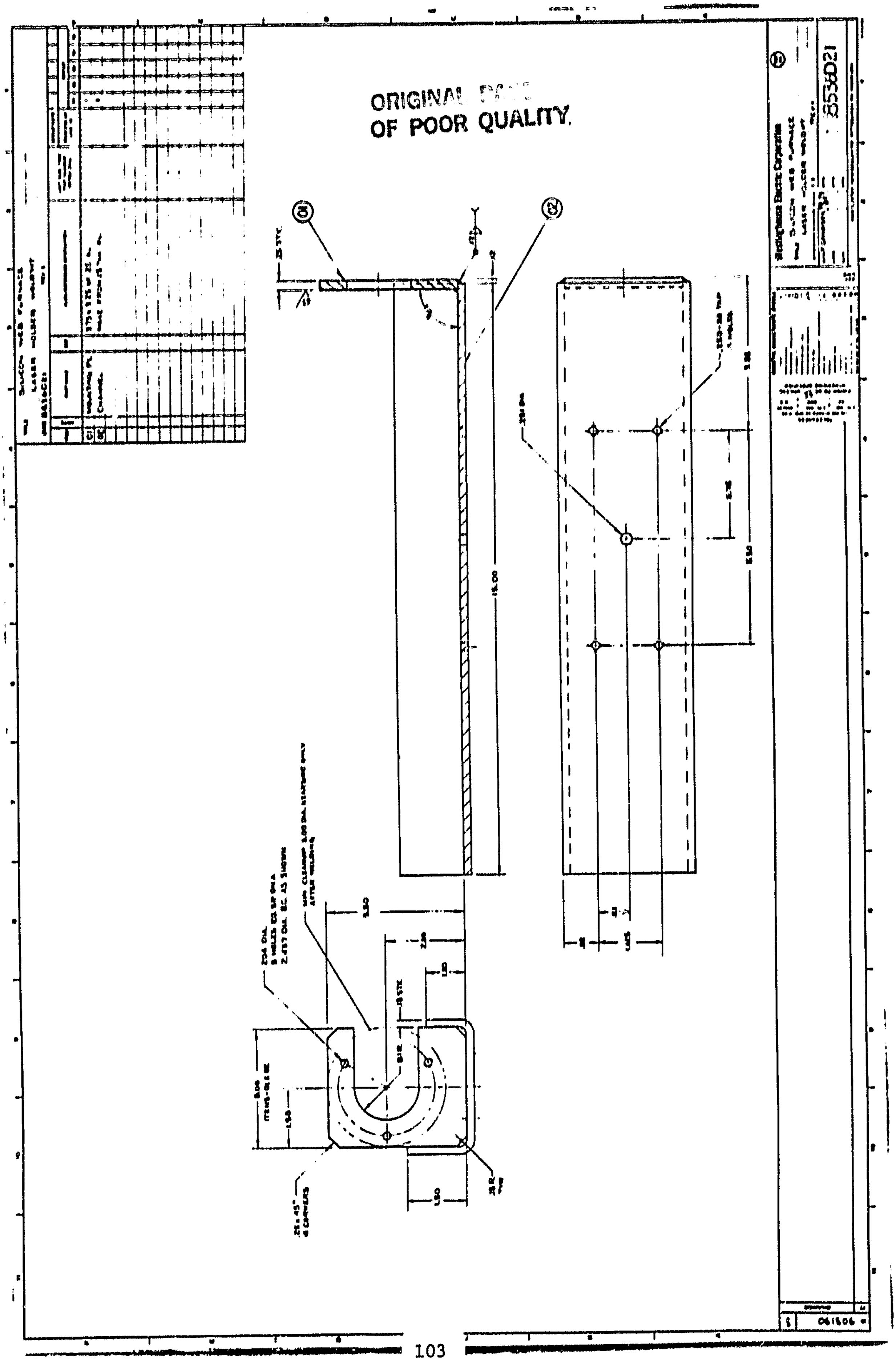

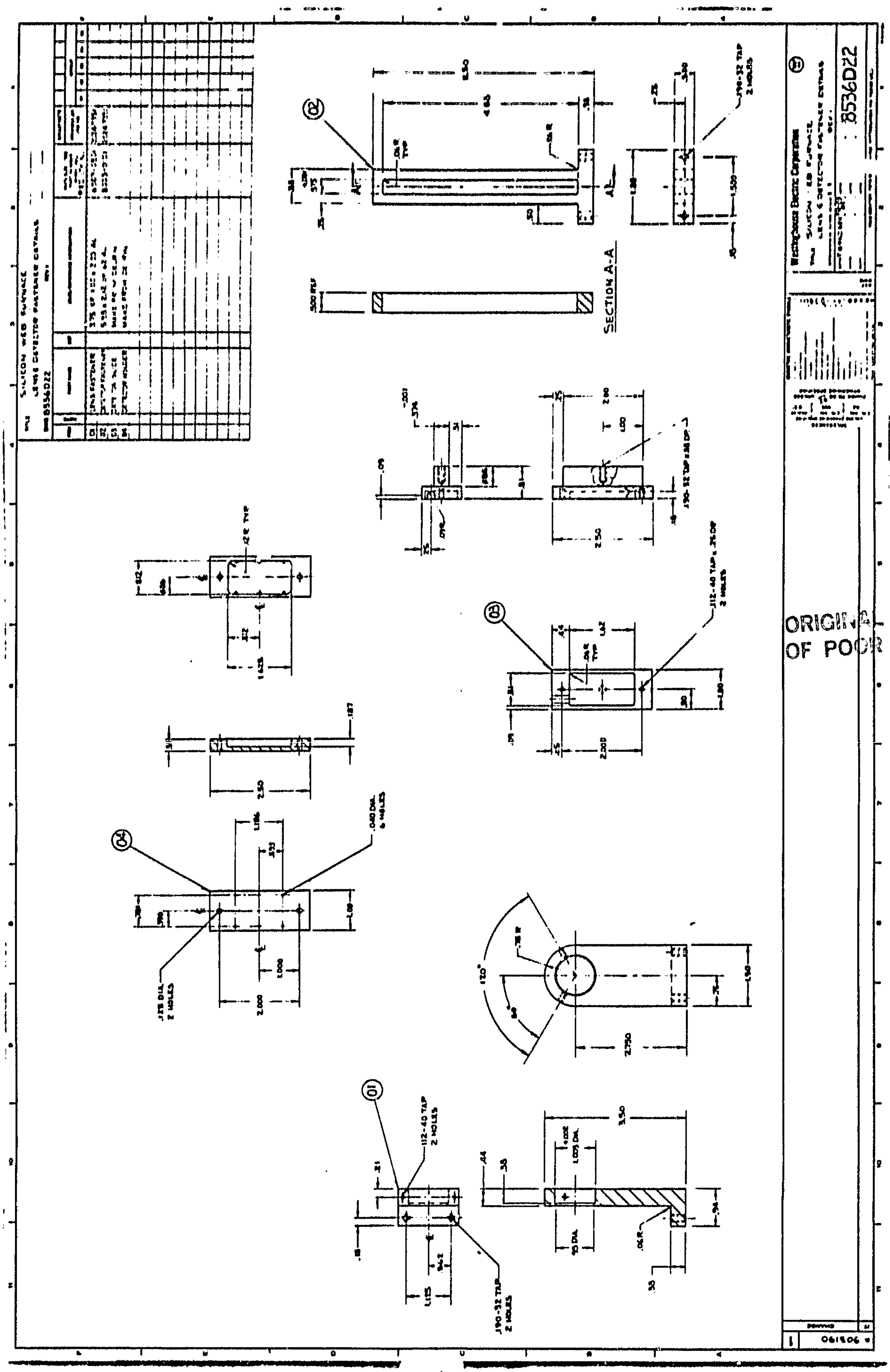
SECTION A-A
8536D22
Westinghouse Electric Corporation

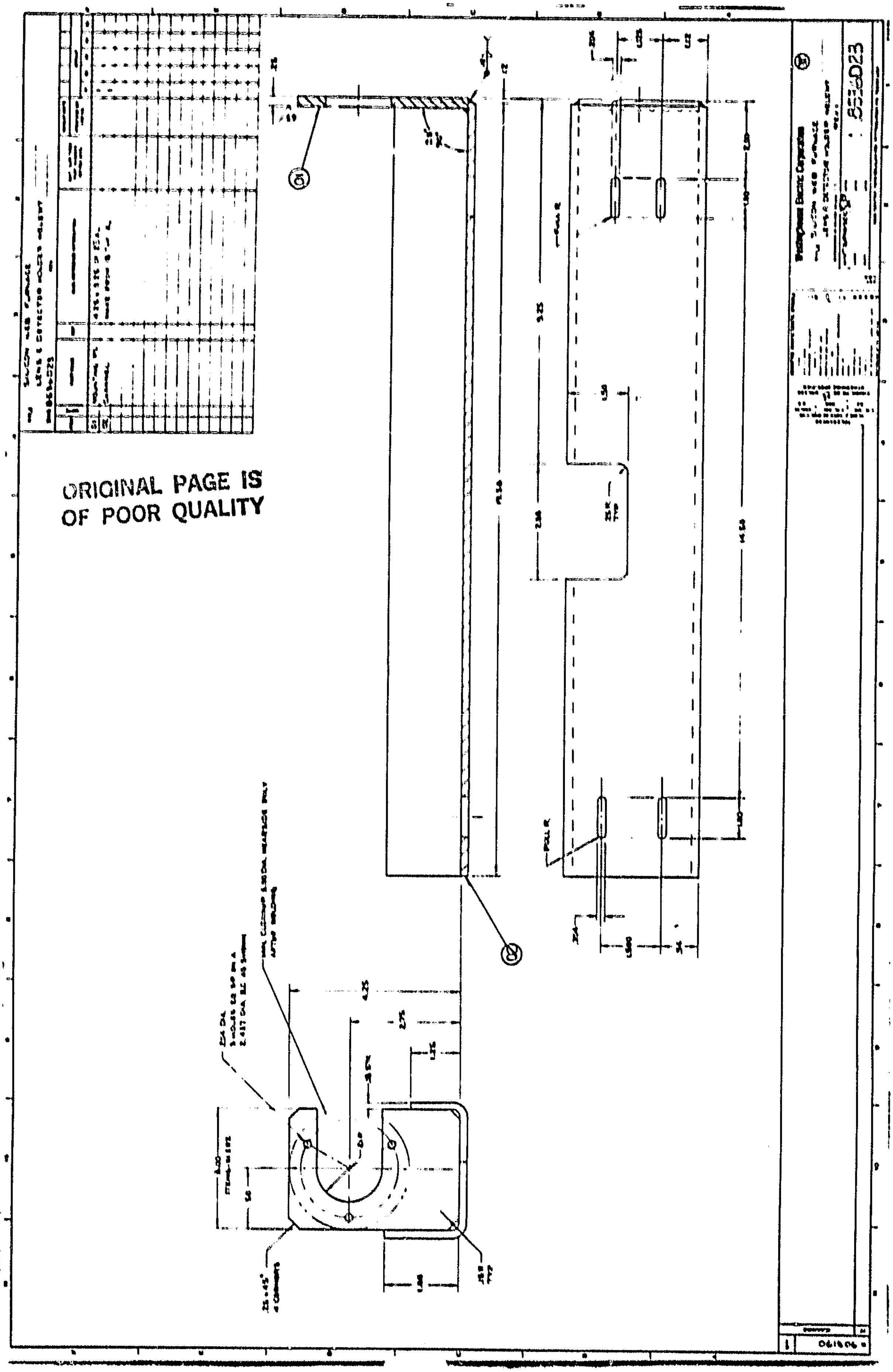

ORIGINAL PAGE IS
OF POOR QUALITY

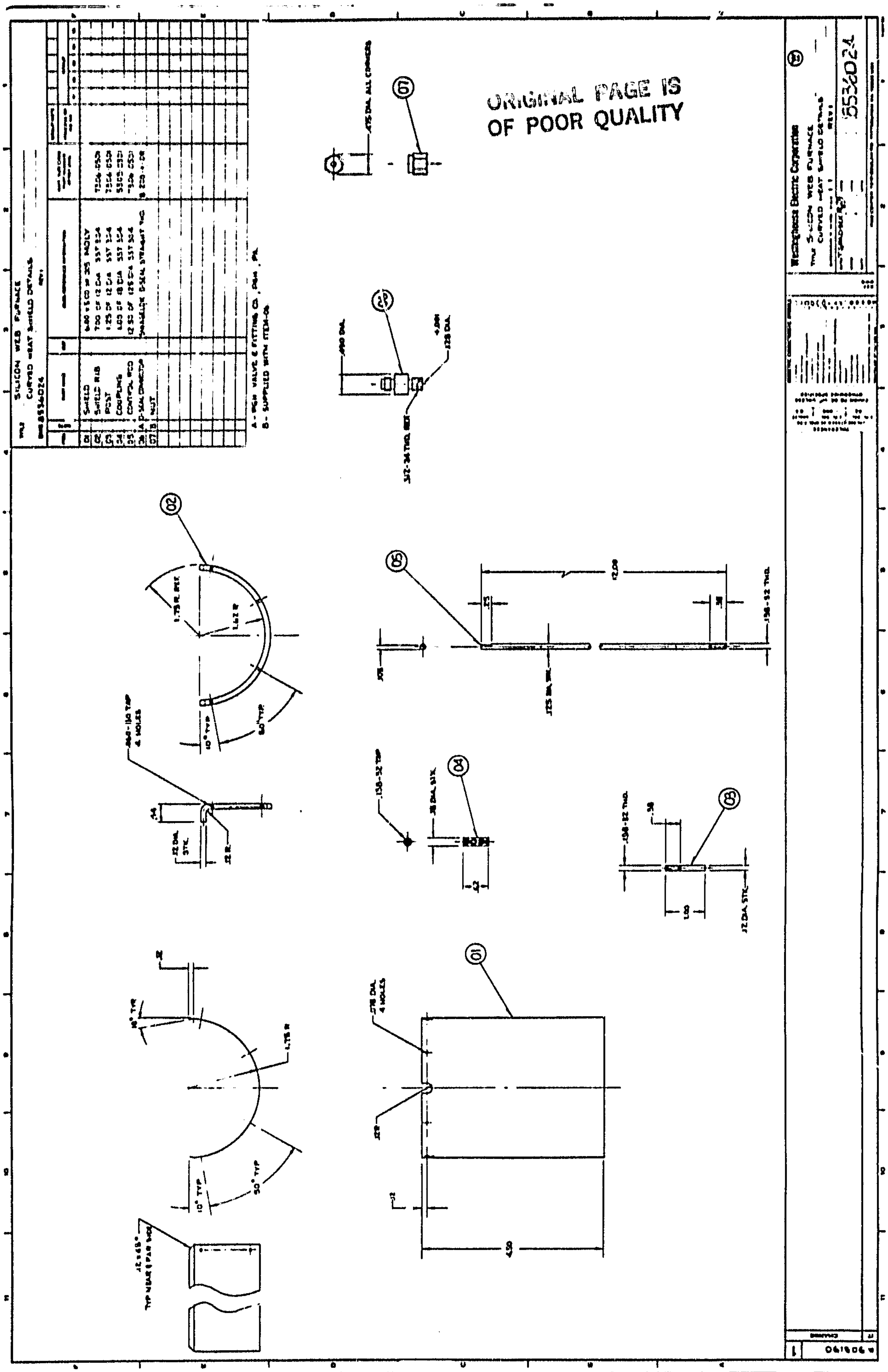

ORIGINAL PAGE IS
OF POOR QUALITY

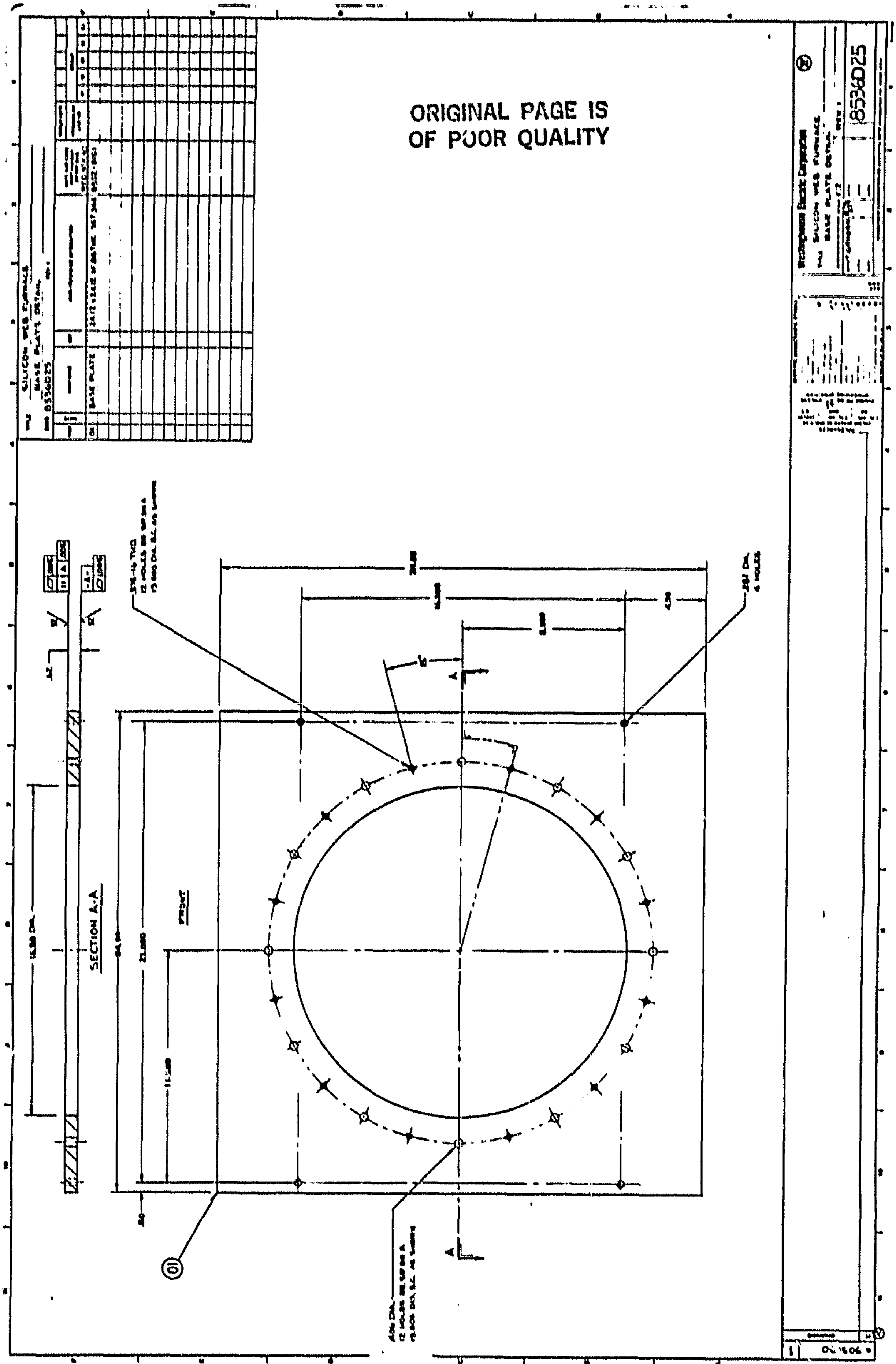

ORIGINAL PAGE IS
OF POOR QUALITY

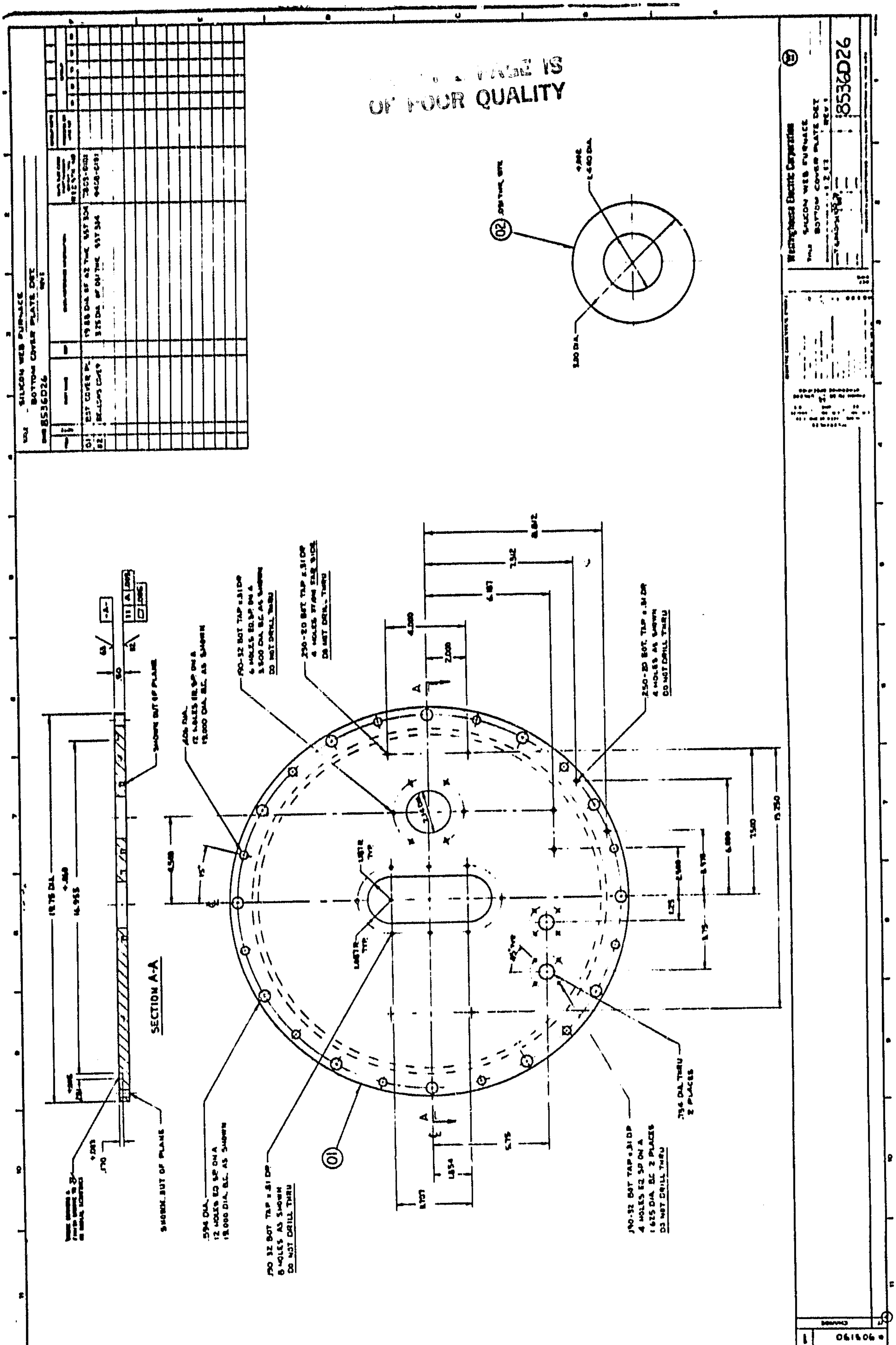

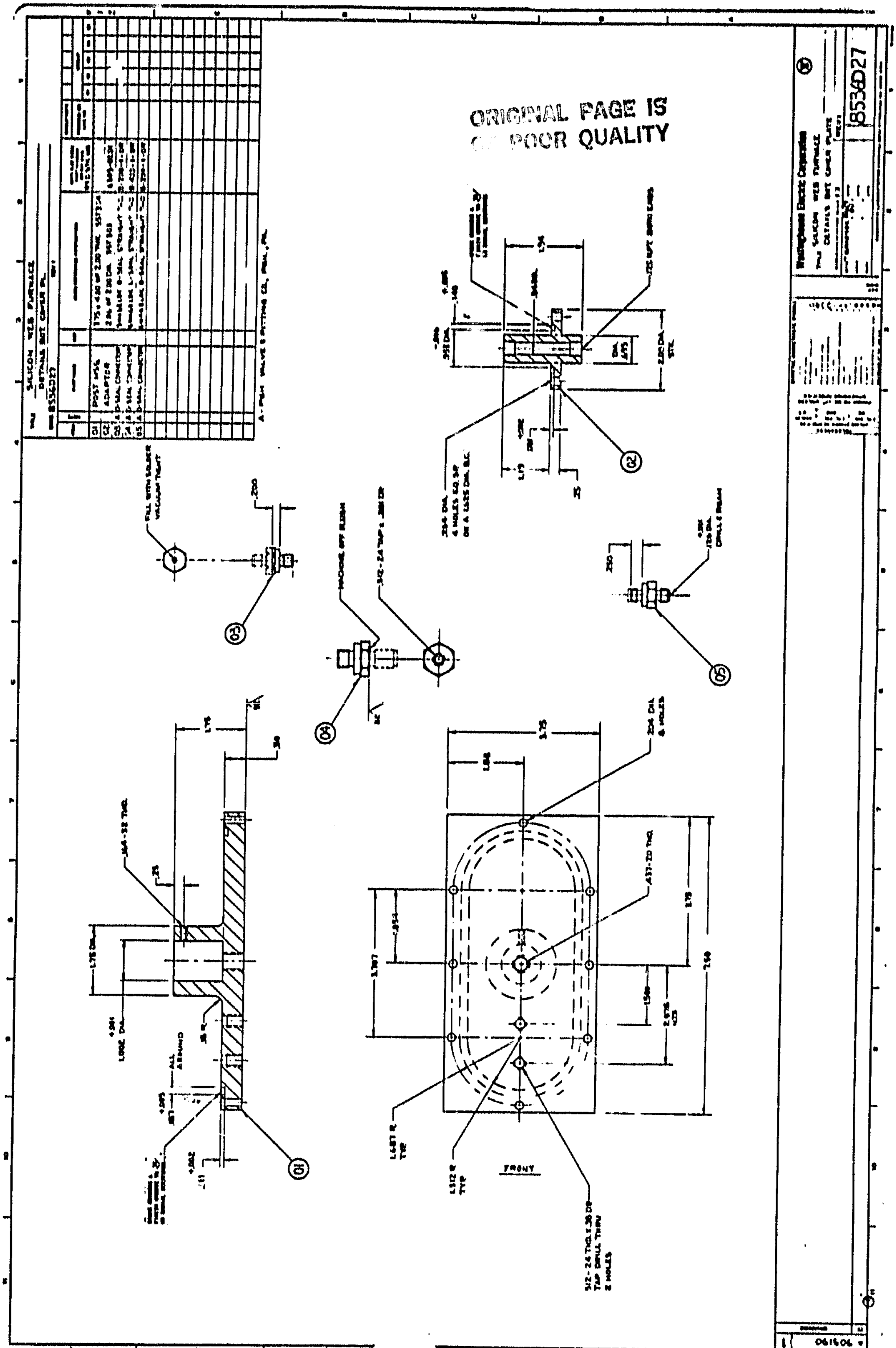

FRONT

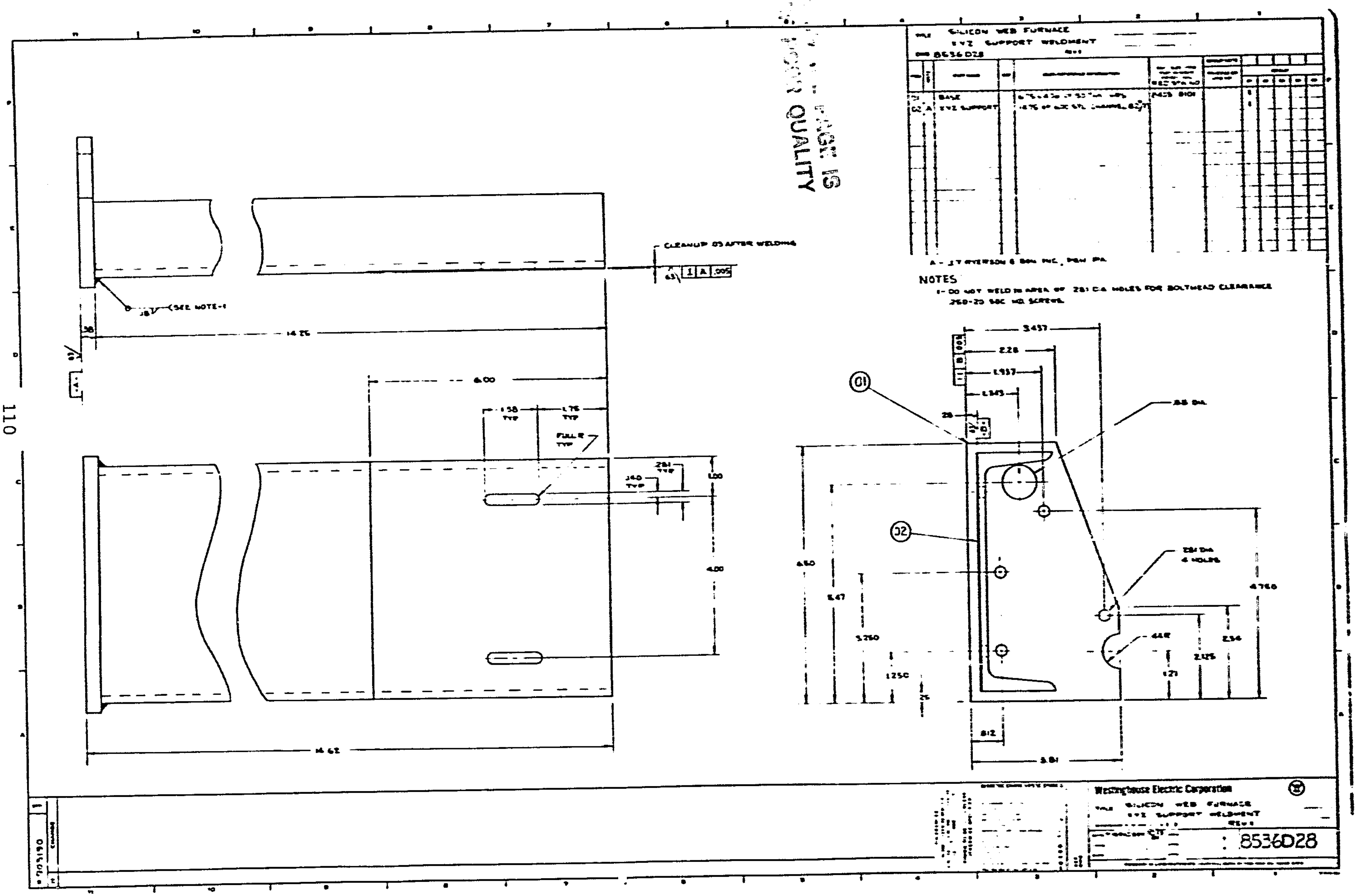
SILICON WEB FURNACE
XYZ SUPPORT WELDMENT
8536D28
BASE
XYZ SUPPORT
A - J.T. RYERSON & SON INC., PGH PA
NOTES
1 - DO NOT WELD IN AREA OF .281 DIA HOLES FOR BOLTHEAD CLEARANCE
.250-20 SOC HD SCREWS.
CLEANUP .03 AFTER WELDING
(SEE NOTE-1
FULL R TYP
.281 DIA 4 HOLES
.88 DIA
.44R
14.25
14.62
6.00
4.00
1.00
3.457
2.28
1.937
1.345
4.50
3.47
3.250
1.250
3.81
.812
4.766
2.34
2.125
1.21
.158 TYP
1.76 TYP
.281 TYP
.140 TYP
Westinghouse Electric Corporation
SILICON WEB FURNACE
XYZ SUPPORT WELDMENT
8536D28
PAGE IS
QUALITY

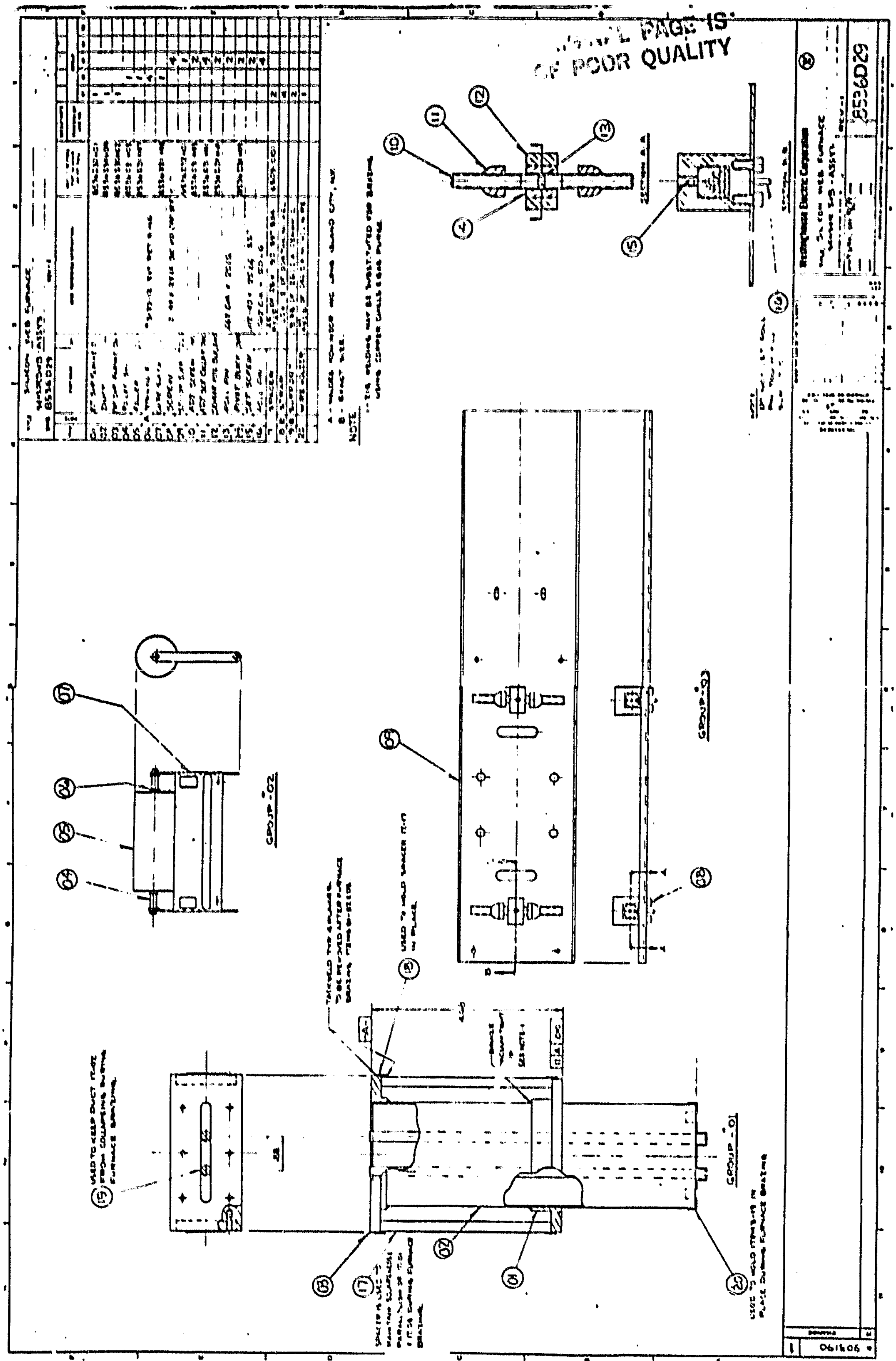
OF POOR QUALITY

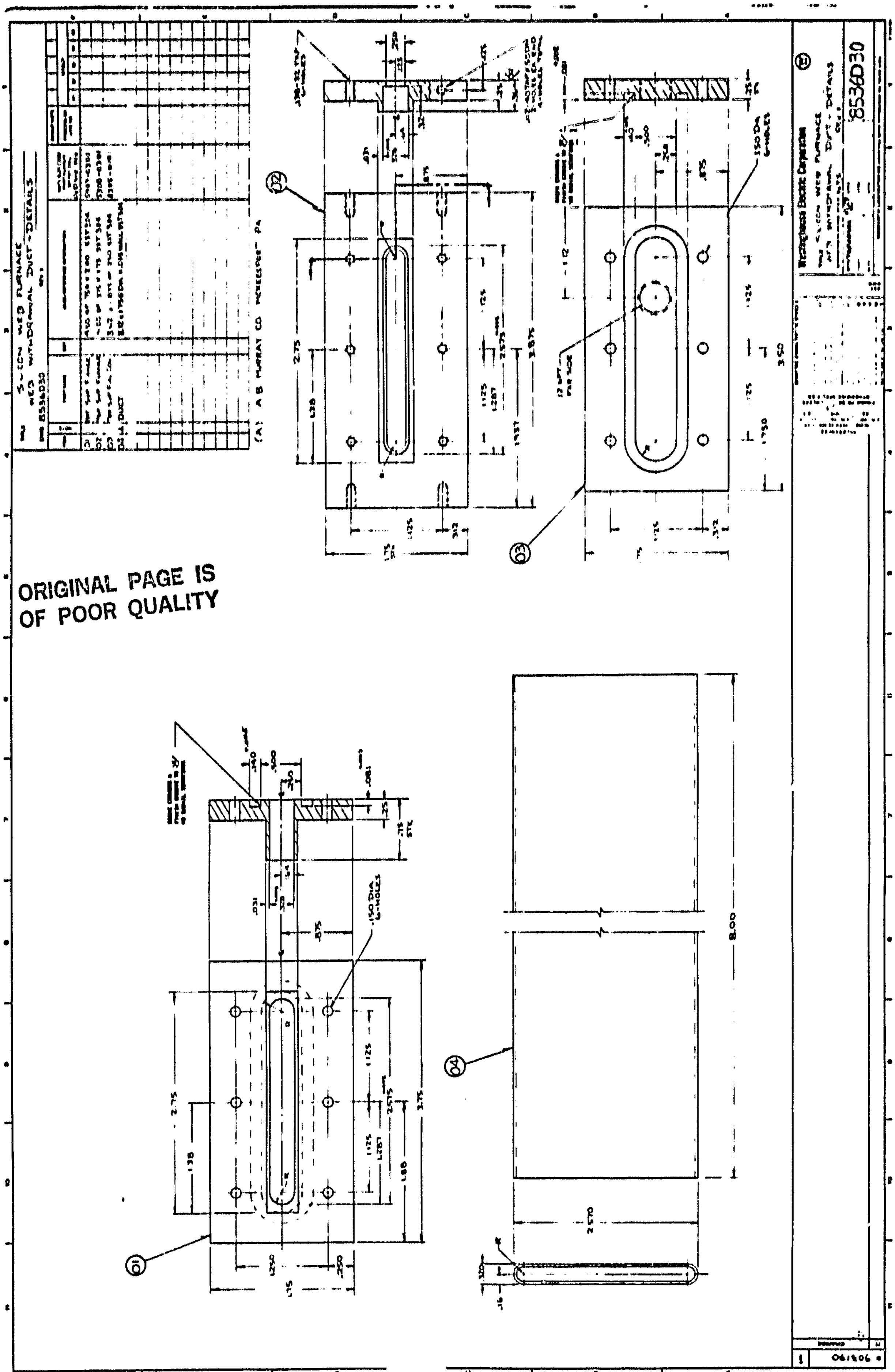

ORIGINAL PAGE IS
OF POOR QUALITY

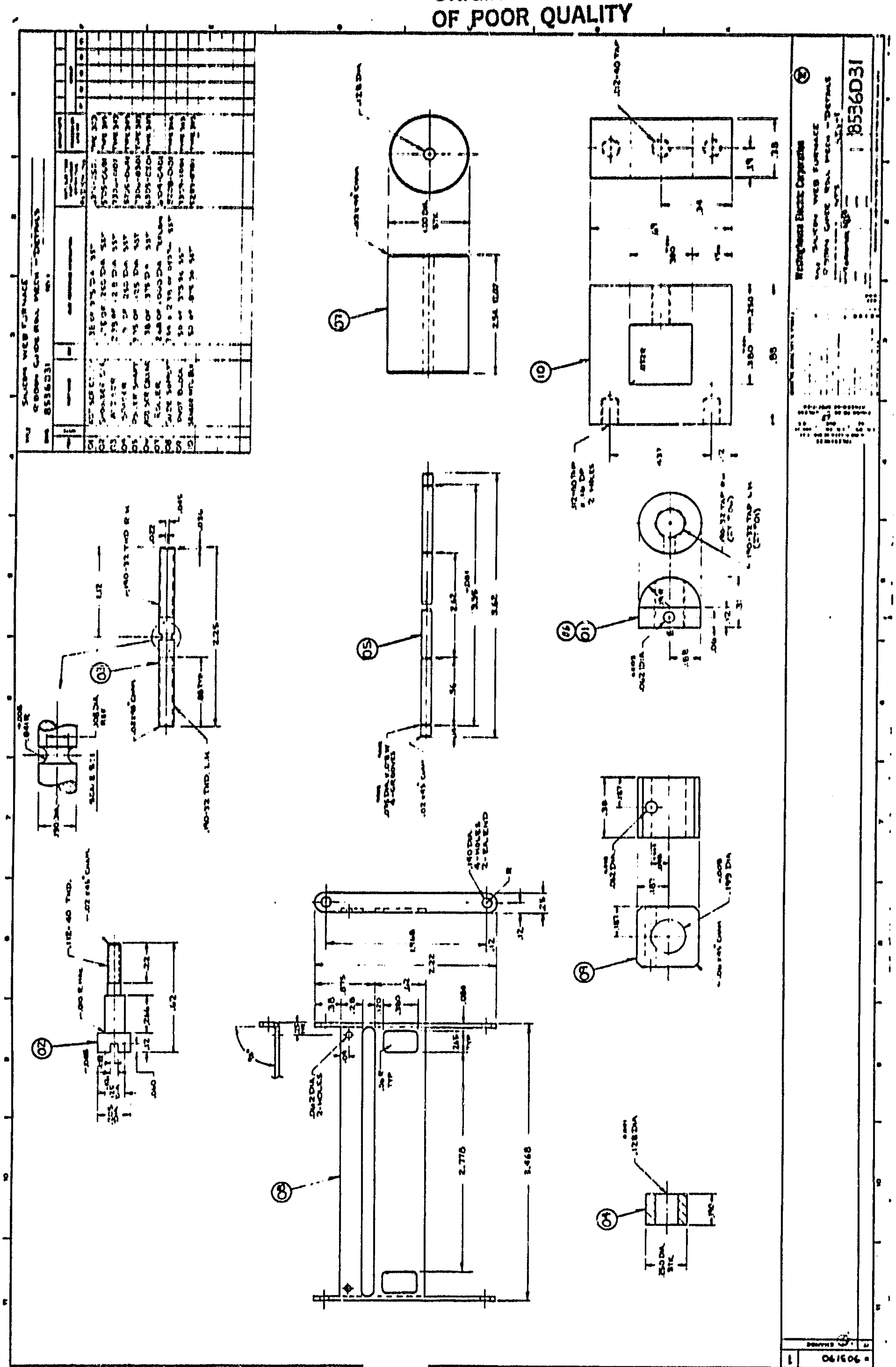

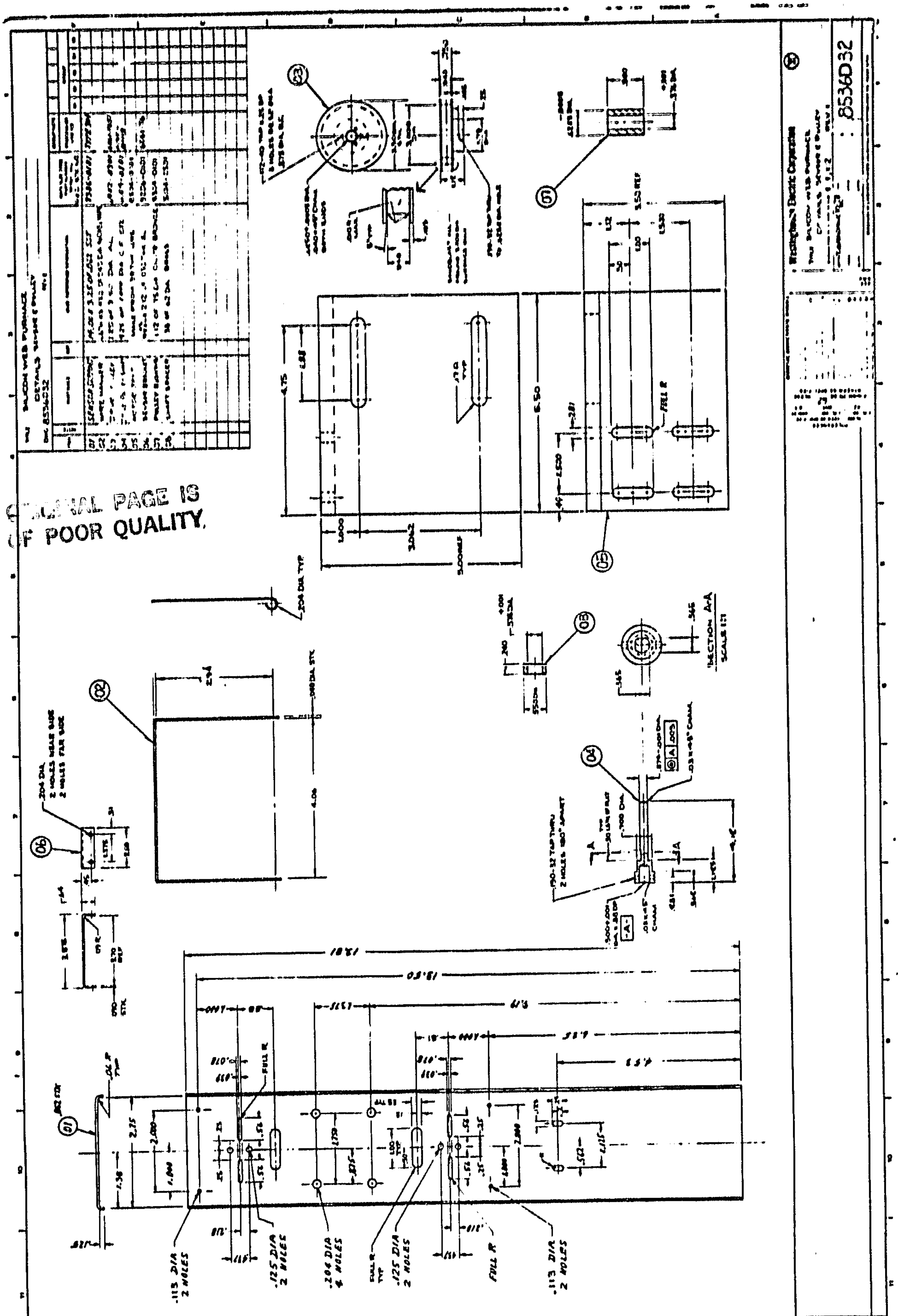
8536D32
SECTION A-A
SCALE 1:1

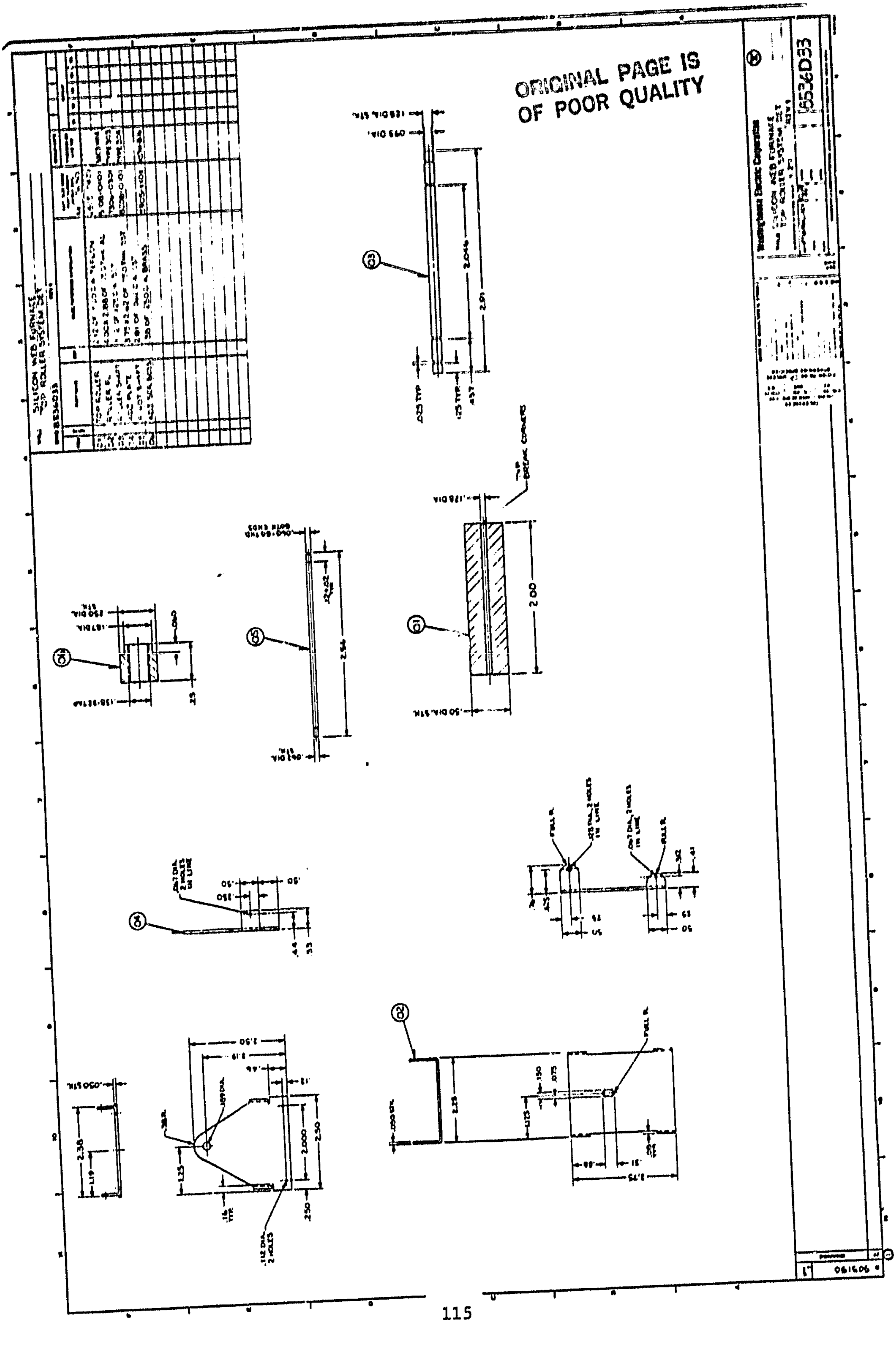

Title:	SILICON WEB FURNACE COIL DETAILS OVAL SUSCEPTOR
DWG	8536D34

Item		Name		Description			
01		COIL POST		18.75 OF .625 DIA [illegible]	[illegible]		
02		ADJ POST		1.75 OF .375 DIA SST 303	[illegible]		
03		ADAPTER		2.95 OF 1.375 DIA SST 303	[illegible]		
04		STANDOFF		.175 OF .52 DIA BRASS	[illegible]	[illegible]	

NOTES:

1. ALL DIMENSIONS ON ITEM 01 ARE BEFORE FORMING.

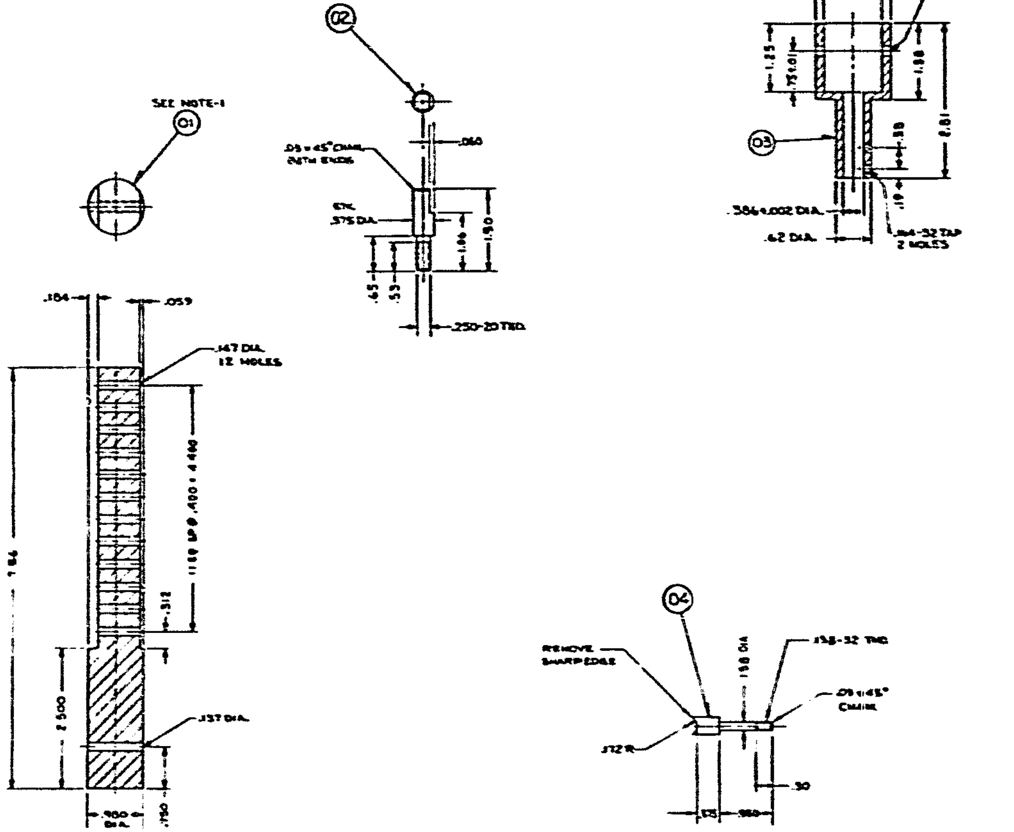

Westinghouse Electric Corporation

SILICON WEB FURNACE COIL DETS OVAL SUSCEPTOR

8536D34

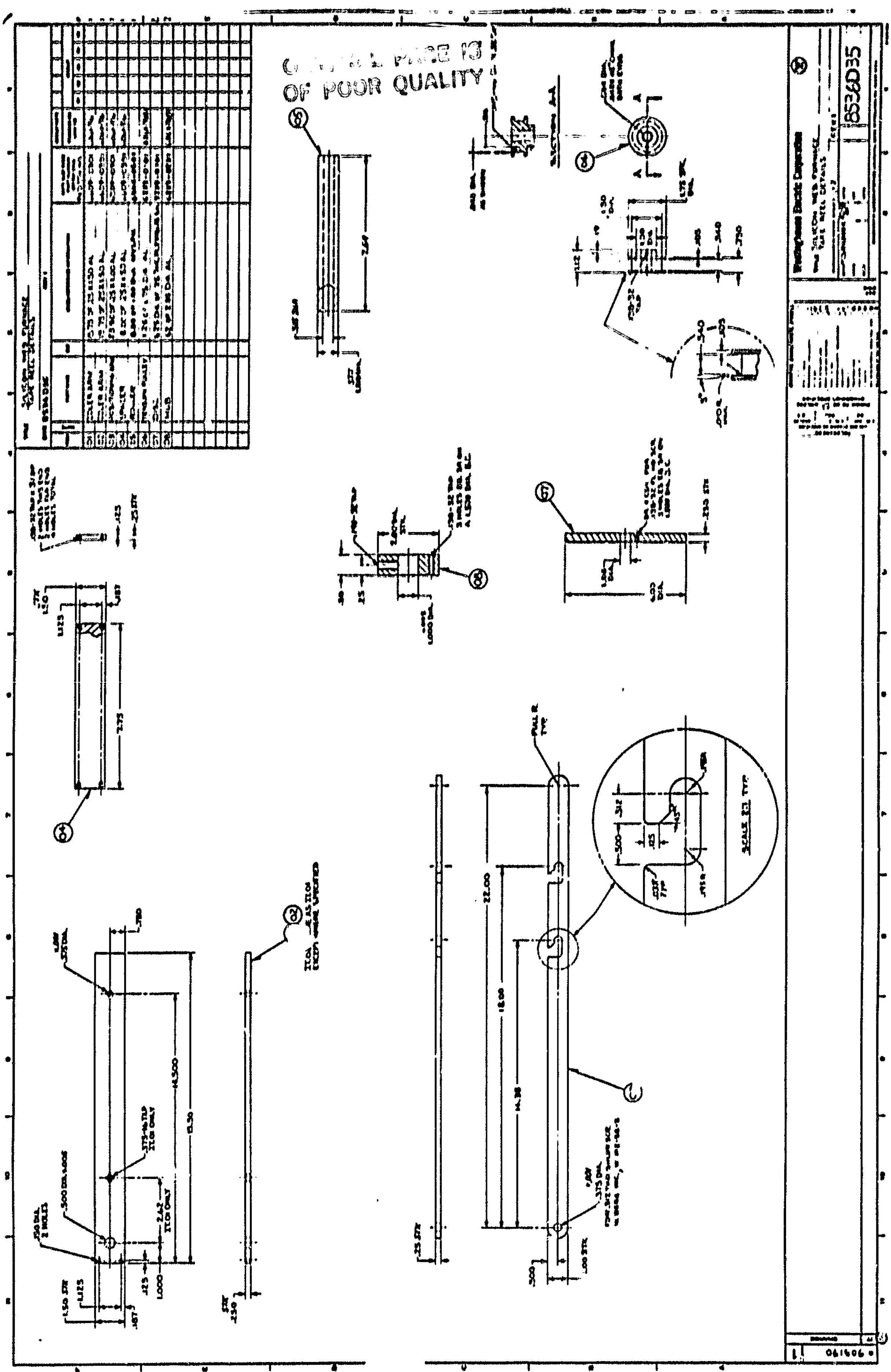
8536D35

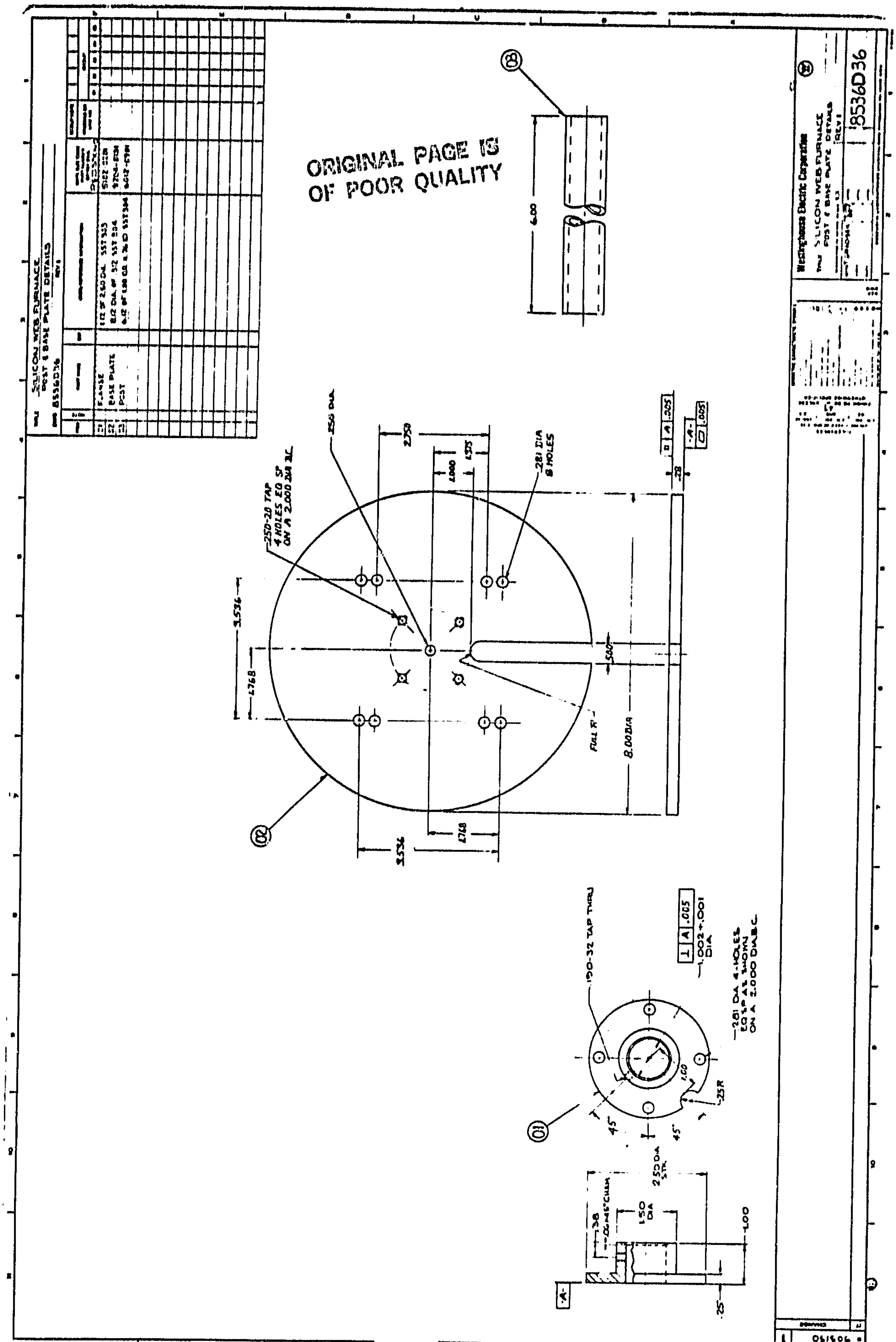

SILICON WEB FURNACE
POST & BASE PLATE DETAILS
8536D36
FLANGE
BASE PLATE
POST
.250-20 TAP
4 HOLES EQ SP
ON A 2.000 DIA B.C.
.281 DIA
8 HOLES
8.00 DIA
FULL R
6.00
.190-32 TAP THRU
.281 DIA 4-HOLES
EQ SP AS SHOWN
ON A 2.000 DIA B.C.
2.500 DIA STK
1.50 DIA
Westinghouse Electric Corporation

ORIGINAL PAGE IS
OF POOR QUALITY

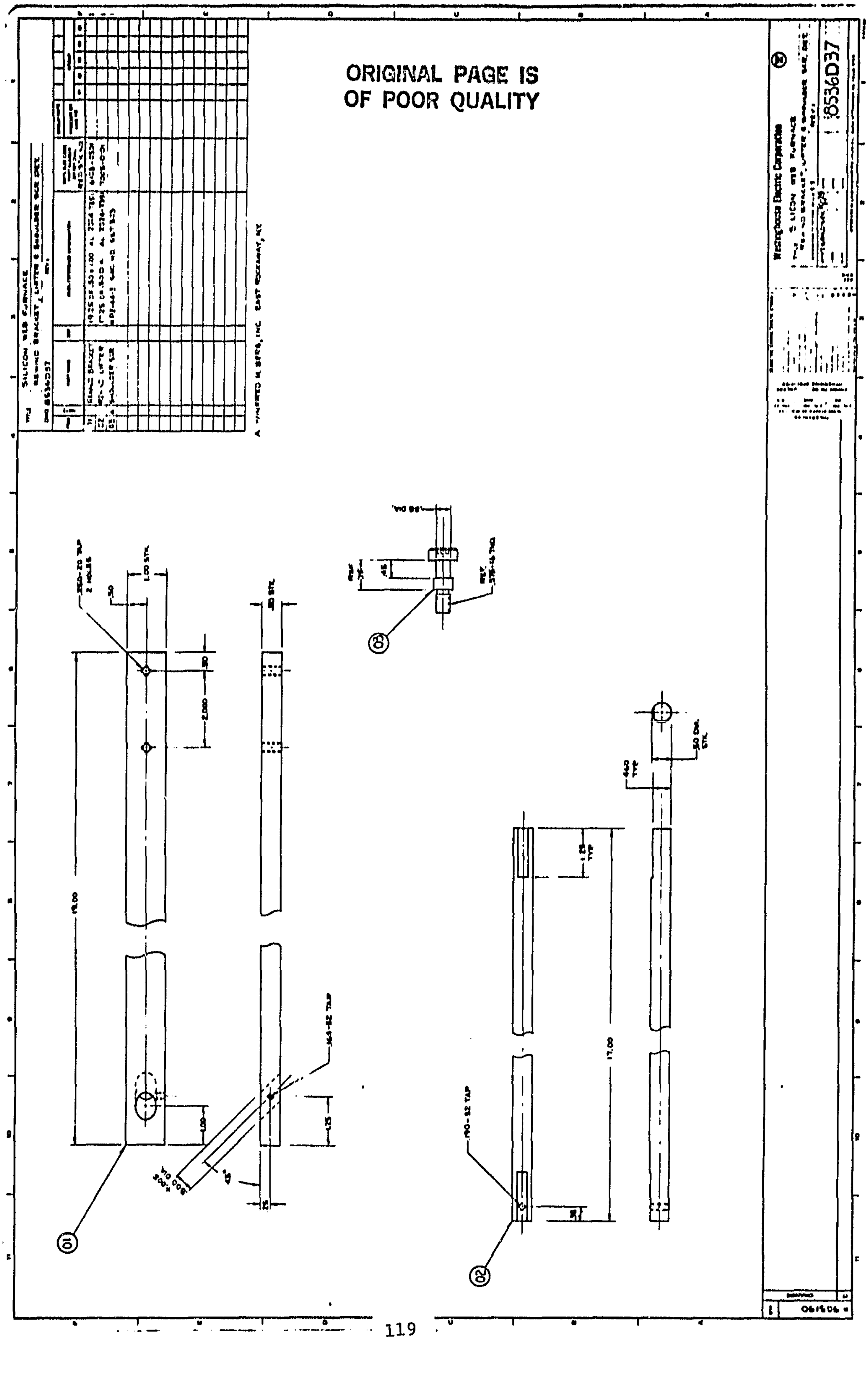

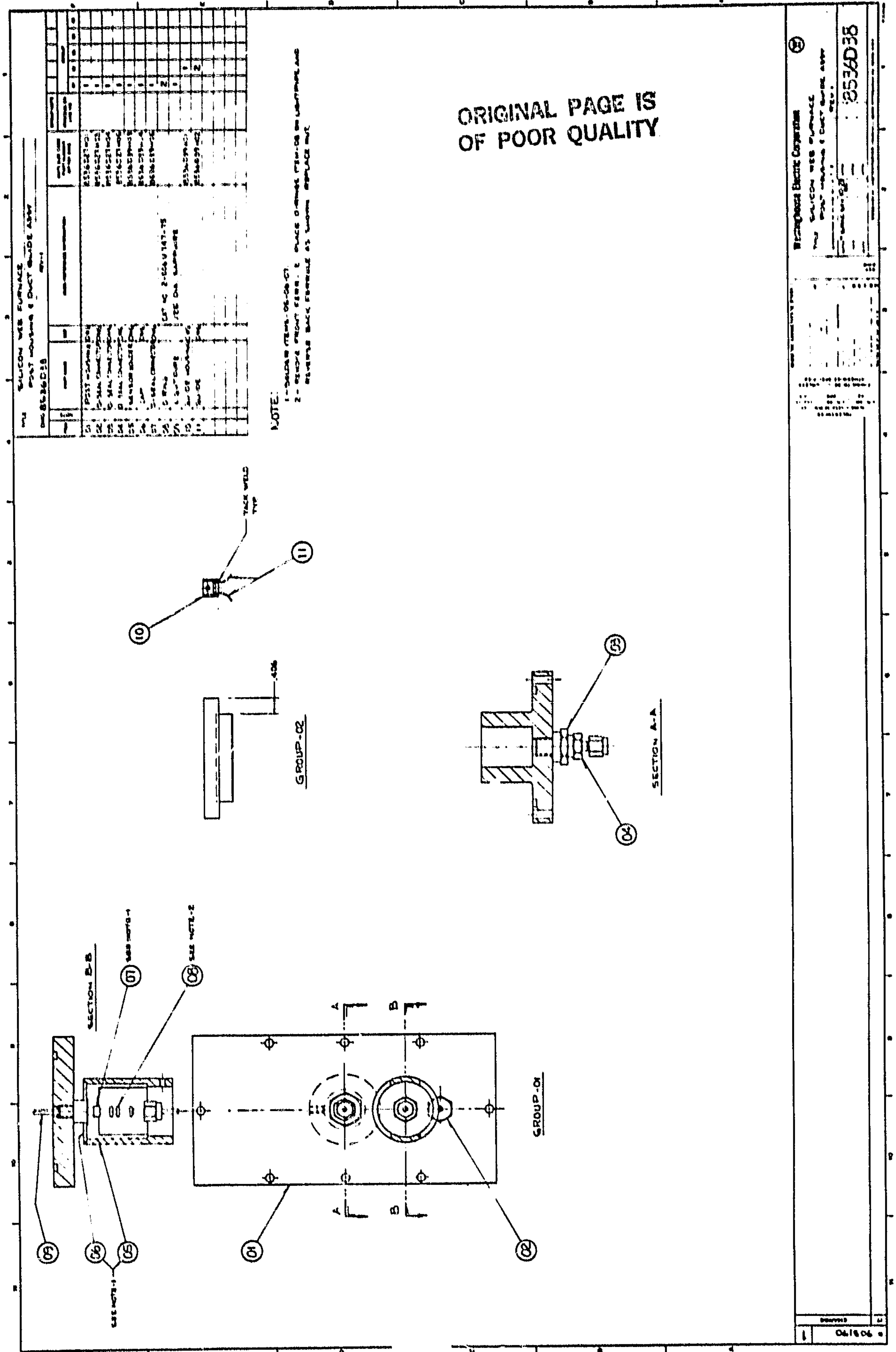
SECTION B-B
SECTION A-A
GROUP-01
GROUP-02
TACK WELD TYP
SEE NOTE-1
SEE NOTE-2
.406
NOTE:
Westinghouse Electric Corporation
SILICON WEB FURNACE

ORIGINAL PAGE IS
OF POOR QUALITY

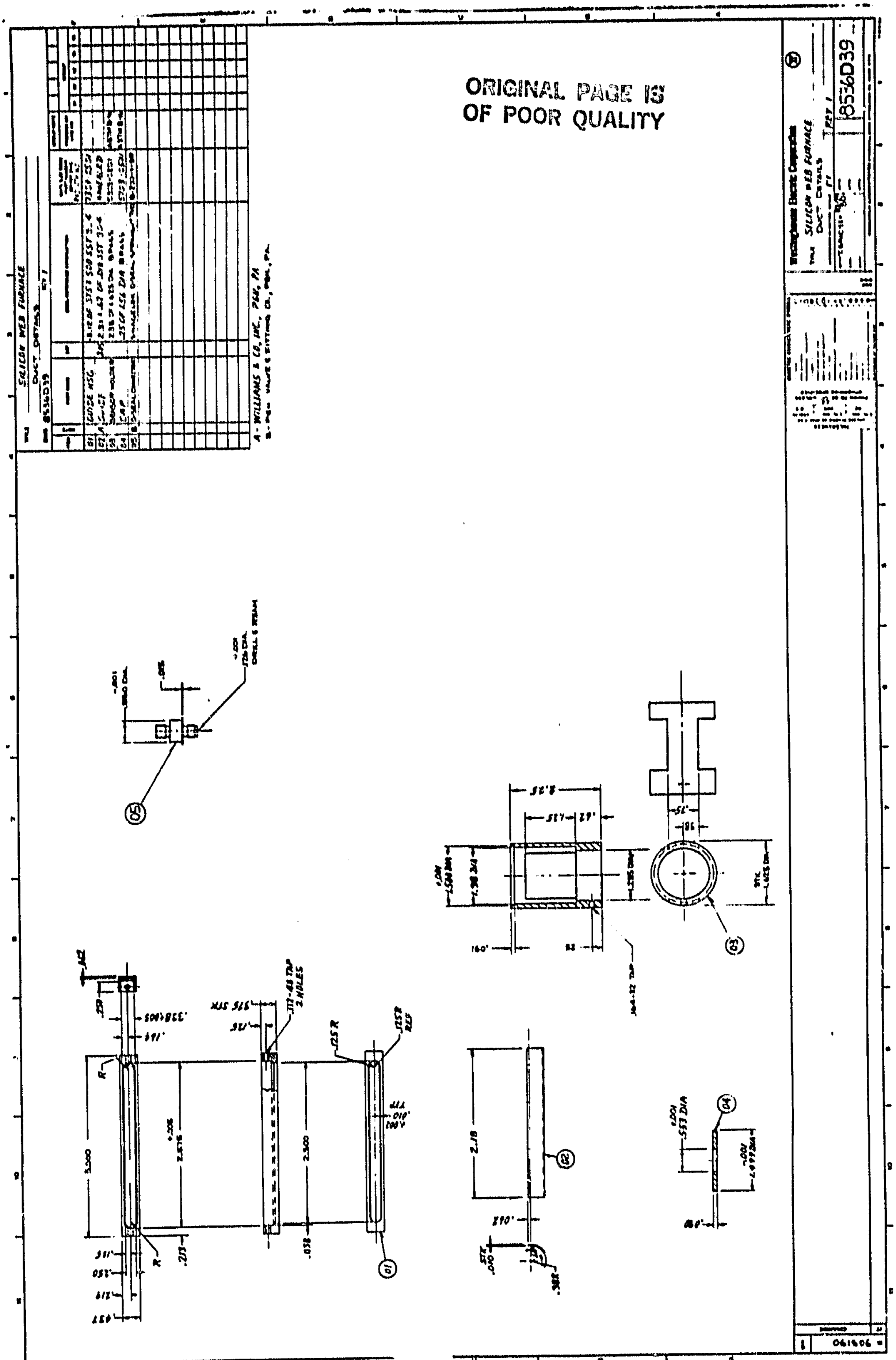

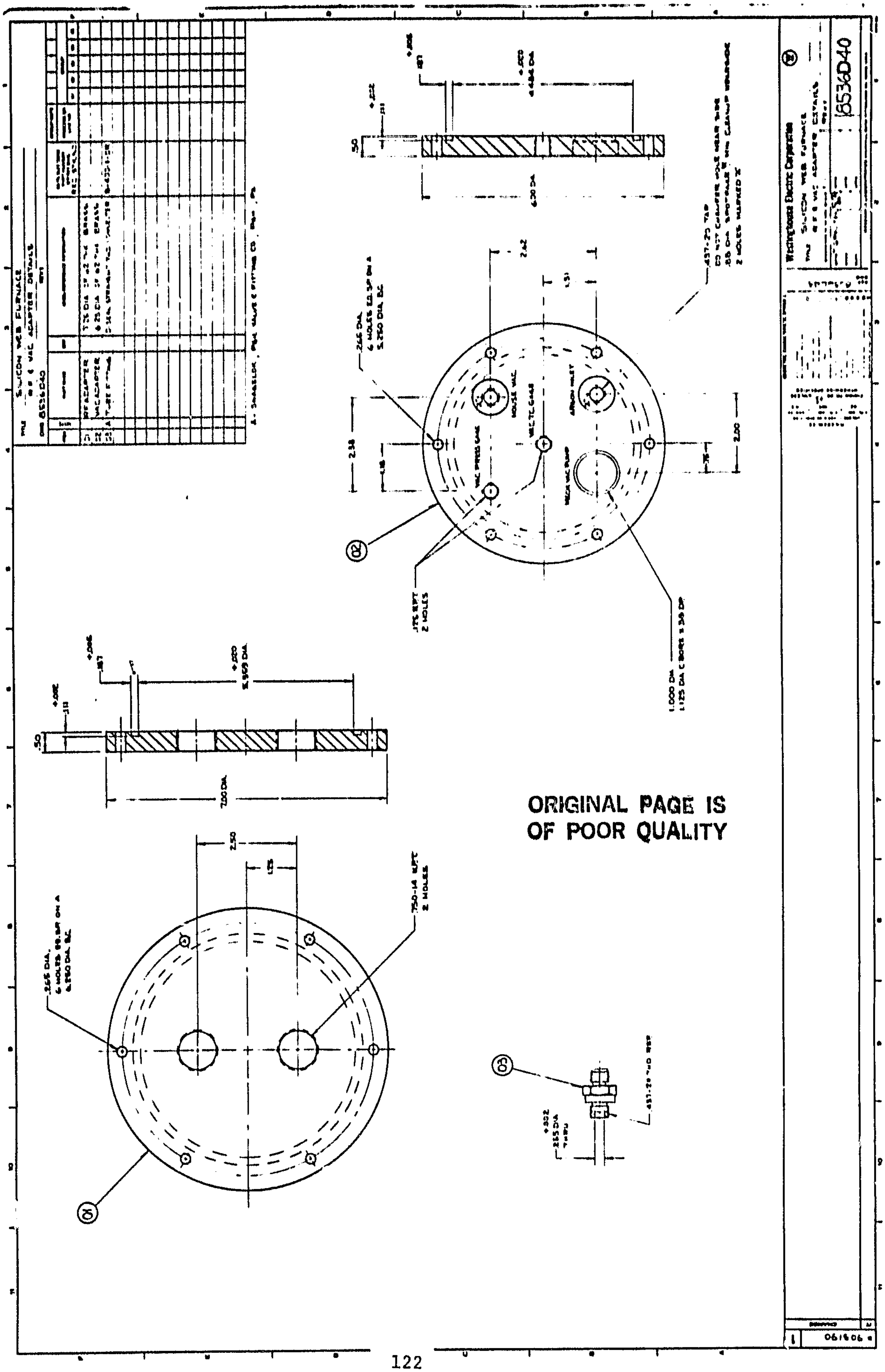
SILICON WEB FURNACE
8536D40
Westinghouse Electric Corporation
ORIGINAL PAGE IS
OF POOR QUALITY

ORIGINAL PAGE IS
OF POOR QUALITY

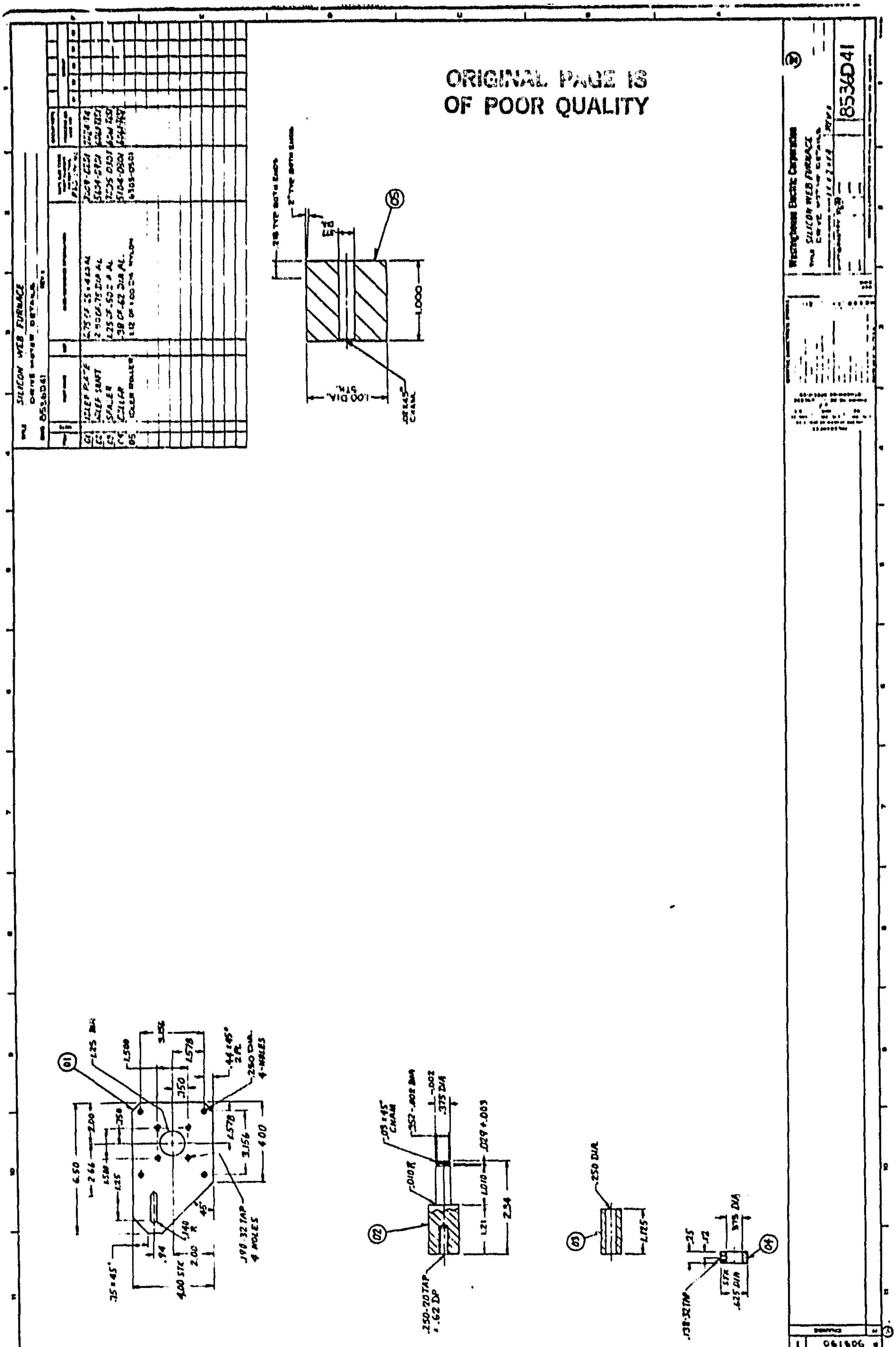

ORIGINAL PAGE IS
OF POOR QUALITY

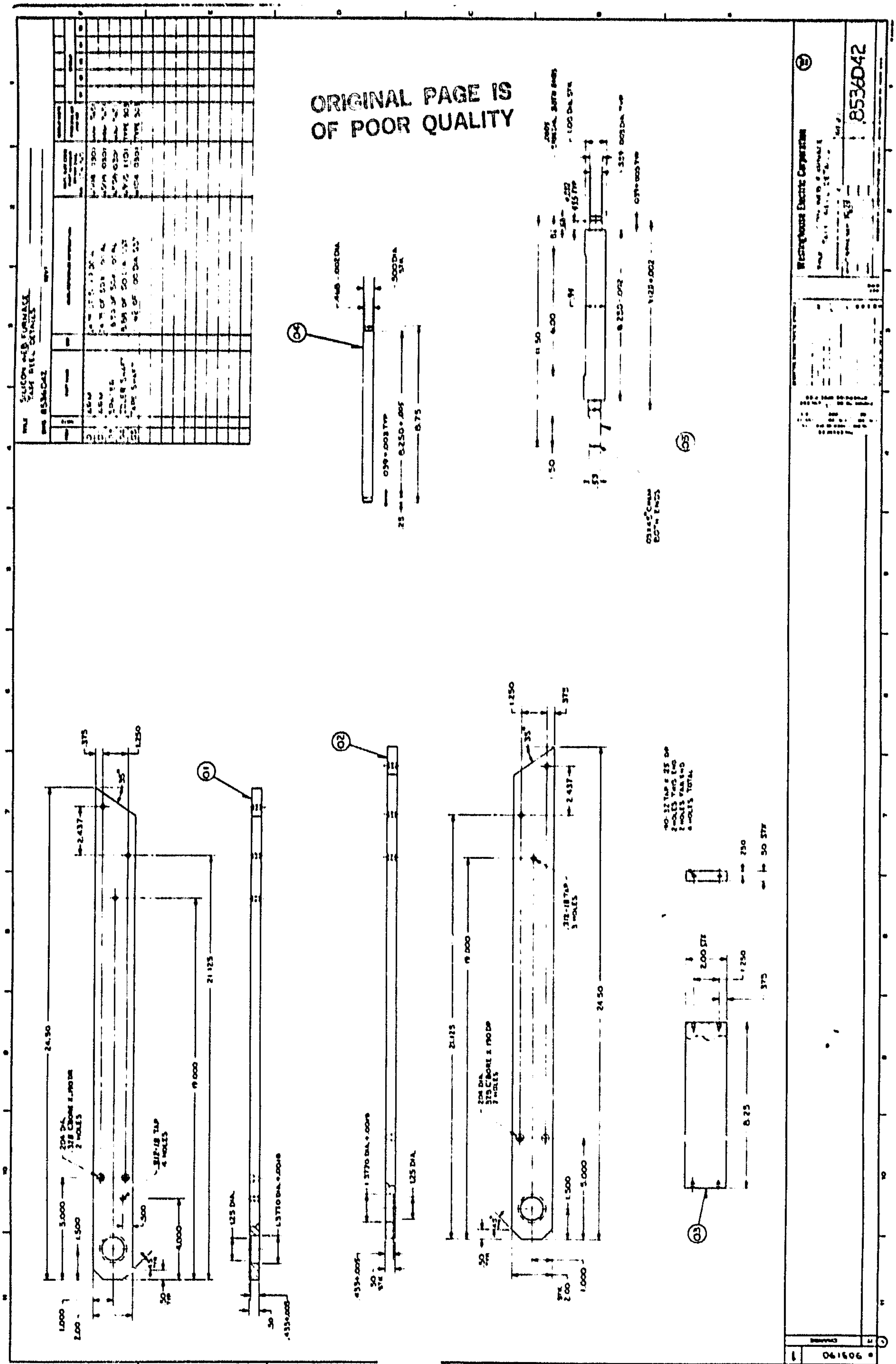

ORIGINAL PAGE IS
OF POOR QUALITY

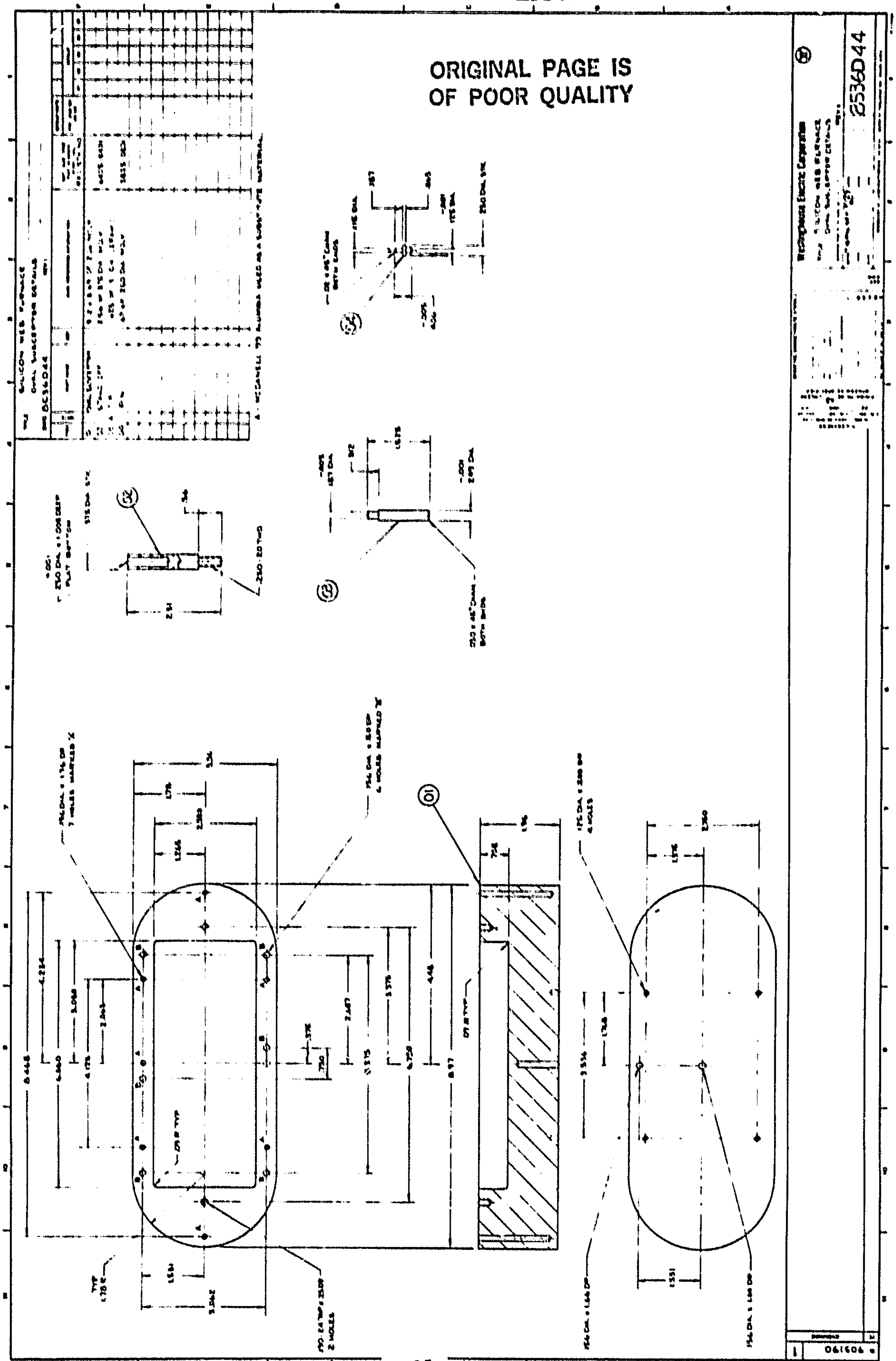

ORIGINAL PAGE IS OF POOR QUALITY

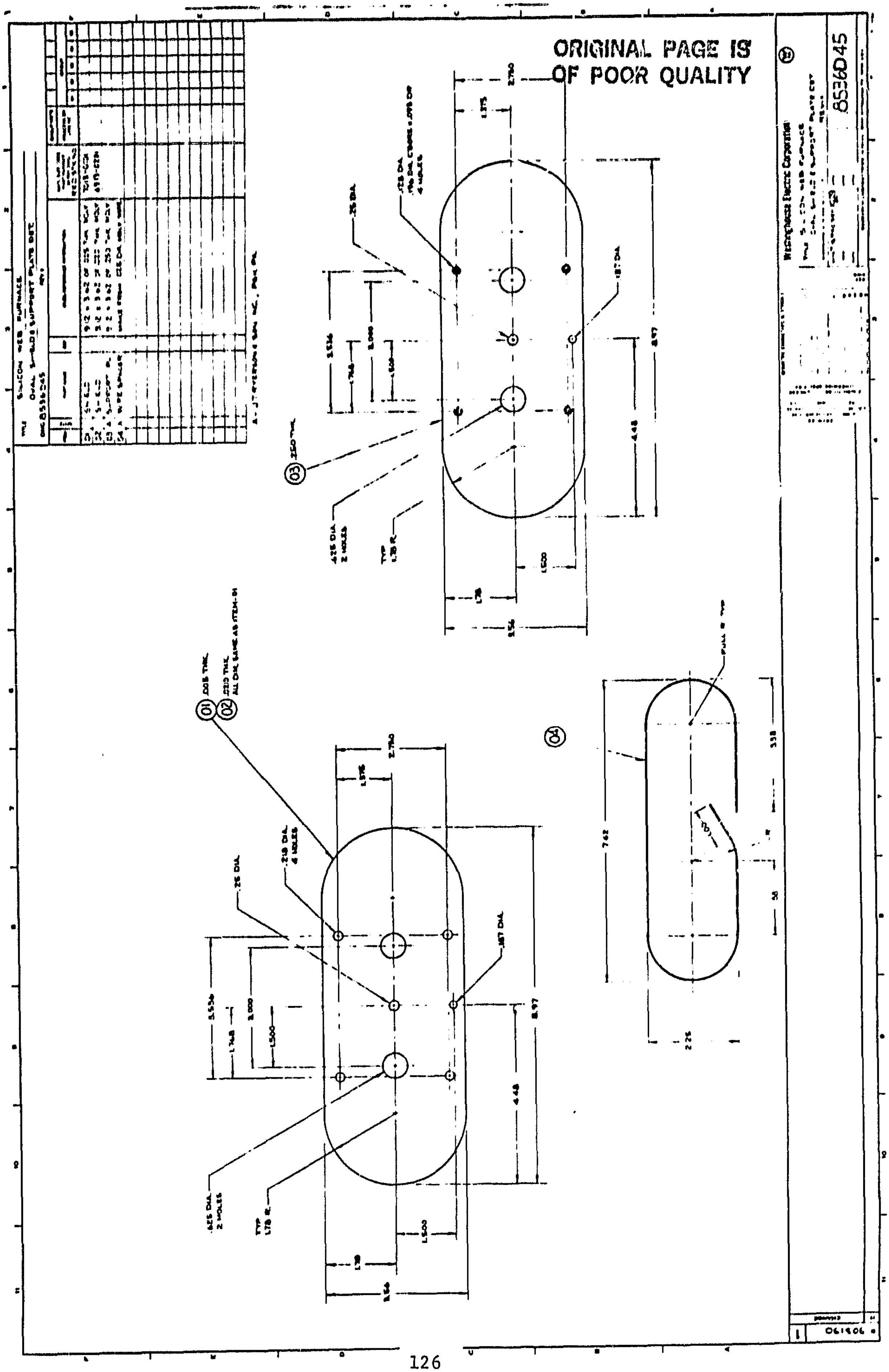

ORIGINAL PAGE IS
OF POOR QUALITY

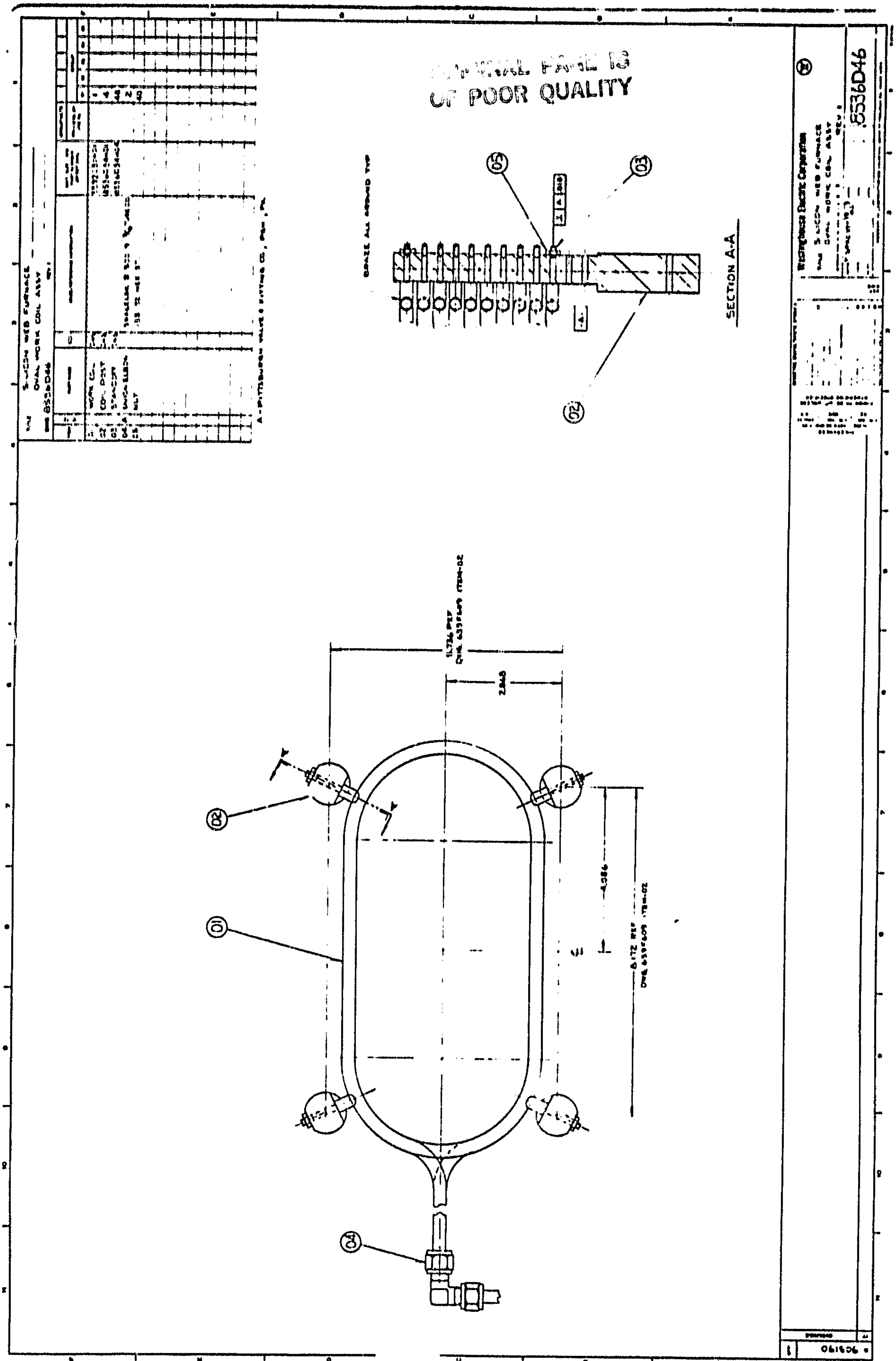

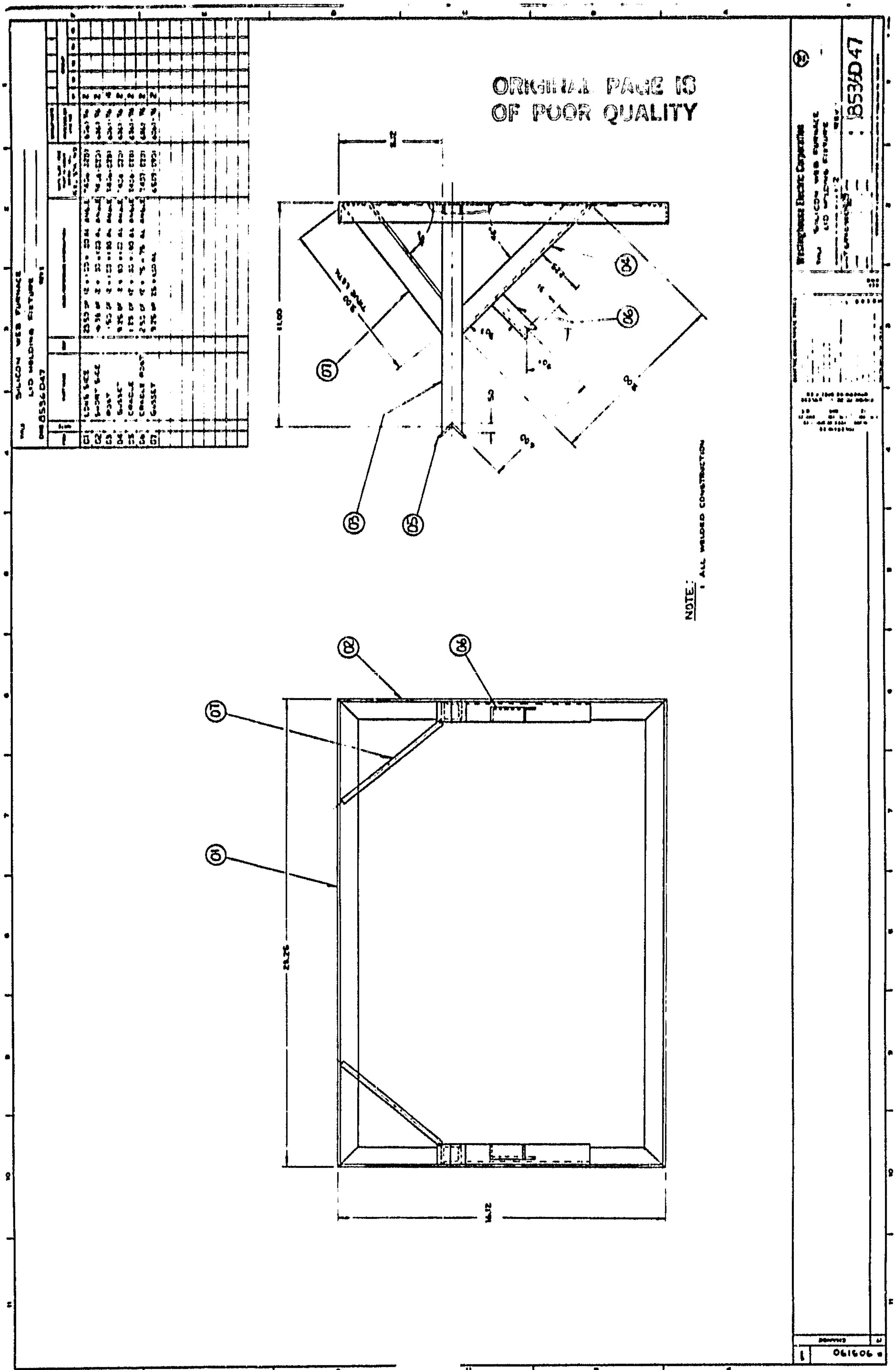
NOTE:
1 ALL WELDED CONSTRUCTION
Westinghouse Electric Corporation
11.00
28.26
16.72

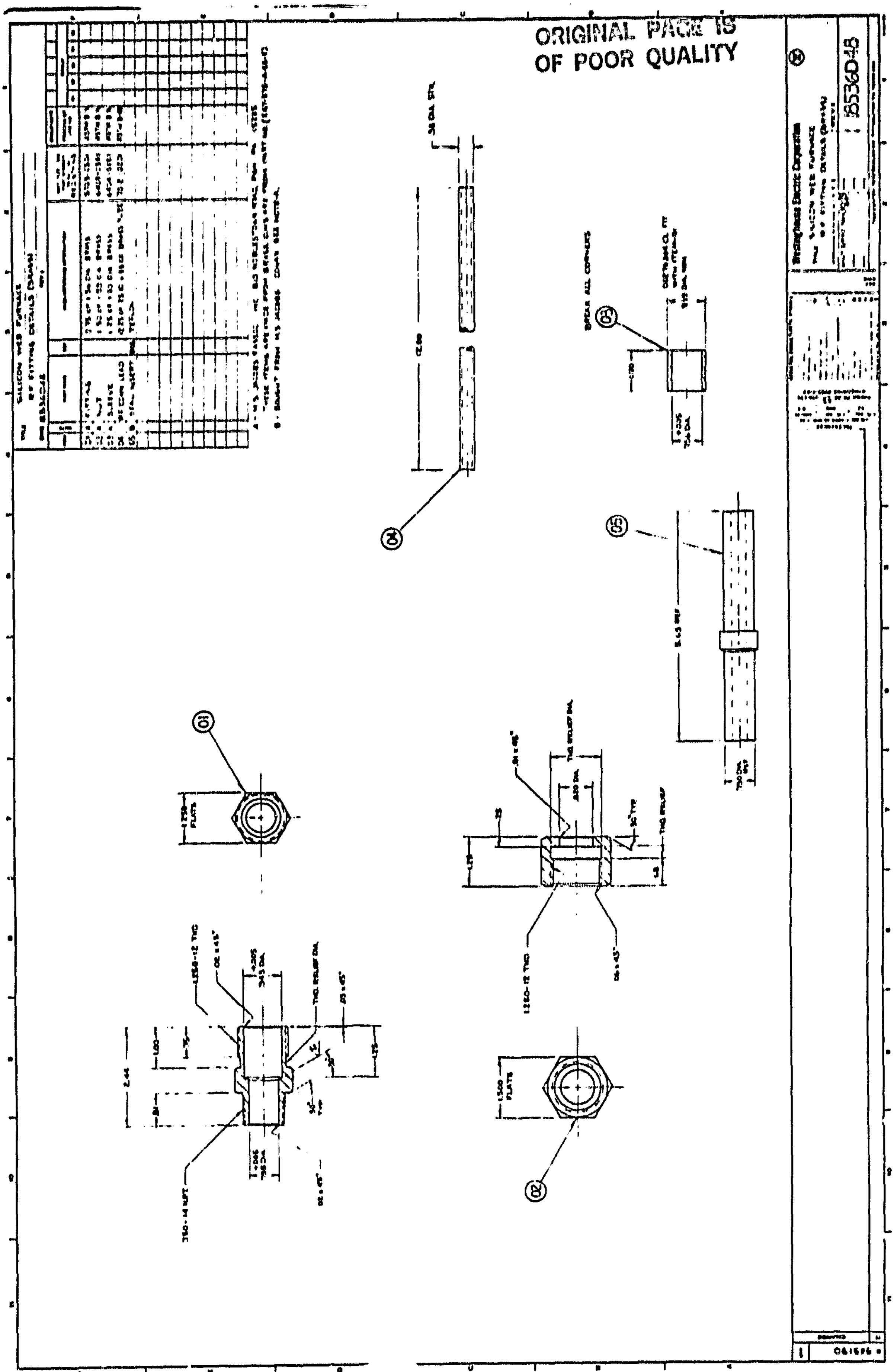

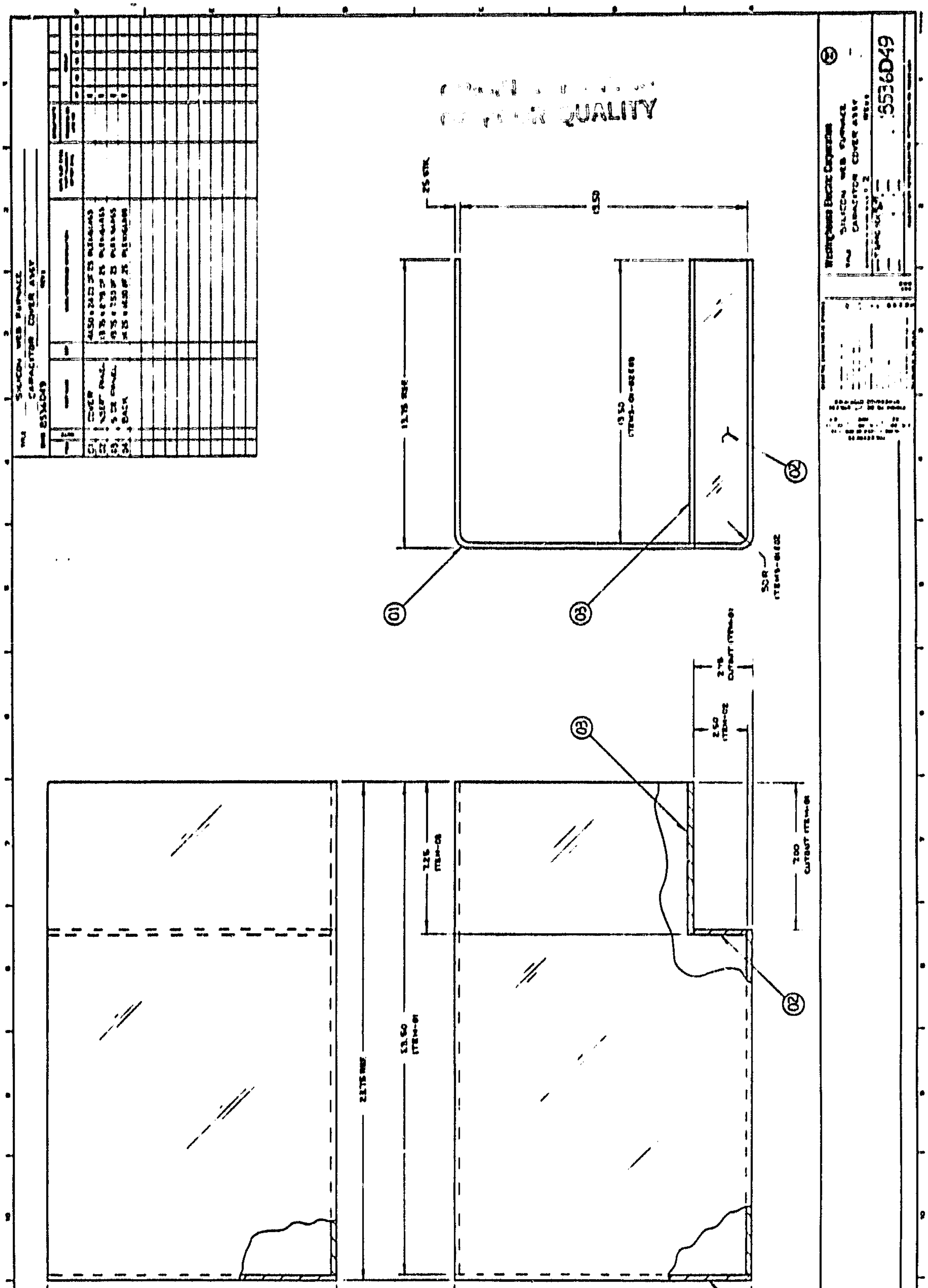

5536D49

ORIGINAL PAGE IS OF POOR QUALITY

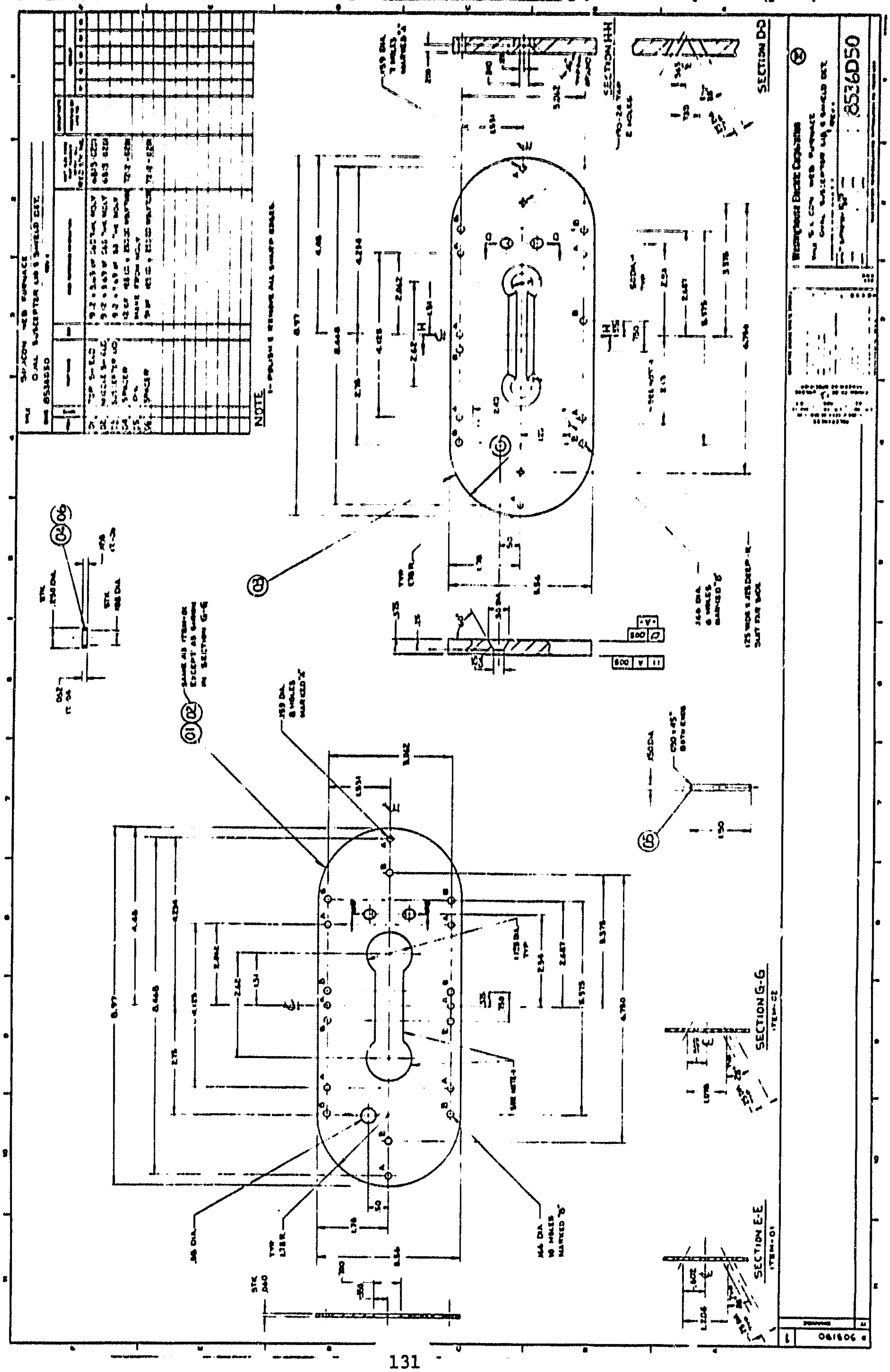

ORIGINAL PAGE IS
OF POOR QUALITY

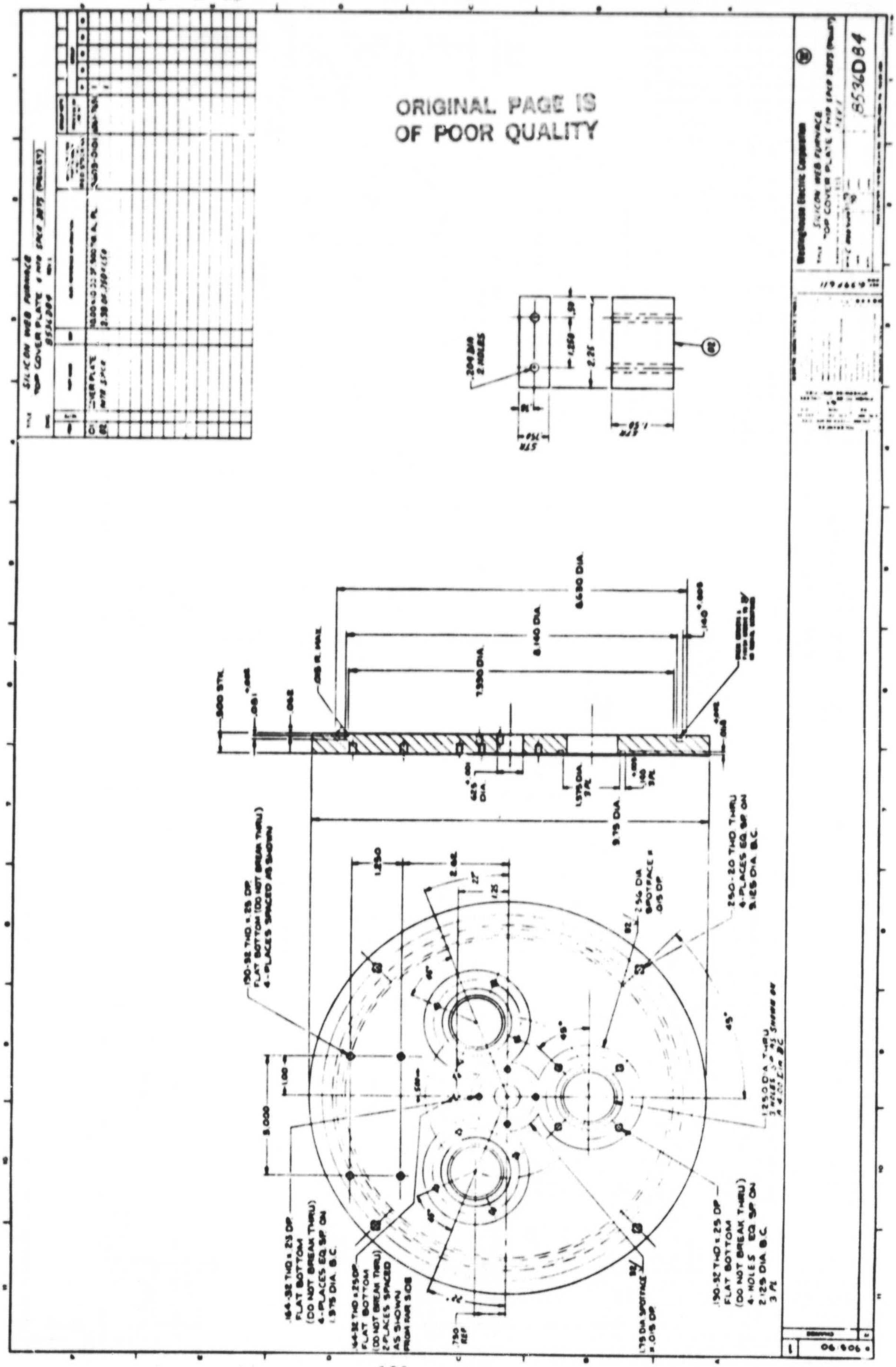

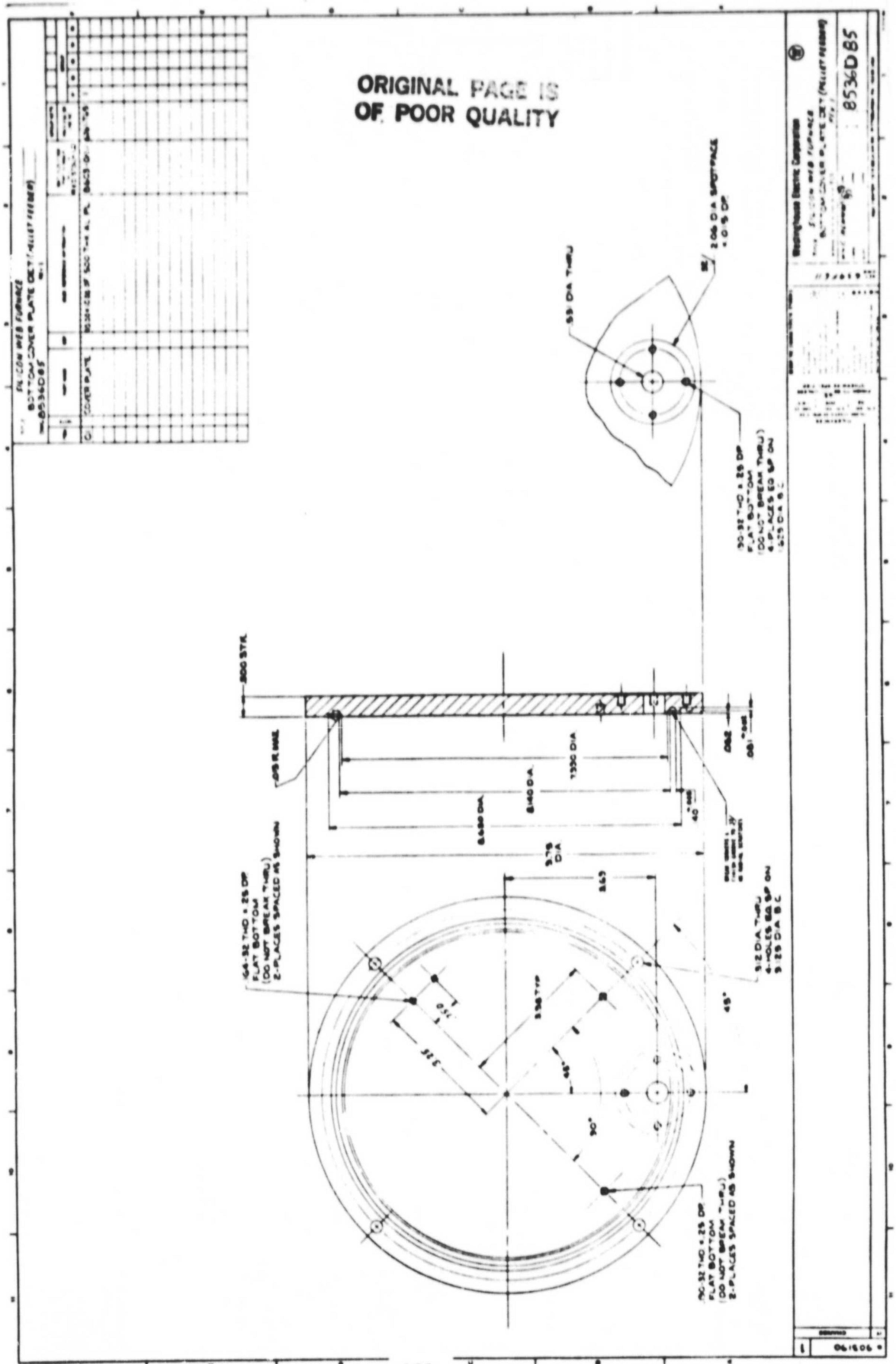
8536D85
.300 STK.
3.75 DIA
45°
90°

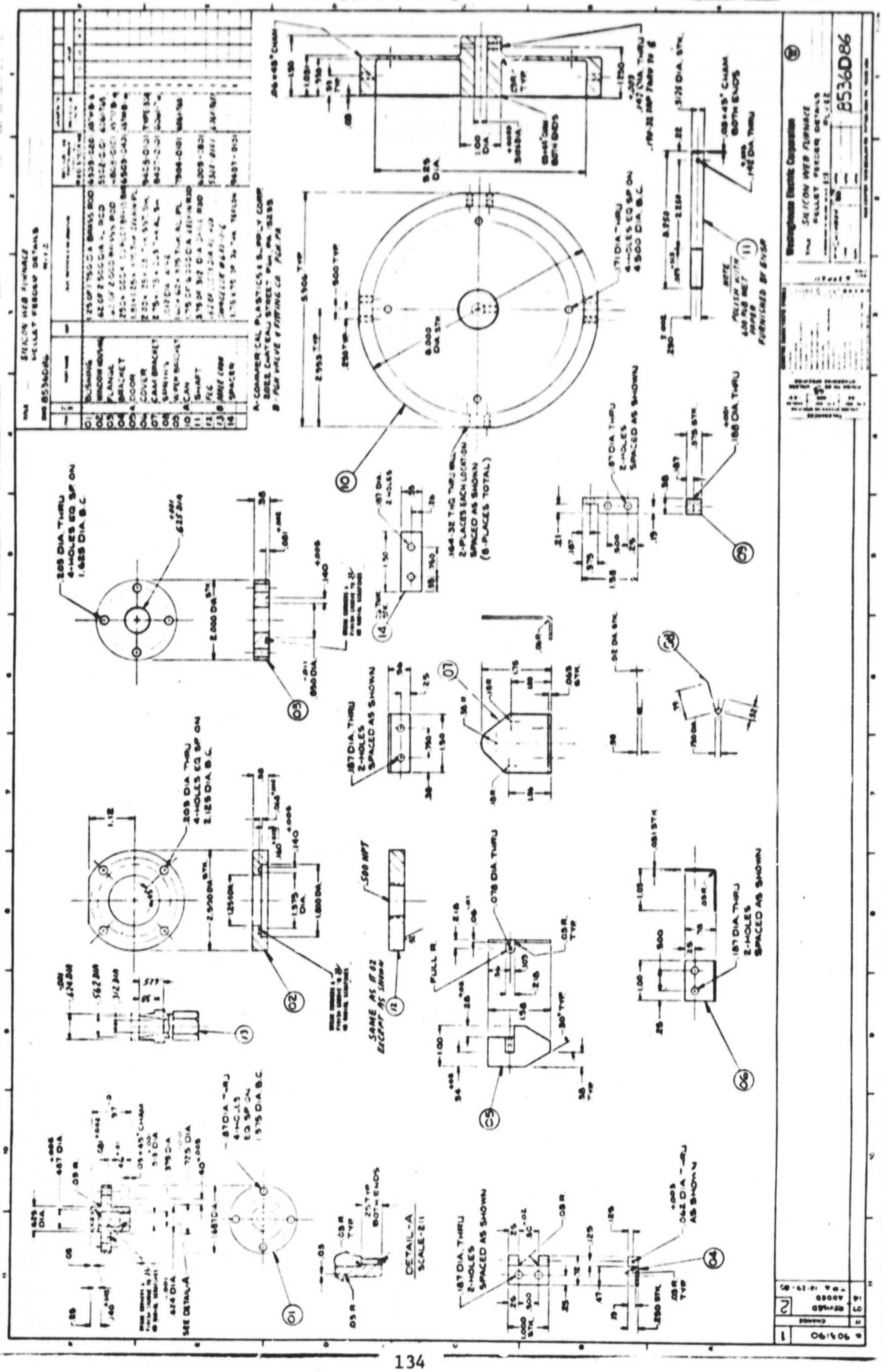
SILICON WEB FURNACE
PELLET FEEDER DETAILS
B536D86
Westinghouse Electric Corporation
DETAIL-A
SCALE-2:1

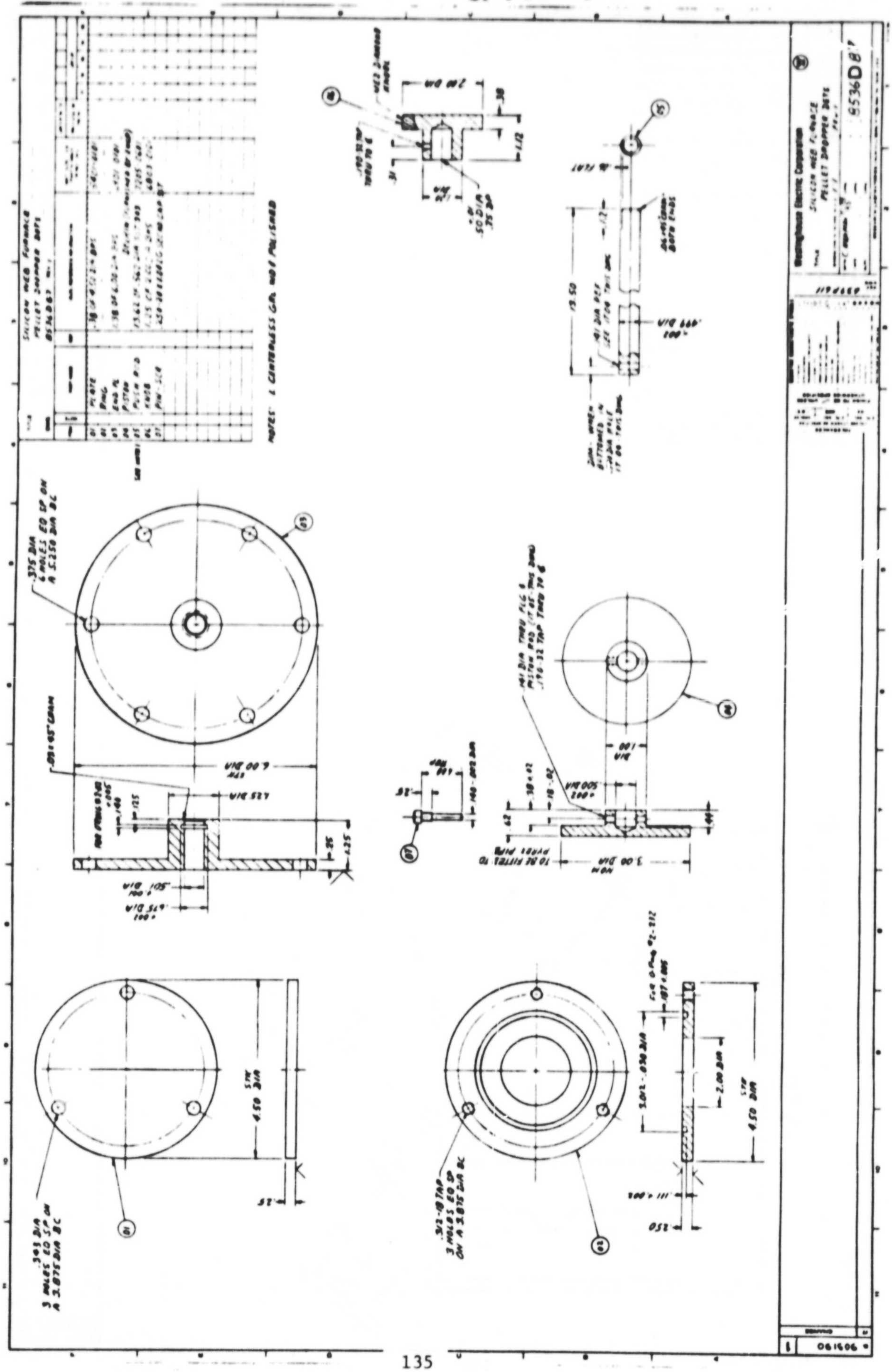

ORIGINAL PAGE IS
OF POOR QUALITY

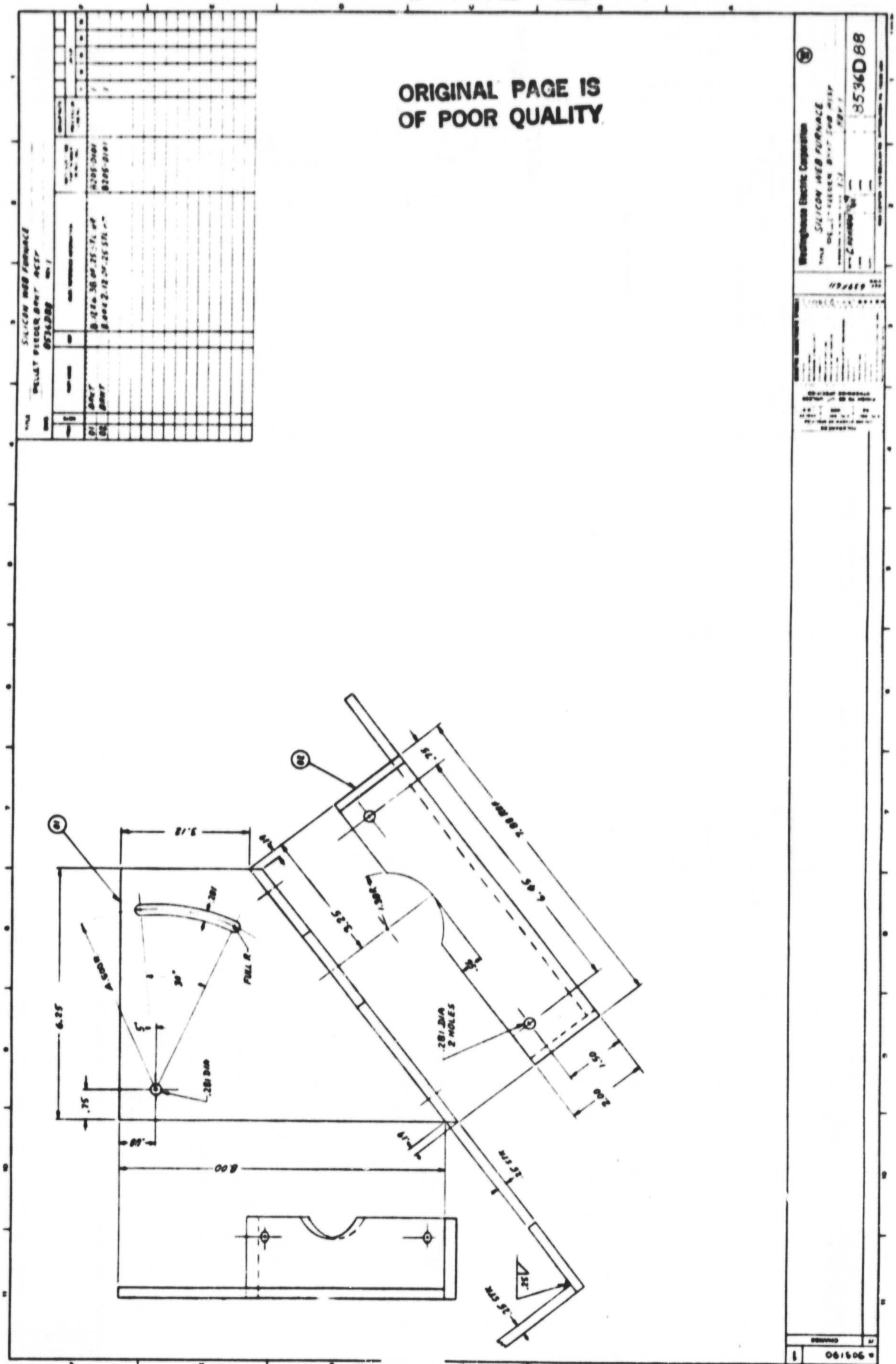

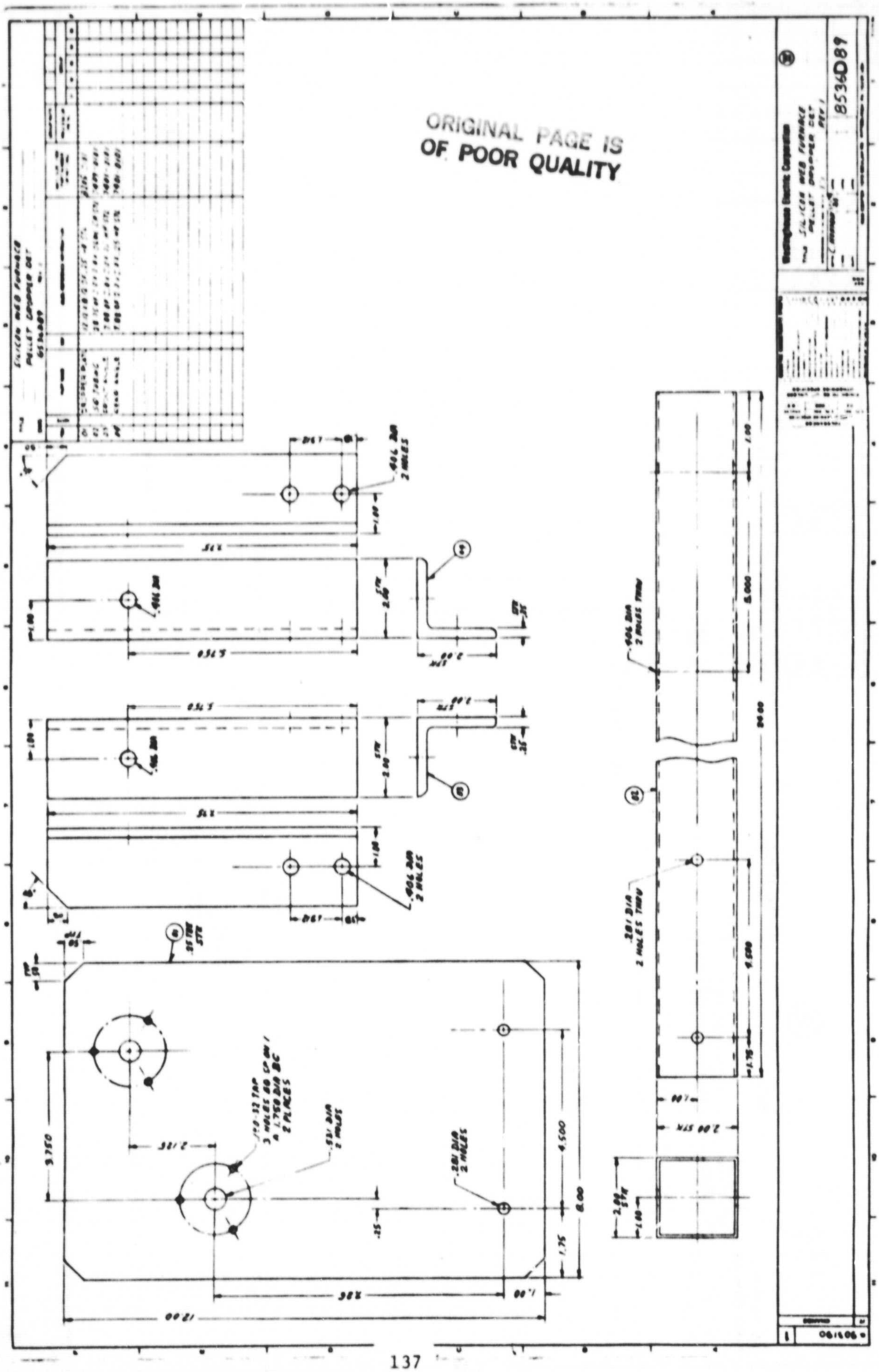
8536D89

ORIGINAL PAGE IS
OF POOR QUALITY

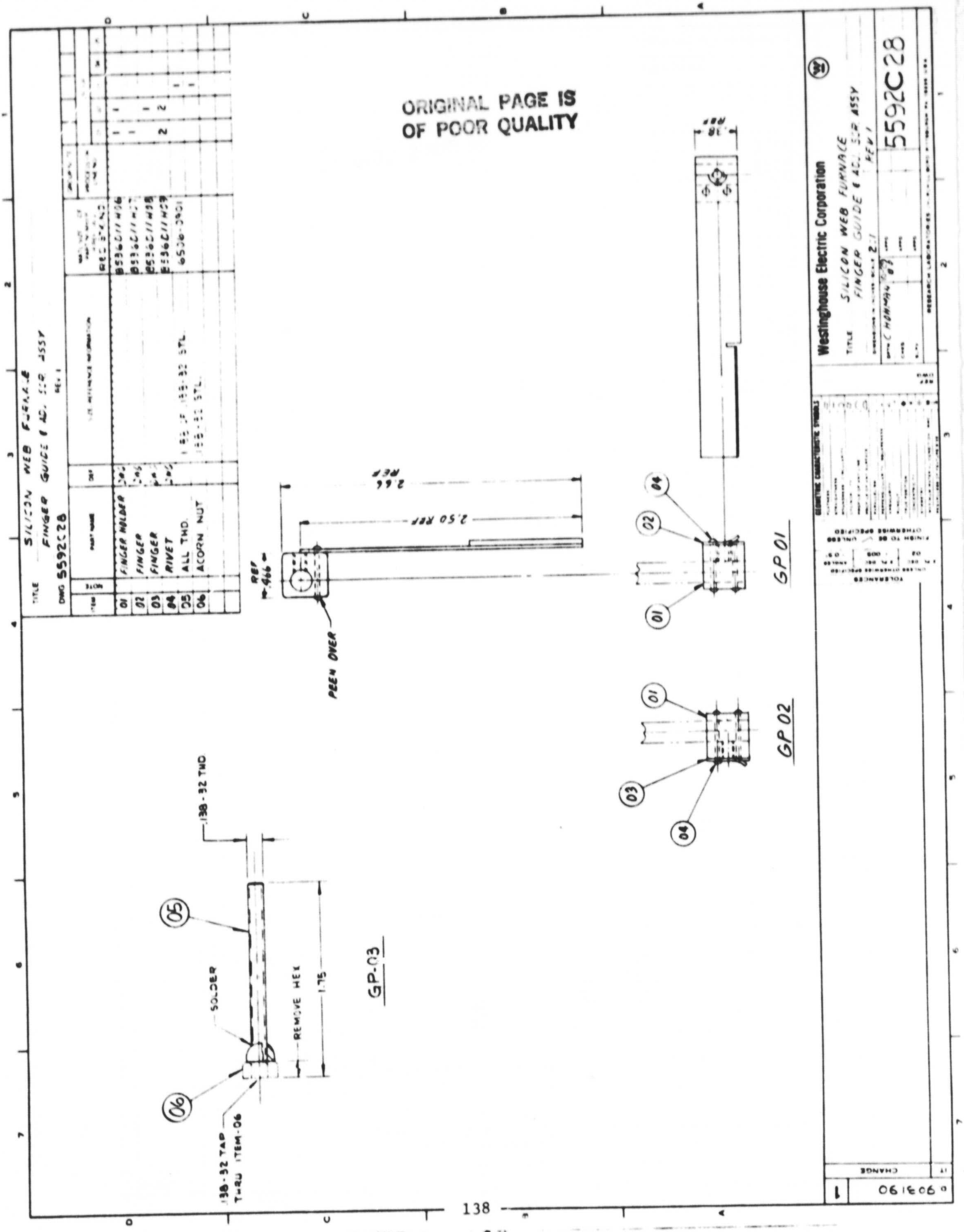

TITLE SILICON WEB WITHDRAW & STORAGE REEL
STORAGE REEL DETAIL WELDMENT
DWG 5592C29

ITEM	NOTE	PART NAME	QTY	SIZE/REFERENCE INFORMATION	R&D STK NO						
01		RIM		MAKE FROM AL		6061-T651	1				
02		RIB		35.50 DIA x .35 THK AL	7304-0101	6061-T651	1				
03		HUB		3.50 OF 3.00 DIA AL	6102-0101	6061-T651	1				

NOTE:

1- MACHINE AFTER WELDING.

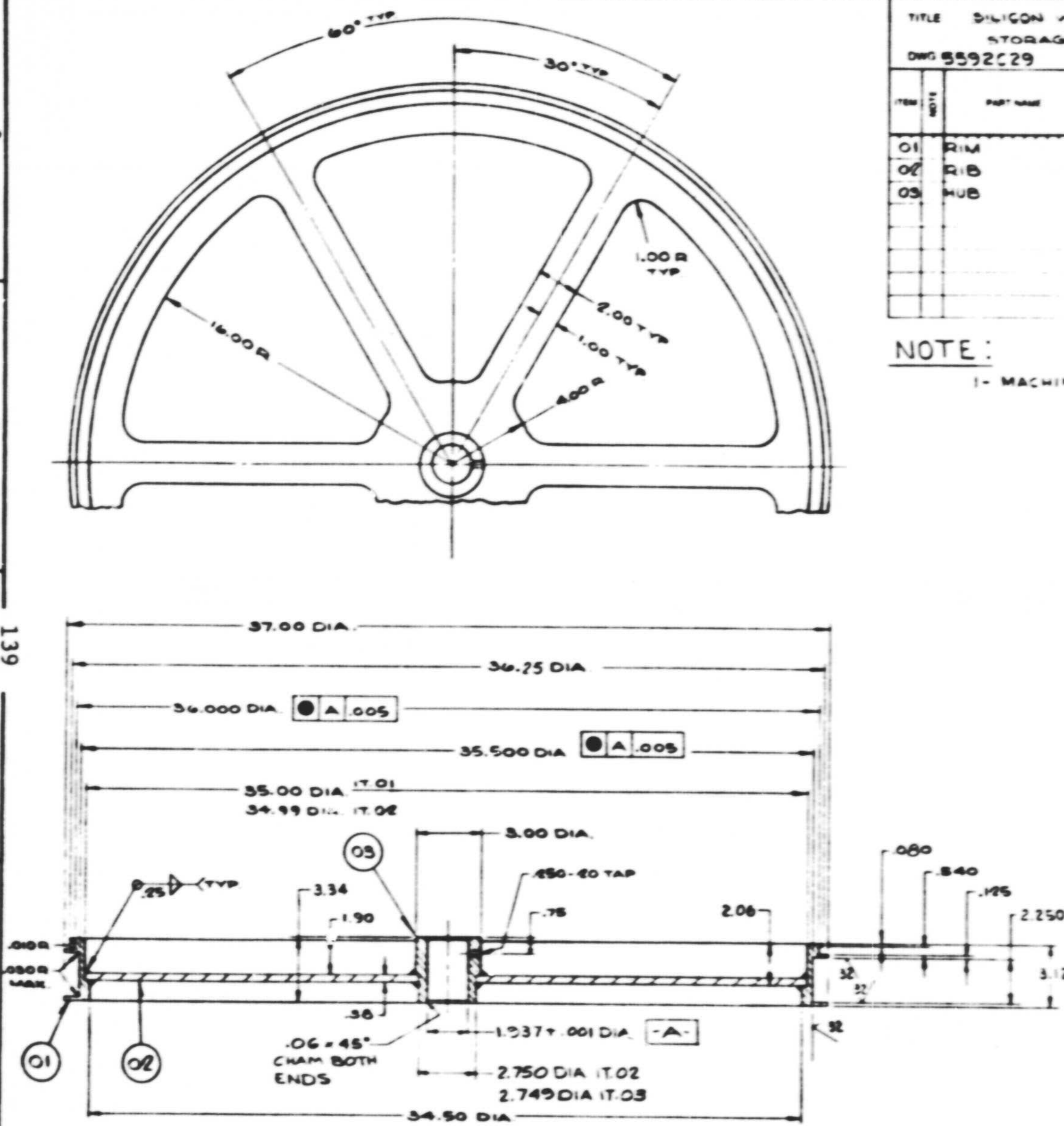

Westinghouse Electric Corporation

TITLE SILICON WEB WITHDRAW & STORAGE REEL
STORAGE REEL DETAIL WELDMENT
REV 1

5592C29

1 CHANGE

06 1506

ORIGINAL PAGE IS
OF POOR QUALITY

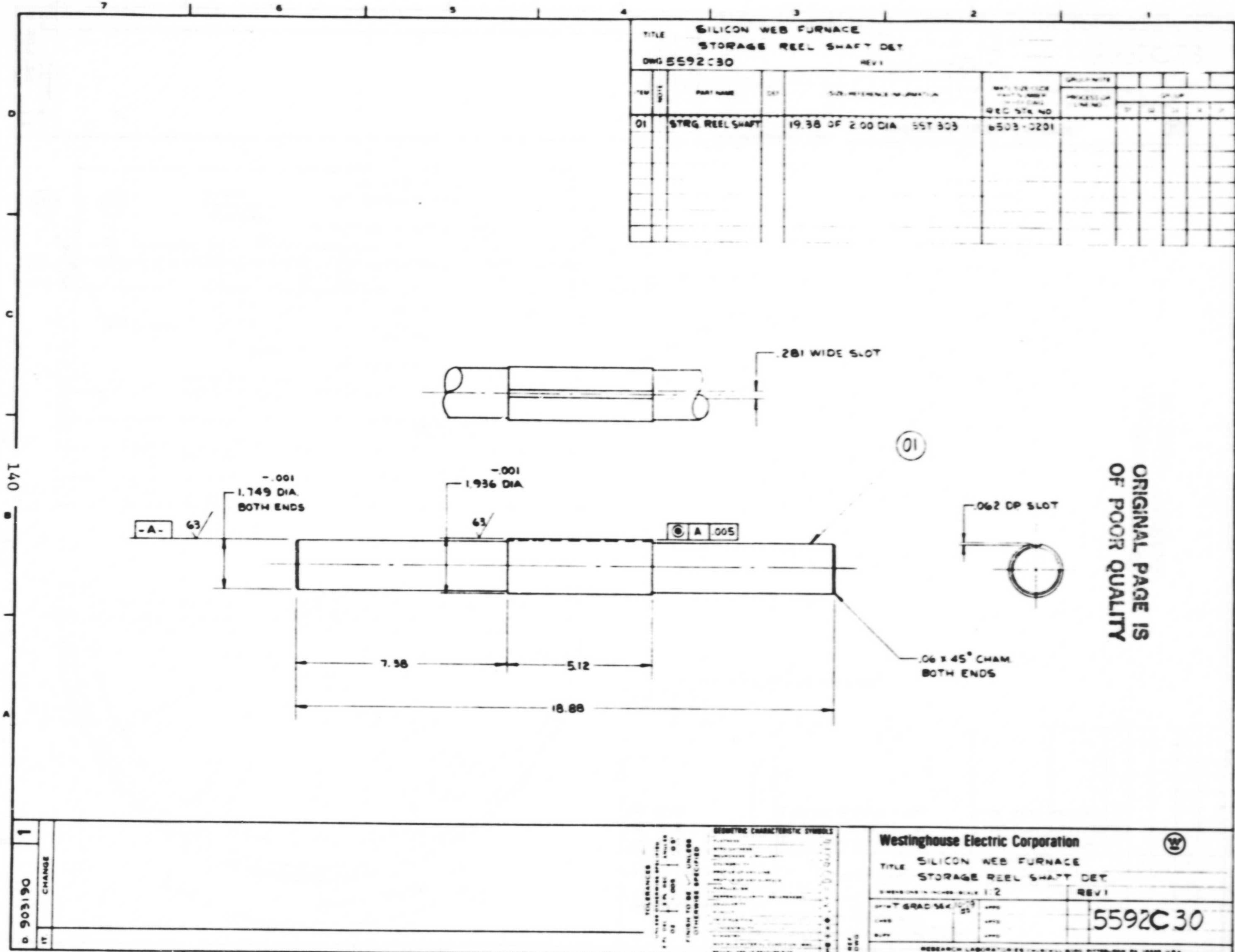

ORIGINAL PAGE IS
OF POOR QUALITY

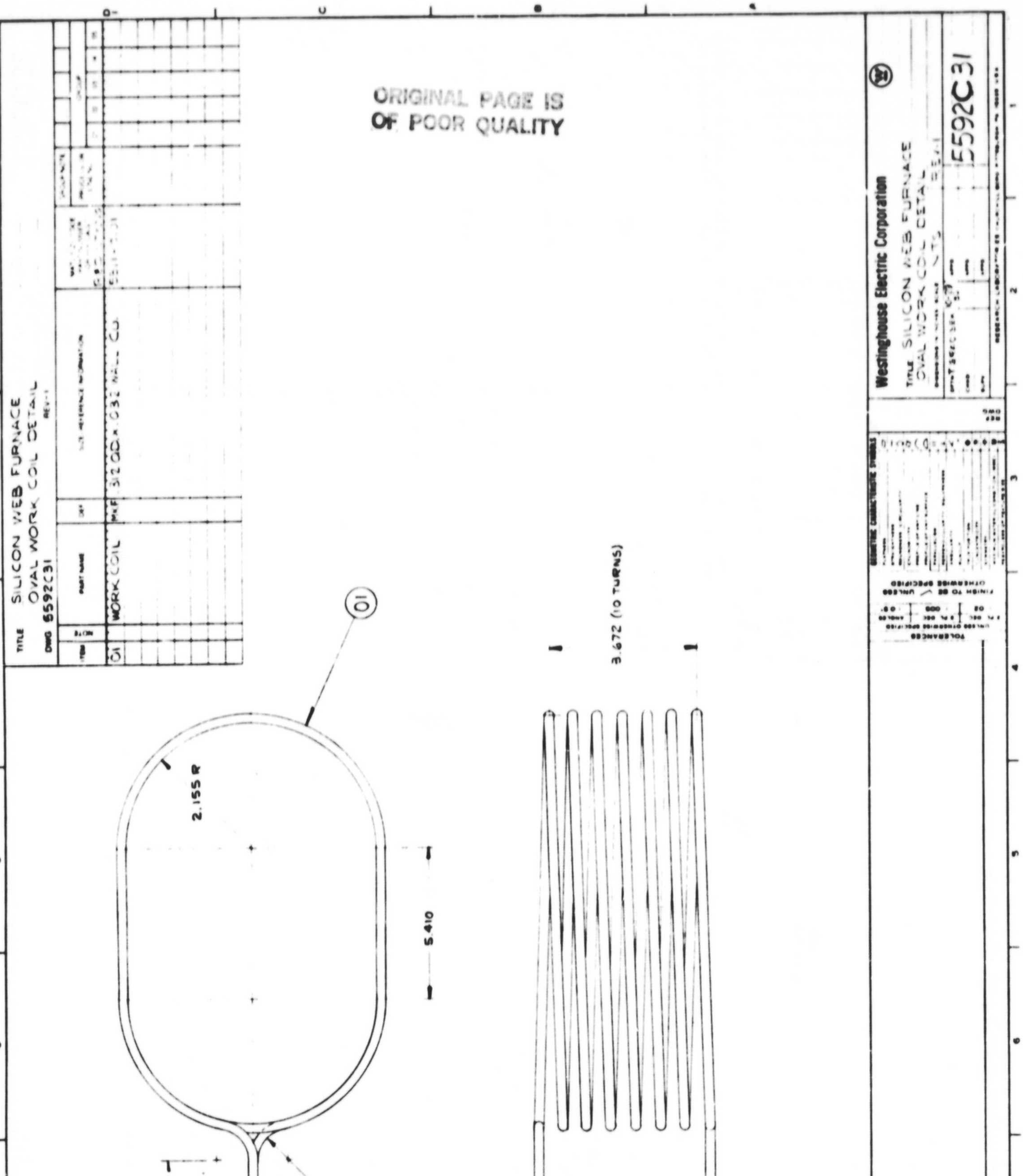

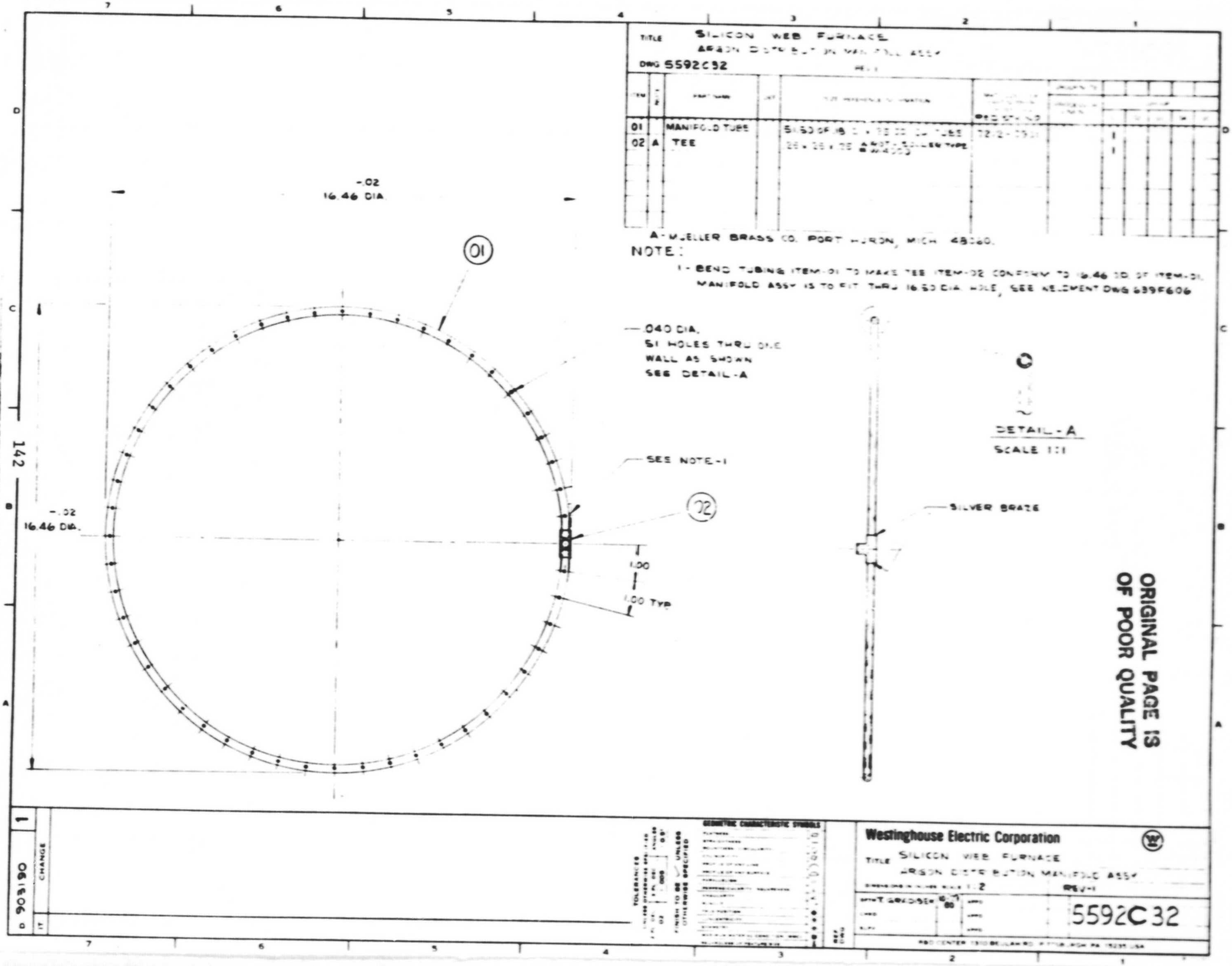
TITLE SILICON WEB FURNACE
ARGON DISTRIBUTION MANIFOLD ASSY
DWG 5592C32
01 MANIFOLD TUBE
02 A TEE
A - MUELLER BRASS CO. PORT HURON, MICH. 48060.
NOTE:
1 - BEND TUBING ITEM-01 TO MAKE TEE ITEM-02 CONFORM TO 16.46 I.D. OF ITEM-01. MANIFOLD ASSY IS TO FIT THRU 16.50 DIA. HOLE, SEE WELDMENT DWG 639F606
-.02
16.46 DIA
01
.040 DIA.
51 HOLES THRU ONE
WALL AS SHOWN
SEE DETAIL-A
DETAIL-A
SCALE 1:1
SEE NOTE-1
02
SILVER BRAZE
1.00
1.00 TYP.
ORIGINAL PAGE IS
OF POOR QUALITY
Westinghouse Electric Corporation
TITLE SILICON WEB FURNACE
ARGON DISTRIBUTION MANIFOLD ASSY
5592C32
061606
CHANGE

TITLE SILICON WEB FURNACE
TAPE REEL BRACKET
DWG 5592C33 REV 1

ITEM	MFR	PART NAME	QTY	SIZE REFERENCE OR DESCRIPTION
01	A	BRACKET		4.75 OF .25 x 2.50 x 2.00 STL ANGLE
02	A	BRACKET		4.75 OF .25 x 2.50 x 2.00 STL ANGLE

A - J.T. RYERSON & SON, PGH PA

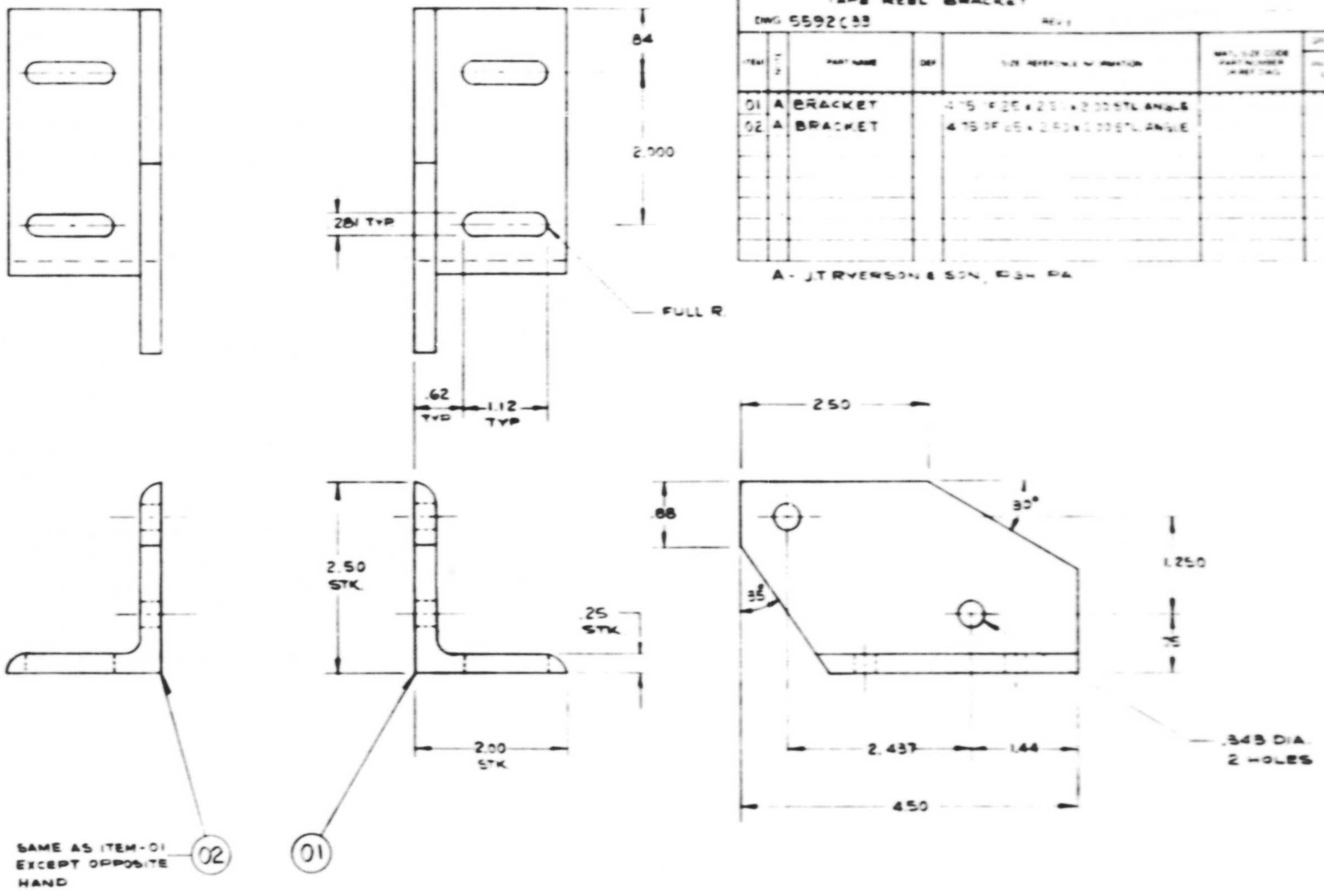

ORIGINAL PAGE IS OF POOR QUALITY

Westinghouse Electric Corporation

TITLE SILICON WEB FURNACE
TAPE REEL BRACKET

5592C33

061506

ORIGINAL PAGE IS
OF POOR QUALITY

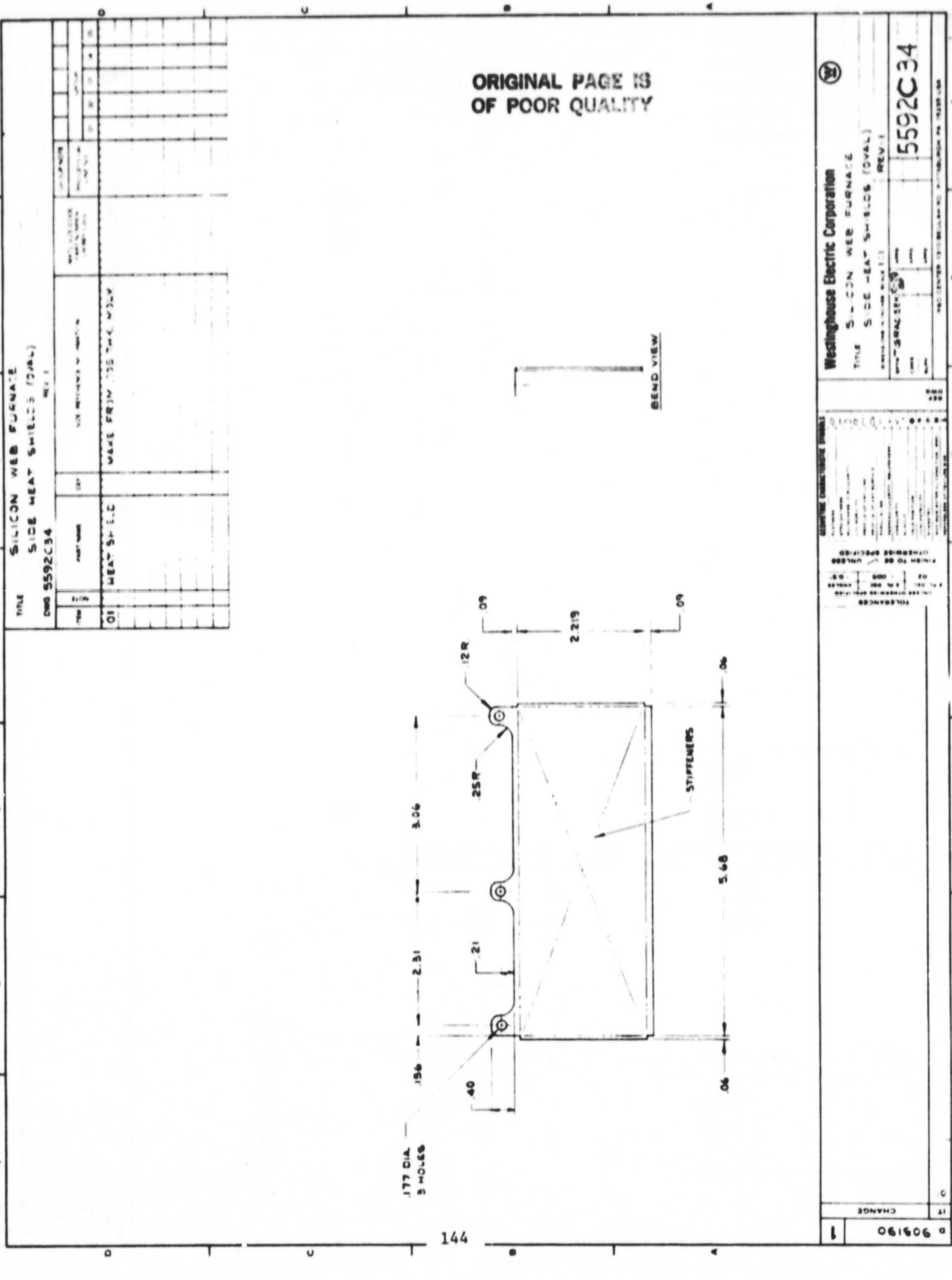

ORIGINAL PAGE IS
OF POOR QUALITY

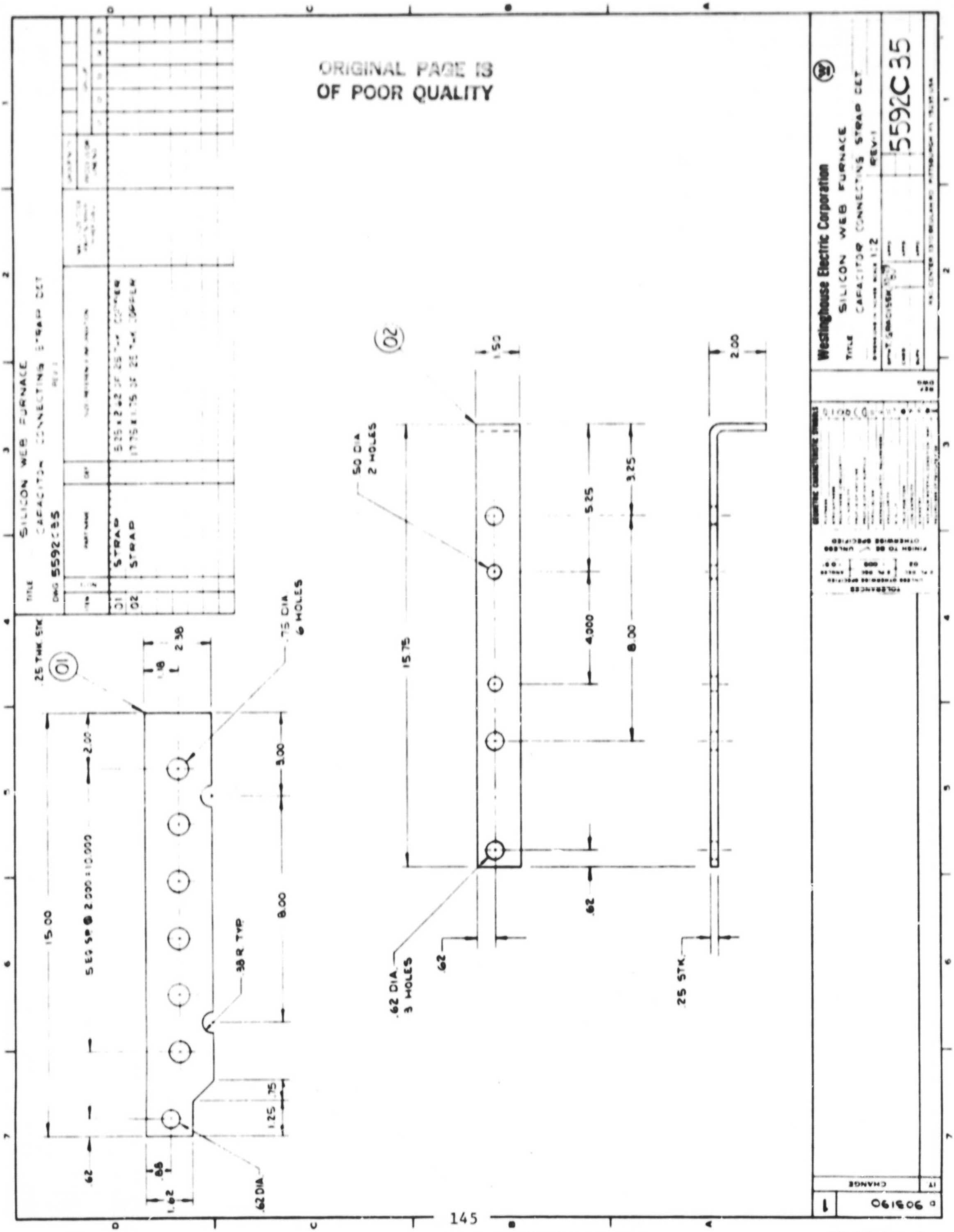

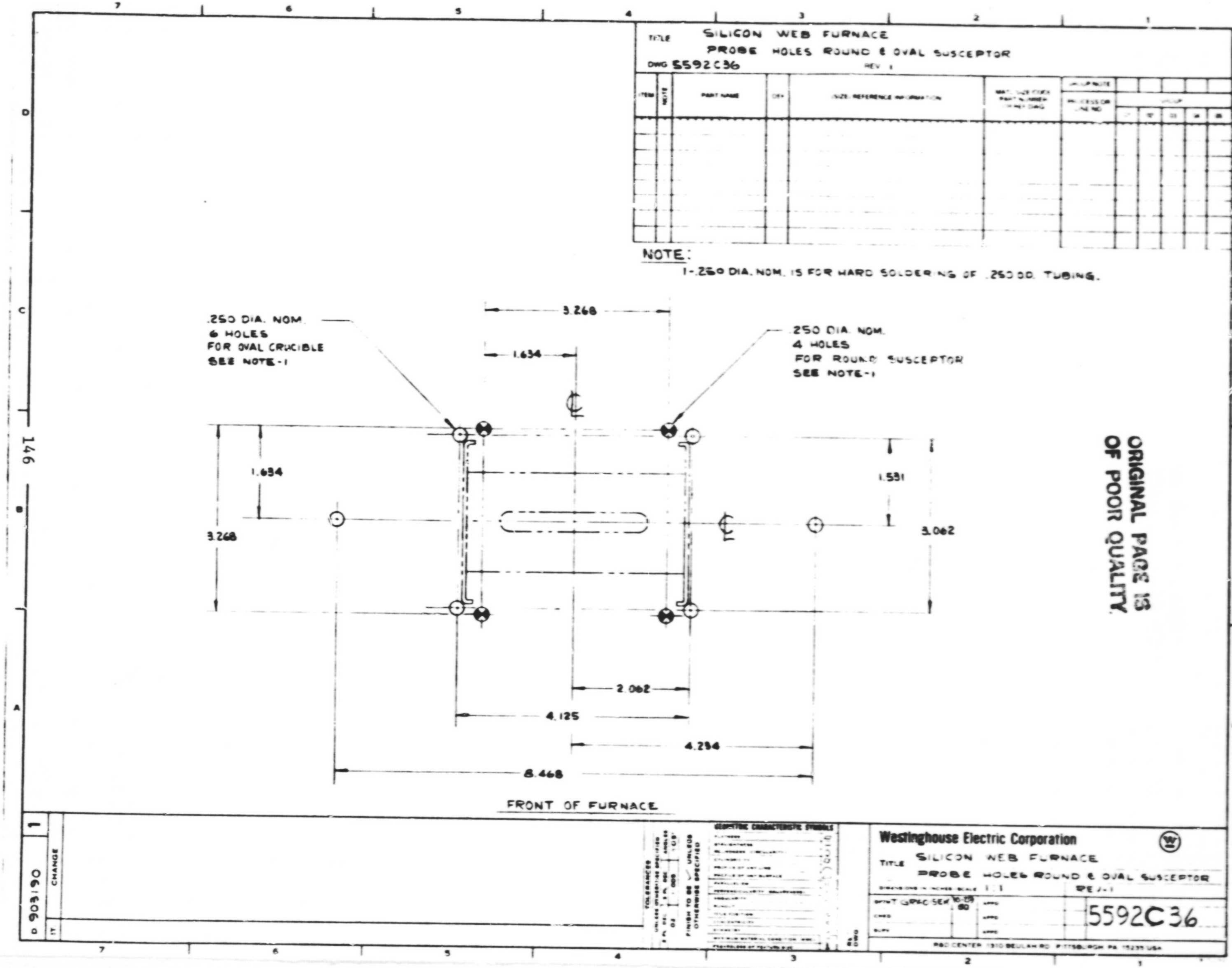
TITLE SILICON WEB FURNACE
PROBE HOLES ROUND & OVAL SUSCEPTOR
DWG 5592C36
REV 1
ITEM
NOTE
PART NAME
QTY
SIZE, REFERENCE INFORMATION
NOTE:
1-.250 DIA. NOM. IS FOR HARD SOLDERING OF .250 O.D. TUBING.
.250 DIA. NOM.
6 HOLES
FOR OVAL CRUCIBLE
SEE NOTE-1
.250 DIA. NOM.
4 HOLES
FOR ROUND SUSCEPTOR
SEE NOTE-1
3.268
1.634
1.634
3.268
1.531
3.062
2.062
4.125
4.294
8.468
FRONT OF FURNACE
ORIGINAL PAGE IS
OF POOR QUALITY
Westinghouse Electric Corporation
TITLE SILICON WEB FURNACE
PROBE HOLES ROUND & OVAL SUSCEPTOR
REV-1
1:1
GPACISEK
5592C36
TOLERANCES
CHANGE
D 903190
1
R&D CENTER 1310 BEULAH RD PITTSBURGH PA 15235 USA

TITLE SILICON WEB FURNACE
GUIDE DETAIL PELLET FEEDER
DWG 5592C52

ITEM	NOTE	PART NAME		
01	A	GUIDE		6.50 x 1.50 OF 1.500 THK DELRIN PL

A-COMMERICAL PLASTICS & SUPPLY CORP
2022 CHATEAU STREET PGH., PA 15233

ORIGINAL PAGE IS
OF POOR QUALITY

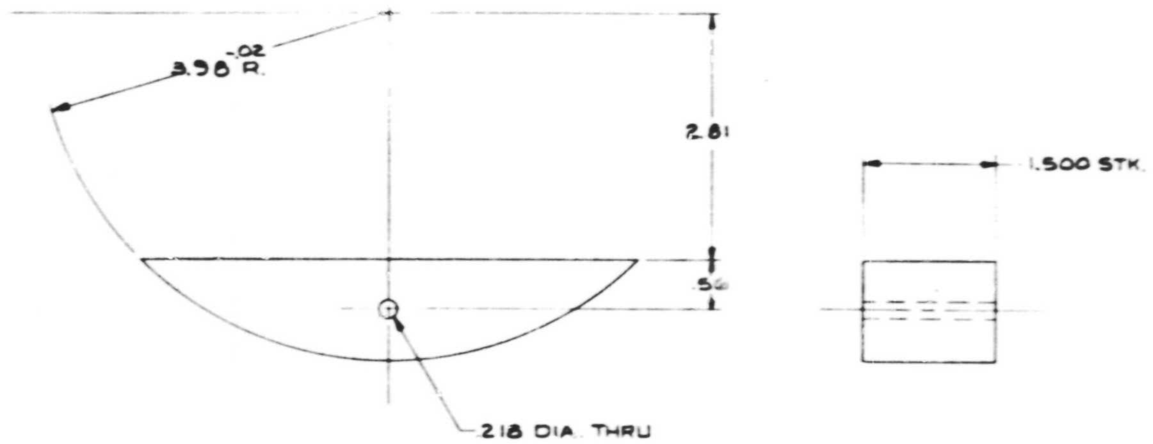

TOLERANCES

GEOMETRIC CHARACTERISTIC SYMBOLS

Westinghouse Electric Corporation

TITLE SILICON WEB FURNACE
GUIDE DETAIL PELLET FEEDER
SCALE 1:1
REV 1
DFTR C. HOHMAN
5592C52

REF 1173E65

1 | CHANGE | 906 SOS

SILICON WEB FURNACE
HOUSING DETAIL
DWG 5592C57 REV 1

ITEM		PART NAME	DESCRIPTION
01	A	HOUSING	8.00 3.25 OF 8.00 SCH 40 AL PIPE 6063-T6 (8.625 OD × .322 WALL) ASTM B-241

A-WILLIAMS & CO. INC., PGH., PA. 15233

NOTES:
1- MACHINE BOTH ENDS TO DIMENSIONS AS NOTED APPROX .25 DEEP

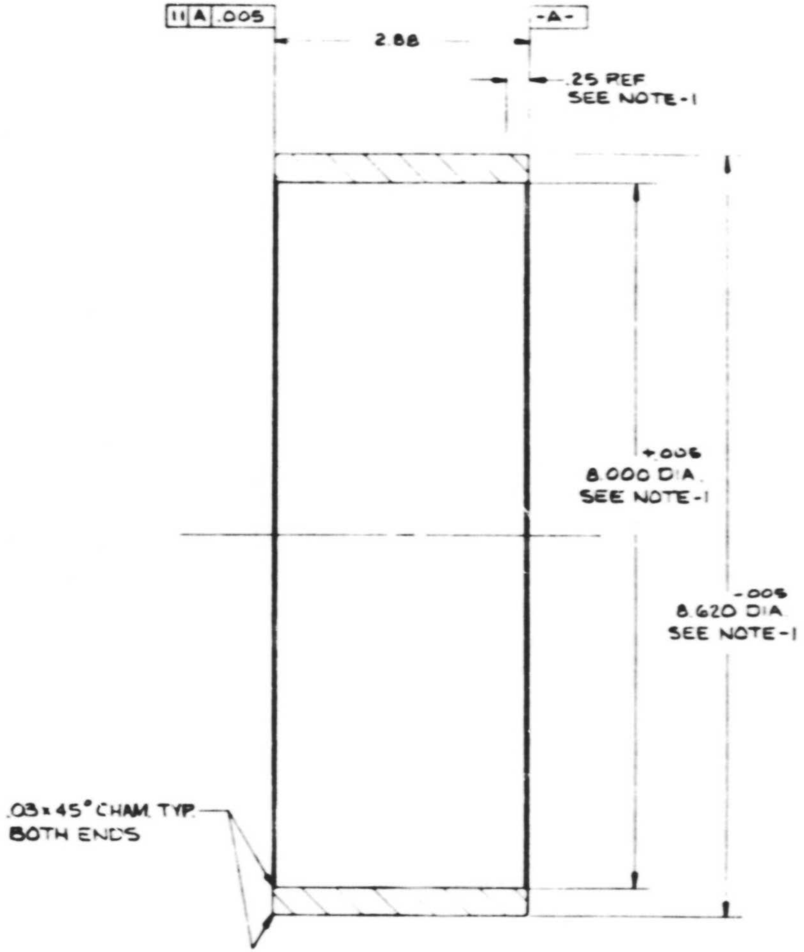

Westinghouse Electric Corporation
TITLE SILICON WEB FURNACE
HOUSING DETAIL
REV 1
C. HOHMAN
5592C57
659F611
D 903190

TITLE SILICON WEB FURNACE MOD-2
OVAL CRUCIBLE DET

DWG 1691B62 REV X23

ITEM	NOTE	PART NAME	DEF	(SIZE) REFERENCE INFORMATION	MATL SIZE CODE PART NUMBER OR REF DWG	GROUP NOTE / PROCESS OR UNIT NO	GROUP 01	02	03	04	5
01		CRUCIELE		CLEAR FUSED QUARTZ							

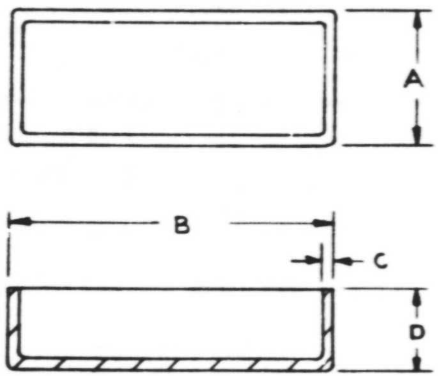

ITEM NO.	A	B	C	D
01	2.493	5.993	.080	.668

TOLERANCE ±.015

ORIGINAL PAGE IS OF POOR QUALITY

IT.	CHANGE
D	905111 903066 903190
01	1
01	2 C WAS .056 MAT'L WAS GE TYPE 214 OR 204 TPG
01	3 .668 WAS .683 +.015 WAS +.000 -.015 TPG

TOLERANCES UNLESS OTHERWISE SPECIFIED: 2 PL DEC, 3 PL DEC, ANGLES

FINISH TO BE √ UNLESS OTHERWISE SPECIFIED

GEOMETRIC CHARACTERISTIC SYMBOLS: FLATNESS, STRAIGHTNESS, ROUNDNESS (CIRCULARITY), CYLINDRICITY, PROFILE OF ANY LINE, PROFILE OF ANY SURFACE, PARALLELISM, PERPENDICULARITY (SQUARENESS), ANGULARITY, RUNOUT, TRUE POSITION, CONCENTRICITY, SYMMETRY, MAXIMUM MATERIAL CONDITION (MMC), REGARDLESS OF FEATURE SIZE

REF DWG 639F573 1297J12 711B32

Westinghouse Electric Corporation

TITLE SILICON WEB FURNACE
OVAL CRUCIBLE DET

DIMENSIONS IN INCHES SCALE ~ REV-X23

DFTM T. GRADISON 10-29-80 APPD
CHKD W. C. J. 10-29-80 APPD
SUPV APPD

1691B62

RESEARCH LABORATORIES CHURCHILL BORO PITTSBURGH PA 15235 U.S.A.

TITLE SILICON WEB FURNACE
OVAL CRUCIBLE ASSY.
DWG 1711B33 REV

ITEM	NOTE	PART NAME		SIZE REFERENCE INFORMATION	MAT'L SIZE CODE PART NUMBER OR REF DWG	GROUP 01
01		CRUCIBLE	DWG		2918B2 -01	1
02		UPPER BARRIER		MAKE FROM .062 QUARTZ PLATE		1
03		ROUND POST		MAKE FROM QUARTZ		2
04		LOWER BARRIER		MAKE FROM .062 QUARTZ PLATE		1

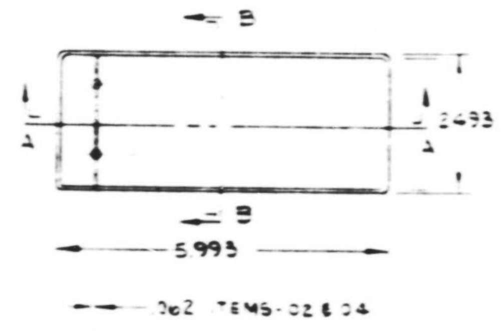

NOTE:
1- ALL FUSED CONSTRUCTION EXCEPT BOTTOM OF LOWER BARRIER ITEM-04 TO BOTTOM OF CRUCIBLE ITEM-01.
2- TOLERANCE ±.015

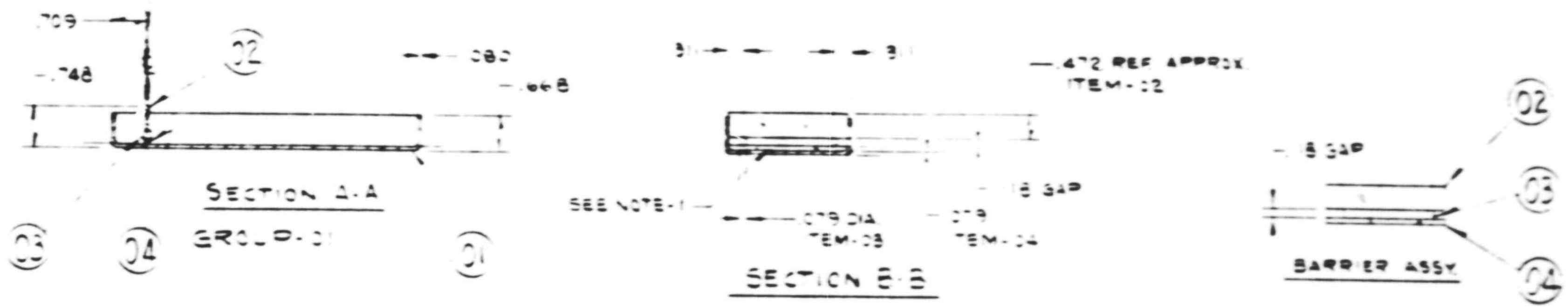

Westinghouse Electric Corporation

TITLE SILICON WEB FURNACE
OVAL CRUCIBLE ASSY
SCALE 1 2 REV
DRAFT GRADISEK 3/83
1711B33

RESEARCH LABORATORIES PITTSBURGH PA U.S.A.

1 | 903190 | CHANGE

TITLE SILICON WEB FURNACE
DOOR SUB-ASSEMBLY PELLET FDR.
DWG 1713B80 REV 1

ITEM	NOTE	PART NAME	DEF	(SIZE) REFERENCE INFORMATION	MAT'L SIZE CODE PART NUMBER OR REF DWG	GROUP NOTE / PROCESS OR LINE NO	GROUP 01	02	03	04	05
01		BRACKET	DWG		8536D86H04		1				
02		DOOR	DWG		8536D86H05		1				
03	A	ROLL PIN	BOS	.062 DIA. x 1.00 LG. CAT. NR. 59-012	-062-1000		1				
04		SPRING	DWG		8536D86H06		1				

A-ELASTIC STOP NUT DIV. AMERACE ESNA CORP.
2330 VAUXHALL ROAD, UNION, N.J. 07083

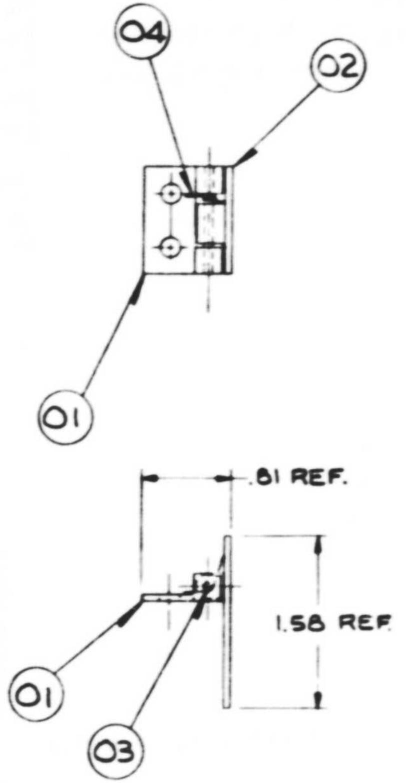

IT	CHANGE
1	D 903190

TOLERANCES UNLESS OTHERWISE SPECIFIED
2 PL. DEC. ±.02 | 3 PL. DEC. ±.009 | ANGLES ±0.5°
FINISH TO BE ✓ UNLESS OTHERWISE SPECIFIED

GEOMETRIC CHARACTERISTIC SYMBOLS
FLATNESS
STRAIGHTNESS
ROUNDNESS (CIRCULARITY)
CYLINDRICITY
PROFILE OF ANY LINE
PROFILE OF ANY SURFACE
PARALLELISM
PERPENDICULARITY (SQUARENESS)
ANGULARITY
RUNOUT
TRUE POSITION
CONCENTRICITY
SYMMETRY
MAXIMUM MATERIAL CONDITION (MMC)
REGARDLESS OF FEATURE SIZE

REF DWG 639F611

Westinghouse Electric Corporation

TITLE SILICON WEB FURNACE
DOOR SUB-ASSEMBLY PELLET FDR.
DIMENSIONS IN INCHES—SCALE 1:1
REV. 1
DFTM C. HOHMAN 12-29 APPD
CHKD APPD
SUPV APPD

1713 B80

RESEARCH LABORATORIES CHURCHILL BORO PITTSBURGH PA 15235 U.S.A.

SKETCH SHEET
WESTINGHOUSE FORM 2444D

ORIGINAL PAGE IS
OF POOR QUALITY

WESTINGHOUSE ELECTRIC CORPORATION

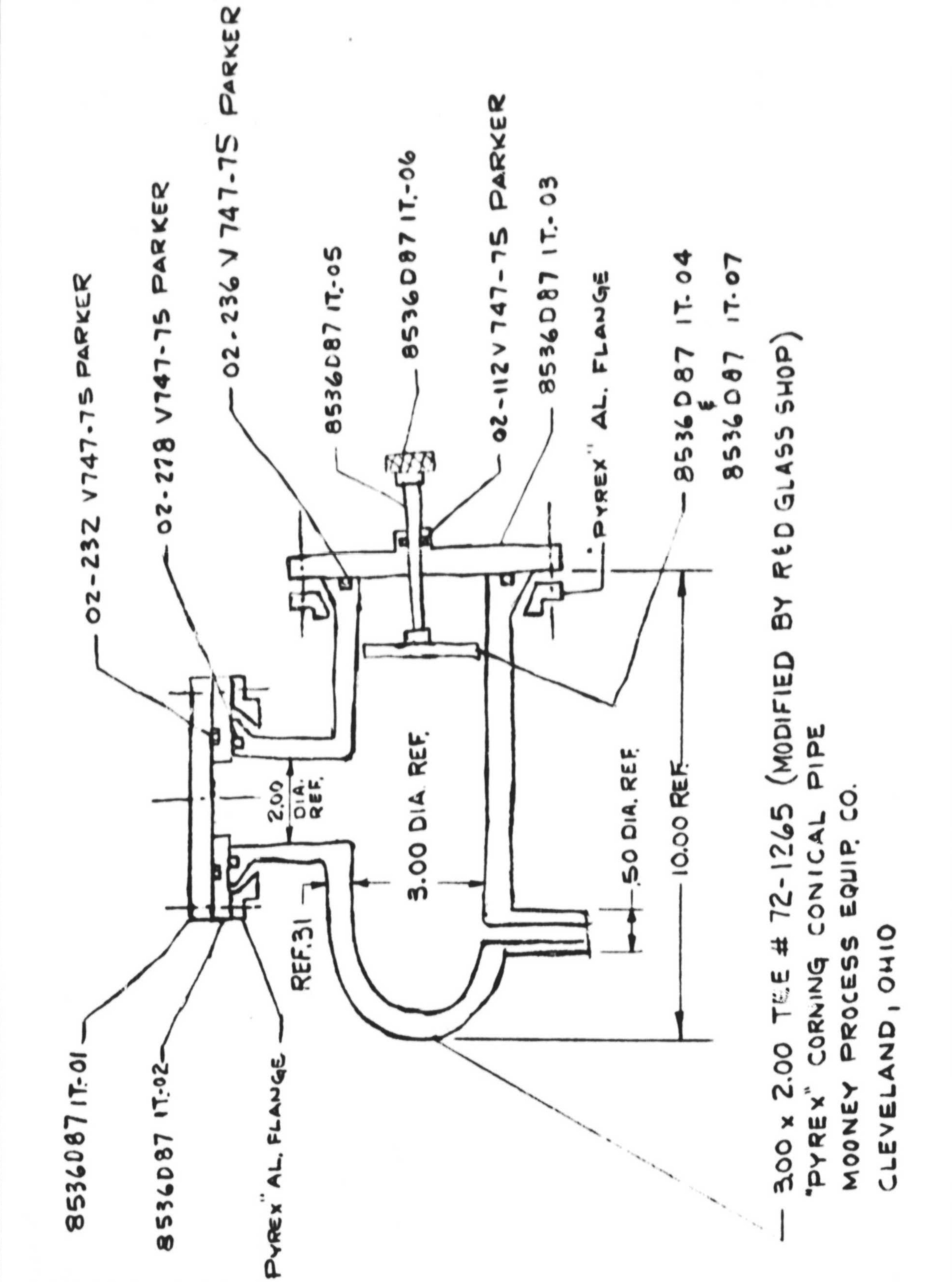

TPG 10-29-80 D.903190

DWG. 7727A96